Topological Defects in Conformal Field Theories, Entanglement Entropy and Indices

Daniel Jaud

München 2017

Topological Defects in Conformal Field Theories, Entanglement Entropy and Indices

Daniel Jaud

Dissertation
an der Fakultät für Physik
der Ludwig–Maximilians–Universität
München

vorgelegt von
Daniel Jaud
aus Schongau

München, den 19.07.2017

Contents

List of Figures

List of Tables

Zusammenfassung

Die hier vorliegende Dissertation befasst sich mit dem Themengebiet der zweidimensionalen konformen Feld Theorien (CFT). Der Schwerpunkt liegt auf der Betrachtung von Defekten in konformen und insbesondere supersymmetrischen konformen Feldtheorien.

Im ersten Teil der Arbeit werden einige Konzepte der konformen Feldtheorien erörtert, welche im weiteren Verlauf der Arbeit benötigt werden. Das dritte Kapitel führt danach in das Themengebiet der Defekte in CFTs ein. Dabei werden deren Klassifikation und Eigenschaften, wie z.B. Klebebedingungen, Fusion, Faltung sowie Transmissivität und Reflexivität, im Detail erläutert.

Seit geraumer Zeit findet die Verschränkungs-Entropie in der Physik zunehmend Beachtung, da diese ein gutes Maß darstellt um die "Stärke" der Verschänkung eines Quantensystems zu beschreiben. Im vierten Kapitel wird darauf eingegangen, wie diese Entropie definiert ist und wie man sie prinzipiell für beliebige Systeme berechnen kann. Insbesondere wird der sogenannte "relpica trick" erläutert, welcher die Verschränkungs-Entropie in zweidimensionalen CFTs mittels Twist-Feldern zu berechnen erlaubt.

Im weiteren Verlauf werden die bereits bekannten Twist Felder auf den supersymmetrischen Fall erweitert. Damit können supersymmetrische Verschränkungs- und Renyi Entropien berechnet und mit den ursprünglichen nicht supersymmetrischen Ergebnissen in Relation gebracht werden.

Da zu Beginn nicht unmittelbar klar ist, ob die supersymmetrischen Twist Felder wirklich im Spektrum der Theorie enthalten sind, wird im darauffolgenden Kapitel eine genauere Betrachtung des Spektrums in supersymmetrischen $\mathbb{Z}_n$ getwisteten Theorien angestellt, um die Konstruktion des supersymmetrischen Twist Feldes zu rechtfertigen.

Das siebte Kapitel dieser Arbeit wird sich mit der Berechnung der Verschänkungs-Entropie in Gegenwart eines topologischen Defektes beschäftigen. Dies wird zeigen, dass die Entropie S in zwei Teile zefällt

$$S = \frac{c}{3} \log L + S_{sub},$$

wobei die gesamte Information des Defektes in dem Term S_{sub} enthalten ist und L die Länge des Verschänkungs-Intervalls darstellt. Das Ergebnis wird an Beispielen dargestellt. Unter anderem wird die Implikation für Coset Theorien untersucht, welche frei von Fixpunkten unter Feldidentifikationen sind. Dabei wird anhand ausgewählter Beispiele ersichtlich, dass die Verschänkungs-Entropie in die einzelnen Bestandteile des Cosets "zerfällt".

Im darauffolgenden Teil wird eine ähnliche Verschränkungs-Entropie, die sogenannte links/ rechts Verschränkungs-Entropie, betrachtet. Die Idee hierbei ist einen Randzustand zu

entfalten und diesen als Defekt zwischen ein und derselben chiralen CFT aufzufassen. Erneut werden die gewonnenen Erkenntnisse an ausgewählten Beispielen erläutert.

Für d Bosonen, welche auf einem Torus kompaktifiziert sind, wurden die dazugehörigen Defekte bereits konstruiert. Indem wir unsere Rechnung aus den vorherigen Kapiteln auf diese Defekte anwenden, können wir einen cross-check mit bereits bekannten Ergebnissen ziehen und unsere Herangehensweise untermauern.

Im letzten Kapitel werden Indizes in der Gegenwart von (topologischen) Defekten betrachtet. Es wird speziell der Witten Index zwischen zwei Randzuständen, in der Gegenwart eines oder mehrerer topologischer Defekte, berechnet. Der resultierende Index lässt sich geometrisch als die Schneidungszahl von D-Branen interpretieren. Anhand ausgewählter Beispiele wird dieser Sachverhalt explizit präsentieren.

Zusätzlich wird das elliptische Geschlecht in Gegenwart topologischer B-Typ Defekte untersucht. Durch die Betrachtung eines speziellen Grenzwertes für das Geschlecht, erhält man einen Ausdruck für den Witten Index in der Gegenwart eben dieser Defekte. Durch die Analyse der Struktur des Index, kann eine Verbindung zu bereits bekannten Resultaten festgestellt werden.

Um die Arbeit thematische abzuschließen, wird zuletzt der Ausdruck für den Witten Index auf die Berechnung der Verschränkungs-Entropie angewendet. Dabei werden wir feststellen, dass nur S_{sub} zu der Entropie beiträgt, d.h. dass es sich wirklich um eine topologische (Intervall L unabhängige) Größe handelt.

Abstract

The following thesis covers the area of two dimensional conformal field theory (CFT). Of particular interest will be special objects within these theories so called *defects* and supersymmetric CFTs. After a short introduction we will review some important concepts concerning CFTs.

In the third chapter we will introduce the notion of defects and discuss their classification and properties such as their gluing conditions, transmissivity and reflectivity, unfolding and their fusion.

The entropy of entanglement has gained importance in various areas of physics over the last years. It has been shown that the entropy of entanglement, or short entanglement entropy, gives a good measure for quantifying the amount of entanglement between two subsystems of a quantum mechanical many-body system. In the fourth chapter we will discuss how one can define entanglement entropy and how it can be calculated. In particular we will consider the so called 'replica trick' which will allow us to calculate entanglement entropies in two-dimensional CFTs via twist fields.

In the following chapter we will generalize the encountered twist fields to a supersymmetric version. With this we can calculate supersymmetric generalizations of Renyi and entanglement entropies and connect the obtained results to the original non-supersymmetric cases.

From the beginning it is not clear right away that the new supersymmetric twist fields really are contained in the spectrum of our theory. Therefore, we will perform a detailed discussion if and how these fields are contained in the spectrum of the $\mathbb{Z}_n$ orbifolded theory.

In chapter seven of this thesis we will calculate the entanglement entropy through a topological defect. We will see that the entropy will decompose into two parts

$$S = \frac{c}{3} \log L + S_{sub},$$

where all the information coming from the defect are contained in the subleading contribution to the entanglement entropy S_{sub}, and L is the length of the entangling region. We will apply our result to various examples, especially to chosen examples of fixed point free coset models. For those we will see that the subleading contribution will decompose into the individual coset parts.

In the following we will consider a related entropy the so called left/right entanglement entropy. By unfolding a boundary state one can interpret it as a topological defect acting

only on the chiral part of the Hilbert space. Performing a similar calculation, as in the chapter before we will highlight our obtained result again with several examples.

For d free bosons compactified on tori the conformal defects have been constructed explicitly. In applying our calculation of the previous chapters to this case we can rederive the entanglement entropy to leading order and compare to known results. In this way we also give a cross-check to our previous calculations.

In the last chapter we will calculate indices in the presence of topological defects. We will start by calculating indices with defects between boundary states. These indices can geometrically be interpreted as the intersection number of D-branes. We will highlight the concepts on explicit examples.

In addition we will calculate the elliptic genus in the presence of a topological B-type defect. By taking a specific limit we can find an expression for the Witten index with a defect insertion. By analysing the structure of the Witten index we can compare our result to already known results which have been performed by calculating the spectrum between permutation branes.

Thematically we will complement the thesis by applying the Witten index to calculate the entanglement entropy in the Ramond sector. Thereby we will observe that there is only a subleading contribution thus defining a topological quantity, i.e. independent of L.

Chapter 1

Introduction

Always there has been a deep interplay between mathematics and physics. Results known for ages in one subject found in many cases applications in the other subject and vice versa. For mathematicians the notion of conformal mappings, which are local angle preserving transformations, have been a toolkit since the development of complex analysis. In the 19th century these conformal mappings first became relevant for physicists in the context of electrodynamics. Especially two dimensional electrostatic problems could be solved by performing a conformal map to a simpler geometry.

In 1918 a special class of conformal transformations, so called Weyl transformations [8], found entrance in one of the most innovative theories of physics: general relativity. Ever since people realized that it is worth studying conformal transformations in more detail. Great progress was achieved when people combined QFT with conformal invariance in the 1960's resulting in conformal field theory (CFT). In this time very interesting and useful theories were constructed e.g. the conformal bootstrap program [9] which is a non-perturbative method to solve and constrain conformal field theories.

When in the 1970's string theory was born conformal field theories once again gained in importance. It's been in that time that a systematic study and classification of 'all' possible CFTs started. By Julian Schwinger it was foreseen that statistical physics at inverse temperature $\beta = 1/T$ is equivalent to imaginary time in QFT. Indeed this relation was proven, to be more precise it has been shown that a conformal field theory can realize a quantum statistical system at criticality. This was the starting point for applications of CFTs to (quantum) critical statistical systems.

With the AdS/CFT correspondence conjectured by Maldacena in 1997 [10] CFTs did arise in another context. The conjecture links theories formulated on AdS-spacetime, in particular quantum gravity theories, with conformal field theories. Thereby the CFTs are assumed to live on the boundaries of the AdS-spacetime. The duality between these two theories represents a major advantage in our understanding of quantum gravity or string theory. Apart from that the correspondence provides a powerful tool for studying strongly coupled quantum systems. This is mainly because the duality is basically a strong-weak-duality, i.e. strongly coupled quantities in one theory are dual to weakly coupled quantities in the other theory that can e.g. be calculated using perturbation theoretical methods.

As mentioned before CFTs find applications in quantum statistical systems, for example the Ising model at critical can be realized via a CFT description. In statistical pyhsics a special interest lies within quantum impurities. These impurities can change the system in a non-trivial way and have been subject of study for several years especially in condensed matter physics [47, 48]. For the CFT side these quantum impurities lead to the notion of conformal defects.

These defects describe critical impurities of low dimensional quantum systems. For two dimensional CFTs defects can be thought of as lines separating two (possibly different) CFTs on each side of the defect. Thereby the defect, or also called interface, acts as a map from one CFT to the other and vice versa. Folding the CFTs along the defect line result in a tensor theory of the two CFTs with the defect representing a boundary condition [39]. In this way the notion of defects can be related to the area of determining boundary states in a CFT. As it turned out the defects generalize in a natural way the notion of boundary conditions by setting local gluing conditions along the defect line. Interfaces and their properties such as their transmissivity and reflectivity [49] or their implementation of symmetries [54] have been studied in various contexts and many of their properties have been discovered [50–54]. For example it has be shown that special defects can implement symmetries or dualities [45, 46] between the various CFTs.

The nature of quantum mechanics is sometimes in contradiction to our experience of the world. In particular this is evident for entangled states for which there is no classical analogue. These states are many-body states with a non-local correlation, i.e. measurement of an observable of an entangled subsystem influences the outcome of the measurement for another subsystem. This fact caused severe doubt on the consistency of the formulation of quantum mechanics. Even A. Einstein was so curios about this non-local correlations between entangled subsystems that it cause him to call them as 'spooky action at a distance' [61]. It was not before J. Bell in 1964 who showed that these correlations have to be inconsistent with reasonable local theories or hidden variables. [62].

In modern physics the concept of entanglement finds many applications e.g. in computations [63, 64] (especially quantum computation), communications [65] and the simulation of physics for strongly correlated systems [66]. Apart from these areas of physics the concept of entanglement also has established in condensed matter physics [70], high energy field theory such as CFT [78] and even in quantum gravity [72, 73] where the entropy of entanglement can be calculated in the AdS/CFT correspondence as the minimal surface in the bulk with the entangling region endpoints as its boundary.

There exist many concepts of how to quantify the information contained in an entangled system [75](for a nice review see [76]). For us of special interest is the so called entropy of entanglement or simply entanglement entropy. The entanglement entropy is basically the von Neumann entropy of the reduced density matrix with respect to one subsystem. Apart from the usual properties of an entropy the entanglement gives a good measure how much entanglement is between two subsystems. Especially for a vanishing entanglement entropy there is no entanglement, i.e. no correlation between the two systems.

Unfortunately the entanglement entropy is not accessible in experiment but another, related entropy called Renyi-entropy [36, 75] can be measured. The entanglement entropy

can be rederived from the Renyi entropy by taking a specific limit. This then connects theoretical predictions with experimental results.

Quantum field theory has been a great success since its development in the 1950's. The theoretical predictions of QED and QCD have been tested with overwhelming precisions in experiments. Nevertheless, there are several open questions that cannot be answered with the standard model of particle physics, e.g. what is the origin of dark matter and energy? Why do we observe a mass hierarchy? Why is the unification of gravity with weak and strong interactions at short distances not possible?

String theory provides a good ansatz for solving these questions, especially the unification of gravity and quantum theory is manifest in string theory. Apart from that supersymmetry is thought to be a good candidate for answering the questions of dark energy and matter. Supersymmetry (short SUSY) is an additional symmetry that transforms bosons into fermions and vice versa [12, 13]. Especially every particle in the standard model has a corresponding superpartner.

The supersymmetry algebra predicts that at each excited energy level there is an equal number of bosons and fermions while for the ground state there is no such correspondence, i.e. the ground state breaks SUSY. This fact inspired E. Witten to his definition of the *Witten index* [14] which is the trace over the entire Hilbert space with a $(-1)^F$ insertion, where F is the fermion number operator. Clearly the Witten index exactly counts the difference of bosonic and fermionic ground states.

In the context of a supersymmetric sigma model, such as the Landau-Ginzburg model, living on a manifold $\mathcal{M}$ the Witten index can in some cases be related to the Euler characteristic of the manifold, i.e.

$$\mathrm{tr}_{\mathcal{H}}(-1)^F = \chi(\mathcal{M}).$$

In this way one can connect quantum theory to geometry. As has been shown [96, 97] there is a deep relation between Landau-Ginzburg models and $\mathcal{N} = 2$ superconformal minimal models. Especially it is known [?, 18] that the Witten index calculated between boundary states of $\mathcal{N} = 2$ minimal models at level k can be interpreted as the intersection number for D-branes of a Landau-Ginzburg theory with superpotential $W = X^{k+2}$.

In this thesis we want to connect the concept of defects with entanglement entropy and indices. Thereby we proceed as follows:

- In the second chapter we review the most important concepts of conformal fields theories creating a setup for the entire work. Apart from general features such as conformal transformations, the energy-momentum tensor and highest weight representations of the Virasoro algebra we will in particular highlight the area of boundary conformal field theories [34, 35, 94] and $\mathcal{N} = 2$ superconformal field theories [28]. A special emphasis thereby will lie on their properties such as the *chiral ring, spectral flow* [15] and the realization via a coset construction.

- After this we will turn to a more detailed discussion on defects. We will learn that defects in some sense generalize boundary conditions already known from the CFT chapter. Highlighting the properties of two special classes of defects called *topological*

and *factorizable* defects we will show how they can be rederived from a boundary state formalism. In particular topological defects implement symmetries and dualities between two CFTs [44–46, 54]. In this context we explicitly introduce the notion of duality, elementary and group like defects.

The connection of defects to boundary states will be seen explicitly by reviewing the so called *folding trick* that has been known to many-body physicist for a long time and first has been applied in the context of conformal interfaces in [39]. By reviewing the notion of transmission and reflection [49] for a defect we will gain a good intuition for the notion of topological and factorizable defects.

General defects inhabit a new feature different from boundary states, namely they can be fused together to yield a new defect. In general the fusion on the quantum level is singular. Therefore, a renormalization procedure has to be applied [41, 55]. Apart from fusing two defects with each other to create a new one it is also possible to fuse a defect onto a boundary state. This in particular has been shown for the case of a topological defect in a rational CFT [44].

- In the fourth chapter we will introduce the concept of entanglement [75, 76] and comment on how it can be quantified by calculating the von Neumann entropy. Also the impact of entanglement on other areas of physics will be discussed. Using the so called *replica trick* [78, 81] the calculation of entanglement entropies can be simplified. Thereby the so called *Renyi entropy* $S^{(n)}$ [36, 75] arises in a natural way which can be analytically continued to yield the ordinary entanglement entropy S in the limit $n \to 1$. Since the Renyi entropy is the only one accessible in experiment we briefly comment on a recent paper where they propose a setup for measuring the entropy [36].

  In a two dimensional CFT the Renyi entropy can be calculated via so called *twist fields* $\mathcal{T}_n$ living in the $\mathbb{Z}_n$ orbifold of the n-times replicated theory CFT^n. We will introduce these twist fields and review how to calculate Renyi entropies for a single and for several entangling intervals. Thereby we will also consider the cases of mapping to other geometries, e.g. systems described at finite temperature or finite size [78].

- In the following two chapters we will generalize the notion of the twist field $\mathcal{T}_n$ to the $\mathcal{N} = 2$ supersymmetric case. The supersymmetric version of $\mathcal{T}_n$ has been constructed in [86] under the condition that it should be a chiral primary field in both left- and right-moving degrees of freedom. To be more precise the supersymmetric field S_n is constructed from $\mathcal{T}_n$ by application of a specific spectral flow that is realized by a vertex operator. After a brief review of their construction we generalize the super- symmetric twist fields to general chiralities in both left- and right-moving degrees of freedom. With these generalized fields we will calculate the supersymmetric version of the Renyi entropy (SRE) for one and several intervals.

  As an interesting result we will see that for a single interval the leading term in the Renyi entropy is identical with the entanglement entropy. This is in contrast to the pure 'bosonic' case where the insertion of twist fields $\mathcal{T}_n$ yield in a leading

term depending on the number of sheets n and just giving the entanglement entropy leading term in the limit $n \to 1$. As it is convenient we also will discuss the properties of the SRE in other geometries and with systems restricted to the right half plane setting boundary conditions along the imaginary axis.

From the beginning it is not clear if the new twist field S_n is really contained in the spectrum of the orbifold theory $\mathcal{M}^n/\mathbb{Z}_n$ of a $\mathcal{N} = 2$ superconformal field theory $\mathcal{M}$. In [84,85] they provide a construction method of these twist fields using the spectral flow. We will generalize their results. In particular we will see that it is crucial how often and in which theory we have to demand the existence and the possibility to apply the spectral flow.

- In chapter 7 we then will calculate the entanglement entropy through a topological defect aligned along the imaginary axis. We will review the method for calculating the partition function on the K-sheeted Riemann surface as introduced in [82]. Our main result for this chapter will be that the entanglement entropy takes the form

$$S = \frac{c}{3} \log L + S_{sub},$$

where all the information coming from the defect are encoded in the sub-leading term S_{sub} of the entropy. We will apply our result to several examples such as duality defects, the Ising model and models based on a $u(1)_k$ and $su(2)_k$ Kac-Moody algebra. Another set of examples is provided by coset models. In calculating the subleading contribution to the entanglement entropy we will see in several examples that for fixed-point free coset models with a $\mathbb{Z}_2$ field identification the subleading term decomposes into the individual coset parts. Thus the entanglement entropy for these coset examples is completely determined by the knowledge of the results for the subleading terms of $su(2)_k$ and $u(1)_k$ theories.

- By Unfolding a boundary one can associate a defect to it acting only on the chiral part of the algebra. In chapter 8 we will review these procedure for Cardy boundary states and calculate the so called *left/right entanglement entropy* first introduced in [87,88] associated to this defect. Again we will highlight our obtained results with several examples, especially for coset theories.

- In chapter 9 we briefly will discuss the (left/right) entanglement entropy through topological interfaces for d bosons compactified on a torus. Performing the same steps as in the calculation for the (left/right) entanglement entropy we reproduce the results obtained in [82, 87] via a direct calculation. In this way we also verify the steps performed in the calculation of the last two chapters.

- In the last chapter we will include defects to calculate indices in $\mathcal{N} = 2$ superconformal theories. In the first part we will review how an index between boundary states in a $\mathcal{N} = 2$ superconformal minimal model is defined. Afterwards we will include topological defects and calculated the associated indices. Since it is known that these

models are realized as the IR fixed point of the Landau-Ginzburg model with super-potential X^{k+2} we can give a geometric interpretation of the index in the presence of one (or several) topological defects in terms of a intersection numbers of D-branes. We will highlight the result with several explicit examples. Next we will show that the same index can also be calculated from unfolding the boundary states. In this way we can also view the index as a torus partition function of the chiral algebra. By introducing the concept of boundary state overlaps with the Ramond ground states we can give a generalization in how to calculate indices for non-topological defects. In particular we will see that the defect induces a metric connecting the boundary brane overlaps.

As another application we will calculate the elliptic genus $\mathcal{E}(\tau, z, D)$ in the presence of a topological B-type defect D. In the limit where $z \to 0$ the elliptic genus exactly reproduces the Witten index. We can compare our obtained result with [21] where they calculated the spectrum between two permutation branes. Unfolding these permutation branes exactly results in the B-type topological defects used in our calculation of the elliptic genus.

Finally to conclude the thesis we apply the result obtained for the elliptic genus to calculate the contribution from the Ramond sector to the entanglement entropy.

Chapter 2

Basics on Conformal Field Theories

In this chapter we review the basic ingredients of conformal field theories which we will need in later chapters of this thesis. Many of the presented concepts can be found in the literature, e.g. [1–4, 6].

2.1 Conformal Transformations & Virasoro Algebra

A conformal field theory (CFT) is a quantum field theory which is invariant under conformal transformations of the coordinates. Thereby conformal transformations are defined as transformations $x^\mu \to x'^\mu(x)$ that leave the metric invariant up to an overall function depending on the coordinates, i.e.

$$g'_{\mu\nu}(x') = \frac{\partial x^\alpha}{\partial x'^\mu} \frac{\partial x^\beta}{\partial x'^\nu} g_{\alpha\beta}(x) = \Omega(x) g_{\alpha\beta}(x). \tag{2.1}$$

Especially this means that under conformal transformations local angles are preserved. Realizations of conformal transformations are given by translations, dilations, rotations and special conformal transformations (SCT= composition of inversion-translation-inversion) CFTs arise in various areas of physics such as condensed matter physics, string theory or the AdS/CFT correspondence but also find applications in two dimensional electrostatics. From now on we will restrict all our discussions to the two-dimensional case. In two dimensions it can be shown that every (anti-)holomorphic transformation is a conformal one (e.g. see figure 2.1). Thus one can complexify the spacetime coordinates according to

$$z = t + ix \tag{2.2}$$
$$\bar{z} = t - ix. \tag{2.3}$$

An infinitesimal transformation is then given by

$$z \to z' = z + \epsilon(z) = z + \sum_{n \in \mathbb{Z}} \epsilon_n \left(-z^{n+1}\right), \tag{2.4}$$

$$\bar{z} \to \bar{z}' = \bar{z} + \bar{\epsilon}(\bar{z}) = \bar{z} + \sum_{n \in \mathbb{Z}} \bar{\epsilon}_n \left(-\bar{z}^{n+1}\right), \tag{2.5}$$

where ϵ_n and $\bar{\epsilon}_n$ are infinitesimal constants. Given a particular n in the series the associated generators for the transformation are given by:

$$l_n = -z^{n+1}\partial_z \quad \text{and} \quad \bar{l}_n = -\bar{z}^{n+1}\partial_{\bar{z}}. \tag{2.6}$$
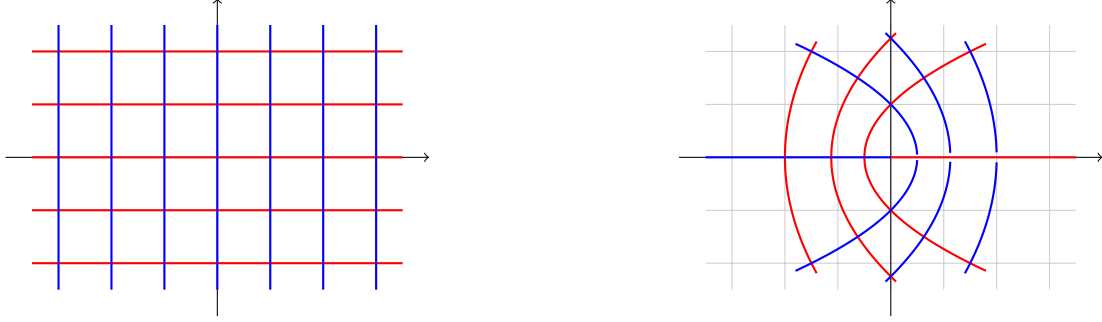
Figure 2.1: Conformal transformation $z \to z^2/2$ in two dimensions.

The generators form an algebra, the so called *Witt algebra*

$$
\begin{aligned}
[l_n, l_m] &= (n-m)l_{n+m} \\
[\bar{l}_n, \bar{l}_m] &= (n-m)\bar{l}_{n+m} \\
[l_n, \bar{l}_m] &= 0
\end{aligned}
\tag{2.7}
$$

A general generator for conformal transformations then takes the form

$$\sum_n \left(\epsilon_n l_n + \bar{\epsilon}_n \bar{l}_n\right). \tag{2.8}$$

With this operator we can generate all conformal transformations of functions $f(z, \bar{z})$. It is important to note that the transformations are analytic near the point $z = 0$, nevertheless, the transformations may introduce poles at $z = 0$.

The Witt algebra allows a central extension which is the quantum version of the conformal generators. The generators L_n (just left movers) then fulfil the so called *Virasoro algebra* Vir_c:

$$[L_m, L_n] = (m-n)L_{m+n} + \frac{c}{12}m(m^2-1)\delta_{m+n}. \tag{2.9}$$

Initially the algebra was discovered in the context of string theory [11]. The constant c is called *central charge* that is a specific quantity for each theory considered. In particular the generators L_{-1}, L_0 and L_1 form a closed subalgebra generating transformations of the form

$$z \to \frac{az+b}{cz+d}, \quad \text{with } a, b, c, d \in \mathbb{C}, \tag{2.10}$$

with the restriction $ad - bc = 1$ for the transformation to be invertible. The above transformation is invariant under the exchange of variable according to $(a, b, c, d) \to$

$(-a, -b, -c, -d)$. These transformations are globally defined on the Riemann sphere $S^2 = \mathbb{C} \cup \infty$ and are generated as before by L_{-1}, L_0 and L_1.[1] The transformations can be identified with the group elements

$$\begin{pmatrix} a & b \\ c & d \end{pmatrix} \in SL(2, \mathbb{C})/\mathbb{Z}_2. \tag{2.11}$$

Especially the generator L_{-1} generates translations of the form $z \to z + b$, L_0 generates dilations and rotations $z \to az$ and L_1 gives rise to special conformal transformations of the form $z \to \frac{z}{cz+1}$.

2.2 The Energy Momentum Tensor

If a theory possesses a symmetry then there usually is a conserved current associated to this symmetry. Considering a conformal symmetry transformation $x^\mu \to x^\mu + \epsilon^\mu(x)$, the current associated to this transformation is given by

$$j_\mu(\epsilon) = T_{\mu\nu}\epsilon^\nu, \tag{2.12}$$

where $T_{\mu\nu}$ are the components of the *energy-momentum tensor*. For the current to be conserved we need:

$$\partial^\mu j_\mu = \left(\partial^\mu T_{\mu\nu}\right)\epsilon^\nu + T_{\mu\nu}\partial^\mu\epsilon^\nu = 0. \tag{2.13}$$

The first term in the sum is zero since the energy-momentum tensor itself is conserved. The second term in the sum can be rewritten as

$$T_{\mu\nu}\partial^\mu\epsilon^\nu = \frac{1}{2}T_{\mu\nu}\left(\partial^\mu\epsilon^\nu + \partial^\nu\epsilon^\mu\right) = \frac{1}{2}T_\mu{}^\mu(\partial \cdot \epsilon). \tag{2.14}$$

Since the expression should be identically zero for all possible transformations $\epsilon(x)$ we find that the energy momentum tensor in a conformal field theory has to be traceless for the current to be conserved, i.e.

$$T_\mu{}^\mu = 0. \tag{2.15}$$

Using complex coordinates it is straight forward to show that there are only two non-vanishing components of the energy-momentum tensor given by

$$T_{zz}(z, \bar{z}) =: T(z) \quad \text{and} \quad T_{\bar{z}\bar{z}}(z, \bar{z}) =: \bar{T}(\bar{z}), \tag{2.16}$$

which represent a chiral and an anti-chiral field respectively. By performing a Laurent expansion around $z = 0$ the energy-momentum tensor can be written in terms of Virasoro

---

[1]Note that L_{-1}, L_0 and L_1 are well defined on the Riemann sphere, this is not true e.g. for L_n with $n \le -2$.

generators as

$$T(z) = \sum_{n \in \mathbb{Z}} L_n z^{-n-2} \tag{2.17}$$

$$\bar{T}(\bar{z}) = \sum_{n \in \mathbb{Z}} \bar{L}_n \bar{z}^{-n-2}. \tag{2.18}$$

Since the modes of the energy-momentum tensor are the Virasoro generators one sees that $T(z)$ (respectively $\bar{T}(\bar{z})$) indeed is the generator of conformal transformations.

2.3 The Operator Product Expansion

In CFTs the notion of *fields* or also called *local operators* is slightly different from the ordinary QFT point of view. In a conformal field theory the term 'field' simply refers to any local operator that one is able to write down. This in particular includes fields Φ, derivatives of fields $\partial^n \Phi$ and also composite operators such as the vertex operator $: \exp(i\Phi) :$ (for properties of the vertex operator see appendix A), where $: \cdot :$ denotes normal ordering. A general field $\Phi(z, \bar{z})$ may be expanded in a Laurent series around $z = 0$ as

$$\Phi(z, \bar{z}) = \sum_{n, \bar{n}} \Phi_{n, \bar{n}} z^{-n-h} \bar{z}^{-\bar{n}-\bar{h}}. \tag{2.19}$$

The constants h and $\bar{h}$ are called *conformal weights* and are specific for each field. They can be related to the known scaling dimension Δ of an operator and its spin s via

$$h = \frac{1}{2}(\Delta + s) \tag{2.20}$$

$$\bar{h} = \frac{1}{2}(\Delta - s) \tag{2.21}$$

In a quantum theory the amplitudes $\Phi_{n, \bar{n}}$ are subjected to be operators as we have seen e.g. in the example of the energy-momentum tensor.

One now can define the so called *operator product expansion* (short OPE), which is a statement about what happens when one brings two local operators close together. The main idea is that two operators that are inserted at close enough points near each other can be represented as a set of new operators sitting at one of the insertion points. We denote the fields by Φ_i, where the label i runs over the set of all possible fields. The OPE is then given by

$$\Phi_i(z, \bar{z}) \Phi_j(w, \bar{w}) = \sum_k C_{ij}^k (z - w)^{h_k - h_i - h_j} (\bar{z} - \bar{w})^{\bar{h}_k - \bar{h}_i - \bar{h}_j} \Phi_k(w, \bar{w}). \tag{2.22}$$

Here h_i (respectively $\bar{h}_i$) is the conformal weight of the field Φ_i and C_{ij}^k are constants. In general the limit $z \to w$ on the right hand side is singular, nevertheless, e.g. in $\mathcal{N} = 2$ superconformal field theories there exist fields, so-called chiral primaries, with the property that their OPE is always non-singular (see section 2.12.3).

2.4   Primary Fields and Transformation Law

A special class of fields are the so called *primary fields*. These fields obey the following transformation rule under a conformal transformation $z \to f(z)$:

$$\Phi(z, \bar{z}) \to \left(\frac{\partial f}{\partial z}\right)^h \left(\frac{\partial \bar{f}}{\partial \bar{z}}\right)^{\bar{h}} \Phi(f(z), \bar{f}(\bar{z})). \tag{2.23}$$

For the OPE of primary fields with the energy-momentum tensor holds

$$T(z)\Phi(w, \bar{w}) = \frac{h}{(z-w)^2}\Phi(w, \bar{w}) + \frac{1}{z-w}\partial_w \Phi(w, \bar{w}), \tag{2.24}$$

$$\bar{T}(\bar{z})\Phi(w, \bar{w}) = \frac{\bar{h}}{(\bar{z}-\bar{w})^2}\Phi(w, \bar{w}) + \frac{1}{\bar{z}-\bar{w}}\partial_{\bar{w}} \Phi(w, \bar{w}). \tag{2.25}$$

The energy-momentum tensor itself is not a primary field, this can be seen from its OPE with itself

$$T(z)T(w) = \frac{c/2}{(z-w)^4} + \frac{2}{(z-w)^2}T(w) + \frac{1}{z-w}\partial T(w). \tag{2.26}$$

Under a conformal transformation the energy-momentum tensor transforms as

$$T(z) \to \tilde{T}(z) = \left(\frac{df}{dz}\right)^2 T(f(z)) + \frac{c}{12}S(f; z), \tag{2.27}$$

where the so called *Schwarzian derivative* has been introduce which is defined by

$$S(f; z) = \frac{(d^3 f/dz^3)}{(df/dz)} - \frac{3}{2}\left(\frac{(d^2 f/dz^2)}{(df/dz)}\right)^2. \tag{2.28}$$

Note that the term coming from the Schwarzian derivative does not depend on T itself which means that when evaluated on states it will give the same result for all of them. Thus it only affects the constant term, i.e. the zero mode, in the energy. This makes it plausible to identify it with the Casimir energy of the system.

The transformation properties of the energy-momentum tensor are essential for performing calculations in different geometries. Consider for example the important case that our CFT is defined on a cylinder [6] parameterized by (in string language)

$$w = \sigma + i\tau \quad, \quad \sigma \in [0, 2\pi). \tag{2.29}$$

By the conformal mapping $z = \exp(-iw)$ we can map the cylinder geometry to the complex plane (see figure 2.2). Thereby constant time slices on the cylinder ($\tau = const.$) are mapped to circles of constant radii in the z-plane where the infinite past $\tau = -\infty$ is mapped to the origin $z = 0$. In this picture the quantization is taken place in the radial direction which is referred to as *radial quantization* [1, 2, 6].

Under the transformation we find using (2.27)for the energy-momentum tensor of the cylinder in terms of the energy-momentum tensor on the complex plane as
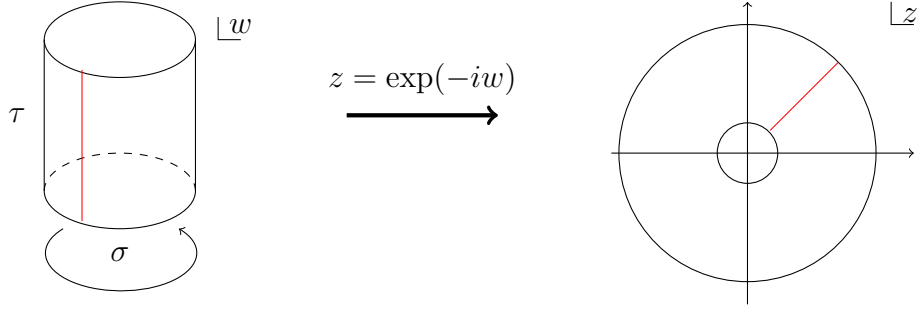
Figure 2.2: Mapping from the cylinder to the complex plane with time evolution along the cylinder axis (red) and its image in the complex plane.

$$T_{cylinder}(w) = -z^2 T_{plane}(z) + \frac{c}{24} = \frac{c}{24} - \sum_{n=-\infty}^{\infty} L_n^{plane} e^{inw}. \tag{2.30}$$

On the cylinder the Hamiltonian generates time translations. We see that these time translations correspond in the plane geometry to dilations generated by L_0^{plane}. Thus the correct identification is

$$L_0^{cyl} = L_0 - \frac{c}{24}. \tag{2.31}$$

The Hamiltonian H_{cyl} on the cylinder thus can be expressed in terms of the generators on the plane as

$$H_{cyl} = L_0^{cyl} + \bar{L}_0^{cyl} = L_0 + \bar{L}_0 - \frac{c}{12}, \tag{2.32}$$

and for the momentum operator P_{cyl}

$$P_{cyl} = L_0^{cyl} - \bar{L}_0^{cyl} = L_0 - \bar{L}_0. \tag{2.33}$$

2.5   Operator-State Correspondence

In a well defined QFT there exists a direct correspondence between fields and states in the Hilbert space. Let us consider a primary field of conformal dimension $(h, \bar{h})$ denoted by $\Phi(z, \bar{z})$. We define an symptotic in-state by

$$|h, \bar{h}\rangle = \lim_{z, \bar{z} \to 0} \Phi(z, \bar{z}) |0\rangle = \Phi_{-h, -\bar{h}} |0\rangle. \tag{2.34}$$

This definition is clear since when mapped to the cylinder $z = 0$ corresponds to infinite past. We see that we have a $1 : 1$ correspondence[2] between the fields and the associated in-state. In a similar way one may define a asymptotic out-state corresponding in the cylinder geometry to infinite future. This means we need to construct an analogous object for $z \to \infty$, i.e. the correct adjoint field. By the conformal map $z = 1/w$ we map points

---

[2]Note that this 1:1 correspondence is special to CFTs

at $z = \infty$ to the origin. Using the transformation law for primary fields (2.23) we find for the field in the new coordinates

$$\tilde{\Phi}(w, \bar{w}) = \Phi(z(w), \bar{z}(\bar{w}))(\partial_w z)^h (\partial_{\bar{w}} \bar{z})^{\bar{h}} = w^{-2h} \bar{w}^{-2\bar{h}} \Phi(1/w, 1/\bar{w}). \qquad (2.35)$$

An asymptotic out-state thus can be defined by

$$\langle h, \bar{h}| = \lim_{w, \bar{w} \to 0} \langle 0| \, \tilde{\Phi}(w, \bar{w}) =$$

$$\lim_{z, \bar{z} \to \infty} \langle 0| \, z^{2h} \bar{z}^{2\bar{h}} \Phi(z, \bar{z}). \qquad (2.36)$$

We see that the adjoint operator (field) is given by

$$[\Phi(z, \bar{z})]^{\dagger} = z^{2h} \bar{z}^{2\bar{h}} \Phi(1/z, 1/\bar{z}). \qquad (2.37)$$

Note that the roles of holomorphic and anti-holomorphic variables are exchanged. To get a better felling of the notion of an adjoint operator let us consider the case of the energy-momentum tensor with conformal weights $(h, \bar{h}) = (2, 2)$. Applying the definition (2.37) on just the holomorphic part we find

$$T^{\dagger}(z) = \bar{z}^{-4} T(1/\bar{z}) = \sum_n L_n (1/\bar{z})^{-n-2} \bar{z}^{-4} = \sum_n L_n \bar{z}^{n-2}. \qquad (2.38)$$

On the other hand we directly find

$$T^{\dagger}(z) = \left(\sum_n L_n z^{-n-2} \right)^{\dagger} = \sum_n L_n^{\dagger} \bar{z}^{-n-2}. \qquad (2.39)$$

Comparing the two results we find the correct identification for the Virasoro generators and their hermitian conjugate

$$L_n^{\dagger} = L_{-n}. \qquad (2.40)$$

2.6 Highest Weight Representation

In this section we briefly discuss the representation theory arising from the Virasoro algebra Vir_c (2.9). Let us begin by defining a *highest weight* state $|h\rangle$ by the following properties (just the holomorphic part)

$$L_n |h\rangle = 0 \quad \text{for} \quad n > 0 \qquad (2.41)$$
$$L_0 |h\rangle = h |h\rangle. \qquad (2.42)$$

In this case the action of L_{-n} for $n > 0$ creates new states with L_0 eigenvalues

$$L_0 L_{-n} |h\rangle = (h + n) L_{-n} |h\rangle. \qquad (2.43)$$

level	L_0 eigenvalue	states
0	h	$\lvert h \rangle$
1	$h+1$	$L_{-1}\lvert h \rangle$
2	$h+2$	$L_{-1}^2\lvert h \rangle$, $L_{-2}\lvert h \rangle$
3	$h+3$	$L_{-1}^3\lvert h \rangle$, $L_{-1}L_{-2}\lvert h \rangle$, $L_{-1}^3\lvert h \rangle$
$\vdots$	$\vdots$	$\vdots$
N	$h+N$	$P(N)$ states

Table 2.1: Possible states at a given level N that can be constructed out of the highest weight state $\lvert h \rangle$. The number at level N is given by $P(N)$, the number of partitions.

We then call $\lvert h \rangle$ a highest weight state and the set of all states, that can be constructed from the highest weight state by applying the negative Virasoro generators, *Verma module* $V_{c,h}$, i.e.

$$V_{c,h} = \{L_{-n_1}\cdots L_{-n_M}\lvert h \rangle \mid n_i \geq 0 \ \forall M \in \mathbb{N}\}. \tag{2.44}$$

States in the Verma module have L_0 eigenvalues $h+N$, where $N = \sum_i n_i$ is called the *level*. Note that a given level N can be realized by several states as shown in table 2.1.

One also calls the states in the Verma module the descendants of the highest weight state, thus the Verma module yields a representation. In principle there can be more than one highest weight state for a given CFT, we will come to this later.

It is important to note that every CFT at least has the vacuum representation build on the highest weight state with $h = 0$. Depending on (h,c) there can also occur states of vanishing or even negative norm. Those states have to be projected out by hands. We won't go into the detail of this procedure related to the so called *Kac-determinant*. For a good discussion see e.g. [1,2].

Theories of special interest the unitary theories. It can be shown that unitary theories, i.e. theories where all states of descendants have positive norm, can only be realized if the central charge and highest weight take the following specific values

$$c = 1 - \frac{6}{m(m+1)} \quad m = 3, 4, \ldots \tag{2.45}$$

$$h_{p,q} = \frac{[(m+1)p - mq]^2 - 1}{4m(m+1)}, \tag{2.46}$$

with $1 \leq p \leq m-1$ and $1 \leq q \leq m$.

We see that in unitary theories only a finite number of highest weight states $\lvert h_{p,q} \rangle$ can occur. Further the central charge also only takes discrete rational values and is bounded from above by $c = 1$ which can e.g. be realized by the free boson CFT. Because the central charge only takes rational values those theories are also called *rational CFT* or *unitary minimal series*.

2.7   Correlation Functions

In ordinary QFT usually one is interested in calculating vacuum expectation values of fields. These can in general be quite complicated. In CFTs the symmetry group $SL(2,\mathbb{C})/\mathbb{Z}_2 \cong SO(3,1;\mathbb{R})/\mathbb{Z}_2$ is so restrictive that it fixes the outcome of two- and three-point functions completely up to a constant. In order to see this consider a set of primary fields $\{\Phi_i(z,\bar{z})\}$ with corresponding conformal weights $(h_i, \bar{h}_i)$. For the N-point function we then have by the transformation properties of the primaries (2.23)

$$\langle \Phi_1(z_1,\bar{z}_1)\cdots\Phi_N(z_N,\bar{z}_N)\rangle = \prod_{j=1}^{N}(\partial f(z_j))^{h_j}(\bar{\partial}\bar{f}(\bar{z}_j))^{\bar{h}_j}\,\langle \Phi_1(f(z_1),\bar{f}(\bar{z}_1))\cdots\Phi_N(f(z_N),\bar{f}(\bar{z}_N))\rangle$$

(2.47)

By this equation the coordinate dependence of the one-,two- and three-point function are fixed by the $SL(2,\mathbb{C})/\mathbb{Z}_2$ conformal symmetry to:

$$\langle \Phi(z,\bar{z})\rangle = 0,$$

(2.48)

$$\langle \Phi_1(z_1,\bar{z}_1)\Phi_2(z_2,\bar{z}_2)\rangle = \frac{k_{12}\delta_{h_1,h_2}\delta_{\bar{h}_1,\bar{h}_2}}{(z_1-z_2)^{2h_1}(\bar{z}_1-\bar{z}_2)^{2\bar{h}_1}},$$

(2.49)

$$\langle \Phi_1(z_1,\bar{z}_1)\Phi_2(z_2,\bar{z}_2)\Phi_3(z_3,\bar{z}_3)\rangle = \frac{k_{123}}{z_{12}^{h_1+h_2-h_3}z_{23}^{h_2+h_3-h_1}z_{13}^{h_1+h_3-h_2}\bar{z}_{12}^{\bar{h}_1+\bar{h}_2-\bar{h}_3}\bar{z}_{23}^{\bar{h}_2+\bar{h}_3-\bar{h}_1}\bar{z}_{13}^{\bar{h}_1+\bar{h}_3-\bar{h}_2}},$$

(2.50)

where $z_{ij} := z_i - z_j$ and similar for the complex conjugated variables. The undetermined constants k_{12} and k_{123} appearing in the equations can not be fixed by the conformal symmetry. It is interesting that in the two point function one has the additional restriction that the fields need to have the same conformal weights in order for the correlator not to be identically zero.

Up to now the correlation functions for $N \leq 3$ fields is entirely determined by the conformal symmetry group. For $N > 3$ fields this is no longer the case since by the conformal symmetry we only can fix three coordinate to lie on specific point on the complex plane. The other $N-3$ coordinates cannot be fixed by the conformal symmetry group. The only thing that one can say is that in general they begin to have a dependence on cross ratios of the coordinates z_i ($i \in \{1,\ldots,N\}$). For example the four-point function (just holomorphic part) takes the form [1, 2, 6]

$$\langle \Phi_1(z_1)\Phi_2(z_2)\Phi_3(z_3)\Phi_4(z_4)\rangle = \mathcal{F}\left(\frac{z_{12}z_{34}}{z_{13}z_{24}}, \frac{z_{12}z_{34}}{z_{23}z_{41}}\right)\prod_{i<j}z_{ij}^{-(h_i+h_h)+h/3}.$$

(2.51)

Here $h = \sum_i h_i$ and $\mathcal{F}$ is an arbitrary function of $4(4-3)/2 = 2$ independent cross ratios and is depending on the full operator content of the theory. General N-point functions are thus given by functions of $N(N-3)/2$ cross ratios where $N-3$ coordinates can be fixed by the conformal group.

2.8   Conformal Ward Identity

Ward identities play an important role in QFTs, especially they are manifestations of symmetries related to the theory considered, e.g. charge conjugation, parity or gauge transformations. In CFTs we obviously have conformal symmetry. Conformal transformations are generated by the energy momentum tensor $T(z)$ (just holomorphic part). For correlation functions we know that these must be invariant under conformal transformations, which means

$$\frac{1}{2\pi i} \oint dz \epsilon(z) \langle T(z)\Phi_1(z_1, \bar{z}_1)\Phi_2(z_2, \bar{z}_2)\rangle = 0. \tag{2.52}$$

By applying the OPEs for the individual primary fields $\{\Phi_i\}$ with the energy momentum tensor we find

$$\frac{1}{2\pi i} \oint dz \; \epsilon(z) \; \langle T(z)\Phi_1(z_1, \bar{z}_1)\cdots\Phi_N(z_N, \bar{z}_N)\rangle =$$

$$\frac{1}{2\pi i} \oint dz \; \epsilon(z) \sum_{j=1}^{N} \left(\frac{h_j}{(z-z_j)^2} + \frac{1}{z-z_j}\partial_{z_j} \right) \langle \Phi_1(z_1, \bar{z}_1)\cdots\Phi_N(z_N, \bar{z}_N)\rangle. \tag{2.53}$$

Since this equation has to be valid for every transformation $\epsilon(z)$ we finally obtain the expression for the *conformal Ward identity*

$$\langle T(z)\Phi_1(z_1, \bar{z}_1)\cdots\Phi_N(z_N, \bar{z}_N)\rangle =$$

$$\sum_{j=1}^{N} \left(\frac{h_j}{(z-z_j)^2} + \frac{1}{z-z_j}\partial_{z_j} \right) \langle \Phi_1(z_1, \bar{z}_1)\cdots\Phi_N(z_N, \bar{z}_N)\rangle. \tag{2.54}$$

The result tells us that if we know the OPE between the energy-momentum tensor and a field, then we immediately know the transformation of the field under conformal symmetry. Alternatively if we know how an field transforms under the conformal symmetry we can deduce (at least) some parts of the OPE of the field with the energy-momentum tensor.

2.9   CFT on the Torus

So far we have just considered the case that our CFT is living on the complex plane or cylinder. We now want to discuss the next complicated manifold, namely a genus 1 manifold, which has the topology of a torus $\mathbb{T}^2$. The torus can be thought of as a cylinder whose ends are sewn together (see fig. 2.3)

It is convenient to describe the torus in terms of the complex plane modulo a lattice (see fig. 2.4), i.e. $\mathbb{T}^2 = \mathbb{C}/(\mathbb{Z} \oplus \tau\mathbb{Z})$. The lattice is spanned by two vectors 1 and τ, where we call $\tau = \tau_1 + i\tau_2$ the *modular parameter*.

Note that since we are considering conformal theories which means especially scale invariant theories, we may always pick one basis vector to be 1. The two real constants τ_1 and τ_2 can be seen as the two cycles of the torus where as in section 2.4 τ_2 can be associated
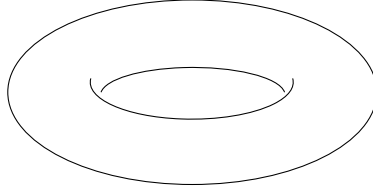
Figure 2.3: The torus as genus 1 surface.

with time translations and τ_1 may be related to spatial rotation. The gray region in figure
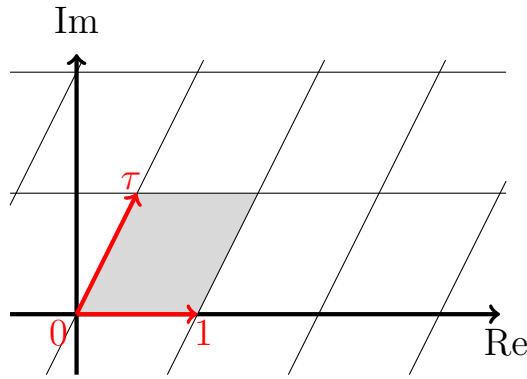
Figure 2.4: Torus in terms of a lattice with basis vectors 1 and τ.

2.4 is called the fundamental domain of the torus. Geometrically the torus is obtained by identifying opposite edges of the fundamental domain. Obviously there are different choices of τ leading to the same lattice and, therefore, to the same torus. Let us consider the following two transformations of the basis vector τ that again lead to the same torus:

1. modular T-transformation: In this case the basis vector τ transforms as

$$T : \tau \to \tau + 1. \tag{2.55}$$

The transformation is illustrated in figure 2.5.

2. modular S-transformation: Under a modular S-transformation τ transforms according to

$$S : \tau \to -\frac{1}{\tau}. \tag{2.56}$$

This has the effect of rotating the lattice with a rescaling of the basis vector along the real axis to 1. The transformation can be illustrated in the easiest way taking τ to be purely imaginary (see fig. 2.6). Clearly the modular S-transformation exchanges the role of the two cycles of the cylinder.
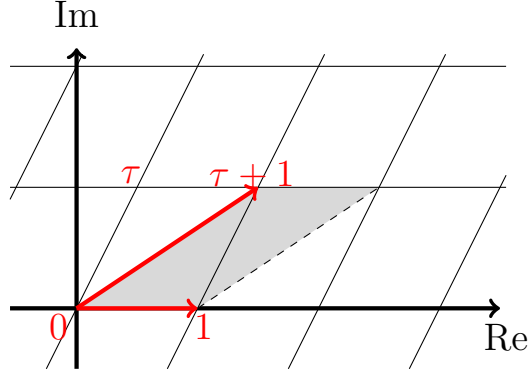
Figure 2.5: Modular T-transformation.
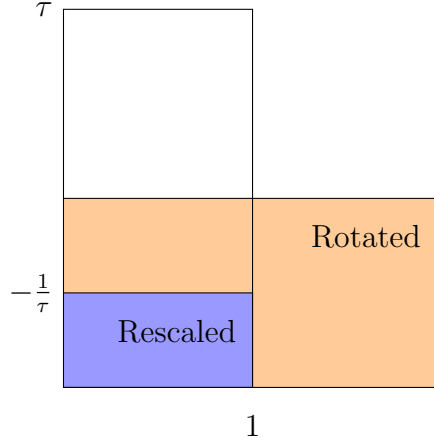
Figure 2.6: Modular S-transformation for τ purely imaginary.

The set of all transformations that leave the torus invariant forms a group and is called *modular group*. It can be shown that the modular T- and S-transformations generate the entire modular group. The most general transformation of the modular parameter thus has the form

$$\tau \to \frac{a\tau + b}{c\tau + d}, \quad a, b, c, d \in \mathbb{Z}; \quad ad - bc = 1. \tag{2.57}$$

Obviously the group is isomorphic to $SL_2(\mathbb{Z})/\mathbb{Z}_2$, where the group $SL_2(\mathbb{Z})$ can be dfined by the set of 2×2 matrices

$$\begin{pmatrix} a & b \\ c & d \end{pmatrix} \tag{2.58}$$

with determinant 1. The $\mathbb{Z}_2$ identification is important since the element $-\mathbb{E}$ cannot be distinguished from $\mathbb{E}$.

Given the modular transformations one may now ask what the fundamental values of τ might be. From the modular T-transformation we know that the real part of τ can be cho-
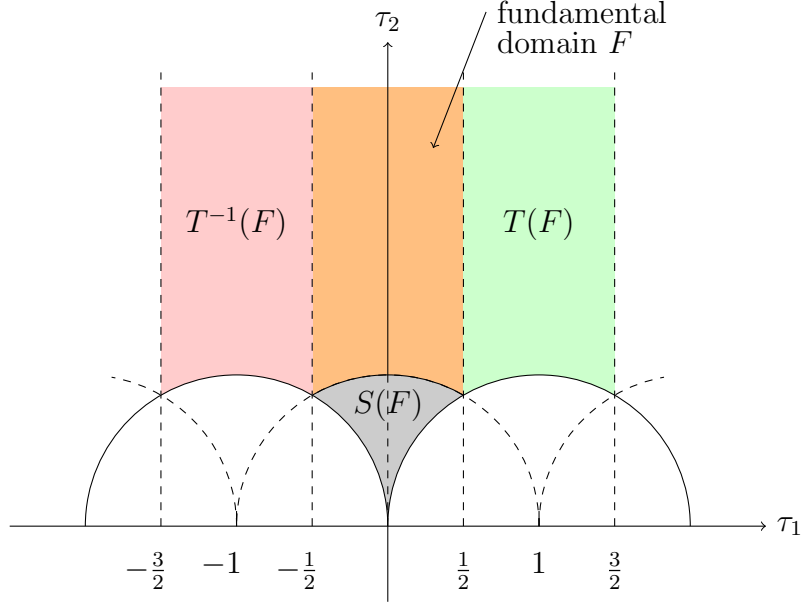
Figure 2.7: Fundamental domain for modular group in the complex upper half plane. In addition we see how the action under modular T- and S-transformations acfts on the fundamental domain.

sen to lie in the fundamental domain $\mathrm{Re}\ \tau \in [-\frac{1}{2}, \frac{1}{2}]$. The modular S-transformation maps points from outside the unit circle to points inside the unit circle. Thus the fundamental domain for the modular parameter τ can be found in the following region (see figure 2.7). All other possible values of τ can now be reconstructed by taking τ and successively applying modular T- and S-transformations.

2.9.1 Torus Partition Function and Modular Matrices

We have seen that the modular parameter τ inhibits information about time and spatial transformations, to be more explicit spatial transformations are generated by

$$\exp(2\pi i \tau_1 P_{cyl}), \tag{2.59}$$

whereas time translations are given by

$$\exp(-2\pi \tau_2 H_{cyl}). \tag{2.60}$$

On the torus we both have time and spatial transformation implying for the partition function

$$Z(\tau, \bar{\tau}) = \mathrm{tr}_{\mathcal{H}} e^{2\pi i \tau_1 P_{cyl}} e^{-2\pi \tau_2 H_{cyl}} = \mathrm{tr}_{\mathcal{H}} \left(q^{L_0 - \frac{c}{24}} \bar{q}^{\bar{L}_0 - \frac{\bar{c}}{24}} \right), \tag{2.61}$$

where $q = \exp(2\pi i\tau)$. For a general Hilbert space which is a direct sum of highest weight representations $\mathcal{H} = \oplus_{i,\bar{i}} M_{i,\bar{i}} \mathcal{H}_i \otimes \bar{\mathcal{H}}_{\bar{i}}$ this partition function can be written as

$$Z(\tau, \bar{\tau}) = \sum_{i,\bar{i}} M_{i,\bar{i}} \chi_i(\tau) \bar{\chi}_{\bar{i}}(\bar{\tau}). \tag{2.62}$$

$M_{i\bar{i}}$ denotes the multiplicities of occurrences of representations $\mathcal{H}_i \otimes \bar{\mathcal{H}}_{\bar{i}}$ in $\mathcal{H}$ and the characters $\chi_i(\tau)$ are defined by

$$\chi_i(\tau) = \mathrm{tr}_{\mathcal{H}_i} q^{L_0 - \frac{c}{24}}, \tag{2.63}$$

and equally for the anti-holomorphic part. Under modular transformations of the torus-parameter the holomorphic characters transform according to

$$\chi_i(\tau + 1) = \sum_j T_{ij} \chi_j(\tau) \tag{2.64}$$

$$\chi_i(-1/\tau) = \sum_j S_{ij} \chi_j(\tau), \tag{2.65}$$

whereas the anti-holomorphic characters transform as

$$\bar{\chi}_{\bar{i}}(\bar{\tau} + 1) = \sum_{\bar{j}} T^*_{\bar{i}\bar{j}} \bar{\chi}_{\bar{j}}(\bar{\tau}) \tag{2.66}$$

$$\bar{\chi}_{\bar{i}}(-1/\bar{\tau}) = \sum_{\bar{j}} S^*_{\bar{i}\bar{j}} \bar{\chi}_{\bar{j}}(\bar{\tau}). \tag{2.67}$$

The matrices appearing in the transformations are called modular T-matrix T_{ij} and modular S-matrix S_{ij} (and the same for the anti-holomorhpic part where $*$ represents complex conjugation). We know that under modular T- and S-transformation our torus doesn't change, therefore, the partition function (2.62) should also be invariant under modular transformations.
This gives rise to the following two conditions

$$Z(\tau, \bar{\tau}) = Z(\tau + 1, \bar{\tau} + 1) \;\leftrightarrow\; \sum_{i,\bar{i}} M_{i,\bar{i}} T_{ij} T^*_{\bar{i}\bar{j}} = M_{j,\bar{j}}, \tag{2.68}$$

and

$$Z(\tau, \bar{\tau}) = Z(-1/\tau, -1/\bar{\tau}) \;\leftrightarrow\; \sum_{i,\bar{i}} M_{i,\bar{i}} S_{ij} S^*_{\bar{i}\bar{j}} = M_{j,\bar{j}}. \tag{2.69}$$

We see that the conditions that arise from modular invariance highly restrict our possible spectra, i.e. $M_{i\bar{i}}$. This means that in contrast to a CFT living on the complex plane for CFTs living on tori the appearing representations and multiplicities are restricted according to the geometry.

For diagonal theories with $M_{i,\bar{\imath}} = \delta_{i,\bar{\imath}}$ it is interesting that we find the 'normalization' condition for the modular S-matrices

$$\sum_i |S_{ij}|^2 = 1. \tag{2.70}$$

The classification of all modular invariant partition functions, i.e. the possible Hilbert spaces that give rise to modular invariant partition function, is, still, an active field of research. In RCFT the classification can be broken down into solving an algebraic problem which, nevertheless, might be quite complicated. In a few cases complete results are known [22–24]. For several families of RCFT's based on the $sl(2)$ algebra a special feature, the so called ADE classification, emerges [22, 23]. Apart from that there exist different approaches to the classification of modular invariant theories e.g. [25, 26] based on Galois theory.

2.10 Fusion Rules and the Verlinde Formula

2.10.1 Fusion Rules

Given two primary fields we can look at the OPE of these fields. The general form is (just holomorphic part)

$$\Phi_i(z)\Phi_j(w) \sim \sum_k C_{ij}^k \Phi_k(w) \, (z-w)^{h_k-h_i-h_j} + \cdots , \tag{2.71}$$

where $C_{ij}^k \in \mathbb{C}$. We now can define the so called *fusion coefficients*

$$N_{ij}^k = \begin{cases} 0 & \text{for } C_{ij}^k = 0 \\ 1 & \text{otherwise} \end{cases} \tag{2.72}$$

These are some integer numbers counting how many independent possibilities exist to obtain the field Φ_k when fusing the two fields Φ_i and Φ_j. In general CFTs the fusion number can be any integer number, in the special cases of rational minimal models [1, 2, 6] they just take values $N_{ij}^k \in \{0, 1\}$.
With the help of the fusion numbers we can define the associated *fusion algebra*

$$[\Phi_i] \times [\Phi_j] = \sum_k N_{ij}^k [\Phi_k]. \tag{2.73}$$

We introduced the notation where $[.]$ labels the set of conformal family for a given field. Thus the fusion algebra tells us which fields of a conformal family can appear when fusing two fields of another family together. This, in fact, doesn't give us the exact OPE but rather an overview which fields might appear.
With the definition (2.73) we see right away that the fusion numbers fulfil the symmetry $N_{ij}^k = N_{ji}^k$, i.e. the algebra is commutative. From the vacuum field Φ_0, which is the identity

element of the algebra, we find $N_{i0}^k = \delta_{ik}$. Since the OPE of primary fields is associative we find on the one hand

$$[\Phi_i] \times ([\Phi_j] \times [\Phi_k]) = [\Phi_i] \times \sum_l N_{jk}^l [\Phi_l] \tag{2.74}$$

$$= \sum_{l,m} N_{jk}^l N_{il}^m [\Phi_m] \tag{2.75}$$

and on the other hand

$$([\Phi_i] \times [\Phi_j]) \times [\Phi_k] = \sum_l N_{ij}^l [\Phi_l] \times [\Phi_k] \tag{2.76}$$

$$= \sum_{l,m} N_{ij}^l N_{lk}^m [\Phi_m]. \tag{2.77}$$

From this follows the equality for the fusion numbers

$$\sum_l N_{jk}^l N_{il}^m = \sum_l N_{ij}^l N_{lk}^m \tag{2.78}$$

2.10.2   Verlinde Formula

Considering rational conformal field theories which consist of a finite number of highest weight representations there is a simple relationship between the fusion coefficients $N_{ij}^k \in \mathbb{Z}_0^+$ and the modular S-matrices:

$$N_{ij}^k = \sum_l \frac{S_{il} S_{jl} S_{kl}^*}{S_{0l}}, \tag{2.79}$$

here as before S_{kl}^* means complex conjugation of the modular S-matrix and the index 0 labels the vacuum representation of the theory. This formula is known as the *Verlinde formula* which connects OPEs with modular transformation properties. It is interesting that this specific combination of sum over modular matrices always gives an integer number.

2.11   Coset Construction

The coset construction is a method for obtaining new CFTs from two known CFTs named G and H [27, 28]. Especially when starting with theories of central charge bigger than one it is possible to construct theories with central charge $c < 1$. In this section we want to review the most important facts about coset constructions.

2.11.1 Kac-Moody Algebras & Sugawara Construction

When dealing with CFT one can, in addition to the Virasoro algebra, have further generators that satisfy other symmetry algebras. Of special interest are the so called *Kac-Moody* algebras $\hat{g}_k$ which are affine Lie algebras g at level k. The Kac-Moody algebra is defined by

$$[j_n^a, j_m^b] = i \sum_c f^{abc} j_{n+m}^c + k \, n \, \delta^{ab} \delta_{n+m,0}, \tag{2.80}$$

where f^{abc} are the structure constants of the Lie algebra and j_n^a are the Laurent modes of the chiral currents $J^a(z)$, where a labels the currents . The level k denotes the central extension of the algebra.

In terms of fields the Kac-Moody algebra translates in the OPE for the chiral currents

$$J^a(z) J^b(w) = \frac{k \delta^{ab}}{(z-w)^2} + \frac{i f^{abc}}{z-w} J^c(w) + \cdots . \tag{2.81}$$

When considering Kac-Moody algebras that are realized by currents of conformal dimension $h = 1$, it is possible to construct generators that fulfil the Virasoro algebra. These Virasoro generators then are bilinear in the current generators. The procedure of constructing these Virasoro generators L_n is known as the *Sugawara construction*

$$L_n = \frac{1}{2(k+C_g)} \sum_{a=1}^{\dim g} \left(\sum_{l \leq -1} j_l^a j_{n-l}^a + \sum_{l \geq 0} j_{n-l}^a j_l^a \right) = \frac{1}{2(k+C_g)} \sum_{a=1}^{\dim g} \sum_l : j_l^a j_{n-l}^a : . \tag{2.82}$$

In terms of fields this can be written as

$$T(z) = \frac{1}{2(k+C_g)} \sum_{a=1}^{\dim g} N(J^a J^a)(z), \tag{2.83}$$

where $N(.)$ denotes normal ordering of the currents. In the formula C_g corresponds to the dual Coxeter number of the Lie algebra g, for cases when $g = su(N)$ it is given by $C_{su(N)} = N$. Further $\dim g$ is the number of generators for the Lie algebra, again for the special case of $su(N)$ it is given by $\dim su(N) = N^2 - 1$.

Given the corresponding Virasoro generators L_n that are constructed via the Sugawara construction from the Kac-Moody algebra current generators, one can determine the central charges associated to these algebra. It is given by the following expression

$$c = \frac{k \dim g}{k + C_g}. \tag{2.84}$$

For later purpose we are interested in theories based on a $u(1)_k$ or $su(2)_k$ Lie-algebra. For the central charges (2.84) we thus find

$$c_{u(1)_k} = 1 \tag{2.85}$$

$$c_{su(2)_k} = \frac{3k}{k+2}. \tag{2.86}$$

2.11.2 Coset Theories

We have seen that rational conformal field theories with central charge $0 < c < 1$ are of special interest since they can (in principle) be solved completely. It turns out that a huge class of rational CFTs can be realized via so called *coset theories*. Therefore, we are starting with a Kac-Moody algebra g_k and a subalgebra h_k. As before the index k labels the levels of the Kac-Moody algebras. To both algebras one can associate the corresponding currents $J_g^a(z)$ in g and J_h^a in h. Obviously since h is a subgroup of g, we can rewrite the currents in h in terms of those in g

$$J_h^a(z) = \sum_b M_b^a J_g^b(z). \tag{2.87}$$

For the OPE this implies

$$J_h^a(z)J_h^b(w) = \frac{kM_l^a M_q^b \delta^{lq}}{(z-w)^2} + \frac{iM_l^a M_q^b f^{lqm}}{z-w} J_g^m(w). \tag{2.88}$$

Choosing the subalgebra h such that it is in the horizontal algebra of g we can use the identities:

$$M_l^a M_q^b f^{lqm} = f^{abc} M_m^c \tag{2.89}$$

$$M_l^a M_q^b \delta^{lq} = \delta^{ab} \tag{2.90}$$

With that we find

$$J_h^a(z)J_h^b(w) = \frac{k\delta^{ab}}{(z-w)^2} + \frac{if^{abc}}{z-w} J_h^c(w), \tag{2.91}$$

which is the closed Kac-Moody algebra at level k for the currents of the horizontal subalgebra h. Given the generators one can construct the Sugawara energy-momentum tensors

$$T_g(z) = \frac{1}{2(k_g + C_g)} \sum_{a=1}^{\dim g} N(J_g^a J_g^a)(z) \tag{2.92}$$

$$T_h(z) = \frac{1}{2(k_h + C_h)} \sum_{a=1}^{\dim h} N(J_h^a J_h^a)(z) \tag{2.93}$$

These can now be used to define the energy-momentum tensor in the coset theory g/h by

$$T_{g/h}(z) = T_g(z) - T_h(z). \tag{2.94}$$

Obviously the central charge in the coset theory is then given by the difference of central charges of g and h, i.e.

$$c_{g/h} = c_g - c_h = \frac{k \dim g}{k + C_g} - \frac{k \dim h}{k + C_h}. \tag{2.95}$$

The definition of $T_{g/h}$ shows that T_g decomposes in two mutually commuting Virasoro subalgebras with $[T_{g/h}, T_h] = 0$. From the difference of the central charges we see that we really can construct theories with $c < 1$. Of course these theories can always be related to the unitary minimal series (2.45).

Let us consider a simple example. Let the coset be given by

$$\frac{g}{h} = \frac{su(2)_k \otimes su(2)_1}{su(2)_{k+1}}. \tag{2.96}$$

The central charge and conformal weights of this coset model can be obtained by using (2.86) and (2.94)

$$c_{g/h} = \frac{3k}{k+2} + 1 - \frac{3(k+1)}{(k+1)+2} = 1 - \frac{6}{(k+2)(k+3)}. \tag{2.97}$$

$$h_{l,m,s} = \frac{l(l+2)}{4(k+2)} + \frac{s(s+2)}{4 \cdot 3} - \frac{m(m+2)}{4(k+3)} \mod 1. \tag{2.98}$$

The exact form of the highest weights can be found by considering so called *branching rules* for the coset decomposition [1–3, 6]. We recognize that theses are precisely the values of the $c < 1$ discrete series (2.45) with $m = k + 2$. The fields appearing in the coset can be labelled by three integer numbers (l, m, s) where

$$l \in \{0, 1, \ldots, k\}, \tag{2.99}$$
$$m \in \{0, 1, \ldots, k+1\}, \tag{2.100}$$
$$s \in \{0, 1\}. \tag{2.101}$$

From this we see that the l labels correspond to $su(2)_k$, the m labels to $su(2)_{k+1}$ and the s labels to $su(2)_1$. The fields are subjected to a so called *field identification* $(l, m, s) \sim (k - l, k + 1 - l, 1 - s)$ and the additional restriction $l + m + s = 0 \mod 2$ reflecting $\mathbb{Z}_2$ symmetry [29]. The concrete identification results from the relation between branching functions and coset characters[3] [1, 2].

The decomposition into commuting Virasoro generators in addition tells us, that the modular S-matrix of the coset theory should be given by

$$S_{g/h} = N S_g S_h^*, \tag{2.102}$$

where N is a normalization constant. For our example this implies

$$S_{l,m,s}^{l',m',s'} = N S_l^{l'} S_m^{*m'} S_s^{s'}. \tag{2.103}$$

The normalization constant can be determined by

$$\sum_{(l,m,s)} |S_{l,m,s}^{l',m',s'}|^2 = 1, \tag{2.104}$$

---

[3]The branching rules and associated branching-functions represent the relations of the highest weight decomposition of g_k into highest weight representations of the subalgebra and the coset $h_k \otimes (g_k/h_k)$.

where the sum runs over distinct labels satisfying the field identifications and the restriction $l + m, s = 0 \mod 2$.

In general coset theories it can occur that several fields are identified with themselves by the field identifications. These so called *fixed points* have to be treated separately when constructing the correct modular S-matrix of the coset [30]. These fixed points always seem to define a new not necessary unitary CFT. This implies that the fixed points have to be resolved in order to obtain the irreducible representations of the coset algebra.

As an example the coset realization of $\mathcal{N} = 1$ minimal models is given by

$$\frac{su(2)_k \oplus su(2)_2}{su(2)_{k+2}}. \tag{2.105}$$

The fields in this model are again labelled by three integers with field identification $(l, m, s) \sim (k - l, k + 2 - l, 2 - s)$. In the case $k = 2$ one obtains field identification fixed points since e.g. the field with labels $(1, 2, 1)$ is identified with itself.

2.12 $\mathcal{N} = 2$ Superconformal Theories

In this section we review the most important concepts when dealing with $\mathcal{N} = 2$ superconformal field theories (SCFT) [1,3,28,31–33]. We will make use of several concepts from SCFT in later chapters.

2.12.1 $\mathcal{N} = 2$ Superconformal Algebra

$\mathcal{N} = 2$ superconformal field theories are quantum field theories that enjoy $\mathcal{N} = 2$ supersymmetry and whose Hilbert spaces form representations of the associated $\mathcal{N} = 2$ superconformal Virasoro algebra (SVA). The SVA can be thought as the ordinary $\mathcal{N} = 0$ Virasoro algebra with an addition $U(1)$ Kac-Moody algebra along with two supersymmetry generators. This means that we have the generators L_n for the highest weights and J_m for the $U(1)$-charges, as well as the two supersymmetry generators $G_r^{\pm}$ that fulfil $(G_s^+)^\dagger = G_{-s}^-$. Here n, $m \in \mathbb{Z}$, whereas $r, s \in \mathbb{Z}$ when we are considering the Ramond-sector (R-sector) of the theory in contrast to $r, s \in \mathbb{Z} + \frac{1}{2}$ corresponding to the Neveau-Schwarz-sector (NS-

sector). The associated $\mathcal{N} = 2$ superconformal Virasoro algebra can be written as [1,3,31]:

$$[L_m, L_n] = (m - n)L_{m+n} + \frac{c}{12}m(m^2 - 1)\delta_{m+n,0}$$

$$[L_m, J_n] = -nJ_{n+m}$$

$$[J_m, J_n] = \frac{c}{3}m\delta_{m+n,0}$$

$$[L_n, G_r^\pm] = \left(\frac{n}{2} - r\right)G_{n+r}^\pm \tag{2.106}$$

$$[J_n, G_r^\pm] = \pm G_{n+r}^\pm$$

$$\{G_r^+, G_s^-\} = 2L_{r+s} + 2(r - s)J_{r+s} + \frac{c}{3}\left(r^2 - \frac{1}{4}\right)\delta_{r+s,0}$$

$$\{G_r^\pm, G_s^\pm\} = 0$$

2.12.2 Highest Weight Representation

Given the generators of the SVA one can build a representation [33] on a highest weight state $|h, q\rangle$ which is labelled by the conformal weight h and $U(1)$-charge q and fulfils

$$L_n |h, q\rangle = J_n |h, q\rangle = G_r^\pm |h, q\rangle = 0 \quad \forall n, r > 0,$$
$$L_0 |h, q\rangle = h |h, q,\rangle,$$
$$J_0 |h, q\rangle = q |h, q\rangle. \tag{2.107}$$

Note that in the NS-sector there is a unique vacuum state $|0, 0\rangle$ whereas in the R-sector there are several ground states $|\frac{c}{24}, \pm\frac{c}{6}\rangle$. Given a highest weight state with conformal weight h and charge q one obtains the descendant states as

$$L_{-n_1} \cdots L_{-n_q} J_{-m_1} \cdots J_{-m_p} G_{-s_1}^+ \cdots G_{-s_a}^+ G_{-r_1}^- \cdots G_{-r_b}^- |h, q\rangle, \tag{2.108}$$

where $n_i, m_i > 0$ and $s_i, r_i \geq 0$. The descendant (2.108) has L_0 and J_0 eigenvalues given by

$$h + \sum_{i=1}^{q} n_i + \sum_{j=1}^{p} m_j + \sum_{k=1}^{a} s_k + \sum_{l=1}^{b} r_l, \tag{2.109}$$

$$q + \sum_{k=1}^{a} 1 - \sum_{l=1}^{b} 1 = q + a - b. \tag{2.110}$$

It can be shown using the SVA and considering the inequality

$$\left|G_{-1/2}^\pm |h, q\rangle\right|^2 \geq 0, \tag{2.111}$$

that any state in the representation satisfies

$$h \geq \frac{1}{2}|q|. \tag{2.112}$$

2.12.3   (Anti-) Chiral Fields

Consider the NS-sector of a $\mathcal{N} = 2$ superconformal theory. Let $|h, q\rangle$ be a state in this Hilbert space. If the state fulfils

$$G^+_{-1/2} |h, q\rangle = 0, \tag{2.113}$$

it is said to be (left-)chiral. Especially these states fulfil

$$|h, q\rangle_{chiral} = |h = \frac{q}{2}, q\rangle . \tag{2.114}$$

We see that for chiral states there is a relation between the conformal weight and $U(1)$ charge. Alternatively an anti-chiral state is defined by

$$G^-_{-1/2} |h, q\rangle = 0, \tag{2.115}$$

from which follows the restriction on the conformal weight and charge

$$|h, q\rangle_{anti-chiral} = |h = -\frac{q}{2}, q\rangle . \tag{2.116}$$

We see that the (anti-) chiral states exactly saturate $(2.112)^4$. This Apart from that all other states in the representation that are neither chiral nor anti-chiral fulfil

$$h > \frac{1}{2}|q|. \tag{2.117}$$

Note that for chiral states the conformal weight can be shown to be bounded by $h_{chiral} \leq c/6$. The same is true for anti-chiral states.

In the Ramond sector chiral states are defined by those annihilated by both G^+_0 and G^-_0. Considering the expectation value

$$\langle h, q| \{G^+_0, G^-_0\} |h, q\rangle , \tag{2.118}$$

one finds using the SVA that chiral states in the Ramond are precisely the ones that satisfy

$$h = \frac{c}{24}. \tag{2.119}$$

Note that chiral states in the NS sector correspond to vacua in the Ramond sector as we will see in section 2.12.5.

2.12.4   Chiral Ring

In the last section we defined chiral and anti-chiral primary fields. It is now interesting to study the OPE between two chiral primary fields $\Phi_a(z)$ and $\Phi_b(w)$. The general form of the OPE is given by

$$\Phi_i(z)\Phi_j(w) = \sum_k \sum_{n \geq 0} C^k_{ij} (z - w)^{h_k + n - h_i - h_j} \partial^n_w \Phi_k(w), \tag{2.120}$$

---

[4]States that saturate the equation are also called BPS states.

where C_{ij}^k are some constants and h_n are the conformal weights of the corresponding fields i, j and k. Since the $U(1)$ charge is a conserved quantity, i.e. $q_i + q_j = q_k$ and we are considering chiral fields we deduce for the difference of the conformal weights using (2.112)

$$h_k - h_i - h_j \geq \frac{1}{2}|q_k| - \frac{1}{2}q_i - \frac{1}{2}q_j = \frac{1}{2}\left(|q_k| - q_k\right) \geq 0. \tag{2.121}$$

For the OPE (2.120) this implies that there are no singular terms. The absence of singular terms in the OPE thus allows us to define a product among the chiral primaries as

$$(\Phi_i \cdot \Phi_j)(w) = \lim_{z \to w} \Phi_i(z)\Phi_j(w) = \sum_k C_{ij}^k \Phi_k(w). \tag{2.122}$$

The defined limit is zero whenever Φ_k is a not a chiral primary state and thus a closed operation action on the chiral primary states. One calls this then the *chiral ring* [15]. Similarly one can also perform the calculations for the anti-chiral primaries obtaining the anti-chiral ring.

2.12.5 Spectral Flow

In $\mathcal{N} = 2$ superconformal theories there is a continuous class of automorphisms that translates the generators of the superconformal algebra to new generators again fulfilling (2.106). These transformations are known as *spectral flow* [15] and are given as follows:

$$\begin{aligned} L_n &\to L_n' = L_n + \eta J_n + \frac{\eta^2}{6}c\,\delta_{n,0}, \\ J_n &\to J_n' = J_n + \frac{c}{3}\eta\,\delta_{n,0}, \\ G_r^\pm &\to G_r'^\pm = G_{r\pm\eta}^\pm. \end{aligned} \tag{2.123}$$

Here η is a continuous parameter, especially we recognise that for $\eta \in \mathbb{Z} + \frac{1}{2}$ we can switch between the NS- and R-sector respectively. Under the spectral flow operation the conformal weights and $U(1)$-charges change according to

$$\begin{aligned} h_\eta &= h - \eta q + \frac{\eta^2}{6}c, \\ q_\eta &= q - \frac{c}{3}\eta. \end{aligned} \tag{2.124}$$

Applying the spectral flow with $\eta = \frac{1}{2}$ to the NS-sector vacuum state $|h, q\rangle = |0, 0\rangle_{NS}$ we obtain a vacuum state in the R-sector to be $|\frac{c}{24}, -\frac{c}{6}\rangle_R$.
The operator performing the spectral flow is realized as the vertex operator

$$U_\eta =: \exp\left(i\eta\sqrt{\frac{c}{3}}\Phi\right) :, \tag{2.125}$$

where $\Phi(z, \bar{z})$ is a free scalar field related to the $U(1)$ current of the SVA as

$$J(z, \bar{z}) = i\sqrt{\frac{c}{3}}\partial\Phi. \tag{2.126}$$

2.12.6 $\mathcal{N} = 2$ Superconformal Minimal Models

In this section we review some important results of $\mathcal{N} = 2$ superconformal minimal models that are given by a coset realization. The $\mathcal{N} = 2$ superconformal minimal models [31] with central charge

$$c = \frac{3k}{k+2}, \quad k \in \{1,\ 2,\ 3,\dots\}, \tag{2.127}$$

can be realized via the coset [16]

$$\frac{su(2)_k \oplus u(1)_2}{u(1)_{k+2}}, \tag{2.128}$$

where k is the level of the associated Kac-Moody algebra. The fields are labelled by three integer numbers (l, m, s). The ranges of these numbers are

$$l = 0,\dots,k \quad m = 0,\dots,2k+3 \ (\mathrm{mod}(2k+4)) \quad s = -1,0,1,2 \ (\mathrm{mod}\ 4). \tag{2.129}$$

In addition one has a $\mathbb{Z}_2$ identification of fields, i.e.

$$(l, m, s) \sim (k-l, k+2+m, 2-s), \tag{2.130}$$

and the additional restriction

$$l + m + s = 0 \ \mathrm{mod}\ 2. \tag{2.131}$$

In the literature sometimes the letter j, instead of l is used, where j is associated with a spin number and is related to l according to $j = l/2$.

Considering the NS-sector we have to restrict to $s = 0, 2$ whereas for the R-sector one has $s = \pm 1$. The conformal weights and $U(1)$-charges in this representations are given by

$$h_{l,m,s} = \frac{l(l+2) - m^2}{4(k+2)} + \frac{s^2}{8} \ \mathrm{mod}\ 1, \tag{2.132}$$

$$q_{l,m,s} = \frac{s}{2} - \frac{m}{k+2} \ \mathrm{mod}\ 2. \tag{2.133}$$

In particular the charges are fractional numbers. We see that the NS-vacuum corresponds to the labels $(0,0,0)$. The chiral primaries in the NS sector correspond to $(l,l,0)$. Since $l \in \{0,\dots,k\}$ there obviously exist $k+1$ chiral primary states. The Ramond ground states can be obtain by spectral flow (2.125) from the NS-sector chiral primaries

$$\text{R vacua:} \quad (l, l+1, 1). \tag{2.134}$$

We see that there are as many chiral primary states in the NS-sector as there are Ramond vacua. The Hilbert space $\mathcal{H}$ decomposes into irreducible highest weight representations of holomorphic and anti-holomorphic super Virasoro algebras

$$\mathcal{H}_{[l,m]} := \mathcal{H}_{[l,m,s]} \oplus \mathcal{H}_{[l,m,s+2]}, \tag{2.135}$$

where by $[l, m, s]$ are meant all fields that satisfy (2.130)-(2.131). Using this notation the NS-sector can be represented as

$$\mathcal{H}_{NSNS} = \bigoplus_{\substack{[l,m]\in J_k \\ l+m \ even}} \mathcal{H}_{[l,m]} \otimes \bar{\mathcal{H}}_{[l,m]}, \tag{2.136}$$

and similar the Ramond sector

$$\mathcal{H}_{RR} = \bigoplus_{\substack{[l,m]\in J_k \\ l+m \ odd}} \mathcal{H}_{[l,m]} \otimes \bar{\mathcal{H}}_{[l,m]}, \tag{2.137}$$

where

$$J_k := \{(l, m)| \ 0 \le l \le k, \ -k-1 \le m \le k+2, \ -1 \le s \le 2\}/\sim, \ \ [l, m] \sim [k-l, k+2+m]. \tag{2.138}$$

For later purpose we already state the corresponding modular S-matrices in the coset representation. These can be determined from the decomposition of characters

$$\chi_l^{su(2)_k}(\tau)\chi_s^{u(1)_2}(\tau) = \sum_{m=-k-1}^{k+2} \chi_m^{u(1)_{k+2}} \chi_{l,m,s}(\tau), \tag{2.139}$$

as

$$S_{L,M,S}^{l,m,s} = \frac{2}{k+2} \sin(l, L)e^{i\pi\frac{mM}{k+2}} e^{-i\pi\frac{sS}{2}}, \tag{2.140}$$

where we introduced the short hand notation

$$\sin(l, L) := \sin\left(\pi \frac{(l+1)(L+1)}{k+2}\right). \tag{2.141}$$

Here the characters of the coset representation can be written in terms of generalized theta functions $\Theta_{a,b}(\tau)$ and string functions $c_a^b(\tau)$ [1, 3] as

$$\chi_{l,m,s}(\tau) = \sum_{a=1}^{k} c_{m-4a-s}^l(\tau)\Theta_{-2m+(4a+s)(k+2),2k(k+2)}(\tau). \tag{2.142}$$

At last let us consider the fusion of two fields in the representation to determine the fusion rules of the minimal models

$$[\Phi_{l_1,m_1,s_1}] \times [\Phi_{l_2,m_2,s_2}] = \sum_{l_3,m_3,s_3} N_{l_1,l_2}^{l_3}\delta_{m_1+m_2,m_3}^{(2k+4)}\delta_{s_1+s_2,s_3}^{(4)}[\Phi_{l_3,m_3,s_3}], \tag{2.143}$$

where $\delta^{(n)}$ is a delta function defined modulo n and $N_{a,b}^c$ are the $su(2)$ level k fusion numbers. We see that the $\mathcal{N} = 2$ minimal model fusion numbers are simply given by

$$N_{l_1,m_1,s_1, \ l_2,m_2,s_2}^{l_3,m_3,s_3} = N_{l_1 l_2}^{l_3}\delta_{m_1+m_2,m_3}^{(2k+4)}\delta_{s_1+s_2,s_3}^{(4)}. \tag{2.144}$$

2.13   Boundary Conformal Field Theory

In this section we will review the basic ingredients for CFTs living on a worldsheet with boundaries. The main references for this section will be [1, 2, 34].

2.13.1   CFT with Boundary

We consider a CFT living on the complex upper half plane with a boundary aligned along the real axis. As our system is fixed to this specific geometry the boundary should not be changed under conformal transformations. Recall that on the full complex plane $(z = x + it \;\; \bar{z} = x - it)$ the conformal mappings are given by

$$z \to w(z) = \sum \epsilon_n z^n \tag{2.145}$$

$$\bar{z} \to \bar{w}(\bar{z}) = \sum_n \bar{\epsilon}_n \bar{z}^n \tag{2.146}$$

where $\epsilon(z)$ and $\bar{\epsilon}(\bar{z})$ are the generators of conformal transformations. On the full complex plane there is no restriction on the generators, on the upper half plane on the other hand we want the boundary to be invariant under the given transformations which relates to

$$\text{Im}[w(z)]|_{z=x} = 0 \quad \leftrightarrow \quad w(z)|_{z=x} = \bar{w}(\bar{z})|_{\bar{z}=x} \quad \leftrightarrow \quad \epsilon_n = \bar{\epsilon}_n. \tag{2.147}$$

We see that the holomorphic and anti-holomorphic generators are identified along the boundary. This gives rise to the interpretation of the anti-holomorphic part being the analytic continuation of the holomorphic part.

2.13.2   Correlation Functions in Presence of a Boundary

In section 2.8 we have seen that correlation functions are solutions to differential equations. Let us now consider the case where our fields live on the upper half plane bounded by some boundary at $z = x$. Under conformal transformations our correlator transforms according to

$$\delta \langle \Phi_1(z_1, \bar{z}_1) \cdots \Phi_N(z_N, \bar{z}_N) \rangle = -\frac{1}{2\pi i} \oint_C dz \, \epsilon(z) \, \langle T(z) \Phi_1(z_1, \bar{z}_1) \cdots \Phi_N(z_N, \bar{z}_N) \rangle +$$

$$\frac{1}{2\pi i} \oint_C d\bar{z} \, \bar{\epsilon}(\bar{z}) \, \langle \bar{T}(\bar{z}) \Phi_1(z_1, \bar{z}_1) \cdots \Phi_N(z_N, \bar{z}_N) \rangle. \tag{2.148}$$

Here the contour integration is performed along the semicircle enclosing the coordinates $(z_j, \bar{z}_j)$ (see figure 2.8).

Along the boundary there is no energy exchange for which we conclude

$$T(z) - \bar{T}(\bar{z})|_{z=\bar{z}=x} = 0. \tag{2.149}$$
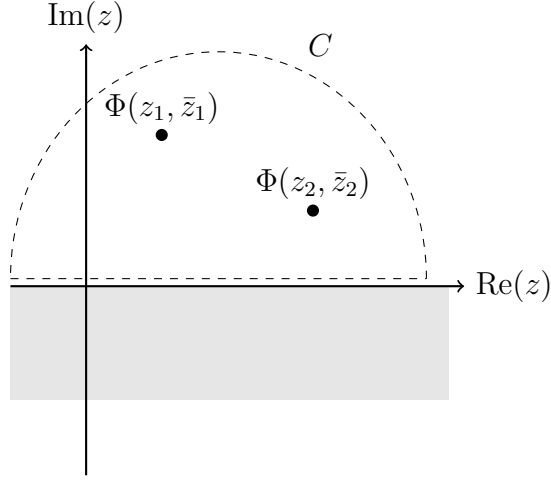
Figure 2.8: Contour for the integration along the semicircle in the upper half plane enclosing the coordinate fields.

Using this equation we see that we can map the anti-holomorphic part of the fields in the upper half plane to the holomorphic part in the lower half plane. With this the anti-holomorphic part of the Ward identities is mapped to the holomorphic part in the lower half plane (see figure 2.9).
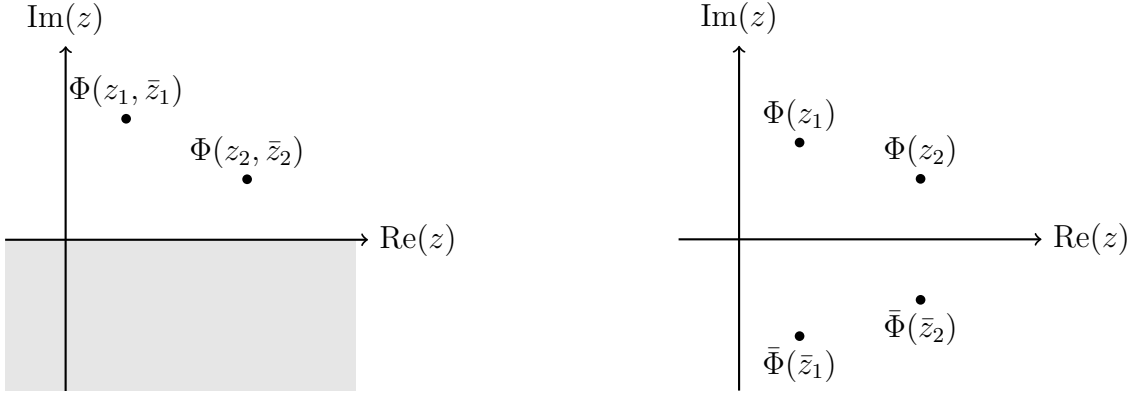
Figure 2.9: Doubling trick for fields on the UHP in presence of a boundary to fields on the complex plane.

The conformal Ward identity in presence of the given boundary thus takes the simpler form

$$\delta\langle\Phi_1(z_1,\bar{z}_1)\cdots\Phi_N(z_N,\bar{z}_N)\rangle = -\frac{1}{2\pi i}\oint_{C-C^*} dz\,\epsilon(z)\,\langle T(z)\Phi_1(z_1)\bar{\Phi}_1(\bar{z}_1)\cdots\Phi_N(z_N)\bar{\Phi}_N(\bar{z}_N)\rangle.$$

$$(2.150)$$

Here the fields are split into their holomorphic and anti-holomorphic parts according to

$$\Phi_i(z, \bar{z}) = \Phi_i(z) + \bar{\Phi}_i(\bar{z}). \tag{2.151}$$

If the fields in question carry some additional degree of freedom, e.g. charge, we have to perform the mapping s.t. it is consistent with the boundary condition, for the charges this would mean that in addition one has for example to perform a charge conjugation, which is quite familiar to the method of mirror charges in ordinary electrostatics, where one introduces charges of opposite signs at the mirrored coordinates in order to solve the boundary conditions for the electric potential.

Considering (2.150) we see that the N-point correlator on the upper half plane fulfils the same differential equation as the $2N$-point correlator on the full complex plane. A nice application of the result is that the one point function for a CFT on the upper half plane (UHP) with some boundary at $z = x = \bar{z}$ is now given by:

$$\langle \Phi(z, \bar{z}) \rangle_{UHP} = \langle \Phi(z)\bar{\Phi}(\bar{z}) \rangle_{\mathbb{C}} = \frac{k_{12}\delta_{h,\bar{h}}}{(z - \bar{z})^{2h}} \tag{2.152}$$

This means in contrast to the one point function on the full complex plane, which is identically zero due to conformal invariance, the one point function on the upper half plane can give a non-zero contribution.

2.13.3 Boundary Conditions and Boundary States

Consider a rational conformal field theory with total Hilbert space

$$\mathcal{H} = \bigoplus_{i,\bar{i}} M_{i,\bar{i}} \mathcal{H}_i \otimes \bar{\mathcal{H}}_{\bar{i}}. \tag{2.153}$$

Assume that the CFT has in addition to the Virasoro generators another set of generators W_n^i ($\bar{W}_n^i$) generating an extended symmetry of our theory.
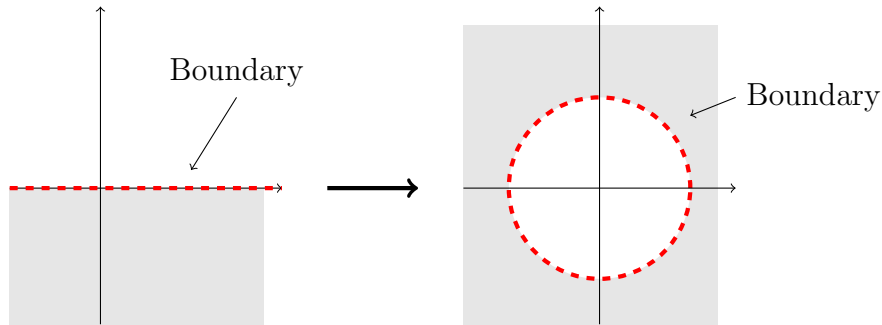
Figure 2.10: Transformation of the upper half plane to the unit disc. The boundary along the real line becomes in the new geometry the boundary of the disc.

In (2.149) we have seen which relation the energy-momentum tensor along the boundary has to fulfil. If we map the upper half plane to the unit disc, the boundary condition becomes such a boundary state in standard radial quantisation (see figure 2.10)

$$L_n - \bar{L}_{-n} = 0 \quad \text{along boundary.} \tag{2.154}$$

Similar considerations apply for the additional symmetry generators. An associated boundary state $|B\rangle$ then has to fulfil the following so called *gluing conditions*

$$(L_n - \bar{L}_{-n})|B\rangle = 0 \quad \text{conformal symmetry} \tag{2.155}$$

$$(W_n^i - (-1)^{h^i}\bar{W}_{-n}^i)|B\rangle = 0 \quad \text{extended symmetry,} \tag{2.156}$$

where we also included the conditions on the boundary state coming from the additional symmetries with $h^i = h(W^i)$. For these additional symmetries it is possible to include the action of an automorphism if desired. When dealing with rational theories there is a important set of fundamental boundary states fulfilling (2.155) and (2.156), called *Ishibashi states* (see [90, 92])

$$|i\rangle\rangle = \sum_{N=0}^{\infty} \sum_{m=1}^{d_i(N)} |i, N; m\rangle \otimes \overline{|h, N; m\rangle} \in \mathcal{H}_i \otimes \bar{\mathcal{H}}_i, \tag{2.157}$$

where N is the level of the highest within the highest weight representation i and $d_i(N)$ is the dimension of the subspace at level N of i.
Here we assumed that $\mathcal{H}_i$ is the conjugated representation of $\bar{\mathcal{H}}_i$. Ishibashi states can be related (in closed string picture) to the character of a representation i by

$$\langle\langle i|q^{\frac{1}{2}\left(L_0 + \bar{L}_0 - \frac{c}{12}\right)}|j\rangle\rangle = \langle\langle i|q^{L_0 - \frac{c}{24}}|j\rangle\rangle = \delta_{ij}\chi_i(q). \tag{2.158}$$

In the second step we used the identification $L_0 = \bar{L}_0$ at the boundary in order to obtain an expression just depending on the chiral algebra. Since a general boundary state $|B\rangle$ has to fulfil the gluing conditions (2.155)-(2.156) it must be a linear combination of Ishibashi states

$$|B_i\rangle = \sum_j \frac{\psi_{ij}}{\sqrt{S_{0j}}}|j\rangle\rangle, \tag{2.159}$$

where we labeld the boundary state in a given representation i by $|B_i\rangle$. The ψ_{ij} are up to now some constants that characterize the boundary condition. It can be shown that these constants are constrained by the so called *Cardy condition* [35] and so-called *sewing-relations* that first were considered in [93, 94]. We won't discuss in detail the sewing-relations, for a detailed and illustrative discussion see [92–94]. The Cardy condition on the other hand is such a fundamental concept that we will review it for the special case of a bulk state space corresponding to a charge-conjugate modular invariant partition function in the next section.

2.13.4 The Cardy Condition

The Cardy condition [35] basically ensures the tree-level loop-channel equivalence. Here we will concentrate on the special case of standard gluing conditions and a bulk state space corresponding to a charge-conjugate modular invariant partition function[5], i.e. $\bar{\mathcal{H}}_{\bar{i}} = \mathcal{H}_{i^+}$. For a more general discussion see [4, 35].

As setup we consider the (open string) partition function on the cylinder with circumference β and length 1 (note that without loss of generality a cylinder of length L can always be rescaled to the cylinder of length 1 in a CFT)

$$Z_{ij}(\beta) = \text{tr}_{\mathcal{H}_{ij}} e^{-\pi\beta(L_0 - \frac{c}{24})}. \tag{2.160}$$

Here $\mathcal{H}_{ij}$ is the space of string states compatible with the boundary conditions i and j at the end of the cylinder[6]. By using that the the boundary conditions preserve the symmetry algebra one finds

$$\mathcal{H}_{ij} = \bigoplus_k N_{ij}^k \mathcal{H}_k, \tag{2.161}$$

where N_{ij}^k are the associated fusion coefficients of the CFT considered. In particular the fusion coefficients arise since we are considering diagonal modular invariant theories without automorphisms. The open string partition function then becomes

$$Z_{ij}(\beta) = \sum_k N_{ij}^k \chi_k(e^{-\pi\beta}). \tag{2.162}$$
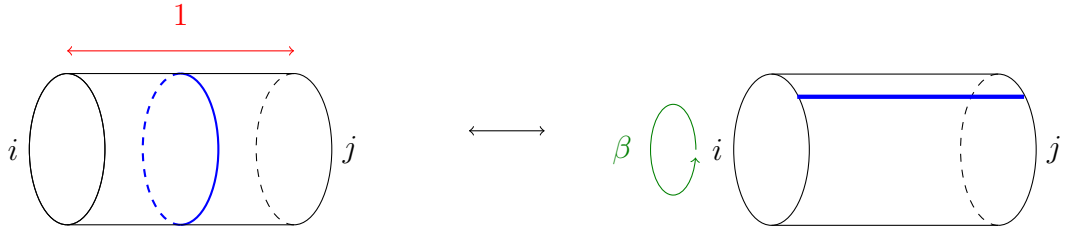
Figure 2.11: Open-closed string duality on the cylinder. The partition function of a closed string moving along the cylinder between its two boundaries can equally be described as the partition function of an open string propagating around the wrapped up dimension.

On the other hand the cylinder partition function may be viewed as a closed string propagating from one boundary to the other, i.e.

---

[5]In chapter 10 we will consider A-type and B-type boundary conditions where some of these considerations will not hold but satisfy the more general results [35].

[6]Here we assume that we are dealing with diagonal theories, i.e. $M_{i\bar{i}} = \delta_{i\bar{i}}$

$$\tilde{Z}_{ij}(\beta) = \langle B_i | e^{-\frac{2\pi}{\beta}(L_0 + \bar{L}_0 - \frac{c}{12})} | B_j \rangle = \sum_m \frac{\psi^*_{im}\psi_{jm}}{S_{0m}} \chi_m(e^{-4\pi/\beta}). \tag{2.163}$$

Performing a modular S-transformation the closed cylinder expression gets transformed to the following expression in the open channel

$$\tilde{Z}_{ij}(\beta) = \sum_{m,k} \frac{\psi^*_{im}\psi_{jm}S_{mk}}{S_{0m}} \chi_k(e^{-\pi\beta}). \tag{2.164}$$

The two partition functions $Z_{ij}(\beta)$ and $\tilde{Z}_{ij}(\beta)$ should yield the same result in order to preserve the tree-channel loop channel duality (see figure 2.11). Thus they have to match. From this one deduces the Cardy condition on the constants ψ_{ij}

$$\sum_m \frac{\psi^*_{im}\psi_{jm}S_{mk}}{S_{0m}} = N^k_{ij}, \tag{2.165}$$

which is solved in the RCFT case by $\psi_{ij} = S_{ij}$ in which case we exactly obtain the Verlinde formula (2.79). For the Cardy boundary state this then implies

$$|B_i\rangle = \sum_j \frac{S_{ij}}{\sqrt{S_{0j}}} |j\rangle\rangle. \tag{2.166}$$

We will see in section 3.1 that defects will also fulfil a consistency condition following similar arguments as the boundary states considered here.

Chapter 3

Generalities on Defects

3.1 Defects and their Classification

The study of one-dimensional interfaces[1] between two-dimensional CFTs [60] has a long history [39, 41, 42, 48]. Locally, an interface sets gluing conditions for all pairs of local fields separated by the interface. In that sense an interface defines a map between the algebras of local fields on the two sides. Similar to a boundary condition, such an interface condition admits local excitations and constitutes a one-dimensional subsector of the full quantum field theory. At a conformal fixed point the interface preserves at least one half of the bulk conformal charges. If the interface runs along the real axis of the complex plane and separates CFT_1 from CFT_2, the condition reads

$$\lim_{y \searrow 0} \left(T^{(1)}(x+iy) - \bar{T}^{(1)}(x-iy) \right) = \lim_{y \nearrow 0} \left(T^{(2)}(x+iy) - \bar{T}^{(2)}(x-iy) \right), \qquad (3.1)$$

where $T^{(n)}$ and $\bar{T}^{(n)}$ are the holomorphic and anti-holomorphic components of the energy-momentum tensor of CFT_n. The requirement (3.1) is a necessary local condition. Similarly as in the case of boundary conditions, further local conditions follow from sewing relations, and global conditions arise from modular constraints on the torus which we will discuss later.

If the time evolution is defined to run orthogonal to the interface or defect - in our setup along the imaginary axis - then it can be realized as an operator I. The gluing conditions (3.1) then tell us that I has to commute with all generators of the conformal transformations, i.e. the Virasoro generators, along the defect. For our setup in which the defect runs along the real line [48] this means

$$\left(L_n^{(1)} - \bar{L}_{-n}^{(1)} \right) I = I \left(L_n^{(2)} - \bar{L}_{-n}^{(2)} \right) \quad \forall n \in \mathbb{Z}. \qquad (3.2)$$

In some sense, conformal interfaces generalise the notion of conformal boundary conditions (2.155), which are the special solutions where both sides of (3.1) are equal to zero, or occur

---

[1]Sometimes interfaces are also referred to as defects but in principle there is a difference between these two objets. In general defects live at a given point in the moduli space, whereas interfaces are intertwiners between different CFTs.

if one side of the interface is trivial. In this case the defect is called *purely reflecting* or alternatively *factorizable*. The notion of 'reflective' will become more clear in section 3.2 and 3.3. For the interface this implements

$$\left(L_n^{(1)} - \bar{L}_{-n}^{(1)} \right) I = 0 \qquad 0 = I \left(L_n^{(2)} - \bar{L}_{-n}^{(2)} \right). \tag{3.3}$$

Another set of special solutions to (3.1) is obtained when the interface commutes with both the left- and the right-moving Virasoro algebra, such that (3.1) is solved separately for the holomorphic and the anti-holomorphic component of the energy-momentum tensor

$$L_n^{(1)} I = I L_n^{(2)} \qquad \bar{L}_n^{(1)} I = I \bar{L}_n^{(2)}. \tag{3.4}$$

Evidently, this can only happen when the theories on the two sides have equal left- and right-moving central charges. Note that equality of central charges not automatically implies equality of the two CFTs. An interface corresponding to such a solution can be freely deformed and moved on the Riemann surface, as long as it does not cross any operator insertions $\mathcal{O}$ (see figure 3.1). These interfaces were dubbed *topological* in [40].
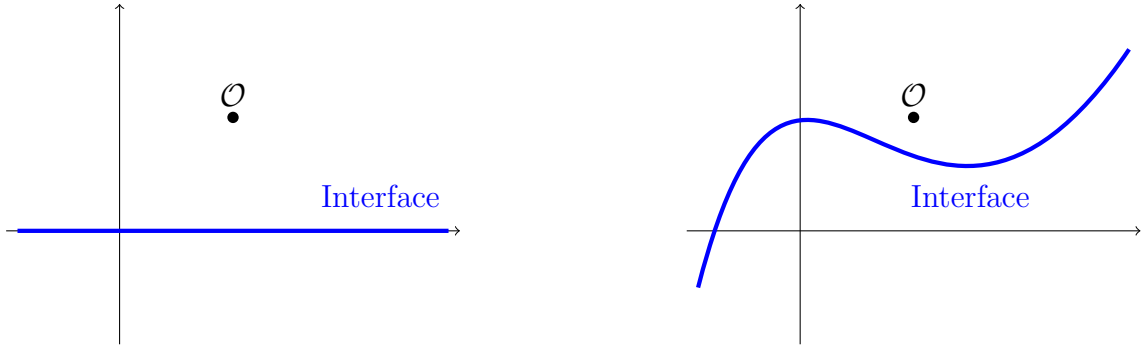
Figure 3.1: Possible deformation of a topological defect.

Initially introduced in [42], topological interfaces have been studied in particular in rational CFTs [46, 54]. Topological defects have a broad range of applications. For example it has been shown in [44] that topological defects map primary fields of CFT_1 to primary fields of CFT_2 and also D-branes from CFT_1 to branes in CFT_2. Another interesting feature (see [45]) is that all automorphisms of a CFT including mirror symmetry and T-duality are implemented by a topological defect.

A topological interface [60] can be regarded as an operator on the space of states, acting as a constant map between (left-right pairs of) isomorphic Virasoro representations[2]. In the case where the conformal symmetry is enhanced to a larger chiral symmetry algebra, the

---

[2]Note that the notion of 'map' is not true for non-topological interfaces.

topological interface condition may or may not respect the additional symmetry. Topological interfaces between CFT_1 and CFT_2 thus naturally fall into classes corresponding to the preserved common symmetry subalgebra. For a given topological interface, we consider the decomposition of the space of states of CFT_n ($n = 1, 2$) with respect to this common subalgebra,

$$\mathcal{H}^{(n)} = \bigoplus_{(i\bar{\imath})} M_{i\bar{\imath}}^{(n)} \mathcal{H}_i \otimes \mathcal{H}_{\bar{\imath}}. \tag{3.5}$$

The indices i and $\bar{\imath}$ label (generally different) irreducible highest weight representations of the two chiral parts of the common subalgebra. The non-negative integers $M_{i\bar{\imath}}^{(n)}$ give the multiplicities of the pair of representations $(i, \bar{\imath})$. We will assume that our theories are unitary and have a discrete spectrum of highest weight states of the chiral subalgebra, and that there is a unique vacuum state.

An operator corresponding to a general topological interface will then be denoted

$$I_A = \sum_{\mathbf{i}} d_{A\mathbf{i}} \, \|\mathbf{i}\| \, . \tag{3.6}$$

We use bold-face indices $\mathbf{i}$ to refer to a pair of left-right products of irreducible representations in the two adjacent CFTs,

$$\mathbf{i} \equiv (i, \bar{\imath}; \alpha, \beta) \, . \tag{3.7}$$

Here, $(i, \bar{\imath})$ labels the transmitted pair of representations. The indices $\alpha = 1, 2, \ldots, M_{i\bar{\imath}}^{(1)}$ and $\beta = 1, 2, \ldots, M_{i\bar{\imath}}^{(2)}$ are the multiplicity labels of this pair on the two sides of the interface. The symbol $\|\mathbf{i}\|$ in (3.6) denotes the Ishibashi-type projector which acts as an intertwiner between the two pairs of representations, *i.e.*

$$\|\mathbf{i}\| : \mathcal{H}_i \otimes \mathcal{H}_{\bar{\imath}}^{(\alpha)} \; \rightarrow \mathcal{H}_i \otimes \mathcal{H}_{\bar{\imath}}^{(\beta)} \tag{3.8}$$

and

$$J_n \|\mathbf{i}\| = \|\mathbf{i}\| J_n \; , \tag{3.9}$$

where J_n denotes any symmetry generator.

One important property of topological interfaces is that they admit a fusion product, i.e. a composition of interfaces. The fusion product has the geometric interpretation of moving the interface lines on top of each other, and interpreting the result as a topological interface between the two remaining CFTs (see section 3.4). While fusion may also be defined for the more general conformal interfaces, it is particularly straightforward in the topological case, where it basically consists of map composition [42]. When writing the coefficients $d_{AB\mathbf{i}}$ of the fusion product $I_{AB} = I_A I_B$ we will suppress the summation over multiplicity labels,

$$d_{AB\mathbf{i}} = \sum_{\gamma} d_{A(i\bar{\imath};\alpha,\gamma)} d_{B(i\bar{\imath};\gamma,\beta)} \; \equiv \; d_{A\mathbf{i}} d_{B\mathbf{i}} \, . \tag{3.10}$$

The fusion product, which we will discuss in more detail in section 3.4, extends to fusion of a topological interface with (non-topological) conformal interfaces, in particular with boundary conditions.

For topological defects the coefficients $d_{A\mathbf{i}}$ are subjected to a consistency condition [42]. To determine the coefficients let us consider the modular S-transformation of the torus partition function with a pair of two closed defect lines. Due to the open-closed string duality there are two possible viewpoints of this partition function. One possible way is to consider time slices parallel to the defect line. This results in the expression

$$Z_{A,B} = \mathrm{Tr}\left(I_A^\dagger I_B \tilde{q}^{L_0 - \frac{c}{24}} \bar{\tilde{q}}^{\bar{L}_0 - \frac{c}{24}}\right) =$$

$$\sum_{\mathbf{i}} d_{A\mathbf{i}}^* d_{B\mathbf{i}} \chi_i(\tilde{q}) \bar{\chi}_{\bar{i}}(\bar{\tilde{q}}) =$$

$$\sum_{(i,\bar{i};\alpha,\beta)} d_{A^*(i,\bar{i};\alpha,\beta)} d_{B(i,\bar{i};\alpha,\beta)} \chi_i(\tilde{q}) \bar{\chi}_{\bar{i}}(\bar{\tilde{q}}). \tag{3.11}$$

Here A^* labels the orientation reversed interface with corresponding defect operator $\mathcal{D}_{A^*} = \mathcal{D}_A^\dagger$. The other possible way is to consider time evolution along, i.e. parallel to the defect line. Let $\mathcal{N}_{i\bar{i}\,A}^{\ \ B} \in \mathbb{N}^0$ denote the multiplicity of Virasoro representations $(i,\bar{i})$ appearing in the Hilbert space in the chosen time evolution, i.e.

$$\mathcal{H}_{A,B} = \mathcal{N}_{i\bar{i}\,A}^{\ \ B} \mathcal{H}_i \otimes \bar{\mathcal{H}}_{\bar{i}}, \tag{3.12}$$

then the partition function can be alternatively expressed as

$$Z_{A,B} = \sum_{(i,\bar{i};\alpha,\beta)} \mathcal{N}_{i\bar{i}\,A}^{\ \ B} \chi_i(q) \bar{\chi}_{\bar{i}}(q). \tag{3.13}$$

Performing a modular S-transformation on (3.13) we can relate the result with (3.1) to obtain a consistency relation on the coefficients

$$\mathcal{N}_{i\bar{i}\,A}^{\ \ B} = \sum_{j,\bar{j}} S_{ij} S_{\bar{i}\bar{j}} d_{A^*(i,\bar{i};\alpha,\beta)} d_{B(i,\bar{i};\alpha,\beta)}. \tag{3.14}$$

Here S_{ij} is an element of the modular S-matrix. In particular we observe that the right-hand side of the last equation should be a positive integer. The condition (3.14) restricts the possible values of coefficients $d_{A\mathbf{i}}$, and it also requires that linear superpositions of interfaces must have integer coefficients.

We refer to interfaces which cannot be decomposed into a superposition of other interfaces with positive coefficients as *elementary interfaces*. The set of elementary interfaces forms a basis for all topological interfaces of the same class. Obviously any interface for which at least one of the $\mathcal{N}_{j\bar{j}\,A}^{\ \ A}$ is equal to 1 is elementary. In fact, due to the operator-state correspondence in the theory on the interface any elementary interface has at least $\mathcal{N}_{00\,A}^{\ \ A} = 1$, i.e. the vacuum in parallel time evolution occurs with multiplicity 1.

Consider a set of topological interfaces I_A for which $d_{A\mathbf{i}}$ provides a unitary transformation from projectors $\|\mathbf{i}\|$ to the I_A. It can be shown [42] that the corresponding $\mathcal{N}_{\bar{i}i\,A}^{\;\;\;B}$ form a representation of a tensor product of fusion algebras,

$$\sum_B \mathcal{N}_{\bar{i}i\,A}^{\;\;\;B} \mathcal{N}_{j\bar{j}\,B}^{\;\;\;C} = \sum_{\mathbf{k}} N_{ij}^{\;\;k} N_{\bar{i}\bar{j}}^{\;\;\bar{k}} \mathcal{N}_{k\bar{k}\,A}^{\;\;\;C}. \tag{3.15}$$

In the last formula, the $N_{ij}^{\;\;k}$ are the fusion rules of the chiral algebra. It is easy to see that a topological interface I_A in such a set is elementary.

A particular instance where we know a set of $d_{A\mathbf{i}}$ that provides a change of basis occurs in rational CFT, *i.e.* in theories where the index set $\{\mathbf{i}\}$ in (3.5) is finite. The simplest case are the diagonal theories — theories which are charge conjugation invariant ($i = \bar{\imath}$), and where the multiplicities for all chiral algebra representations are 1. In such a theory there are topological defects[3] of the form

$$\mathcal{D}_{\mathbf{a}} = \sum_i \frac{S_{ai}}{S_{0i}} \|i\|. \tag{3.16}$$

The projector on irreducible representations can also be written in terms of Ishibashi states[4]

$$\|i\| = |i\rangle\rangle\langle\langle i|. \tag{3.17}$$

These defects have $\mathcal{N}_{0a}^{\;\;a} = N_{0a}^{\;\;a} = 1$ and are, therefore, elementary. They provide a basis for the set of topological defects which respect the chiral symmetry. The fusion of such defects can now be easily expressed as

$$\mathcal{D}_a \mathcal{D}_b = \sum_c N_{ab}^{\;\;c} \mathcal{D}_c. \tag{3.18}$$

We see that for topological defect the fusion amounts in an algebra for the defects.

In cases where the chiral algebra admits a global symmetry G, we find among the topological interfaces the so-called symmetry defects. Each element $g \in G$ can be associated to a topological defect $\mathcal{D}_g$. By definition, these interfaces glue any field to its image under the symmetry operation. Hence, they implement an action of G through

$$\mathcal{D}_g^\dagger = \mathcal{D}_{g^{-1}}, \qquad \mathcal{D}_g \mathcal{D}_h = \mathcal{D}_{gh} \qquad \forall h, g \in G. \tag{3.19}$$

A broader class of interfaces are the duality interfaces introduced in [46]. Their defining property is that

$$I\,I^\dagger = \bigoplus_{g \in G} \mathcal{D}_g, \tag{3.20}$$

---

[3]In this paper we usually refer to interfaces as defects if the CFTs on the two sides are identical.

[4]A general projector acting on representations $(i, \bar{\imath})$ can be written as $P^{(i,\bar{\imath})} = \sum_{N,\bar{N}} (|i, N\rangle \otimes |\bar{\imath}, \bar{N}\rangle)(\langle i, N| \otimes \langle \bar{\imath}, \bar{N}|)$, where N is the level of the descendant.

where G is a finite symmetry group of the CFT. The fusion product of a duality interface with its adjoint contains a superposition of group-like defects corresponding to a symmetry (sub-)group. Duality defects were first introduced in the context of RCFT [46], where they can be used to relate CFTs with the same chiral algebra but different modular invariants. However, the definition can be extended also to the non-rational context. Prominent examples for duality interfaces implement dualities such as T-duality in free field theories [54], or the Kramers-Wannier duality in the Ising model [45].

3.2 The Folding Trick

Consider a defect along the imaginary axis separating CFT$_1$ and CFT$_2$, where the CFTs in principle can differ from each other. Folding the theories along the defect line (see figure 3.2) we obtain a new theory which is the tensor theory of the two individual theories

$$\text{CFT}_1 \otimes \overline{\text{CFT}}_2. \tag{3.21}$$

Here the folding exchanges left- and right -movering degrees of freedom of CFT$_2$ denoted by $\overline{\text{CFT}}_2$. This so called *folding trick* is well known in condensed matter physics and has e.g. been applied in the context of conformal defects[5] in [39]. After the folding the defect corresponds to a boundary in the tensor theory of the two CFTs. The gluing conditions (3.1) become in the folded picture

$$(L_n^{(1)} + L_n^{(2)} - \bar{L}_{-n}^{(1)} - \bar{L}_{-n}^{(2)}) |B_D\rangle = 0, \tag{3.22}$$

where $|B_D\rangle$ is the associated boundary corresponding to the defect.
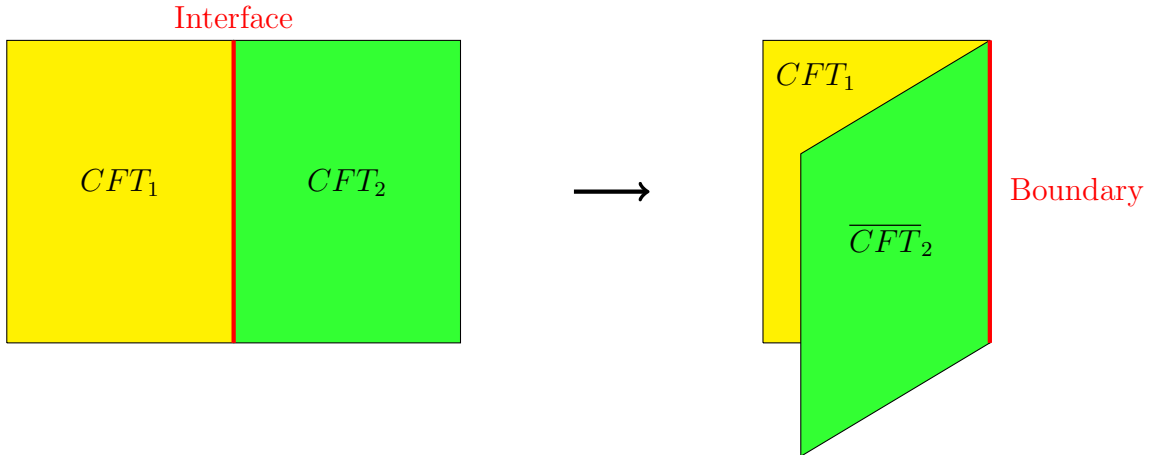
Figure 3.2: Folding Trick: CFT$_2$ is folded along the interface, in this way the interface becomes a boundary of CFT$_1 \otimes \overline{\text{CFT}}_2$.

---

[5]A defect is denoted *conformal* if its gluing conditions are compatible with all possible conformal transformations that leave the shape of the defect invariant.

Alternatively when starting with a boundary state that obeys (3.22) one may ask for solutions to this equation. A trivial solution is given by (see [39])

$$|B\rangle_{reflect} = |B_1\rangle \otimes |B_2\rangle, \tag{3.23}$$

where the boundary state factorizes into individual boundary states for CFT_1 and CFT_2. In this case $L_n - \bar{L}_{-n}$ vanishes for each theory separately. This implies that the component T_{xt} of the energy momentum tensor is zero along the interface which means that there is no energy transfer across the wall and the two theories are decoupled from each other. Unfolding the boundary state we, therefore, obtain a totally reflective defect given by

$$D_{fac} = |B_1\rangle \langle \bar{B}_2|, \tag{3.24}$$

satisfying (3.3). The opposite case is when one considers purely transmitting solutions that fulfil

$$\left(L_n^{(1)} - \bar{L}_{-n}^{(2)}\right)|B\rangle_{trans} = 0 = \left(L_n^{(2)} - \bar{L}_{-n}^{(1)}\right)|B\rangle_{trans}. \tag{3.25}$$

by unfolding the boundary state we gain a topological defect D_{trans} satisfying (3.4). Let us consider an explicit example to emphasise the result. Consider a topological defect $\mathcal{D}_a$ in a RCFT which is given by

$$\mathcal{D}_a = \sum_{(i,\bar{i})} \frac{S_{ai}}{S_{0i}} P^{(i,\bar{i})}, \tag{3.26}$$

where the projector $P^{(i,\bar{i})}$ is given by

$$P^{(i,\bar{i})} = \sum_{N,\bar{N}} (|i,N\rangle_1 \otimes |\bar{i},\bar{N}\rangle_1)(\langle i,N|_2 \otimes \langle \bar{i},\bar{N}|_2). \tag{3.27}$$

As before this topological defect satisfies the commutation relations

$$[L_n, \mathcal{D}_a] = [\bar{L}_n, \mathcal{D}_a] = 0 \tag{3.28}$$

$$[W_n, \mathcal{D}_a] = [\bar{W}_n, \mathcal{D}_a] = 0. \tag{3.29}$$

The folding procedure now tells us, that we first have to interchange left- and right-movers for the second CFT, i.e. $\langle i,N|_2 \otimes \langle \bar{i},\bar{N}|_2 \to \langle \bar{i},\bar{N}|_2 \otimes \langle i,N|_2$, and then hermitian conjugate the obtained result, i.e. $\langle \bar{i},\bar{N}|_2 \otimes \langle i,N|_2 \to |\bar{i},\bar{N}\rangle_2 \otimes |i,N\rangle_2$.

Thus the corresponding boundary state that can be deduced from the topological defect by following the folding procedure is given by

$$|a\rangle_{\mathcal{P}} = \sum_i \frac{S_{ai}}{S_{0i}} \sum_{N,M} (|i,N\rangle_1 \otimes U\overline{|i,N\rangle}_2) \otimes (|i,M\rangle_2 \otimes U\overline{|i,M\rangle}_1). \tag{3.30}$$

The state $|a\rangle_{\mathcal{P}}$ is called permutation boundary state. The notion of permutation becomes clear since under the folding the commutation relations for the defect become the following (permuted) gluing conditions on the permutation state

$$L_n^{(1)} - \bar{L}_{-n}^{(2)} = 0, \quad W_n^{(1)} - (-1)^{hW}\bar{W}_{-n}^{(2)} = 0 \tag{3.31}$$

$$L_n^{(2)} - \bar{L}_{-n}^{(1)} = 0, \quad W_n^{(2)} - (-1)^{hW}\bar{W}_{-n}^{(1)} = 0 \tag{3.32}$$

The obtained permutation branes are special classes of more general permutation branes discussed e.g. in [67–69].

3.3   Reflection and Transmission

In section 3.1 we have considered the properties of topological and factorizable (also called purely reflective) defects. The notion of topological was somewhat clear from the fact that one can continuously deform the defect line as long as one doesn't cross any field insertions. The notion of purely reflective, nevertheless, was somewhat arbitrary. It, therefore, would be preferable to have a good criterion to distinguish the two cases appart from their gluing conditions. In [49] they introduced the concept of *transmission* $\mathcal{T}$ and *reflection* $\mathcal{R}$ coefficients related to a general conformal interface aligned along the real line. The coefficients are defined by

$$\mathcal{R} = \frac{\langle T^{(1)}\bar{T}^{(1)} + T^{(2)}\bar{T}^{(2)}\rangle_{1|2}}{\langle (T^{(1)} + \bar{T}^{(2)})(\bar{T}^{(1)} + T^{(2)})\rangle_{1|2}}, \tag{3.33}$$

$$\mathcal{T} = \frac{\langle T^{(1)}T^{(2)} + \bar{T}^{(1)}\bar{T}^{(2)}\rangle_{1|2}}{\langle (T^{(1)} + \bar{T}^{(2)})(\bar{T}^{(1)} + T^{(2)})\rangle_{1|2}}. \tag{3.34}$$

$T^{(1)}$ and $\bar{T}^{(1)}$ are inserted at the point iy within the upper half plane, whereas $T^{(2)}$ and $\bar{T}^{(2)}$ are inserted at $-iy$ on the lower half plane. Obviously $\mathcal{T} + \mathcal{R} = 1$. From the definition of the reflection and transmission one now can consider the special cases corresponding to topological and factorizable defects (see [49]). For the case of topological defects the transmission yields $\mathcal{T}_{top} = 1$ and, therefore, $\mathcal{R}_{top} = 0$. This means that a topological defect is purely transmissive, i.e. there is no loss of energy or momentum when crossing the defect line. In contrast the transmission of factorizable interfaces can be calculated to give $\mathcal{T}_{fac} = 0$ from which immediately follows $\mathcal{R}_{fac} = 1$. This confirms the notion of purely reflective since there is no energy or momentum transfer through the defect. General interfaces interpolate between these two extremes, i.e. for a general defect the transmission takes values $\mathcal{T} \in [0,1]$.
Let us consider a simple example namely the free boson interfaces preserving $u(1)^2$ Kac-Moody symmetries. The interface operators between two free boson theories were constructed first in [39, 41]. As usual the interface operator $I_{12} : \mathcal{H}_2 \rightarrow \mathcal{H}_1$ between the two

Hilbert spaces commutes with the Virasoro algebra, i.e.

$$(L_n^1 - \bar{L}_{-n}^1)I_{12} = I_{12}(L_n^2 - \bar{L}_{-n}^2). \tag{3.35}$$

Here the superscript labels the Virasoro generators of the two individual theories. Since tha Virasoro generators for the free boson are quadratic in the modes (see appendix B) the gluing conditions for them have to fulfil [39, 41, 55]

$$\begin{pmatrix} a_n^1 \\ -\bar{a}_{-n}^2 \end{pmatrix} I_{12} = I_{12}\Lambda \begin{pmatrix} a_n^2 \\ -\bar{a}_{-n}^2 \end{pmatrix} \quad \text{for} \quad \Lambda \in O(1,1) \tag{3.36}$$

At this point we are not interested in the explicit form of the defect operators, we will review them in more detail in section 9.1. The transmission of the defect in this case can be related to the gluing matrix and is given by

$$\mathcal{T} = \frac{1}{|\Lambda_{22}|}. \tag{3.37}$$

It has been shown [55] that for d-bosons living on tori the notion of transmission can be generalized to

$$\mathcal{T}_{tori} = \frac{1}{|\det \Lambda_{22}|}, \tag{3.38}$$

where Λ_{22} is now a $d \times d$ matrix.

3.4   More on Fusion of Defects

In this section we want to discuss the fusion of interfaces in more detail. We already encountered in section 3.1 that the fusion is basically the composition of two defects. Here we now want to give a more profound definition of the fusion. Consider, therefore, three possibly different CFTs (CFT$_n$, $n = 1, 2, 3$) and interfaces I_{12} and I_{23}, where I_{ij} maps from CFT$_j$ to CFT$_i$. For the total system we consider the setup as shown in the one-dimensional graphical representation [55] (see figure 3.3) where CFT$_2$ of size δ lies within CFT$_1$ and CFT$_3$.
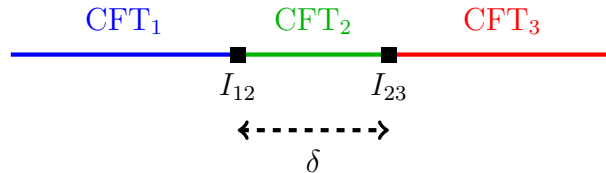
Figure 3.3: Setup for three CFTs and interfaces between them.

Fusion now amounts in taking the limit $\delta \to 0$ (figure 3.4), i.e. shrinking the middle region such that CFT$_1$ and CFT$_3$ are now separated by a new interfaces denoted by $I_{12} \circ I_{23}$ (see [41, 55]).

<div align="center">

CFT$_1$ CFT$_3$

$I_{13} = I_{12} \circ I_{23}$

</div>
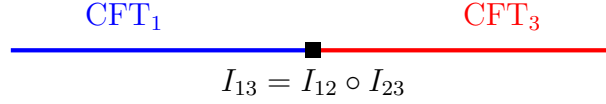
Figure 3.4: Performing the limit $\delta \to 0$. In general this limit is divergent and one has to apply a renormalization scheme, i.e. subtract divergent terms.

Classically the limit is well defined but since we are dealing with quantum theories a regularization is required. This amounts in the 'quantum' definition of the fusion

$$I_{12} \circ I_{23} := \lim_{\delta \to 0} \mathcal{R}_\delta[I_{12} e^{-\delta H_2} I_{23}], \tag{3.39}$$

where $\mathcal{R}_\delta$ denotes the renormalization procedure which can be achieved by local counter terms [41, 55] and H_2 is the Hamiltonian of CFT$_2$. We already know that topological interfaces 'commute' with Virasoro generators of the left and right moving algebra and, therefore, also with the Hamiltonian ($I_{ij}^{top} H_j = H_i I_{ij}^{top}$), i.e. in this case the fusion is simply the composition of interfaces

$$I_{12}^{top} \circ I_{23}^{top} := \lim_{\delta \to 0} \mathcal{R}_\delta[I_{12}^{top} e^{-\delta H_2} I_{23}^{top}] = \lim_{\delta \to 0} \mathcal{R}_\delta \ e^{-\delta H_1}[I_{12}^{top} I_{23}^{top}] = I_{12}^{top} I_{23}^{top}. \tag{3.40}$$

Note that the last equation is also true if only one of the two interfaces is topological.

Apart from fusion interfaces together with each other there is also the possibility to fuse them with a boundary state. Especially in RCFTs it was shown in [44] that the action of a topological defect D_a (3.16) on Cardy boundary states $|B_b\rangle$ (2.166) is straight forward

$$D_a |B_b\rangle = \sum_i \frac{S_{ai}}{S_{0i}} ||i|| \left(\sum_j \frac{S_{bj}}{\sqrt{S_{0j}}} |j\rangle\rangle \right) = \sum_c N_{ab}^c |B_c\rangle, \tag{3.41}$$

where the fusion coefficients arise from the Verlinde formula (2.79). In particular we see that fusion in general results in a superposition of new boundary states.

Chapter 4

Entanglement Entropy

In quantum mechanics a general state is a superposition of eigenstates for an observable $\mathcal{O}$. Performing a measurement of $\mathcal{O}$ on such a superposition state will exhibit randomness in the possible outcomes. For general many-body quantum systems the superposition between various possible configurations often results in correlations between the outcomes of the measurements for different parts of the system. The correlated subsystems are then said to be *entangled*, i.e. the measurement on one system affects the outcome of a measurement on the other system.

The appearing non-local correlations between entangled subsystems caused Einstein to describe entanglement as 'spooky action at a distance' [61]. Bell showed in 1964 (see [62]) these correlations between entangled subsystems have to be inconsistent with reasonable local theories of classical hidden variables.

Nowadays entanglement has far-reaching applications e.g. in computation [63,64], communication [65] and the simulation of physics for strongly correlated systems [66]. Also the concept of entanglement finds applications in many other areas of physics e.g. condensed matter physics [70,71], high energy field theory [78] and even quantum gravity [72–74].

Often entanglement is quantified by the *entropy of entanglement* or for short *entanglement entropy*. Thereby entanglement entropy is a measure of how quantum information is stored in a quantum state.

We will now presume as follows: in the next section we will introduce the mathematical formulation of entanglement and introduce the so called entanglement entropy which will turn out to be a good measure for entanglement [75,76]. We will discuss the concepts for the specific example of two spin-1/2 systems. Afterwards we will introduce the so called replica trick which is a mighty tool for calculating entanglement entropies before in the last part we will consider the formulation of entanglement entropies in terms of twist fields.

4.1 Generalities on Entanglement Entropy

In this section we review the basic concepts regarding entanglement entropy and how it can be calculated. Consider a Hilbert $\mathcal{H}$ space which is divided into two subsystems A

and B such that $\mathcal{H} = \mathcal{H}_A \otimes \mathcal{H}_B$. See for example figure 4.1 as an illustrative example of a one-dimensional chain divided into two subsystems or figure 4.2 for a two-dimensional system.
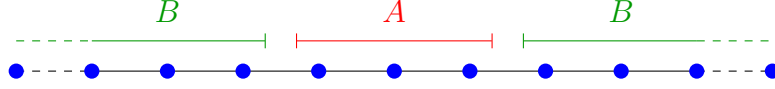
Figure 4.1: One-dimensional quantum chain divided into two subsystems.
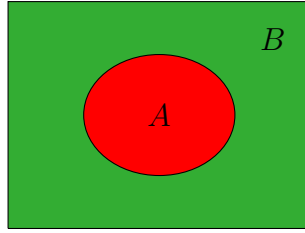
Figure 4.2: Two-dimensional quantum system divided into two subsystems (areas) A and B.

For a given pure state $|\psi\rangle \in \mathcal{H}$ one can define the associated density matrix ρ via

$$\rho = |\psi\rangle \langle\psi| . \tag{4.1}$$

We are now interested in the information coming from the subsystem A (or B), thus we integrate out the degrees of freedom coming from the system B (or A) by taking the partial trace to obtain the reduced density matrix ρ_A (or ρ_B)

$$\rho_A = \text{tr}_{\mathcal{H}_B}\rho \quad (\rho_B = \text{tr}_{\mathcal{H}_A}\rho). \tag{4.2}$$

By tracing out one system we end up in a pure or mixed state for ρ_A depending on the correlations present between the subsystem A and B. To be more precise if there is no correlation between the two subsystems ρ_A corresponds to a pure state and to a mixed state if A and B are correlated.

The *entanglement entropy* (from now on also denoted by EE) is defined as the von-Neumann entropy

$$S_{EE} = -\text{tr}_{\mathcal{H}_A}\rho_A \log \rho_A. \tag{4.3}$$

This entropy gives a good measure for the entanglement between the two subsystems but not for the entanglement of a subsystem with itself. We say that the state $|\psi\rangle$ is entangled if the corresponding EE is bigger than zero, and unentangled if the entropy is zero. This allows us to give an alternative definition of entanglement regarding the decomposition of the state $|\psi\rangle$. Namely a state $|\psi\rangle \in \mathcal{H}$ is called unentangled iff it can be written as

$$|\psi\rangle = |\psi\rangle_A \otimes |\psi\rangle_B , \tag{4.4}$$

where $|\psi\rangle_A \in \mathcal{H}_A$ and $|\psi\rangle_B \in \mathcal{H}_B$. Clearly this is the case if there is no correlation between the two different subsystems. Graphically this can be shown as follows where quantum correlations are illustrated by arrows between different parts[1].
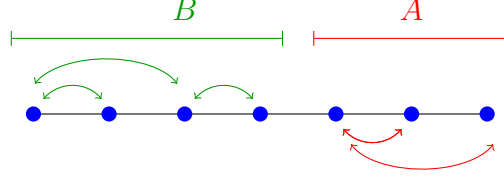
Figure 4.3: Example of a unentangled state $|\psi\rangle = |\psi_A\rangle \otimes |\psi_B\rangle$ with correlations only between the individual subsystems. There are no correlations between states of subsystem A and B (no arrows that connect between A and B). The reduced density matrix $\rho_A = |\psi_A\rangle \langle \psi_A|$ then corresponds to a pure state with vanishing entanglement entropy.

If the state $|\psi\rangle$ cannot be decomposed according to (4.4) it is called an entangled state. Graphically for an entangled state there are correlations between the different subsystems (see figure 4.4).
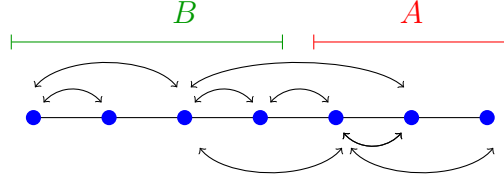
Figure 4.4: Example of an entangled system. The correlations are now not only restricted to the individual subsystems A and B but also range from one subsystem to another.

Example: von-Neumann entropy for a two spin-1/2 system

Consider the following state in a two spin-1/2 system

$$|\psi\rangle = \cos\theta \, |+\rangle_A \, |-\rangle_B + \sin\theta \, |-\rangle_A \, |+\rangle_B \,, \tag{4.5}$$

where we already labelled the states corresponding to the subsystems A and B. We can calculate the reduced density matrix with respect to the system B as

$$\rho_A = tr_{\mathcal{H}_B} |\psi\rangle \langle \psi| =$$

$$_B\langle +|\psi\rangle\langle\psi|+\rangle_B +_B \langle -|\psi\rangle\langle\psi|-\rangle_B =$$

---

[1]Note that we are just interested in the correlations between A and B and not into the correlations (entanglement) of A with itself (respectively B with itself)

$$\cos^2\theta \, |+\rangle_A \langle+|_A + \sin^2\theta \, |-\rangle_A \langle-|_A \, . \tag{4.6}$$

Written as a matrix this is represented as

$$\rho_A = \begin{pmatrix} \cos^2\theta & 0 \\ 0 & \sin^2\theta \end{pmatrix} . \tag{4.7}$$

With this it is now straight forward to calculate the entanglement entropy as

$$S_A = -\mathrm{tr}_{\mathcal{H}_A} \rho_A \log \rho_A =$$

$$-\mathrm{tr} \begin{pmatrix} \cos^2\theta & 0 \\ 0 & \sin^2\theta \end{pmatrix} \log \left[\begin{pmatrix} \cos^2\theta & 0 \\ 0 & \sin^2\theta \end{pmatrix} \right] =$$

$$-\mathrm{tr} \begin{pmatrix} \cos^2\theta & 0 \\ 0 & \sin^2\theta \end{pmatrix} \begin{pmatrix} \log\cos^2\theta & 0 \\ 0 & \log\sin^2\theta \end{pmatrix} =$$

$$- \cos^2\theta \log(\cos^2\theta) - \sin^2\theta \log(\sin^2\theta). \tag{4.8}$$

We see that for $\cos^2\theta = \frac{1}{2}$ the two systems are maximally entangled with $S_A = \log 2$. On the other hand if $\cos^2\theta = 0$ or 1 there is no entanglement $S_A = 0$ and the state $|\psi\rangle$ really takes the form $|\psi\rangle = |\psi\rangle_A \otimes |\psi\rangle_B$ as required for a unentangled state.
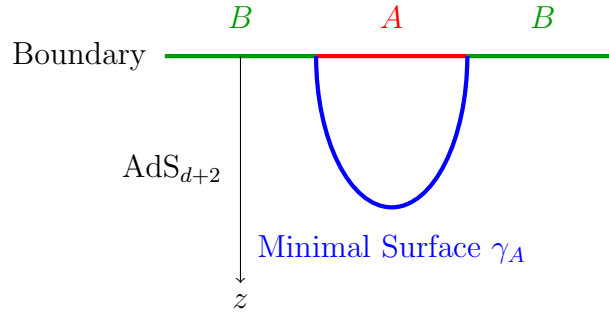
Figure 4.5: Holographic calculation of the entanglement entropy via the calculation of the minimal surface using the AdS/CFT correspondence.

In 2006 very important progress in our understanding of entanglement was made in [73] which goes under the name of *holographic entanglement entropy*. Holographic entanglement links in a beautiful way the study of entanglement to gravity and thermodynamics. Explicitly it was shown using the AdS/CFT correspondence [10] that the entanglement entropy is proportional to the minimal surface γ_A in the bulk of AdS_{d+2} [72](see figure 4.5) where ∂A is the boundary of the region A in CFT_{d+1}, i.e.

$$S_A = \frac{\mathrm{Area}(\gamma_A)}{4G_N^{(d+2)}}, \tag{4.9}$$

where $G_N^{(d+2)}$ is the Newton constant in $d+2$ dimensions.

4.2   The Replica Trick

From now on we will consider a 2d CFT with complex coordinates $z = x + it$, $\bar{z} = x - it$. We want our entangling region A at initial time $t = 0$ to be aligned along the real axis with endpoints u and v (see figure 4.6).
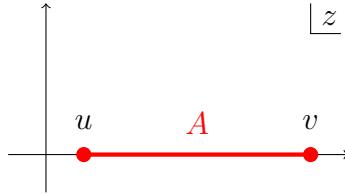
Figure 4.6: Entangling region at $t = 0$.

Often it is too difficult to calculate the von-Neumann entropy (4.3) directly. In order to find an analytic expression for the EE one applies the so called *replica trick* [74, 77–79, 81]. By replicating the sheets and gluing along the cuts A one can calculate the quantity

$$\mathrm{tr}\rho_A^n =: \frac{Z_n}{Z^n}, \; n \in \mathbb{N}. \tag{4.10}$$

Here the trace is now taken over states in the n-sheeted Riemann surface $\mathcal{R}_{N,n}$, where N is the number of intervals, Z_n is the partition function on $\mathcal{R}_{N,n}$ and Z is the partition function on the original sheet. Again $\mathcal{R}_{N,n}$ is the Riemann surface obtained by replicating
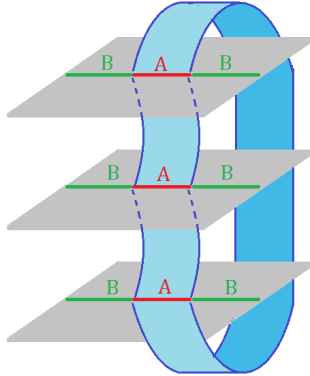
Figure 4.7: Replica trick for $n = 3$. The three sheets are replicated and cyclically sewn together along the interval A.

the original surface n-times and gluing the sheets together along the N intervals. The genus of the surface is $g = (n-1)(N-1)$, i.e. for a single interval $N = 1$ the genus is zero corresponding to the topology of $\mathbb{C}$.

In figure 4.7 we illustrate the procedure for calculating $tr\rho_A^3$ where the sheets are sewn together along the interval A. It is now convenient to introduce the so called *Renyi-entropy* which is defined by

$$S_{Renyi} = \frac{1}{1-n} \log \mathrm{tr}\rho_A^n. \tag{4.11}$$

Experimentally the Renyi-entropy is the only accessible quantity to measure. For example in [36] a setup was proposed for measuring the n-th Renyi entropy. Adopting the notation of the paper n pairs of half chains are arranged in a cross geometry (see figure 4.8). A quantum switch positioned at the centre of the cross controls the way of connection between the two chains. Explicitly for $n = 2$ the two pairs of half chains are connected through the switch by selectively forbidding tunnelling to one of the neighbours. It can be shown that the overlap of the ground states of this configuration (see figure 4.8 left) corresponding to different connections is directly proportional to the n-th Renyi entropy. By studying Rabi oscillations of the quantum switch the Renyi entropy thus can be measured.
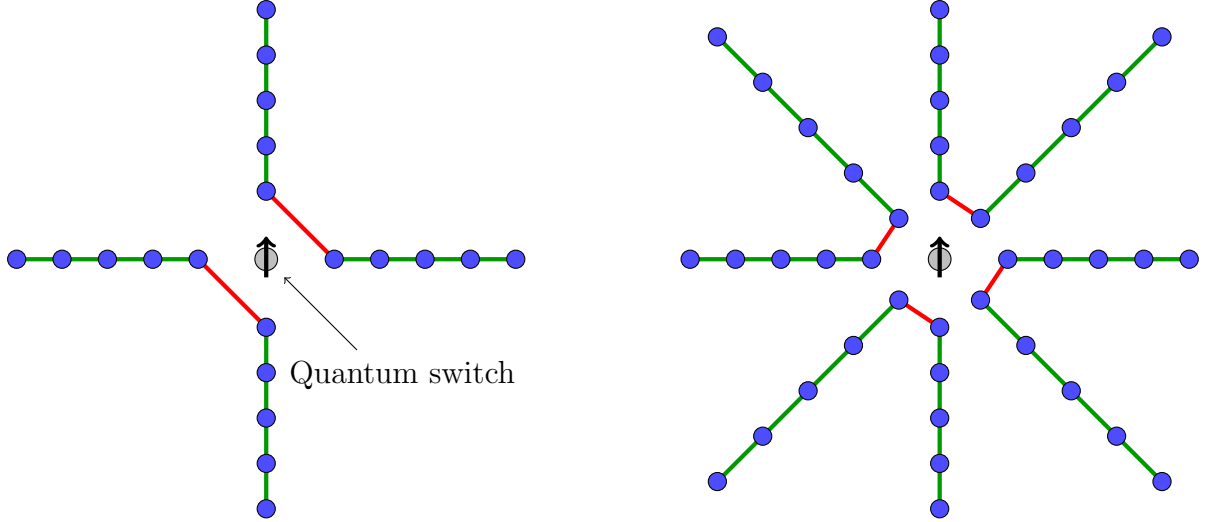
Figure 4.8: Proposal for measuring the n-th Renyi entropy via a cross geometry connected by a quantum switch. The left graph is a proposal for measuring $n = 2$ Renyi entropy. On the right graph is an example for measuring $n = 4$ Renyi entropy.

Having found an expression for the n-th Renyi entropy (4.11) one can analytically continue the expression to $\mathbb{R}^+$. The entanglement entropy is then found by taking the limit

$$S_A = \lim_{n \to 1} \frac{1}{1-n} \log \mathrm{tr}\rho_A^n = (1 - \partial_n) \log \mathrm{tr}\rho_A^n|_{n=1}. \tag{4.12}$$

This means that, instead of calculating the difficult expression (4.3) the problem reduces to the calculation of Renyi entropies, especially in calculating $tr\rho_A^n$. In the next section we will discuss how this quantity can be calculated in the context of two-dimensional CFTs.

4.3 How to Derive $tr\rho_A^n$

In the last section we stated how the entanglement entropy can be derived from the Renyi entropy which basically results in calculating $tr\rho_A^n$ using the replica trick. Here we now want to show how to derive $tr\rho_A^n$. In particular this will lead us to the notion of twist fields that we will discuss in detail in the following section.
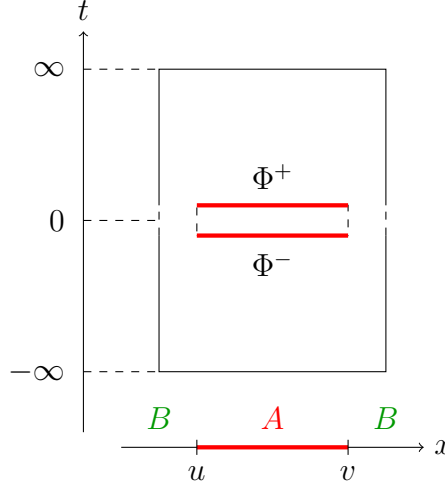
Figure 4.9: Path-integral representation for the reduced density matrix $[\rho_A]_{\Phi_+\Phi_-}$.

The easiest way to derive $tr\rho_A^n$ is using the path-integral formalism. We consider a two dimensional system with Euclidean coordinates $(x, t) \in \mathbb{R}^2$ an assume that the entangling region A is a single interval aligned along the real axis $x \in [u, v]$ at $t = 0$. The ground state wave function ψ of this system can be found by path-integrating from $t = -\infty$ to $t = 0$, i.e.

$$\psi(\Phi(x, t = 0)) = \int_{t=-\infty}^{\Phi(x,t=0)} \mathcal{D}\Phi \; e^{-S(\Phi)}, \tag{4.13}$$

where we denoted by $\Phi(x, t)$ the field defining our CFT. The values of the field $\Phi(x, t)$ at the boundary $t = 0$ depend on the spatial coordinate x. The entries of the total density matrix for this system are then given by

$$[\rho]_{\Phi_0 \Phi_0'} = \psi(\Phi_0)\psi^*(\Phi_0'). \tag{4.14}$$

Here we introduced the shorthand notation $\Phi_0(x) := \Phi(x, t = 0)$. The complex conjugate wave function ψ^* can be obtained in the path-integral formalism by integrating from $t = +\infty$ to $t = 0$. In order to obtain the reduced density matrix ρ_A we need to integrate out the degrees of freedom coming from the subsystem B, i.e. we need to integrate Φ_0 on B assuming $\Phi_0(x) = \Phi_0'(x)$ when $x \in B = \mathbb{R} \setminus [u, v]$. Performing the integration we have for

the entries of the reduced density matrix

$$[\rho_A]_{\Phi^+\Phi^-} = \frac{1}{Z} \int_{t=-\infty}^{t=\infty} \mathcal{D}\Phi \; e^{-S(\Phi)} \prod_{x\in A} \delta(\Phi(x,+0)-\Phi^+(x)) \cdot \delta(\Phi(x,-0)-\Phi^-(x)). \quad (4.15)$$

Here Z is the vacuum partition function added s.t. $tr_{\mathcal{H}_A}\rho_A = 1$. $\Phi^\pm$ are the fields that are obtained by approaching 0 from $t = \pm\infty$ to zero (see figure 4.9).
In order to obtain an expression for $tr\rho_A^n$ we take n copies of $[\rho_A]_{\Phi^+\Phi^-}$, i.e.

$$[\rho_A]_{\Phi_1^+\Phi_1^-}[\rho_A]_{\Phi_2^+\Phi_2^-}\cdots[\rho_A]_{\Phi_n^+\Phi_n^-}, \quad (4.16)$$

and successively take the traces. In the path-integral formalism this is realized by gluing the set of fields according to $\Phi_i^+(x) = \Phi_{i+1}^-(x)$ with $i = 1,\ldots,n-1$ and $\Phi_n^+(x) = \Phi_1^-(x)$, and integrating Φ_i^+. In this way as said before the trace over the replicated reduced density matrix is given in terms of a path-integral on a n-sheeted Riemann surface $\mathcal{R}_n$ via

$$\text{tr}_A\rho_A^n = \frac{1}{Z^n} \int_{(x,t)\in\mathcal{R}_n} \mathcal{D}\Phi \; e^{-S(\Phi)} \equiv \frac{Z_n}{Z^n}. \quad (4.17)$$

For a graphical representation again consider figure 4.7.

4.4 Entanglement Entropy via Twist Fields

The replica trick is a useful tool for the calculation of entanglement entropy, in particular it has been shown in [78] that Z_n/Z^n, for a single entangling interval transforms under conformal transformations like a two point function of primary fields, so called *twist fields* $\mathcal{T}_n$ of lowest conformal dimensions

$$h_n = \bar{h}_n = \frac{c}{24}\left(n - \frac{1}{n}\right), \quad (4.18)$$

living in the orbifold theory $\mathbb{C}^{\otimes n}/\mathbb{Z}_n$ of n replicated sheets. For a single interval one can map the Riemann surface via a uniformizing transformation to the complex plane since the genus of $\mathcal{R}_n$ is one. The twist fields are then inserted at the end points of the gluing interval (see figure 4.10). These fields can be considered a special kind of twist field, called branch-point twist fields [37]. The notion of branch-point twist fields is natural since the twist fields are related to the branch points in the n-sheeted Riemann surface. The twist and adjoint twist field implement in a natural way the cyclic symmetry on the sheets

$$\mathcal{T} : i \to i+1 \bmod n \quad (4.19)$$
$$\bar{\mathcal{T}} : i \to i-1 \bmod n. \quad (4.20)$$

The relation to the trace of the replicated density matrix is then given by

$$\text{tr}\rho_A^n = c_n\langle\mathcal{T}_n(u)\bar{\mathcal{T}}_n(v)\rangle = c_n\left(\frac{v-u}{\epsilon}\right)^{-\frac{c}{6}\left(n-\frac{1}{n}\right)}, \quad (4.21)$$
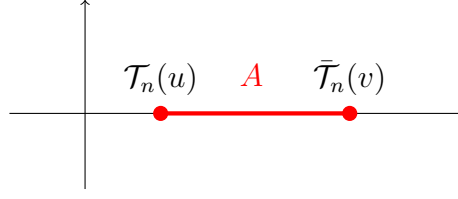
Figure 4.10: Insertion of twist fields at interval end points.

where c_n is a normalization constant with the property $c_1 = 1$ and ϵ is a UV cut-off[2] regularising the limit $v - u \to \epsilon \ll 1$ due to short range correlations between the entangling regions A and B (see figure 4.11).
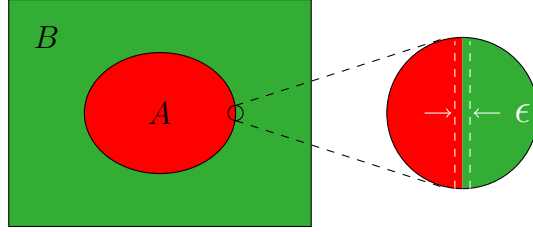
Figure 4.11: Zoomed out example for short range correlations with UV cut-off ϵ.

For the entanglement entropy we then find using (4.12):

$$S = \lim_{n \to 1} \frac{1}{1 - n} \log c_n \left(\frac{v - u}{\epsilon} \right)^{-\frac{c}{6}\left(n - \frac{1}{n}\right)} = \frac{c}{3} \log \frac{l}{\epsilon} - c_1'. \tag{4.22}$$

Here we defined the interval length to be $l = v - u$ and

$$c_1' := \lim_{n \to 1} \frac{1}{n - 1} \log c_n = \frac{\partial \log c_n}{\partial n}\Big|_{n=1}. \tag{4.23}$$

Similarly one obtains the n-sheeted partition function for N disjoint intervals with end points (u_i, v_i) [78], i.e. $A = [u_1, v_1] \cup [u_2, v_2] \cup \cdots \cup [u_N, v_N]$, by inserting the twist and adjoint-twist fields at the corresponding end points (see figure 4.12) and calculate the vacuum expectation value

$$\text{tr}\rho_A^n = c_n^N \langle \mathcal{T}_n(u_1)\bar{\mathcal{T}}_n(v_1) \cdots \mathcal{T}_n(u_N)\bar{\mathcal{T}}_n(v_N) \rangle =$$

$$c_n^N \left| \frac{\prod_{j<i\leq N}(u_i - u_j)(v_i - v_j)}{\prod_{i,j\leq N}(v_i - u_j)} \right|^{\frac{c}{6}\left(n - \frac{1}{n}\right)} \mathcal{F}_{n,N}(\{x\}), \tag{4.24}$$

---

[2]Note that ϵ sets a natural length scale of the system, i.e. for lattice mocels ϵ simply would correspond to the lattice spacing.

where $\{x\}$ is the set of all cross ratios that can be built out of the points u_i, v_j and $\mathcal{F}$ is a function depending on the full operator content of the theory. Note that the $2N$-point function exactly takes the form as mentioned before in section 2.7. For the function $\mathcal{F}$ there exists no general form, i.e. it must be calculated explicitly in each theory considered. The entanglement entropy for the case of N disjoint intervals then takes the form
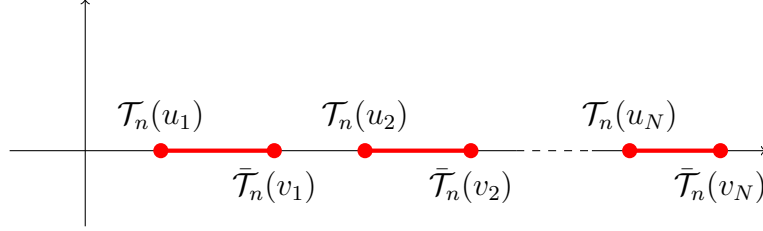
Figure 4.12: Insertion of twist fields at interval end points for several intervals.

$$S_A = \frac{c}{3} \log \left| \frac{\prod_{j<i \leq N}(u_i - u_j)(v_i - v_j)}{\prod_{i,j \leq N}(v_i - u_j)} \right| - Nc_1' - \frac{\mathcal{F}_{1,N}'(\{x\})}{\mathcal{F}_{1,N}(\{x\})}. \tag{4.25}$$

Since the genus for more than one interval is bigger than zero we expected the partition function not only to be a function containing the data of the insertion points, conformal weights of the twist fields and the central charge but also on additional information e.g. fusion coefficients or similar which are encoded in $\mathcal{F}$ [78, 80].

4.5 Mapping to other geometries

So far we have considered our system at zero temperature and infinite size. It would be interesting to calculate the entanglement entropy for other setups. For a single interval it is known [78] that $\mathrm{tr}\rho_A^n$ transforms like a two point function of primary fields $\mathcal{T}_n$ under general conformal transformations. This means that we can easily map to other geometries obtained by a conformal map $z \to w(z)$ as

$$\langle \mathcal{T}_n(z_1, \bar{z}_1)\bar{\mathcal{T}}_n(z_2, \bar{z}_2)\rangle = |w'(z_1)w'(z_2)|^{2h_n} \langle \mathcal{T}_n(w_1, \bar{w}_1)\bar{\mathcal{T}}_n(w_2, \bar{w}_2)\rangle. \tag{4.26}$$

Of special interest is the transformation $z \to w = (\beta/2\pi)\log z$ that maps each sheet in the z-plane to the infinitely long cylinder of circumference β (see figure 4.13) where we have periodic boundary conditions in z along the time axis. The sheets that before were sewn together along the branch cut are now sewn together along a branch cut joining the two images of the points u and v on the cylinder.

By mapping to the cylinder we obtain an expression for $\mathrm{tr}\rho_A^n$ in a thermal mixed state at finite temperature $T = \beta^{-1}$ by arranging the branch cut to lie along the cylinder axis. For
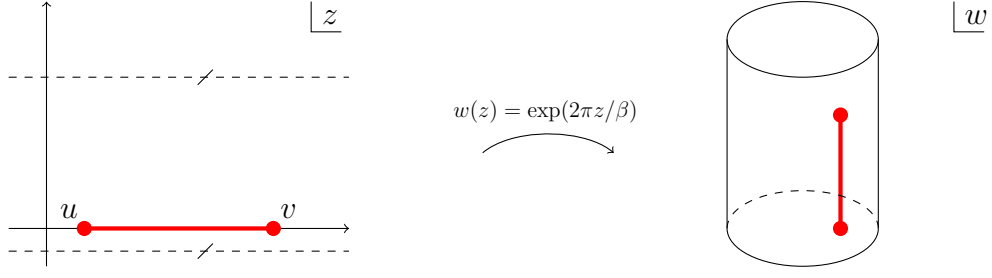
Figure 4.13: Transformation from the complex plane to the infinite cylinder with periodic boundary conditions perpendicular to the cylinder axis.

the entanglement entropy one obtains in this new geometry after some simple algebraic manipulations

$$S_{cyl} = \frac{c}{3} \log \left(\frac{\beta}{\pi \epsilon} \sinh \frac{\pi l}{\beta} \right) - c_1', \tag{4.27}$$

where again $l = v - u$. One can now consider two different limits namely the high temperature limit where $l \gg \beta$ and the zero temperature limit $l \ll \beta$:

$$S = \begin{cases} \frac{c}{3} \log \frac{l}{\epsilon} - c_1' & l \ll \beta \\ \frac{\pi c}{3\beta} l - c_1' & l \gg \beta \end{cases} \tag{4.28}$$

We see that in the zero temperature limit $l \ll \beta$ we exactly recover (4.22).

Orientating the branch cut perpendicularly to the cylinder axis corresponding to the replacement $\beta \to iL$ one obtains an expression for the entanglement entropy for a finite 1D system of length L with periodic boundary conditions at zero temperature (see figure 4.14)

$$S = \frac{c}{3} \log \left(\frac{\pi L}{\epsilon} \sin \frac{\pi l}{L} \right). \tag{4.29}$$

In order to obtain an expression for the entanglement entropy at finite temperature and finite size one has to consider periodic boundary conditions both along and perpendicularly to the cylinder axis. In this case one obtains the topology of a torus.
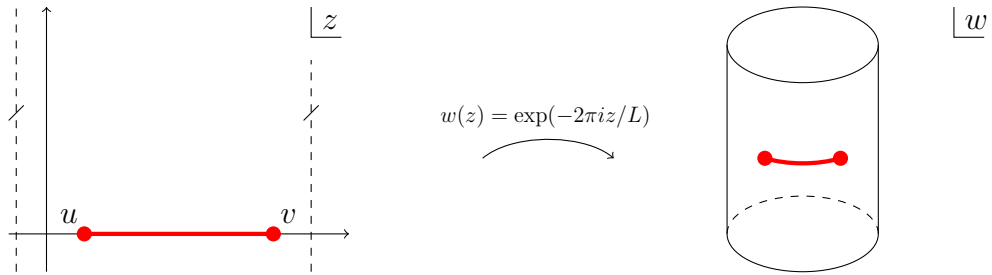
Figure 4.14: Transformation from the complex plane to the infinite cylinder with periodic boundary conditions parallel to the cylinder axis.

4.6   Boundary Entropy

We now review the concept of a boundary entropy first introduced by J. Cardy. In the context of entanglement entropy in two-dimensional CFTs the notion of boundary entropy was introduced [38]. Consider a cylinder of length L and circumference β. The partition function on this cylinder can be thought of as a quantum statistical mechanics partition function for a one-dimensional quantum field theory living on an interval of length L, at the temperature $1/\beta$ [34]. In the thermodynamic limit where L/β is large only the ground state contributes to the partition function since all excited states are exponentially suppressed, i.e.

$$Z_{ij}(L, \beta) \sim \langle i|0\rangle \langle 0|j\rangle e^{\pi c L/6\beta}. \tag{4.30}$$

It is important to realize that $|0\rangle$ is not the boundary state corresponding to the vacuum representation but the ground state of the vacuum representation. Following the standard procedures from statistical mechanics we can deduce that the free energy is

$$F_{ij} = -\frac{1}{\beta} \ln Z_{ij}. \tag{4.31}$$

From this one can derive the associated entropy in leading order

$$S_{ij} = -\beta^2 \partial_\beta F_{ij} = \frac{\pi c}{3\beta} L + s_i + s_j. \tag{4.32}$$

The first term is the usual contribution in the high temperature limit (4.28). The two extra contributions $s_i = \ln\langle i|0\rangle$ and $s_j = \ln\langle j|0\rangle$ can be identified with the boundary entropy related to the two boundary states. Note that $g_i = \langle i|0\rangle$ is nothing but the g-factor associated to a boundary state [38].

Chapter 5

EE for SUSY Twist fields

In this chapter we want to generalize the idea of purely 'bosonic' twist fields $\mathcal{T}_n$ to the supersymmetric case, i.e. we want to construct a supersymmetric version of a twist field, in particular a twist field that saturates a chirality condition between its conformal weight and $U(1)$ charge. We consider the same setup as n the chapter before, i.e. we are considering the twist field $\mathcal{T}_n$ coming from the permutation symmetry. In [86] such a supersymmetric twist field has been constructed for the cases that it is both chiral in the left and right moving sector. Here chiral means the explicit relation between conformal weight and $U(1)$ charge (2.114). We first review the construction of this twist field before we generalize it to other chiralities and apply the supersymmetric twist fields to the calculating SUSY Renyi entropies and the associated entanglement entropies.

5.1 Construction of SUSY Twist Field

5.1.1 Review of SUSY Twist Field Construction

The construction of supersymmetric twist fields is mainly based on [86]. Here we just review the main steps of the construction. We start by considering a $\mathcal{N} = 2$ superconformal field theory with the ordinary 'bosonic' twist field $\mathcal{T}_n$. As discussed before $\mathcal{N} = 2$ SCFT has some very special properties. In Particular, it contains a special class of operators, so called chiral operators (see section 2.12.3) that have the defining equation between their conformal weight h and R-charge R

$$h = \frac{1}{2}R. \tag{5.1}$$

The chiral operators form the *chiral ring* (see section 2.12.4) which controls properties of their correlation functions. As before there exists a second class of operators, so called anti-chiral operators whose defining equation is

$$h = -\frac{1}{2}R. \tag{5.2}$$

Obviously $\mathcal{T}_n$ is not a chiral operator since its conformal weight and R-charge are given by

$$h(\mathcal{T}_n) = h_n = \frac{c}{24}\left(n - \frac{1}{n}\right), \tag{5.3}$$

$$R(\mathcal{T}_n) = 0. \tag{5.4}$$

The idea is to construct a chiral operator S_n out of $\mathcal{T}_n$ which then represents a supersymmetric extension. Therefore, consider a general $\mathcal{N} = (2,2)$ SCFT $\mathcal{M}$ with central charge c. As usual the Renyi entropy of this theory can be derived by studying the cyclic orbifold $\mathcal{M}^n/\mathbb{Z}_n$. The operator of lowest dimension in the $\mathbb{Z}_n$ twisted theory is exactly given by $\mathcal{T}_n$. The $U(1)_R$ current on $\mathcal{M}^n$ is given by

$$J = \sum_{j=1}^{n} J_j, \tag{5.5}$$

where J_j is the $U(1)_R$ current on each individual sheet $\mathcal{M}$. It is straightforward to show that $\mathcal{T}_n$ commutes with J. By defining a canonically normalized scalar field $H(z,\bar{z}) =: H_L(z) + H_R(\bar{z})$ this can be related to the current via

$$J = i\sqrt{\frac{cn}{3}}\partial H. \tag{5.6}$$

It is now interesting to study the properties of a new twist field defined by

$$\mathcal{T}_n(\alpha) = \mathcal{T}_n e^{i\alpha H}. \tag{5.7}$$

The conformal weight and R-charge of this new operator satisfy

$$h(\mathcal{T}_n(\alpha)) = h(\mathcal{T}_n) + \frac{\alpha^2}{2} \tag{5.8}$$

$$R(\mathcal{T}_n(\alpha)) = \alpha\sqrt{n}. \tag{5.9}$$

The idea is now to tune α in such a way that $\mathcal{T}_n(\alpha)$ becomes a chiral operator in order to easily calculate correlation functions using the properties of the chiral ring. This means we want

$$h(\mathcal{T}_n(\alpha)) = \frac{1}{2}R(\mathcal{T}_n(\alpha)) \quad \leftrightarrow \quad \alpha = \alpha_n = \frac{n-1}{2}\sqrt{\frac{c}{3n}}. \tag{5.10}$$

The supersymmetric (chiral) version of the twist field is, therefore, given by

$$S_n := \mathcal{T}_n(\alpha_n) = \mathcal{T}_n e^{i\alpha_n H}. \tag{5.11}$$

Note that the conformal weight of this operator takes the much simpler form

$$h(S_n) = \frac{c}{12}(n-1). \tag{5.12}$$

It is natural to ask if this new twist field really is contained in the spectrum of the orbifolded theory. In [84,85] they show that S_n really is contained in the theory. Thereby they make use of the existence of the spectral flow in the original supersymmetric theory denoted $\mathcal{M}$ and on the orbifolded theory $\mathcal{M}^n/\mathbb{Z}_n$. We will discuss the arguments that show that S_n really is contained in the spectrum of $\mathcal{M}^n/\mathbb{Z}_n$ in detail in chapter 6.

We will now turn back in calculating Renyi and entanglement entropies with this ew field. Given this new operator S_n we can now also generalize the Renyi entropy for general N intervals

$$S_A^{(n)} = \frac{1}{1-n} \log(\mathrm{tr}\rho_A^n), \tag{5.13}$$

with

$$\mathrm{tr}\rho_A^n = c_n \langle \mathcal{T}_n(u_1)\mathcal{T}_n^*(v_1)\cdots\mathcal{T}_n(u_N)\mathcal{T}_n^*(v_N)\rangle, \tag{5.14}$$

to its supersymmetric version, the so called *supersymmetric Renyi entropy* (SRE), by replacing the 'bosonic' twist fields $\mathcal{T}_n$ by their chiral analogous S_n and including an additional normalization constant f_n which in general depends on the chiral structure and is a function of n, i.e.

$$S_A^{(n)}(susy) = \frac{1}{1-n} \log \mathcal{O}_n, \tag{5.15}$$

with

$$\mathcal{O}_n = c_n f_n \langle S_n(u_1)S_n^*(v_1)\cdots S_n(u_N)S_n^*(v_N)\rangle. \tag{5.16}$$

From the SRE one can derive the supersymmetric version of the entanglement entropy performing the usual limit

$$S_A(susy) = \lim_{n\to 1} S_A^{(n)}(susy). \tag{5.17}$$

It turns out that $S_A(susy) = S_A - f_1'$, i.e. the supersymmetric version of the Renyi entropy gives the ordinary entanglement entropy in the limit $n \to 1$ up to an additional constant coming from the additional normalization constant. Nevertheless, the leading order behaviour of $S_A(susy)$ is the same as S_A.

5.1.2 Generalization to Other Chiralities

Following the same ideas as in the previous section it is now straightforward to construct supersymmetric versions of twist fields with other chiralities, by making the ansatz

$$\mathcal{T}_n(\alpha, \epsilon, \bar{\epsilon}) = \mathcal{T}_n e^{i\alpha(\epsilon H_L + \bar{\epsilon} H_R)}, \tag{5.18}$$

with $\epsilon, \bar{\epsilon} \in \{\pm 1\}$. The conformal weight and R-charge of the left and right moving parts satisfy

$$h(\mathcal{T}_n(\alpha, \epsilon, \bar{\epsilon})) = \bar{h}(\mathcal{T}_n(\alpha, \epsilon, \bar{\epsilon})) = h(\mathcal{T}_n) + \frac{\alpha^2}{2} \tag{5.19}$$

$$R_L(\mathcal{T}_n(\alpha, \epsilon, \bar{\epsilon})) = \epsilon\alpha\sqrt{n} \tag{5.20}$$

$$R_R(\mathcal{T}_n(\alpha, \epsilon, \bar{\epsilon})) = \bar{\epsilon}\alpha\sqrt{n} \tag{5.21}$$

The SUSY twist fields which are chiral/antichiral in the holomorphic and anti-holomorphic parts are now given by

$$S_n(z, \bar{z}, \epsilon, \bar{\epsilon}) = \mathcal{T}_n(z, \bar{z}) e^{i\alpha_n(\epsilon H_L(z) + \bar{\epsilon} H_R(\bar{z}))}. \tag{5.22}$$

Especially the chiral (c) and antichiral (a) fields are obtained by giving the variables ($\epsilon, \bar{\epsilon}$) the following values:

$$(c, c) \Leftrightarrow (1, 1) \tag{5.23}$$
$$(c, a) \Leftrightarrow (1, -1) \tag{5.24}$$
$$(a, c) \Leftrightarrow (-1, 1) \tag{5.25}$$
$$(a, a) \Leftrightarrow (-1, -1). \tag{5.26}$$

5.2 Renyi & Entanglement Entropy for Different Chiralities

In this section we want to apply our supersymmetric twist fields of given chiralities to calculate supersymmetric Renyi entropies and associated entanglement entropies. We proceed as follows: first we study the case of a single interval. We will calculate the SRE and entanglement entropy for all possible chiralities. As it is convenient we also consider our system in other geometries. As a next step we will consider the case of several disjoint intervals of different chiralities before discussing in the end systems with boundaries.

5.2.1 Single Interval

Having defined the supersymmetric twist field (5.22) for general chiralities we can calculate the SRE for a single interval. Within the interval the corresponding chirality structure for the left- and right-movers has to be preserved in order not to break SUSY. This means that we want to calculate the NS vacuum expectation value

$$\langle S_n(\epsilon, \bar{\epsilon}; u, \bar{u}) S_n^*(\epsilon, \bar{\epsilon}; v, \bar{v}) \rangle =$$

$$= \langle \mathcal{T}_n(u) \mathcal{T}_n^*(v) \rangle \cdot \langle : e^{i\epsilon\alpha_n H(u) + i\bar{\epsilon}\alpha_n H^*(\bar{u})} :: e^{-i\epsilon\alpha_n H(v) - i\bar{\epsilon}\alpha_n H^*(\bar{v})} : \rangle =$$

$$= |u - v|^{-\frac{c}{6}\left(n - \frac{1}{n}\right)} \cdot |u - v|^{-2\alpha_n^2} = |u - v|^{-4h(S_n)}. \tag{5.27}$$

In our calculation we used some facts on expectation values of vertex operators. For a detailed discussion see appendix A.

We see that the result (5.27) is independent of the choice of $\epsilon, \bar{\epsilon}$ and thus gives the same result for all chiral/antichiral structures. For the trace then holds (including normalization factors):

$$\mathcal{O}_n = \text{tr}\rho^n = c_n f_n(\epsilon, \bar{\epsilon}) |u - v|^{-4h(S_n)}, \tag{5.28}$$

where again c_n is the usual 'bosonic' normalization corresponding to the twist field $\mathcal{T}_n$ and $f_n(\epsilon, \bar{\epsilon})$ accounts for the additional 'fermionic' contribution realized by the vertex operator. For the SRE we thus find

$$S_{SUSY}^{(n)} = \frac{c}{3} \log |u - v| - \frac{\log c_n}{n-1} - \frac{\log f_n(\epsilon, \bar{\epsilon})}{n-1}. \tag{5.29}$$

We see that the leading term contribution to the Renyi entropy is constant for any number of sheets n in the $\mathbb{Z}_n$ twisted theory. This is in contrast with the pure bosonic case where the leading term also depends on the number of sheets (4.21) and the leading term approaches $\frac{c}{3} \log |v - u|$ just in the limit $n \to 1$. The supersymmetric version of the entanglement entropy then follows by taking the limit $n \to 1$ of the SRE, i.e.

$$S(susy) = \frac{c}{3} \log |u - v| - c_1' - f_1'(\epsilon, \bar{\epsilon}) \tag{5.30}$$

where c_1' and $f_1'(\epsilon, \bar{\epsilon})$ are the first derivatives with respect to n evaluated at $n = 1$. Comparing this result to the usual case (just bosonic twist field (4.22)) we see that the results agree up to an additional constant $-f_1'(\epsilon, \bar{\epsilon})$ coming from the fermionic extension.

5.2.2 Single Interval SUSY Renyi Entropy and EE in Other Geometries

Since $\langle S_n(\epsilon, \bar{\epsilon}; u, \bar{u}) S_n^*(\epsilon, \bar{\epsilon}; v, \bar{v}) \rangle$ also transforms like a two point function of 'bosonic' and 'fermionic' twist fields separately we can easily map to other geometries. For example we can map to the infinite cylinder with circumference β via $w = \exp(2\pi z/\beta)$, i.e. we are considering the system at finite temperature $T = 1/\beta$. For the SRE we, therefore, obtain in the cylinder geometry

$$S_{cyl}^{(n)}(susy) = \frac{c}{3} \log \left(\frac{\beta}{\pi} \sinh \frac{\pi l}{\beta} \right) - \frac{\log c_n}{n-1} - \frac{\log f_n(\epsilon, \bar{\epsilon})}{n-1}. \tag{5.31}$$

The mapping is shown in figure 5.1.
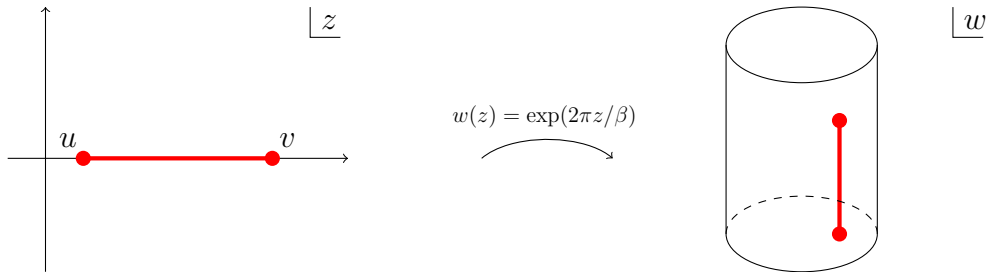
Figure 5.1: Transformation from the complex plane to the infinite cylinder with periodic boundary conditions perpendicular to the cylinder axis.

As usual one can consider the low and high temperature limits where $\beta \gg l$ or $\beta \ll l$, i.e.

$$
S_{cyl}^{(n)}(susy) = \begin{cases} \frac{c}{3} \log l - \frac{\log c_n}{n-1} - \frac{\log f_n}{n-1} & \text{for } \beta \gg l \\ \frac{c}{3} \frac{\pi l}{\beta} - \frac{\log c_n}{n-1} - \frac{\log f_{n,1}}{n-1} & \text{for } \beta \ll l \end{cases} \tag{5.32}
$$

For the SUSY EE we, therefore, obtain in the given limits

$$
S_{SUSY,cyl} = -c_1' - f_1'(\epsilon, \bar{\epsilon}) + \begin{cases} \frac{c}{3} \log l & \text{for } \beta \gg l \\ \frac{c\pi l}{3\beta} & \text{for } \beta \ll l \end{cases} \tag{5.33}
$$

Analogously we can map to a finite size interval of length L with periodic boundary conditions via $w = \exp(2\pi i z/L)$ (see figure 5.2). In this geometry the Renyi entropy is

$$
S_{finite}^{(n)}(susy) = \frac{c}{3} \log \left(\frac{L}{\pi} \left| \sin \frac{\pi l}{L} \right| \right) - \frac{\log c_n}{n-1} - \frac{\log f_1(\epsilon, \bar{\epsilon})}{n-1}. \tag{5.34}
$$
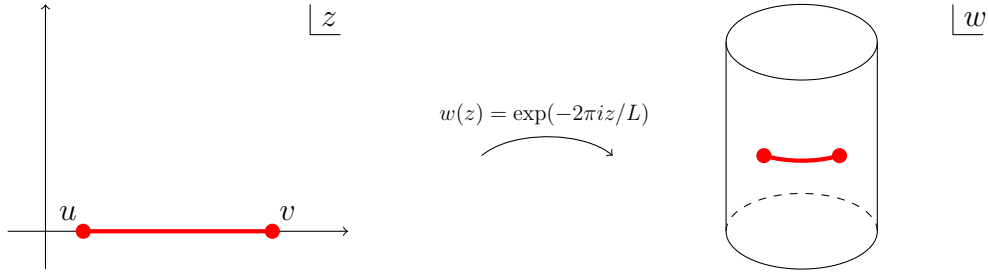
Figure 5.2: Transformation from the complex plane to the infinite cylinder with periodic boundary conditions parallel to the cylinder axis.

Again performing the limit $n \to 1$ we find for the SUSY EE

$$
S_{finite}(susy) = -c_1' - f_1'(\epsilon, \bar{\epsilon}) + \begin{cases} \frac{c}{3} \log l & \text{for } L \gg l \\ \log l + \log \left(\frac{1}{\pi} \left(1 - \frac{l}{L} \right) \right) & \text{for } L \approx l \end{cases} \tag{5.35}
$$

Note that in all cases we omitted the UV cut-off which we called ϵ in (4.22). Further we see that leading order terms of the SREs are again constant and the results for the EE in the different geometries match with the pure 'bosonic' case [78] up to an additional constant $-f_1'(\epsilon, \bar{\epsilon})$.

5.2.3   Several Intervals

In this section we now want to consider the case of several disjoint intervals

$$
A = [u_1, v_1] \cup \cdots \cup [u_N, v_N], \tag{5.36}
$$

where we assume the intervals to be ordered by $u_i < v_i < u_j < v_j \ \forall i < j$. Within each interval the associated chiral/antichiral structure has to be preserved to preserve SUSY. We are thus interested in the quantity

$$\langle \prod_{j=1}^{N} S_n(u_j, \bar{u}_j, \epsilon_j, \bar{\epsilon}_j) S_n^*(v_j, \bar{v}_j, \epsilon_j, \bar{\epsilon}_j) \rangle, \tag{5.37}$$

with $\epsilon_j, \bar{\epsilon}_j \in \{\pm 1\}$ the chiralities/antichiralities in each interval. Again it is possible to decompose this expectation value into a part containing the 'bosonic' twist fields and another containing the 'fermionic' twist fields.

The contribution associated to the 'bosonic' twist fields $\mathcal{T}_n$ is given by

$$\langle \mathcal{T}_n(u_1) \mathcal{T}_n^*(v_1) \cdots \mathcal{T}_n(u_N) \mathcal{T}_n^*(v_N) \rangle =$$
$$\left(\frac{\prod_{j<k}(u_k - u_j)(v_k - v_j)}{\prod_{j,k}(v_k - u_j)} \right)^{4h(\mathcal{T}_n)} \mathcal{F}_{n,N}(\{x\}). \tag{5.38}$$

Here $\mathcal{F}_{n,N}(\{x\})$ is a function of all cross ratios x and explicitly depends on the full operator content of the theory. This in particular means that $\mathcal{F}_{n,N}(\{x\})$ has to be calculated for each case separately (see [78]).

The contribution from the vertex operators reads

$$\langle \prod_{j=1}^{N} : e^{i\alpha_n(\epsilon_j H_L(u_j) + \bar{\epsilon}_j H_R(\bar{u}_j))} :: e^{-i\alpha_n(\epsilon_j H_L(v_j) + \bar{\epsilon}_j H_R(\bar{v}_j))} : \rangle =$$
$$\left(\frac{\prod_{j<k}[(u_k - u_j)(v_k - v_j)]^{\epsilon_j \epsilon_k + \bar{\epsilon}_j \bar{\epsilon}_k}}{\prod_{j,k}(u_k - v_j)^{\epsilon_j \epsilon_k + \bar{\epsilon}_j \bar{\epsilon}_k}} \right)^{\frac{c}{12}\frac{1-n}{n}}. \tag{5.39}$$

Using the identity

$$\sum_{i,j} = 2\sum_{i<j} + \sum_{i,j} \delta_{i,j}, \tag{5.40}$$

we, therefore, obtain an expression for the SRE

$$S_A^{(n)}(susy) = \frac{N \log c_n + \log f_n(\{\epsilon, \bar{\epsilon}\}) + \log \mathcal{F}_{n,N}(\{x\})}{1-n} +$$
$$+ \frac{c}{3} \sum_{i=1}^{N} \log|v_i - u_i| + \frac{c}{6} \sum_{j>i=1}^{N} \left(\frac{n+1}{n} + \frac{n-1}{2n}(\epsilon_i \epsilon_j + \bar{\epsilon}_i \bar{\epsilon}_j) \right) \log \frac{|v_j - u_i|^2}{|u_j - u_i| \cdot |v_j - v_i|}. \tag{5.41}$$

In this form we learn that the SRE of several intervals decomposes into the sum of SREs of single intervals

$$\frac{c}{3} \sum_{i=1}^{N} \log|v_i - u_i|, \tag{5.42}$$

up to a part containing the information about the cross-entangling between the individual intervals

$$\frac{c}{6}\sum_{j>i=1}^{N}\left(\frac{n+1}{n}+\frac{n-1}{2n}(\epsilon_i\epsilon_j+\bar{\epsilon}_i\bar{\epsilon}_j)\right)\log\frac{|v_j-u_i|^2}{|u_j-u_i|\cdot|v_j-v_i|}. \tag{5.43}$$

Explicitly we see that the sum over the single intervals is independent of the choice for the chiralities (exactly as we discovered before). Note that for N intervals $c_{n,N}=c_n^N$ holds. In contrast to the single interval case, the total SRE now explicitly depends on the choice of the $\epsilon_i,\bar{\epsilon}_i$. In the single interval case the leading order term in the SRE is independent of the number of sheets n. This is no longer the case for several intervals but again the additional contributions coming from the 'fermionic' extension drop in the limit $n\to 1$ reproducing the results found in [78] up to an additional constant, i.e.

$$S_A(susy)=\lim_{n\to 1}S_A^{(n)}(susy)=-Nc_1'-f_1'(\{\epsilon,\bar{\epsilon}\})-\frac{\mathcal{F}_{1,N}'(\{x\})}{\mathcal{F}_{1,N}(\{x\})}+$$

$$+\frac{c}{3}\sum_{i=1}^{N}\log|v_i-u_i|+\frac{c}{3}\sum_{j>i=1}^{N}\log\frac{|v_j-u_i|^2}{|u_j-u_i|\cdot|v_j-v_i|}. \tag{5.44}$$

5.2.4   SUSY Renyi & EE for R Vacua

So far we have calculated the SRE as NS-sector vacuum expectation values of supersymmetric twist fields. In this section we calculate the SUSY entropies via R-sector vacua expectation values. Therefore, we start with the NS vacuum in the $\mathbb{Z}_n$ twisted theory and spectral flow to the Ramond ground states

$$|0,0\rangle_{NS}\to|\frac{nc}{24},\pm\frac{nc}{6}\rangle_R=\lim_{t\to-\infty}e^{\pm i\beta_n H(x+it,x-it)}|0,0\rangle_{NS}=\lim_{t\to\infty}e^{\pm i\beta_n H(x-it,x+it)}|0,0\rangle_{NS},$$
$$\tag{5.45}$$

where $\beta_n=\sqrt{nc/12}$. Note that in the limit $t\to-\infty$ the insertion coordinate x is basically irrelevant thus we can set it to zero $x=0$ without loss of generality.

For the adjoint ground states one finds

$$_R\langle\frac{nc}{24},\mp\frac{nc}{6}|=\lim_{t\to\infty}{}_{NS}\langle 0,0|e^{\mp i\beta_n H(it,-it)}|2t|^{2\beta_n^2}. \tag{5.46}$$

Here the factor $|2t|^{2\beta_n^2}$ comes from the fact that we normalize the R-sector ground states to one, i.e.[1]

$$_R\langle\frac{nc}{24},\mp\frac{nc}{6}|\frac{nc}{24},\pm\frac{nc}{6}\rangle_R=1. \tag{5.47}$$

---

[1]In $\mathcal{N}=2$ theories with moduli the correlation function $_R\langle 0|0\rangle_R=\exp(-K)$ is an interesting function on the moduli space, where K is the Kähler potential. This means it is crucial that we choose the ground states to be normalized.

Alternatively one could define the normalized Ramond vacuum right away by

$$|\frac{nc}{24}, \pm\frac{nc}{6}\rangle_R := 2^{\beta_n} \lim_{t\to-\infty} e^{\pm i\beta_n H(x+it,x-it)} |0,0\rangle_{NS} \tag{5.48}$$

We now proceed in calculating the associated Renyi entropy in the Ramond vacuum for a single entangling interval. The result can easily be generalized to several intervals. For the single interval in the R-sector we find for the expectation value

$$\langle\frac{nc}{12}, \mp\frac{nc}{6}| S_n(u)S_n^*(v) |\frac{nc}{12}, \pm\frac{nc}{6}\rangle =$$

$$= \langle T_n(u)T_n^*(v)\rangle\cdot$$

$$\cdot \lim_{t'\to\infty} |t'|^{2\beta_n^2} \langle: e^{\mp i\beta_n H(it',-it')} :: e^{i\alpha_n H(u+it,u-it)} :: e^{-i\alpha_n H(v+it,v-it)} :: e^{\pm i\beta_n H(-it',it')} :\rangle =$$

$$= |u-v|^{-4h(S_n)}. \tag{5.49}$$

We see that for both vacua we get the same result. Since both Ramond vacua contribute equally to the entropy the right identification for the trace of the n-sheeted density matrix in the Ramond sector reads

$$\mathrm{tr}\rho_{A,R}^n = c_n f_n(\epsilon, \epsilon) \sum_{\lambda=\pm 1} \langle\frac{nc}{12}, -\lambda\frac{nc}{6}| S_n(u)S_n^*(v) |\frac{nc}{12}, \lambda\frac{nc}{6}\rangle =$$

$$2c_n f_{n,1} |v-u|^{-4h(S_n)}. \tag{5.50}$$

For the SRE in Ramond vacua we thus find

$$S_{SUSY,R}^{(n)} = \frac{4h(S_n)}{n-1} \log|u-v| - \frac{\log c_n}{n-1} - \frac{\log f_{n,1}}{n-1} + \log 2 = S_{SUSY,NS}^{(n)} + \log 2. \tag{5.51}$$

We see that compared to the result for the NS-vacuum we have an additional term $\log 2$. This term can be identified with the logarithm of the number of Ramond ground states[2]. Similar considerations can be made for the cases of different chiralities and several intervals and the results will always take the form

$$S_{SUSY,R}^{(n)}(\{\epsilon, \bar{\epsilon}\}) = S_{SUSY,NS}^{(n)}(\{\epsilon, \bar{\epsilon}\}) + \log 2. \tag{5.52}$$

5.3   Systems with Boundaries

Let us now consider the case of a system bounded from one side by a boundary. On the boundary we have consistency conditions in which fields may appear. In $\mathcal{N} = 2$ superconformal field theories there exist two type of boundaries A- and B-type. For A-type boundaries the charges of left- and right-movers have to fulfil $q - \bar{q} = 0$ whereas for

---

[2]Note that the number of Ramond ground states depends strongly on the theory under consideration, i.e. usually it is not equal 2 (see e.g. $\mathcal{N} = 2$ minimal models with $k + 1$ different Ramond ground states.

B-type boundaries they satisfy $q + \bar{q} = 0$. In the case of our supersymmetric twist field $S(u, u, \epsilon, \bar{\epsilon})$ the charges of left- and right-movers are proportional to ϵ and $\bar{\epsilon}$ (5.20)-(5.21). We take the boundary to run along the imaginary axis and our fields to live on the right half plane (see figure 5.3). Thus for A-type boundaries only twist fields with $S(l, l, \epsilon, \epsilon)$ ending on the boundary are allowed whereas for B-type boundaries only $S(l, l, \epsilon, -\epsilon)$ contributes. Explicitly this means that (c, c) and (a, a) fields couple to A-type boundaries whereas (a, c) and (c, a) fields couple to B-type boundaries. In the following we are interested in calculating the SRE and EE for a single interval in the presence of such a boundary. Thereby we will distinguish the cases of the interval ending on the boundary from that of the interval being separated from the boundary by a distance x.

5.3.1 Entangling Region Ending on Boundary

In the first case we are interested in the entangling region ending on the boundary (figure 5.3). As said before depending on the boundary only the twist fields with the correct chiral structure contribute.
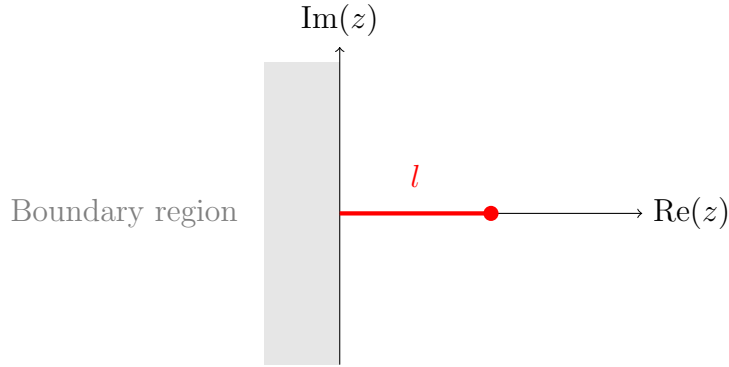
Figure 5.3: Entangling region ending on a boundary.

In order to calculate the upper diagram we have to insert a single twist field at $z = \bar{z} = l$. For the case where one just considers $\mathcal{T}_n$ the calculation has been performed in [78]. Note that we do not need a twist field insertion at $z = 0$ due to our choice of geometry. We thus want to calculate

$$\mathrm{tr}\rho^n = \langle \mathcal{B}_n| S_n(l, l, \epsilon, \bar{\epsilon}) |0\rangle = \langle \mathcal{B}_n|0\rangle \langle 0| S_n(l, l, \epsilon, \bar{\epsilon}) |0\rangle_{RHP} =:$$

$$g_{\mathcal{B}}^{(n)} c_n^{1/2} f_n^{1/2}(\epsilon, \bar{\epsilon})(2l)^{-2h(S_n)} \delta_{\mathcal{B},(\epsilon,\bar{\epsilon})}, \tag{5.53}$$

where $\delta_{\mathcal{B},(\epsilon,\bar{\epsilon})}$ is understood to be non-zero iff the chiralities fulfil the boundary conditions. Here $\mathcal{B}_n$ is the boundary state in the n-times replicated theory mapped by a uniformizing transformation to $\mathbb{C}$. In our calculation we applied Cardy's doubling trick in order to evaluate the one-point function on the right half-plane via a two point function of only holomorphic operators on the whole complex plane. This leads to an total interval length of $2l$, instead of just l. The normalization constants are simply the square roots of the

usual constants since we just have a single twist field insertion and $g_{\mathcal{B}}^{(n)} = \langle \mathcal{B}_n | 0 \rangle$ is the g-factor of the replicated boundary state.

Assuming that our twist field is compatible with the boundary conditions we find for the SRE

$$S_A^{(n)} = \frac{c}{6} \log(2l) - \frac{1}{2} \frac{\log c_n}{n-1} - \delta_{\mathcal{B},(\epsilon,\bar{\epsilon})} \frac{1}{2} \frac{f_n(\epsilon,\bar{\epsilon})}{n-1} - \frac{g_{\mathcal{B}}^{(n)}}{n-1}. \tag{5.54}$$

Taking the limit $n \to 1$ we obtain the supersymmetric entanglement entropy as

$$S_A = \frac{c}{6} \log(2l) - \frac{c_1'}{2} - \delta_{\mathcal{B},(\epsilon,\bar{\epsilon})} \frac{f_1'(\epsilon,\bar{\epsilon})}{2} + \log g_{\mathcal{B}}, \tag{5.55}$$

where $g_{\mathcal{B}} = |\langle 0 | \mathcal{B} \rangle|$ is the g-factor associated to the boundary in the unreplicated theory. In particular the result shows us that the prefactor of the leading order term is one half of the one we find in the case of no boundary. This reflects nothing but the area law. Further we reproduce the results obtained in [78] up to an additional constant coming from the 'fermionic' normalization. Note that we have omitted the UV cut-off in the leading order term.

5.3.2 Entangling Region Away From the Boundary

Next we want to calculate the SRE and supersymmetric EE for the case that we again have a boundary aligned along the imaginary axis, where the entangling region of length l is away from the boundary by some distance x (see figure 5.4)
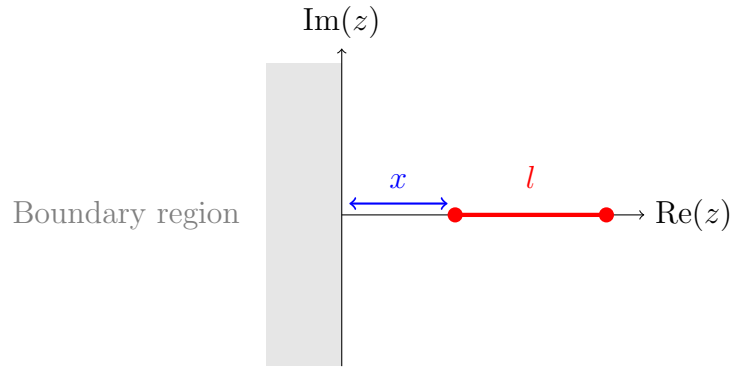
Figure 5.4: Entangling region away from the boundary.

Since our entangling region is not ending on the boundary we need to insert a twist field and an adjoint twist field at $u = x$ and $v = x + l$. For the trace of the replicated theory we thus find

$$\text{tr}\rho^n = c_n f_n(\epsilon,\bar{\epsilon}) \langle \mathcal{B}_n | S_n(x,x,\epsilon,\bar{\epsilon}) S_n^*(x+l,x+l,\epsilon,\bar{\epsilon}) | 0 \rangle =$$

$$c_n f_n(\epsilon,\bar{\epsilon}) \langle \mathcal{B}_n | e^{x(H_n - \frac{nc}{12})} | 0 \rangle \langle 0 | S_n(x,x,\epsilon,\bar{\epsilon}) S_n^*(x+l,x+l,\epsilon,\bar{\epsilon}) | 0 \rangle_{RHP} =$$

$$c_n f_n(\epsilon,\bar{\epsilon}) \langle \mathcal{B}_n | 0 \rangle \langle 0 | S_n(x,x,\epsilon,\bar{\epsilon}) S_n^*(x+l,x+l,\epsilon,\bar{\epsilon}) | 0 \rangle_{RHP}. \tag{5.56}$$

For the vacuum expectation value on the right half plane we find using the Cardy doubling trick

$$\langle 0 | S_n(x, x, \epsilon, \bar{\epsilon}) S_n^*(x + l, x + l, \epsilon, \bar{\epsilon}) | 0 \rangle_{RHP} = \delta_{\mathcal{B},(\epsilon,\bar{\epsilon})} \left(\frac{2xl^2(2x + 2l)}{(2x + l)^2} \right)^{-2h(S_n)} \tilde{\mathcal{F}}_{n,1}(x, l).$$

(5.57)

Here as in the case with no boundary we obtain a function $\tilde{\mathcal{F}}$ of all cross ratios which has to be calculated for each individual case. The SRE is thus given by

$$S_A^{(n)} = \frac{c}{6} \log \left(\frac{4xl^2(x + l)}{(2x + l)^2} \right) - \frac{\log c_n}{n - 1} - \delta_{\mathcal{B},(\epsilon,\bar{\epsilon})} \frac{\log f_n(\epsilon, \bar{\epsilon})}{n - 1} - \frac{\log \tilde{\mathcal{F}}_{n,1}(x, l)}{n - 1} - \frac{\log g_{\mathcal{B}}^{(n)}}{n - 1}. \quad (5.58)$$

The supersymmetric entanglement entropy can thus be found in the usual manner and takes the form

$$S_A(x, l) = \frac{c}{6} \log \left(\frac{4xl^2(x + l)}{(2x + l)^2} \right) - c_1' - \delta_{\mathcal{B},(\epsilon,\bar{\epsilon})} f_1'(\epsilon, \bar{\epsilon}) - \frac{\tilde{\mathcal{F}}_{1,1}'(x, l)}{\tilde{\mathcal{F}}_{1,1}(x, l)} + \log g_{\mathcal{B}}. \quad (5.59)$$

Considering the case $x \to \infty$, i.e. when our entangling interval is far away from the boundary we find

$$\lim_{x \to \infty} S_A(x, l) = \frac{c}{3} \log l - c_1 - \delta_{\mathcal{B},(\epsilon,\bar{\epsilon})} f_1'(\epsilon, \bar{\epsilon}) - \lim_{x \to \infty} \frac{\tilde{\mathcal{F}}_{1,1}'(x, l)}{\tilde{\mathcal{F}}_{1,1}(x, l)} + \log g_{\mathcal{B}}. \quad (5.60)$$

We see that in this setup the leading order behaves like the one of a free theory, i.e. without boundary (5.30). In this way one is able to match the expressions for the subleading contributions i.e. in that limit we can relate the boundary entropy to the functions of cross ratios as

$$\log g_{\mathcal{B}} = \lim_{x \to \infty} \frac{\tilde{\mathcal{F}}_{1,1}'(x, l)}{\tilde{\mathcal{F}}_{1,1}(x, l)}. \quad (5.61)$$

Chapter 6

SUSY Twist Fields

In the last chapter we constructed the supersymmetric version of a twist field. Nevertheless, as we know from section 4.4 these twist fields have to live in the orbifold theory $\mathcal{M}^n/\mathbb{Z}_n$. It is thus natural to ask if our new twist field S_n is really contained in the spectrum of $\mathcal{M}^n/\mathbb{Z}_n$. This is similar to the question if one can find a field in the the 'mother' theory $\mathcal{M}$ that becomes S_n in $\mathcal{M}^n/\mathbb{Z}_n$. We will see that S_n really is contained in the spectrum of $\mathcal{M}^n/\mathbb{Z}_n$ and can be constructed from the vacuum in $\mathcal{M}$. Thereby one has to demand the existence of spectral flow in both $\mathcal{M}$ and $\mathcal{M}^n/\mathbb{Z}_n$.

6.1 State content of the SUSY twist operators

For this section we first review the results for the chiral spectrum of symmetric products [84, 85]. Starting with a supersymmetric (chiral) theory $\mathcal{M}$ with fields of conformal weight h and R-charge R, there is an operator in the $\mathbb{Z}_n$ twisted sector $\mathcal{M}^n/\mathbb{Z}_n$ with weight and R-charge given by

$$twist: \qquad h^n = \frac{h}{n} + \frac{c}{24}\frac{n^2 - 1}{n}, \quad R^n = R. \qquad (6.1)$$

Here we use the notation where we denote conformal weights and R-charges in the twisted sector by h^n and R^n. This has not to be confused with the n-th power of the conformal weight and R-charge of a field in $\mathcal{M}$.

From (6.1) we see that the conformal weight transforms in a non-trivial way whereas the charge remains invariant under twisting.

In the paper [84] they provide a procedure for mapping a chiral state to the $\mathbb{Z}_n$ twisted sector using the spectral flow (2.124) via

$$h_{NS} = \frac{R_{NS}}{2}, \ R = R_{NS} \qquad\qquad h_{NS}^n = \tfrac{1}{2}R_{NS} + \tfrac{c}{12}(n-1), \ R_{NS}^n = R_{NS} + \tfrac{c}{6}(n-1)$$

$$\left. \eta=\tfrac{1}{2} \right\downarrow \qquad\qquad\qquad\qquad\qquad\qquad \left\uparrow \eta=-\tfrac{1}{2} \right.$$

$$h_R = \tfrac{c}{24}, \ R_R = R_{NS} - \tfrac{c}{6} \xrightarrow[twist]{} h_R^n = \tfrac{nc}{24}, \ R_R^n = R_{NS} - \tfrac{c}{6}$$

Here R and NS in the indices label the Ramond and Niveau-Schwarz sector and η corresponds to the spectral flow (2.124). The left side of the diagram corresponds to a single theory $\mathcal{M}$ where we apply the spectral flow of $\mathcal{M}$. By 'twist' we exactly mean the operation that transforms conformal weights and R-charges of $\mathcal{M}$ to conformal weights and R-charges in the twisted sector by (6.1). The right hand side of the diagram then is understood to live in $\mathcal{M}^n/\mathbb{Z}_n$. We will use this convention for all following diagrams.

A similar manipulation, following the same arguments, can also be done for anti-chiral states, i.e.

$$h_{NS} = -\frac{R_{NS}}{2}, \ R = R_{NS} \qquad\qquad h_{NS}^n = -\frac{1}{2}R_{NS} + \frac{c}{12}(n-1), \ R_{NS}^n = R_{NS} - \frac{c}{6}(n-1)$$

$$\left. \eta=-\frac{1}{2} \right\downarrow \qquad\qquad\qquad\qquad\qquad\qquad\qquad \uparrow \eta=\frac{1}{2}$$

$$h_R = \frac{c}{24}, \ R_R = R_{NS} + \frac{c}{6} \xrightarrow{\quad twist \quad} h_R^n = \frac{nc}{24}, \ R_R^n = R_{NS} + \frac{c}{6}$$

Note that in contrast to the chiral states the spectral flows run in opposite directions.

After this short review we turn back to the paper by Giveon and Kutasov [86]. There they construct the SUSY twist operator in the $\mathcal{M}^n/\mathbb{Z}_n$ theory using the chirality condition for the NS-sector. For the chiral case the weight and charge are given by

$$h(S_n) = \frac{1}{2}R(S_n) = \frac{c}{12}(n-1) \ \leftrightarrow \ h_{NS}^n = \frac{1}{2}R_{NS}^n. \tag{6.2}$$

Comparing to the first commutative diagram we can determine the conformal weight and charge of the associated field in $\mathcal{M}$

$$h_{NS} = 0 = R_{NS}, \tag{6.3}$$

thus corresponding to a NS ground state (vacuum).

By similar considerations, using the second diagram, we can determine the weight and charge for an anti-chiral twist with

$$h(\bar{S}_n) = -\frac{1}{2}R(\bar{S}_n) = \frac{c}{12}(n-1), \tag{6.4}$$

leading to

$$h_{NS} = 0 = R_{NS}, \tag{6.5}$$

which is identical to the chiral state.

The following diagram concludes the possible ways to construct a (anti-)chiral state from the field with weight and R-charge $(0,0)$

$$\left(\tfrac{c}{24}, -\tfrac{c}{6}\right) \xrightarrow{\quad twist \quad} \left(\tfrac{nc}{24}, -\tfrac{c}{6}\right)$$

$$\Big\downarrow \eta = -\tfrac{1}{2}$$

$$\left(\tfrac{c}{12}(n-1), \tfrac{c}{6}(n-1)\right) \quad chiral$$

$$\Big\downarrow \eta = \tfrac{n-1}{n}$$

$$\eta = \tfrac{1}{2}$$

$$(0,0)$$

$$\eta = -\tfrac{1}{2}$$

$$\left(\tfrac{c}{12}(n-1), -\tfrac{c}{6}(n-1)\right) \quad anti-chiral$$

$$\Big\uparrow \eta = \tfrac{1}{2}$$

$$\left(\tfrac{c}{24}, \tfrac{c}{6}\right) \xrightarrow{\quad twist \quad} \left(\tfrac{nc}{24}, \tfrac{c}{6}\right)$$

Note that for the construction to work we need the existence of the spectral flow both in $\mathcal{M}$ and $\mathcal{M}^n/\mathbb{Z}_n$.

Next we discuss an alternative way to obtain a chiral state in the twisted sector (starting with a chiral state in $\mathcal{M}$).

$$h = R/2, \ R$$

$$\Big\downarrow \eta_c = \tfrac{1-n}{2}$$

$$h', \ R' \xrightarrow{\quad twist \quad} h^n = R^n/2, \ R^n$$

where

$$h' = \frac{n}{2}R + \frac{c}{24}(n-1)^2 \tag{6.6}$$

$$R' = R + \frac{c}{6}(n-1) \tag{6.7}$$

$$h^n = \frac{R}{2} + \frac{c}{12}(n-1) \tag{6.8}$$

$$R^n = R + \frac{c}{6}(n-1). \tag{6.9}$$

From this statement we see that we first can perform a spectral flow with $\eta_c = (1-n)/2$ and then twist to obtain a chiral state in $\mathcal{M}^n/\mathbb{Z}_n$. Note that performing a spectral flow with $\eta = (1-n)/2$ is equivalent to applying $(n-1)$-times the spectral flow with $\eta = -1/2$, thus for this construction to work we only need the existence of the spectral flow in the mother theory $\mathcal{M}$ in contrast to the construction discussed before. The same construction also holds for antichiral states where $\eta_{ac} = -\eta_c$.

In contrast to the construction before we now end up either in the NS- or R-sector depending on whether $(n-1)$ is even or odd. This can be seen by the following diagram

$$
\begin{array}{c}
\text{NS} \\
\eta{=}{-}1/2 \downarrow \\
\text{RR} \\
\eta{=}{-}1/2 \downarrow \\
\vdots \\
\eta{=}{-}1/2 \downarrow \\
\text{RR} \\
\eta{=}{-}1/2 \downarrow \\
\text{NS} \xrightarrow[twist]{} \text{NS}
\end{array}
$$

if $(n-1)$ is even or

$$
\begin{array}{c}
\text{NS} \\
\eta{=}{-}1/2 \downarrow \\
\text{RR} \\
\eta{=}{-}1/2 \downarrow \\
\vdots \\
\eta{=}{-}1/2 \downarrow \\
\text{NS} \\
\eta{=}{-}1/2 \downarrow \\
\text{RR} \xrightarrow[twist]{} \text{RR}
\end{array}
$$

if $(n-1)$ is odd. This means starting with a chiral state we need $(n-1)$ to be even in order to obtain an chiral state in the NS-twisted theory or alternatively the second construction is only valid for $(n-1)$ even.

In an alternative construction we just need the existence of the spectral flow in the $\mathbb{Z}_n$ twisted theory. We motivate the construction starting with an NS chiral vacuum state. Twisting this field results in the usual twist field $\mathcal{T}_n$. Performing now a spectral flow with $\eta = \frac{n-1}{2n}$ results in the chiral twist field S_n as introduced in the paper by Giveon and Kutasov. The construction described here illustrates that the SUSY twist field they construct is nothing else than the chiral field obtained by spectral flowing from the bosonic twist field $\mathcal{T}_n$ to S_n. Thus the additional contribution to the bosonic twist $\exp(i\alpha_n H)$ can be interpreted as the spectral flow operator. Schematically this means

$$(0,\ 0) \xrightarrow{\quad twist \quad} (\tfrac{c}{24}\tfrac{n^2-1}{n},\ 0)$$
$$\Big\downarrow \eta=\tfrac{1-n}{2n}$$
$$(\tfrac{c}{12}(n-1),\ \tfrac{c}{6}(n-1))$$

Or in terms of fields

$$vac. \xrightarrow{\quad twist \quad} \mathcal{T}_n$$
$$\Big\downarrow \eta=\tfrac{1-n}{2n}$$
$$\mathcal{S}_n$$

Note that in the $\mathbb{Z}_n$ twisted theory (central charge nc) the spectral flow operator is given by

$$U_\eta =: \exp\left(i\eta\sqrt{\frac{nc}{3}}H\right) :, \tag{6.10}$$

where the weights and R-charges in the twisted theory ($c_{total} = nc$) transform according to

$$h \to h - \eta R + \frac{nc}{6}\eta^2 \tag{6.11}$$

$$R \to R - \frac{nc}{3}\eta. \tag{6.12}$$

Obviously the construction is also valid for anti-chiral states with the spectral flow running in opposite direction. Concluding we have the following commutative diagram for the states

$$(0,0) \xrightarrow{\quad twist \quad} (\tfrac{c}{24}\tfrac{n^2-1}{n},0)$$
$$\eta=\tfrac{1-n}{2}\Big\downarrow \qquad\qquad \Big\downarrow \eta_t=\tfrac{1-n}{2n}=\tfrac{\eta}{n}$$
$$(\tfrac{c}{24}(n-1)^2,\tfrac{c}{6}(n-1)) \xrightarrow{\quad twist \quad} (\tfrac{c}{12}(n-1),\tfrac{c}{6}(n-1))$$

and equally for the associated fields

$$vac. \xrightarrow{\quad twist \quad} \mathcal{T}_n$$
$$\eta=\tfrac{1-n}{2}\Big\downarrow \qquad\qquad \Big\downarrow \eta_t=\tfrac{1-n}{2n}=\tfrac{\eta}{n}$$
$$field \xrightarrow{\quad twist \quad} \mathcal{S}_n$$

From this perspective it is interesting to note that it doesn't matter if we first twist and then flow or vice versa. Especially $\eta_t = \frac{1-n}{2n} = \frac{\eta}{n}$ shows that the spectral flow in the twisted sector is the same as acting on each individual component with the original flow. Further the construction gives the same result if we apply it to more general chiral states $(R/2, R)$ or to anti-chiral states $(-R/2, R)$ with the opposite flows $\eta' = -\eta$ and $\eta'_t = -\eta_t$.

A last possible way to construct the twisted SUSY field is shown in the following diagram by an interplay between non trivial spectral flowing on both sides of the theories (we just

discuss the case for starting with the chiral vacuum state but the construction is also valid for starting with other chiral states with $R \neq 0$):

$$(0,0)$$

$$\eta(m)=\frac{1-m}{2} \Bigg\downarrow$$

$$\left(\tfrac{c}{24}(m-1)^2, \tfrac{c}{6}(m-1)\right) \xrightarrow{\ twist\ } \left(\tfrac{c}{24}\tfrac{(m-1)^2}{n} + \tfrac{c}{24}\tfrac{n^2-1}{n}, \tfrac{c}{6}(m-1)\right)$$

$$\Bigg\downarrow \eta_t(m)=\frac{m-n}{2n}$$

$$\left(\tfrac{c}{12}(n-1), \tfrac{c}{6}(n-1)\right)$$

Here $m \in \mathbb{R}$. Especially we see that for $m = 2\mathbb{Z}$ our state remains in the NS-sector, whereas when $m = 2\mathbb{Z}+1$ we obtain a twisted state in the R-sector. Further we recognize that for $m = 0$ we exactly reproduce the construction shown in [84] and in the beginning of this section. This shows that their construction only gives states in the NS-sector and omits the possibility to also find states in the R-sector of the twisted theory that obey a chirality condition between the conformal weights and R-charges.

6.2 Concluding Remarks on the Spectrum

We summarize the results from the last section: to any field of conformal dimension and charge (h, R) in an $\mathcal{N} = 2$ superconformal theory there is a field in the $\mathbb{Z}_n$ twisted sector with

$$(h^n, R^n) = \left(\frac{h}{n} + \frac{c}{24}\frac{n^2-1}{n}, R \right). \tag{6.13}$$

For a chiral state $(h = R/2, R)$ in $\mathcal{M}$ there is one corresponding chiral state in the $\mathbb{Z}_n$ twisted sector with

$$(h^n, R^n) = \left(\frac{R}{2} + \frac{c}{12}(n-1), R + \frac{c}{6}(n-1) \right). \tag{6.14}$$

For an anti-chiral state $(h = -R/2, R)$ in $\mathcal{M}$ there is one corresponding anti-chiral state in the $\mathbb{Z}_n$ twisted sector with

$$(h^n, R^n) = \left(-\frac{R}{2} + \frac{c}{12}(n-1), R - \frac{c}{6}(n-1) \right). \tag{6.15}$$

For the constructions to work it is crucial that the spectral flow on $\mathcal{M}$ ($\mathcal{M}^n/\mathbb{Z}_n$ respectively) exist. This is always the case since we are considering space time supersymmetric theories.

Chapter 7

Entanglement Entropy through Topological Interfaces

7.1 General Setup

We want to calculate the entanglement entropy through a topological interface separating two identical CFTs of the same central charge. As we have seen in section 4.2 the entropy was defined via a limit of a partition function $Z(n) = Z_n/Z^n$ on the n-sheeted Riemann surfaces.

We will now first briefly review the construction of $Z(n)$ (see also [82,83]), which in principle will allow us to derive the entanglement entropy through general, i.e. not necessarily topological, interfaces that are connecting two (also possibly different) CFTs.
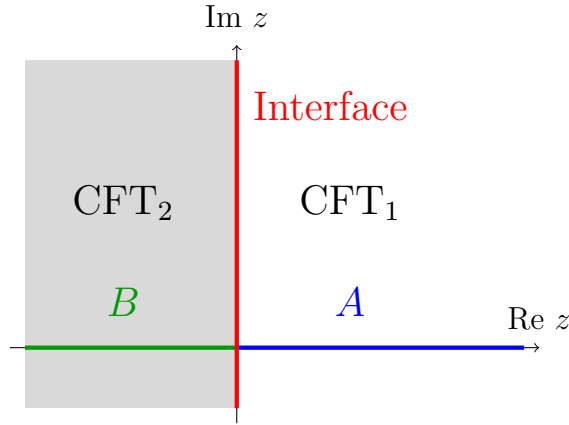
Figure 7.1: Setup for the two CFTs with an interface aligned along the imaginary axis.

Consider the complex plane and let the interface I be placed along the imaginary axis where we have the two CFTs on each side with CFT_1 on $\mathrm{Re}\, z > 0$ and CFT_2 on $\mathrm{Re}\, z < 0$.

In our setup time flows along the defect line and we divide our system, at initial time zero, in the two subsystems A and B consisting of the positive and negative real axis (see figure 7.1).

We can now apply the replica trick in order to evaluate the partition function on the n-sheeted surface which consists of n copies of the complex plane, glued together cyclically along a branch cut on the positive real axis (see figure 7.2 left). As usual to be able to calculate the partition function we have to introduce a UV cut-off $\epsilon = |z|$ and an IR cut-off $L = |z|$ and change the coordinates by a uniformizing transformation according to $w = \log z$. It is important to note that this coordinate transformation is compatible with the gluing conditions (3.1) imposed by the interface along the imaginary axis. The new geometry obtained is that of a cylinder (see figure 7.2 right).
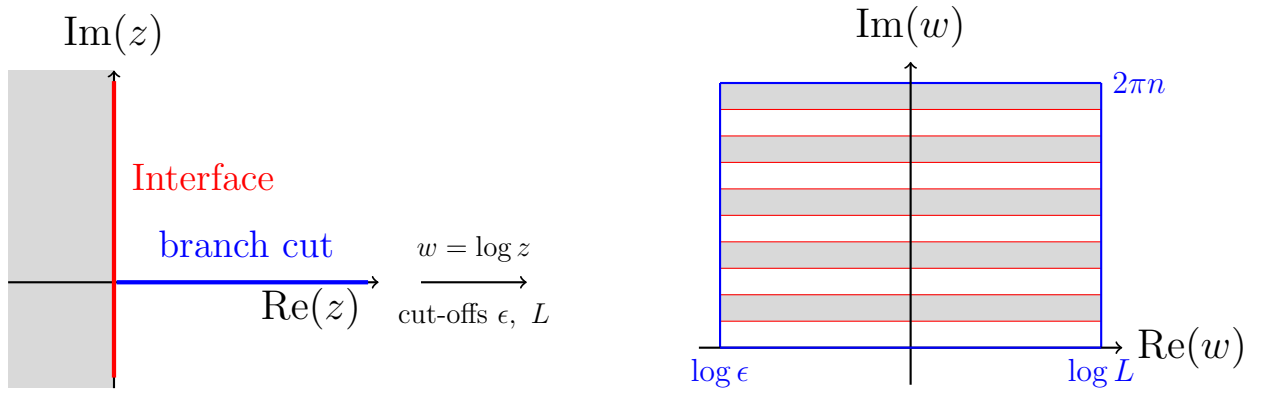
Figure 7.2: *left*: n-sheeted Riemann surface with branch cut along the real axis. *right*: mapping to the cylinder geometry.

In [82] it is shown that one can regularize the partition function by imposing periodicity in Re w and choosing $\epsilon = \frac{1}{L}$. It is important to recognize that the periodicity condition can be imposed since the UV and IR cut-offs are very small/large respectively. Having applied all the transformations and identifications the partition function then becomes the torus partition function

$$Z(n) = \mathrm{tr}_{\mathcal{H}_1}\left(I e^{-\delta H_2} I^\dagger e^{-\delta H_1} \cdots I^\dagger e^{-\delta H_1}\right) = \mathrm{tr}_{\mathcal{H}_1}\left(I e^{-\delta H_2} I^\dagger e^{-\delta H_1}\right)^n, \tag{7.1}$$

where H_1 and H_2 are the Hamilton operators of CFT$_1$ and CFT$_2$ respectively,

$$\delta := \frac{2\pi^2}{\log L/\epsilon} = \frac{\pi^2}{\log L}, \tag{7.2}$$

and the trace runs over all the states of the first Hilbert space in the replicated theory. For general interfaces I the calculation and analytic continuation of the partition function can be quite complicated. For free field examples, i.e. for a single free boson [82] or a single free fermion [83], this partition function has been calculated for conformal defects. From now on we only will consider the cases of topological interfaces. In this case the partition function simplifies considerably and we will be able to calculate it in a straightforward manner as we will see in the next section.

7.2 Calculation of the Entanglement Entropy through Topological Interfaces

We have already seen in section 3.1 that topological defects commute with both chiral and anti-chiral Virasoro algebras (if the two CFTs are identical). This means that when assuming the defect I and the adjoint defect $I^\dagger$ to be topological and the CFTs on both sides to be the same we can rewrite the partition function as

$$Z(n) = \text{tr}_{\mathcal{H}_1}\left[\left(II^\dagger\right)^n e^{-2\delta n H_1}\right]. \tag{7.3}$$

As we already have discussed a general topological defect can be written as a sum of weighted projectors on a given representation, i.e.

$$I_A = \sum_{\mathbf{i}} d_{A\mathbf{i}}||\mathbf{i}||, \tag{7.4}$$

where again

$$\mathbf{i} = (i, \bar{i}; \alpha, \beta), \tag{7.5}$$

with $(i, \bar{i})$ the labels of the representations, $\alpha = 1, 2, \ldots, M_{i\bar{i}}^{(1)}$ and $\beta = 1, 2, \ldots, M_{i\bar{i}}^{(2)}$ are the multiplicity labels of the representation pair on the two sides of the interface. For the torus partition function this results in

$$Z(n) = \sum_{(i,\bar{i})} \text{Tr}\left(d_{A\mathbf{i}} d_{A^*\mathbf{i}}\right)^n \, tr_{\mathcal{H}_i \otimes \mathcal{H}_{\bar{i}}} e^{-2\delta n(L_0 + \bar{L}_0 - \frac{c}{12})} =$$

$$\sum_{(i,\bar{i})} \text{Tr}\left(d_{A\mathbf{i}} d_{A^*\mathbf{i}}\right)^n \chi_i\left(e^{-2\delta n}\right) \bar{\chi}_{\bar{i}}\left(e^{-2\delta n}\right). \tag{7.6}$$

Here $\chi_i(q)$ are the characters of the chiral representations and similar for the anti-chiral ones, further Tr denotes the trace over the multiplicity indices. We can now perform a modular S-transformation

$$\chi_i(q) = \sum_j S_{ij}\chi_j(\tilde{q}), \tag{7.7}$$

with $\tilde{q} = \exp(2\pi^2/\delta n)$ and similarly for the antichiral characters. The partition function in the modular S-transformed channel then takes the form

$$Z(n) = \sum_{(i,\bar{i})} \sum_{(j,\bar{j})} \text{Tr}\left(d_{A\mathbf{i}} d_{A^*\mathbf{i}}\right)^n S_{ij} S_{\bar{i}\bar{j}} \chi_j\left(e^{-\frac{2\pi^2}{\delta n}}\right) \bar{\chi}_{\bar{j}}\left(e^{-\frac{2\pi^2}{\delta n}}\right). \tag{7.8}$$

In the large L limit, i.e. $\delta \ll 1$, only the vacuum will contribute to the sums in the characters, i.e.

$$\chi_j\left(e^{-\frac{2\pi^2}{\delta n}}\right) \bar{\chi}_{\bar{j}}\left(e^{-\frac{2\pi^2}{\delta n}}\right) \xrightarrow{\delta \ll 1} \delta_{j,0} e^{\frac{\pi^2 c}{12\delta n}} \cdot \delta_{\bar{j},0} e^{\frac{\pi^2 c}{12\delta n}} = \delta_{j,0} \delta_{\bar{j},0} e^{\frac{\pi^2 c}{6\delta n}}. \tag{7.9}$$

For the partition function this implies

$$Z(n) \approx \underbrace{\sum_{(i,\bar{i})} \mathrm{Tr}\, (d_{A\mathbf{i}} d_{A^*\mathbf{i}})^n \, S_{i0} S_{\bar{i}0} \, e^{\frac{\pi^2 c}{6\delta n}}}_{=B(n)}. \tag{7.10}$$

One notices that the factor $B(n)$ contains all the information about the topological interface. Applying now the formula for the entanglement entropy (4.12) we find

$$S = (1 - \partial_n) \log Z(n)|_{n=1} \approx (1 - \partial_n) \left. \left(\frac{\pi^2 c}{6\delta n} + \log B(n) \right) \right|_{n=1} =$$

$$\frac{c}{3} \log L + \left[\log B(1) - \frac{B'(1)}{B(1)} \right]. \tag{7.11}$$

Here we used in the last line the definition of δ and a prime denotes the derivative with respect to n. Note that time in the channel described in (7.8) runs parallel to the interface. From (3.14) we, therefore, find that

$$B(1) = \mathcal{N}_{\mathbf{0}A}^{A} \tag{7.12}$$

is a non-negative integer. It is the multiplicity of the vacuum representation in the twisted torus partition function in the channel where time evolves along the interface and its conjugate. If the interface is elementary we have $B(1) = 1$. For the derivative of $B(n)$ one obtains

$$B'(1) = \sum_{(i,\bar{i})} S_{i0} S_{\bar{i}0} \, \mathrm{Tr}\, (d_{A^*\mathbf{i}} \, d_{A\mathbf{i}}) \, \log (d_{A^*\mathbf{i}} \, d_{A\mathbf{i}}) \,. \tag{7.13}$$

Inserting this into the formula for the entanglement entropy it becomes

$$S = \frac{c}{3} \log L + \left[\log \mathcal{N}_{\mathbf{0}A}^{A} - \frac{1}{\mathcal{N}_{\mathbf{0}A}^{A}} \sum_{(i,\bar{i})} S_{i0} S_{\bar{i}0} \, \mathrm{Tr}\, (d_{A^*\mathbf{i}} \, d_{A\mathbf{i}}) \, \log (d_{A^*\mathbf{i}} \, d_{A\mathbf{i}}) \right]. \tag{7.14}$$

Within CFT_1 we now can define [60]

$$p_{(i\bar{i},\alpha\alpha')}^{A} = \frac{d_{A^*\mathbf{i}} \, d_{A\mathbf{i}} \, S_{i0} S_{\bar{i}0}}{\mathcal{N}_{\mathbf{0}A}^{A}}, \tag{7.15}$$

where the multiplicity labels α and α' both run from 1 to $M_{i\bar{i}}^{(1)}$. For every pair $(i, \bar{i})$, the matrix $p_{\mathbf{i}}^{A} \equiv p_{(i\bar{i},\alpha\alpha')}^{A}$ is a positive-semidefinite Hermitian matrix[1], *i.e.* the eigenvalues of the $p_{\mathbf{i}}^{A}$ are real and positive or zero. Moreover, by (3.14) we have

$$\sum_{(i,\bar{i})} \mathrm{Tr}\, p_{\mathbf{i}}^{A} = 1 \,. \tag{7.16}$$

---

[1]Recall that in unitary theories $S_{i0} > 0$

The set of all eigenvalues, therefore, forms a probability distribution. In a quantisation where time runs orthogonally to the interface, the value of $\operatorname{Tr} p_{\mathbf{i}}^A$ is the probability of finding the system CFT_1 in the Ishibashi-type state associated to the sector $(i, \bar{\imath})$, after tracing out CFT_2. Such a state is thermal within its sector, and the set of $p_{\mathbf{i}}^A$ should, therefore, be understood as defining a reduced density matrix. Further we observe that the distribution corresponding to the identity defect in CFT_1 is given by

$$p_{\mathbf{i}}^{id} = S_{i0} S_{\bar{\imath}0}\, \delta_{\alpha\alpha'} \qquad (\alpha, \alpha' = 1,\, 2, \ldots, M_{i\bar{\imath}}^1)\,. \tag{7.17}$$

Equation (7.14) can now be written as

$$S = \frac{c}{3} \log L - \sum_{(i,\bar{\imath})} \operatorname{Tr} p_{\mathbf{i}}^A \, \log \frac{p_{\mathbf{i}}^A}{p_{\mathbf{i}}^{id}}\,. \tag{7.18}$$

This is our main result of this section [60]. The quantity

$$s(I_A) := - \sum_{(i,\bar{\imath})} \operatorname{Tr} p_{\mathbf{i}}^A \, \log \frac{p_{\mathbf{i}}^A}{p_{\mathbf{i}}^{id}} \tag{7.19}$$

is the negative of the relative entropy — the Kullback-Leibler divergence [56] — of the probability distribution associated to I_A on the CFT_1 side, measured with respect to the probability distribution associated to the identity defect $\mathcal{D}_{id}$ of CFT_1. One interpretation of this quantity is the amount of information lost when the probability distribution is wrongly assumed to be given by $\mathcal{D}_{id}$, while it is in reality given by I_A.

The relative entropy is always non-negative, and vanishes only if the compared probability distributions agree.[2] Therefore, we have $s(I_A) \leq 0$, which corresponds to the intuition that an interface cannot enhance the transmissivity beyond the one of the identity defect in CFT_1.

We have $s(I_A) = 0$ if and only if $p^A = p^{\mathrm{id}}$. This is the case precisely if $d_{A^*\mathbf{i}} d_{A\mathbf{i}}$ is the identity matrix for all pairs of representations $(i, \bar{\imath})$ which appear in CFT_1. A necessary requirement for the existence of an interface with this property is that the representation multiplicities of CFT_2 must not be smaller than those of CFT_1. Since both CFTs are unitary and have a single vacuum state, modular invariance, in fact, forces CFT_1 and CFT_2 to have identical spectra. Since the necessary condition $d_{A^*\mathbf{i}} d_{A\mathbf{i}} = 1$ then means that the fusion product of the defect and its conjugate is the identity, we have

$$\exists I : s(I) = 0 \quad \Leftrightarrow \quad Z_{\mathrm{CFT}_1} = Z_{\mathrm{CFT}_2} \quad \text{and} \quad I^\dagger I = \mathcal{D}_{id} \quad \text{in } \mathrm{CFT}_1\,. \tag{7.20}$$

For general CFT_1 and CFT_2 we may give a simple upper bound for s, based on the restricted data we have been employing so far. Without loss of generality every interface I between CFT_1 and CFT_2 can be associated with a set of diagonal matrices $p_{\mathbf{i}}$. Each of these matrices $p_{\mathbf{i}}$ has at most $T_{i\bar{\imath}} = \min(M_{i\bar{\imath}}^{(1)}, M_{i\bar{\imath}}^{(2)})$ eigenvalues different from 0. Varying the

---

[2]Continuous distributions have to agree almost everywhere.

remaining eigenvalues we look for the maximal value of s under the linear constraint (7.16). This is only one constraint out of the set (3.14), such that this calculation will obviously lead to an upper bound. A maximal value of s would be achieved for the distribution

$$p_{\mathbf{i}} = \mathrm{diag}(p_{(i\bar{i},1)}, \ldots, p_{(i\bar{i},T_{i\bar{i}})}, 0, \ldots, 0) \quad \text{with} \quad p_{(i\bar{i},\alpha)} = \frac{S_{i0} S_{\bar{i}\bar{0}}}{\sum_{(j,\bar{j})} T_{j\bar{j}} S_{j0} S_{\bar{j}\bar{0}}} \, . \tag{7.21}$$

This distribution yields the upper bound

$$s \leq \log \left(\sum_{(i,\bar{i})} T_{i\bar{i}} \, S_{i0} S_{\bar{i}\bar{0}} \right) \, . \tag{7.22}$$

The bound is strictly smaller than zero if there is at least one $(i, \bar{i})$ with $T_{i\bar{i}} < M_{i\bar{i}}^{(1)}$. As we have seen above, this is equivalent to having at least one pair $(i, \bar{i})$ where $M_{i\bar{i}}^{(1)} \neq M_{i\bar{i}}^{(2)}$. The bound (7.22) is zero if and only if the theories CFT_1 and CFT_2 have the same spectrum. In cases where the CFTs on the two sides are identical, the distribution (7.21) is in particular obtained from the identity defect.

We emphasise [60] that different interfaces can lead to the same distribution (7.15), and thus to the same entanglement entropy. In particular, fusing any interface on either side with a symmetry defect of the respective theory will leave the distribution unaltered. The reference distribution p^{id} of (7.17) is, therefore, also obtained from any symmetry defect in CFT_1. On the other hand, every defect whose fusion product with a particular topological interface leaves the probability distribution of the interface unaltered is a symmetry defect. The distributions also do not change if we superpose the same interface multiple times. This is obvious from the interpretation of the probability distribution mentioned above. Note that an interface I formally has the same probability distribution as λI for any rescaling $\lambda \in \mathbb{C}^*$, and, therefore, in particular for superpositions of the same interface[3]. However, the change in the entanglement entropy is difficult to compute for general superposition and fusion. This is so because it is in general difficult to see how closely the probability distribution of the resulting interface follows $p_{\mathbf{i}}^{id}$.

For concreteness, let us now consider the defects (3.16) in a rational theory with diagonal modular invariant. By (7.15), the interfaces (3.16) of diagonal RCFTs lead to a probability distribution

$$p_i^a = |S_{ia}|^2 \, . \tag{7.23}$$

From our result (7.18) we, therefore, obtain the entanglement entropy

$$S = \frac{c}{3} \log L - \sum_i |S_{ia}|^2 \log \left| \frac{S_{ia}}{S_{i0}} \right|^2 \, . \tag{7.24}$$

For later purpose it is useful to define the subleading contribution to the entanglement

---

[3]This is in agreement with our remark from the beginning of the chapter

entropy via

$$s(\mathcal{D}_a) := -\sum_i |S_{ia}|^2 \log \left|\frac{S_{ia}}{S_{i0}}\right|^2, \tag{7.25}$$

thus (7.24) can alternatively be written as

$$S(\mathcal{D}_a) = \frac{c}{3} \log L + s(\mathcal{D}_a). \tag{7.26}$$

Remark: In this whole section we have considered topological interfaces. For non-topological interfaces (see e.g. [82,83]) the leading term in the entanglement entropy takes the form

$$S = \frac{\sigma}{3} \log L, \tag{7.27}$$

i.e. the prefactor is no longer constant but a continuous function σ. In the case of a free boson or a free fermion [82,83] it has been shown that σ is a function depending on the transmissivity $\mathcal{T}$ of the interface. For general interfaces it is not clear if σ is a function just depending on the transmissivity.

7.3   Examples for Entanglement Entropies

In the following section we will calculate the entanglement entropies for several non-trivial examples.

7.3.1   Duality Inferfaces

As a class of examples we consider the duality interfaces (3.20). Here I, $I^\dagger$ project the theory onto a sector invariant under a symmetry group G. States that are invariant under the action of I (respectively $I^\dagger$) pick up a factor $|G|$ which is simply the order of the group. On the level of equation (7.1) this means that

$$Z(n) = Tr\left((II^\dagger)^n e^{-2\delta Hn}\right) = Tr\left((\oplus_{g\in G}\mathcal{D}_g)^n e^{-2\delta Hn}\right) = |G|^n\ Tr_{inv}\left(e^{-2\delta Hn}\right), \tag{7.28}$$

where in the last line the trace is taken only over the invariant subsector of the initial Hilbert space. This partition function is a projection of an initial partition function, which is in line with the fact that correlators of invariant fields in orbifold theories are obtained by projection from the initial theory. In the calculation of the entanglement entropy the prefactor $|G|^n$ will drop out (this is true for all factors of the form x^n), so that effectively we consider the entanglement of an initial system with a projected system.

However, if we consider the system with only the trivial defect inserted the projection only contains a factor $|G|^{-1}$. This single factor leads to a shift in the entanglement entropy for duality interfaces, i.e.

$$S = \frac{c}{3} \log L - \log |G|. \tag{7.29}$$

This can alternatively be phrased in terms of the probability distributions introduced earlier as

$$p_{\mathbf{i}}^{duality} = p_{\mathbf{i}}^{id}|G| \text{ for } \mathbf{i} \text{ invariant}, \quad p_{\mathbf{i}}^{duality} = 0 \text{ otherwise} . \tag{7.30}$$

The shift in the entanglement entropy encodes the information loss under a projection.

7.3.2   Ising Model

The critical Ising model is described by three primaries id, ϵ, σ. For comparison of the fields with the conventional description of the Ising model on the lattice see [6]. It is an example of a diagonal rational theory. The S-matrix of the Ising model is given by

$$S_{ij} = \frac{1}{2} \begin{pmatrix} 1 & 1 & \sqrt{2} \\ 1 & 1 & -\sqrt{2} \\ \sqrt{2} & -\sqrt{2} & 0 \end{pmatrix}, \quad \text{with } i, j \in \{id, \epsilon, \sigma\} . \tag{7.31}$$

The three elementary topological defects of the Ising model are, therefore,

$$\begin{aligned}
\mathcal{D}_{id} &= \|id\| + \|\epsilon\| + \|\sigma\| , \\
\mathcal{D}_{\epsilon} &= \|id\| + \|\epsilon\| - \|\sigma\| , \\
\mathcal{D}_{\sigma} &= \sqrt{2}\|id\| - \sqrt{2}\|\epsilon\| .
\end{aligned}$$

The defect corresponding to the vacuum id is the identity defect. The defect $\mathcal{D}_{\epsilon}$ is a symmetry defect implementing the $\mathbb{Z}_2$ symmetry of the Ising model. The presence of these two defects does not result in a shift of the entanglement entropy. The third defect $\mathcal{D}_{\sigma}$ implements Kramers-Wannier duality [45]. It satisfies the fusion rule

$$\mathcal{D}_{\sigma}\mathcal{D}_{\sigma} = \mathcal{D}_{id} + \mathcal{D}_{\epsilon} . \tag{7.32}$$

From our formula (7.24) we deduce that the entanglement entropy of $\mathcal{D}_{\sigma}$ is

$$S(\sigma) = \frac{c}{3} \log L - \log 2 , \tag{7.33}$$

which also agrees with the result (7.29) for duality interfaces where the order of the group is 2. The result also reproduces the constant shift in the entanglement entropy observed in [83].

7.3.3 $u(1)_k$ Interfaces

Let us now consider a theory based on $u(1)_k$ which is realized via a free boson compactified on a circle of radius $R = \sqrt{2k}$, for which the central charge is $c = 1$. The modular S-matrix of such a theory is given by

$$S_m^{m'} = \frac{1}{\sqrt{2k}} \exp\left(-i\pi \frac{mm'}{k}\right) , \tag{7.34}$$

where $m, m' \in \{-k+1, \ -k+2, \dots, k\}$. Our topological defect is labelled by a number m and takes the form

$$\mathcal{D}_m = \sum_{m'=-k+1}^{k} \frac{S_m^{m'}}{S_0^{m'}} ||m'||. \tag{7.35}$$

Using formula (7.25) for the subleading contribution to the entanglement entropy

$$s(\mathcal{D}_m) = - \sum_{m'=-k+1}^{k} \left| S_m^{m'} \right|^2 \log \left| \frac{S_m^{m'}}{S_0^{m'}} \right|^2 \tag{7.36}$$

we see that it is identically zero for all possible defects with labels m, since $|S_m^{m'} / S_0^{m'}| = 1$. The entanglement entropy in this case is, therefore, simply given by

$$S(\mathcal{D}_m) = \frac{1}{3} \log L \quad \forall m. \tag{7.37}$$

In this sense the defects act as symmetry defects on the space of states.

7.3.4 $su(2)_k$ Interfaces and the Large k Limit

In this section we present an example also discussed in [60]. The diagonal WZW model based on the chiral algebra $su(2)$ at level k has irreducible representations labelled by half-integer spins s. Using the index convention $i = 2s$, the integer label i runs from 0 to k. The modular S matrix is given by

$$S_{ij} = \sqrt{\frac{2}{k+2}} \sin\left(\frac{\pi(i+1)(j+1)}{k+2}\right). \tag{7.38}$$

By (7.24), the entanglement entropy in the presence of an elementary defect $\mathcal{D}_l$ of the form (3.16) reads

$$S(\mathcal{D}_l) = \frac{c}{3} \log L + s(\mathcal{D}_l) \tag{7.39}$$

with

$$s(\mathcal{D}_l) = -\frac{2}{k+2} \sum_{i=0}^{k} \sin^2\left(\frac{\pi(l+1)(i+1)}{k+2}\right) \log \frac{\sin^2\left(\frac{\pi(l+1)(i+1)}{k+2}\right)}{\sin^2\left(\frac{\pi(i+1)}{k+2}\right)} \tag{7.40}$$

Note that the defect $\mathcal{D}_k$ does not change the entanglement entropy, since this defect simply implements the $\mathbb{Z}_2$-symmetry acting on the representation labels as $l \to k - l$. For small values of k some results for the subleading term to the entanglement entropy are given in table 7.1.

At large k one obtains the WZW model based on $su(2)$. In this limit the model can be presented as three bosons of total central charge $c = 3$ on a target space S^3 with non-vanishing H-flux at large radius. The $\mathbb{Z}_2$-symmetry now corresponds to the reflection

k	$s_{su(2)_k}(\mathcal{D}_l)$
1	0 for $l = 0, 1$
2	0 for $l = 0, 2$
	$-\log 2$ for $l = 1$
3	0 for $l = 0, 3$
	$-4\left(a^2 \log \frac{a^2}{b^2} + b^2 \log \frac{b^2}{a^2}\right)$ for $l = 1, 2$

Table 7.1: Values of $s(\mathcal{D}_l)$ for small values of k, here $a := \frac{1}{\sqrt{5}}\sin(\pi/5)$ and $b := \frac{1}{\sqrt{5}}\sin(2\pi/5)$

symmetry of the three-sphere. At any k, the theory contains elementary defects $\mathcal{D}_l$ for non-negative integers $l \leq k$. To find their geometric interpretation, we recall a few facts about the interpretation of symmetry preserving boundary states. Quite generally, symmetry preserving D-branes on group manifolds wrap conjugacy classes [57, 58], which can be automorphism-twisted. In particular, the symmetry preserving (Cardy-)states of a WZW model wrap ordinary conjugacy classes of the underlying group G. To give an interpretation to defects, we first use the folding trick to map defects to permutation boundary conditions [67] for the WZW model based on $G \times G$. Geometrically, these branes wrap twisted conjugacy classes where the automorphism is the permutation of the two factors, and the conjugacy class of $(g_1, g_2) \in G \times G$ takes the form [59]

$$C_\omega(g_1, g_2) = \left\{ (h_1^{-1}g_1h_2, h_2^{-1}g_2h_1) \mid h_1 \in G_1, h_2 \in G_2 \right\}. \tag{7.41}$$

The multiplication map $m : G \times G \to G$ maps these conjugacy classes to the conjugacy classes in the diagonal G. Indeed, the twisted conjugacy classes of $G \times G$ correspond precisely to the pre-images of the conjugacy classes of G under the multiplication map [59]. In the case of $SU(2)$ they take the form $S^3 \times S^2$, as the regular untwisted conjugacy classes of $SU(2)$ are generically isomorphic to S^2. The conjugacy classes of ± 1 are special and correspond to points. This gives a geometric interpretation to the fact that the defects $\mathcal{D}_l$ carry the same labels as Cardy boundary states. Indeed, the label l corresponds to a polar angle distinguishing the different 2-spheres $S^2 \subset S^3$ of a single $SU(2)$.

We now compute the entanglement entropy in the large k limit while keeping the label l fixed. In the limit $k \to \infty$ as said before the subleading contribution to the entanglement entropy becomes an integral

$$s(\mathcal{D}_l) = -\lim_{k \to \infty} \frac{2}{k+2} \sum_{i=0}^{k} \sin^2\left(\frac{\pi(l+1)(i+1)}{k+2}\right) \log \frac{\sin^2\left(\frac{\pi(l+1)(i+1)}{k+2}\right)}{\sin^2\left(\frac{\pi(i+1)}{k+2}\right)}$$

$$= -2 \int_0^1 dx \, \sin^2(\pi(l+1)x) \log\left(\frac{\sin^2(\pi(l+1)x)}{\sin^2(\pi x)}\right). \tag{7.42}$$

In particular, we see that in the large k limit, the probability distribution of the interface

is a continuous sine-square distribution

$$p_l(x) = 2\sin^2[\pi(l+1)x], \quad x \in [0,1]. \tag{7.43}$$

The integration can be performed by elementary methods. We first split the logarithmic term. The first of the two resulting summands,

$$\int_0^1 dx \, \sin^2(\pi(l+1)x)\log(\sin^2(\pi(l+1)x)) = \frac{1}{\pi}\int_0^\pi dy \, \sin^2 y \log(\sin^2 y) = \frac{1}{2} - \log 2 \tag{7.44}$$

is independent of l. In the other summand we use $2\sin^2 x = 1 - \cos(2x)$ to obtain

$$-\int_0^1 dx \, \sin^2(\pi(l+1)x)\log(\sin^2(\pi x)) =$$
$$= -\frac{1}{2\pi}\int_0^\pi dy \, \log(\sin^2 y) + \frac{1}{2\pi}\int_0^\pi dy \, \cos(2(l+1)y)\log(\sin^2 y). \tag{7.45}$$

The first integral on the right-hand side of (7.45) yields $-\int_0^\pi dy \, \log\sin^2 y = 2\pi\log 2$. In the second integral we use partial integration to obtain

$$\int_0^\pi dy \, \cos(2(l+1)y)\log(\sin^2 y) =$$
$$= -\frac{1}{l+1}\int_0^\pi dy \, \sin(2(l+1)y)\cot(y) = -\frac{\pi}{l+1}. \tag{7.46}$$

Using (7.44) – (7.46), (7.42) becomes

$$s(\mathcal{D}_l) = -\frac{l}{l+1} \qquad , l \ll k. \tag{7.47}$$

In particular, the contribution to the entanglement entropy from such an elementary defect $\mathcal{D}_l$ is given by a rational number.

However, there is a second class of defects, for which the approximations made in the calculation leading to the result (7.47) do not hold. This is in particular the case if we pick l such that $l + 1$ divides $k + 2$ and take the limit keeping the ratio $(l+1)/(k+2)$ fixed. Let us for example consider the case $l = k/2$ (k even), geometrically corresponding to the equatorial two-sphere, which is the fixed point under the involution $l \to k - l$. In this case the probabilities p_i^l vanish for i odd, and take the value $2/(k+2)$ for i even. Using similar methods as above, the entanglement entropy in the limit $k \to \infty$ becomes

$$s(\mathcal{D}_{\frac{k}{2}}) = -\log 4 \qquad (k \to \infty). \tag{7.48}$$

Since $\log 4 > 1$ one sees that $-s(\mathcal{D}_{\frac{k}{2}})$ deviates substantially from the value (7.47). In fact, plotting of $-s(\mathcal{D}_l)$ at finite even k one observes a peak in the entanglement at $l = k/2$. Similar, less pronounced peaks are obtained at other values where $l + 1$ divides $k + 2$.

For generic defects, $l + 1$ does not divide $k + 2$, but of course $(l + 1)/(k + 2)$ is, still, a rational number that we denote l'/n, where l', n are coprime. It is natural to ask what happens if, instead of l (as in the computation leading to (7.47)) we keep l'/n fixed when taking the large k limit. In this case we find from (7.39) the expression

$$s(\mathcal{D}_{\frac{l'(k+2)}{n} - 1}) = -\log(2n) - H(n) \qquad (k \to \infty), \tag{7.49}$$

where $H(n)$ is the entropy of a probability distribution $p_m = \frac{2}{n} \sin^2(\frac{\pi m}{n})$ for $m = 1, 2, \ldots, n$,

$$H(n) = \sum_{m=1}^{n} \frac{2}{n} \sin^2(\tfrac{\pi m}{n}) \log \left(\tfrac{2}{n} \sin(\tfrac{\pi m}{n})^2 \right). \tag{7.50}$$

Note that the values of s in (7.49) are multiply degenerate, as the right-hand side does not depend on l'. The entropies (7.49) are bounded from below by $s(\mathcal{D}_{\frac{k}{2}})$, showing again that the defect corresponding to the equatorial two-sphere has minimum entanglement entropy. On the other hand, for $n \gg l'$ they quickly approach the value -1 from below, such that this asymptotic expression, in fact, comes rather close to the approximation (7.47).

We will not go much further into details, and, instead plot the entanglement entropy correction $-s(\mathcal{D}_l)$ at a finite value of k together with the approximation (7.47) in figure 7.3. The plot illustrates that the values of $s(\mathcal{D}_l)$ approach the asymptotic values (7.47) rather well for generic values of l. It also illustrates the peaks of the values at the special points where (7.49) deviates strongly from (7.47).
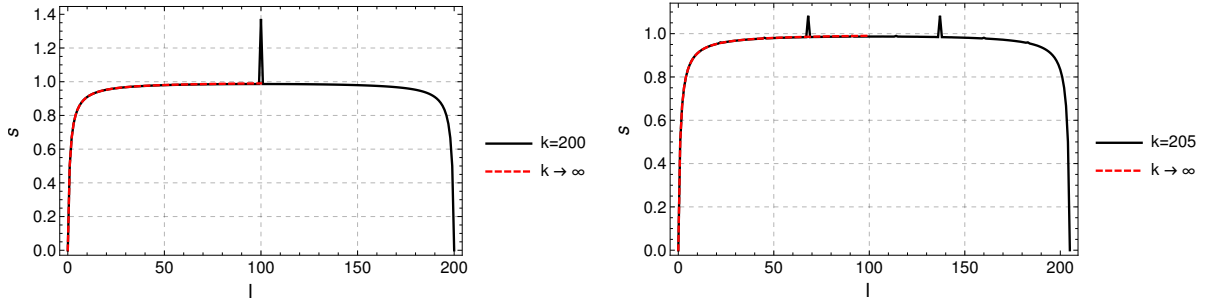
Figure 7.3: Plots of $-s(\mathcal{D}_l)$ for large values of k, together with the asymptotic values (7.47). The peaks in the plots are captured by the asymptotic expression (7.49).

A nice pattern arises when we consider the fusion product of elementary defects at fixed labels l and $\tilde{l}$ for $k \to \infty$. For finite k, the product of topological defects $\mathcal{D}_{l \times \tilde{l}} = \mathcal{D}_l \mathcal{D}_{\tilde{l}}$ has the usual decomposition

$$\mathcal{D}_{l \times \tilde{l}} = \sum_c N_{l\tilde{l}}{}^c \mathcal{D}_c \tag{7.51}$$

in terms of elementary defects, where $N_{l\tilde{l}}{}^c$ are the $su(2)_k$ fusion rules. We can use the fact that the number of vacua contained in the fusion product at large k is

$$\mathcal{N}_{0\,l \times \tilde{l}}^{l \times \tilde{l}} = \min(l, \tilde{l}) + 1. \tag{7.52}$$

For the probability distribution of $\mathcal{D}_{l \times \tilde{l}}$ this implies

$$p_i^{l \times \tilde{l}} = \frac{2}{\min(l, \tilde{l}) + 1} \frac{\sin^2(\frac{\pi(l+1)(i+1)}{k+2}) \sin^2(\frac{\pi(\tilde{l}+1)(i+1)}{k+2})}{(k+2) \sin^2(\frac{\pi(i+1)}{k+2})}. \tag{7.53}$$

The expression for $s(\mathcal{D}_{l \times \tilde{l}})$ in the large-k limit can be written as two summands, by splitting off the part involving the logarithm of the factor $\min(l, \tilde{l}) + 1$ in (7.53). The subleading part to the entanglement entropy in the large k-limit is then given by

$$-2 \int_0^1 \frac{\sin^2(\pi(l+1)x) \sin^2(\pi(\tilde{l}+1)x)}{\min(l+1, \tilde{l}+1) \cdot \sin^2(\pi x)} \log\left(\frac{\sin^2(\pi(l+1)x) \sin^2(\pi(\tilde{l}+1)x)}{\sin^4(\pi x)}\right) dx. \tag{7.54}$$

We want to prove that this is a rational number. In order to see this, the basic integral that has to be evaluated is

$$-\frac{1}{\pi} \int_0^\pi \frac{\sin^2((l+1)x) \sin^2((\tilde{l}+1)x)}{\sin^2(x)} \log\left(\sin^2((l+1)x)\right) dx. \tag{7.55}$$

By the two representations of Clausen's function Cl_1 we can express the logarithmic factor in terms of the sum

$$\log(\sin^2(y)) = -\log 4 - \sum_{k=1}^\infty \frac{2 \cos(2ky)}{k}. \tag{7.56}$$

We note that the $\log 2$ terms cancel out in (7.54), so it is enough to keep only the sum over cosines from the right-hand side of (7.56) for further calculations. One might be concerned that while the individual terms in the summation over k give rational results, resummation may yet yield something non-rational. In order to see that this is not the case we eliminate the sine functions in the denominator of (7.55) by writing the remaining sine functions in the numerator in terms of spread polynomials [98]

$$\sin^2(nx) = \sum_{p=0}^{n-1} \frac{n}{n-p} \binom{2n-1-p}{p} (-4)^{n-1-p} \sin^{2(n-p)}(x) =: \sum_{\{p\}} \sin^{2p}(x). \tag{7.57}$$

Since we are not interested in the precise value of the finite result, the only relevant property for us is that the spread polynomials have rational coefficients and finite order. We define the summation symbol on the right-hand side to indicate a finite sum of trigonometric functions with rational coefficients. The right hand side can be deduced further using the identity

$$\sin^{2p}(x) = \frac{1}{2^{2p}} \binom{2p}{p} + \frac{2}{2^{2p}} \sum_{r=0}^{p-1} (-1)^{p-r} \binom{2p}{r} \cos(2(n-r)x) =: \sum_{\{r\}} \cos(2rx). \tag{7.58}$$

The purpose of writing (7.57) and (7.58) is to demonstrate that (7.54) can indeed be written in the form

$$\frac{1}{\pi} \int_0^\pi \sum_{\{s\}} \cos(2sx) \sum_{k=1}^\infty \cos(2k(l+1)x) \frac{1}{k} \, dx \, . \tag{7.59}$$

By the integral identity $\int_0^\pi \cos(nx) \cos(mx) \, dx = \frac{\pi}{2} \delta_{n,m}$, the finite sum over s reduces the infinite sum over k to a rational result. This concludes the argumentation that the entanglement entropy in the large k-limit takes the form

$$s(\mathcal{D}_{l \times \tilde{l}}) = -\frac{p}{q} + \log(\min(l, \tilde{l}) + 1) \, , \tag{7.60}$$

where p and q are natural numbers depending on the labels l and $\tilde{l}$. Note that the argument in the logarithm is the number of elementary defects in the decomposition of the fusion product. However, the fact that this logarithm directly reflects the number of elementary defects in the decomposition is true only if each of these elementary defects appears with multiplicity 1.

7.4 Entanglement Entropy for Coset Theories

We now want to discuss the entanglement entropy through topological interfaces where our theory is given by a coset construction. Especially we are interested in coset theories with a $\mathbb{Z}_2$ identification of fields. Further we only consider cosets that are free of field identification fixed points such as the parafermionic coset $su(2)_k/u(1)_k$, the coset $su(2)_k \otimes su(2)_1/su(2)_{k+1}$ corresponding to the unitary minimal series or the coset representing the $\mathcal{N} = 2$ minimal models $su(2)_k \otimes u(1)_2/u(1)_{k+2}$.

7.4.1 Parafermionic Coset

Let us consider the simplest possible coset corresponding to a parafermionic theory. We will first briefly review some general aspects of the parafermionic coset construction before we come to the calculation of the subleading term to the entanglement entropy. The parafermions are defined by the coset

$$\frac{su(2)_k}{u(1)_k}, \quad k \in \mathbb{N}^+ . \tag{7.61}$$

The associated central charge at given level k of these models is then given by

$$c = c_{su(2)_k} - c_{u(1)_k} = \frac{3k}{k+2} - 1 = \frac{2(k-1)}{k+2} . \tag{7.62}$$

The chiral algebra of the parafermionic theory has a set of irreducible highest weight representations $\mathcal{H}_{(l,m)}$ with labels (l, m) where $0 \leq l \leq k$ and m is an integer defined modulo $2k$, i.e. we may pick the range to be $-k + 1 \leq m \leq k$. The same is true for the

anti-chiral algebra. The pairs (l, m) are subjected to the constraint $l + m = 0$ mod 2 and a field identification equivalence relation $(l, m) \sim (k - l, k + m)$. We will label the set of distinct irreducible representations by $PF(k) = \{(l, m)\}$ adopting the notation used for example in [91]. The characters $\chi_{(l,m)}$ of the representation (l, m) can be determined by the decomposition of $su(2)_k$ characters χ_l in terms of the parafermionic ones at the same level k

$$\chi_l(\tau) = \sum_{m=-k}^{k+1} \chi_{l,m}(\tau) \frac{\Theta_{m,k}(\tau)}{\eta(\tau)}, \tag{7.63}$$

where

$$\Theta_{m,k}(\tau) := \sum_{n \in \mathbb{Z} + \frac{m}{2k}} e^{2\pi i \tau k n^2}, \quad -k + 1 \leq m \leq k, \tag{7.64}$$

are the generalized theta-functions. For a more detailed discussion see [1, 2, 91]. It is important to note that the representations with labels (l, m) and $(l, -m)$ are distinct, whereas representations with labels (l, m) and $(k - l, k + m)$ are the same.

The L_0 eigenvalue of the highest weight state $|l, m\rangle$ of the representation (l, m) is given by

$$h_{l,m} = \begin{cases} \frac{l(l+2)}{4(k+2)} - \frac{m^2}{4k} & \text{for} \quad -l \leq m \leq l \\ \frac{l(l+2)}{4(k+2)} - \frac{m^2}{4k} + \frac{m-l}{2} & \text{for} \quad l \leq m \leq k - l \end{cases} \tag{7.65}$$

Note that for k even the fundamental domain can always be chosen s.t.

$$PF(k) = \{(l, m) | 0 \leq l \leq k, \ 0 \leq m \leq k, \ l + m = 0 \text{ mod } 2\}, \tag{7.66}$$

whereas for k odd one may always choose the fundamental domain to be

$$PF(k) = \{(l, m) | 0 \leq l \leq \frac{k-1}{2}, \ -k + 1 \leq m \leq k, \ l + m = 0 \text{ mod } 2\}. \tag{7.67}$$

The modular S-matrix $S_{l,m}^{l',m'}$ of this theory is given in terms of the $su(2)_k$ modular matrix

$$S_l^{l'} = \sqrt{\frac{2}{k+2}} \sin\left(\pi \frac{(l+1)(l'+1)}{k+2}\right), \tag{7.68}$$

and the $u(1)_k$ modular matrix

$$S_m^{m'} = \frac{1}{\sqrt{2k}} e^{-i\pi \frac{mm'}{k}}, \tag{7.69}$$

as

$$S_{l,m}^{l',m'} = N S_l^{l'} S_m^{*m'} = N \frac{1}{\sqrt{k(k+2)}} \sin\left(\pi \frac{(l+1)(l'+1)}{k+2}\right) e^{i\pi \frac{mm'}{k}}, \tag{7.70}$$

with N an appropriate normalization constant which can be determined by the condition (see section 2.9.1)

$$\sum_{(l',m')\in PF(k)} \left| S_{l,m}^{l',m'} \right|^2 = 1 \quad \leftrightarrow \quad N = 2. \tag{7.71}$$

Applying the result for the parafermionic modular S-matrix to the expression for the fusion coefficients we obtain the fusion rules of the theory to be

$$N_{(l_1,m_1),(l_2,m_2)}^{(l_3,m_3)} = N_{l_1 l_2}^{l_3} \delta_{n_1+n_2-n_3}^{(2k)} + N_{l_1 l_2}^{k-l_3} \delta_{n_1+n_2-n_3-k}^{(2k)}, \tag{7.72}$$

where

$$N_{ab}^c = \begin{cases} 1 & \text{for } |a-b| \leq c \leq \ min(a+b, 2k-a-b) \\ & a+b+c = 0 \text{ mod } 2 \\ 0 & \text{otherwise} \end{cases} \tag{7.73}$$

are the fusion coefficients of the $su(2)_k$ theory and $\delta^{(2k)}$ is a delta function of period $2k$.
We will now continue by calculating the subleading contribution to the entanglement entropy in the presence of topological defects. By doing this we will distinguish the cases where k is even or odd. In the end we will see that both cases lead to the same result. In addition we will briefly apply the obtained result for the first two non trivial values of k namely $k=2$ which corresponds to the Ising model and $k=3$ corresponding to the three state Potts model.
For our representations of the parafermionic theory the subleading term to the entanglement entropy is again given by

$$s(l,m) := - \sum_{(l',m')\in PF(k)} \left| S_{l,m}^{l',m'} \right|^2 \log \left| \frac{S_{l,m}^{l',m'}}{S_{0,0}^{l',m'}} \right|^2 = -\frac{N^2}{2k} \sum_{(l',m')\in PF(k)} \left| S_l^{l'} \right|^2 \log \left| \frac{S_l^{l'}}{S_0^{l'}} \right|^2. \tag{7.74}$$

In the last step we inserted the expression for the modular S-matrix in the form (7.70) and used that the absolute values of the exponential functions are one. We now want to calculate this expression for the cases where k is even or odd. Starting with the case where k is even we see, that we can write

$$\sum_{(l',m')\in PF(k)} = \sum_{l'=0}^{k} \sum_{\substack{m'=0 \\ l'+m'=0 \text{ mod } 2}}^{k-1} . \tag{7.75}$$

Since all terms in (7.74) are independent of the summation over m' and give equal contribution $k/2$ for l even or odd we find

$$s(l,m) = -\frac{N^2}{2k} \cdot \frac{k}{2} \sum_{l'=0}^{k} \left| S_l^{l'} \right|^2 \log \left| \frac{S_l^{l'}}{S_0^{l'}} \right|^2 = -\sum_{l=0}^{k} \left| S_l^{l'} \right|^2 \log \left| \frac{S_l^{l'}}{S_0^{l'}} \right|^2 = s_{su(2)_k}(l). \tag{7.76}$$

We see that the subleading term is totally determined by the subleading contribution coming only from the $su(2)_k$ representations.

Considering now the case where k is odd we obtain

$$\sum_{\substack{(l',m')\in PF(k)}} = \sum_{l'=0}^{\frac{k-1}{2}} \sum_{\substack{m'=-k+1 \\ l'+m'=0 \bmod 2}}^{k} = \frac{1}{2}\sum_{l=0}^{k} \sum_{\substack{m=-k+1 \\ l+m=0 \bmod 2}}^{k} . \tag{7.77}$$

In the last step we used the properties of the $su(2)_k$ modular S-matrices, i.e. under the transformations $S_l^{l'} = S_{k-l}^{l'}$, in order to let the summation over l' run from 0 to k including a correction factor of $1/2$. Plugging this into (7.74) we obtain the same result as in the k even case namely

$$s(l,m) = s_{su(2)_k}(l). \tag{7.78}$$

Since for all k we obtain the same formula for the subleading term we can thus write down the entanglement entropy for a parafermionic theory in the presence of topological defects

$$S_{PF}(l,m;k) = \frac{2(k-1)}{3(k+2)}\log L + s_{su(2)_k}(l). \tag{7.79}$$

We will now briefly discuss the two simplest models contained in the parafermionic description.

Example 1: $k = 2$ as the Ising model
For $k = 2$ one recovers the Ising model at criticality. In the model there are the three distinct fields with corresponding conformal weight

(l,m)	$h_{l,m}$
$(0,0)$	0
$(0,2)$	$1/2$
$(1,1)$	$1/16$

The corresponding entanglement entropies are, therefore, given by

$$S_{EE} = \frac{1}{6}\log L - \begin{cases} 0 & \text{for } (1,1) \\ \log 2 & \text{for } (0,0) \ \& \ (0,2) \end{cases} \tag{7.80}$$

This reproduces exactly our former result from section 7.3.2 for the entanglement entropies of the Ising model where the correct correspondence to the fields is given by $id \mathrel{\widehat{=}} (0,0)$, $\epsilon \mathrel{\widehat{=}} (0,2)$ and $\sigma \mathrel{\widehat{=}} (1,1)$.

Example 2: $k = 3$ as the three state Potts model

For $k = 3$ we reproduce the fractional spectrum of the three state Potts model with central charge $c = 4/5$ and the right multiplicities of fields. The distinct representations are given by the following table

(l, m)	$h_{l,m}$
$(0, 0)$	0
$(0, 2)$	$2/3$
$(0, -2)$	$2/3$
$(1, -1)$	$1/15$
$(1, 1)$	$1/15$
$(1, 3)$	$2/5$

The entanglement entropy can thus be calculated to give

$$S_{EE} = \frac{4}{15} \log L + \begin{cases} 0 & \text{for } (0,0) \ \& \ (0,-2) \ \& \ (0,2) \\ -8(b^2 - a^2) \log \frac{b}{a} & \text{for } (1,1) \ \& \ (1,-1) \ \& \ (1,3) \end{cases} \tag{7.81}$$

where again $a := \frac{1}{\sqrt{5}} \sin \frac{\pi}{5}$ and $b := \frac{1}{\sqrt{5}} \sin \frac{2\pi}{5}$.

7.4.2 Unitary Minimal Series

In section 2.11.2 we already encountered the coset

$$\frac{su(2)_k \otimes su(2)_1}{su(2)_{k+1}}, \tag{7.82}$$

which can be identified with the unitary minimal series (2.45). The fields in the coset were labelled by three integers (l, m, s), where $l = 0, \ldots, k$, $m = 0, \ldots, k+1$ and $s = 0, 1$. The fields are subjected to the field identification $(l, m, s) \sim (k - l, k + 1 - m, 1 - s)$ and the restriction $l + m + s = 0 \bmod 2$. We can choose the standard range for the representation to be

$$I_k := \{(l, m, s) | 0 \leq l \leq k, \ 0 \leq m \leq k + 1, \ s = 0, l + m \ even\}. \tag{7.83}$$

With this we can determine the normalization constant N for the modular S-matrix of the coset theory

$$S_{l,m,s}^{l',m',s'} = N S_l^{l'} S_m^{m'} S_s^{s'}. \tag{7.84}$$

Here $S_l^{l'}$ is the modular S-matrix of $su(2)_k$, $S_m^{m'}$ of $su(2)_{k+2}$ and $S_s^{s'}$ of $su(2)_1$. We thus want to determine N s.t.

$$\sum_{(l',m',s') \in I_k} |S_{l,m,s}^{l',m',s'}|^2 = 1. \tag{7.85}$$

This can be done using the identities (see appendix C for a prove of the formulas)

$$\sum_{\substack{l'=0 \\ l' \ even}}^{k} |S_l^{l'}|^2 = \sum_{\substack{l'=0 \\ l' \ even}}^{k} \frac{2}{k+2} \sin^2\left(\pi \frac{(l+1)(l'+1)}{k+2}\right) = \frac{1}{2}\left(1 + \delta_{l,k/2}\right), \qquad (7.86)$$

$$\sum_{\substack{l'=0 \\ l' \ odd}}^{k} |S_l^{l'}|^2 = \sum_{\substack{l'=0 \\ l' \ odd}}^{k} \frac{2}{k+2} \sin^2\left(\pi \frac{(l+1)(l'+1)}{k+2}\right) = \frac{1}{2}\left(1 - \delta_{l,k/2}\right). \qquad (7.87)$$

With this the normalization can be determined as

$$\sum_{(l',m',s')\in I_k} |S_{l,m,s}^{l',m',s'}|^2 = 1 = N^2 \sum_{s'=0}^{0} \left(\sum_{\substack{l'=0 \\ even}}^{k} \sum_{\substack{m'=0 \\ even}}^{k+1} + \sum_{\substack{l'=0 \\ odd}}^{k} \sum_{\substack{m'=0 \\ odd}}^{k+1} \right) |S_l^{l'}|^2 |S_m^{m'}|^2 |S_s^{s'}|^2$$

$$\leftrightarrow N = 2. \qquad (7.88)$$

We can now calculate the entanglement entropy through topological interfaces in this coset theory. The subleading term to the entanglement entropy is then given by

$$s(l,m,s) = - \sum_{(l,m,s)\in I_k} |S_{l,m,s}^{l',m',s'}|^2 \log \left| \frac{S_{l,m,s}^{l',m',s'}}{S_{0,0,0}^{l',m',s'}} \right|^2 =$$

$$-4 \sum_{s'=0}^{0} \left(\sum_{\substack{l'=0 \\ even}}^{k} \sum_{\substack{m'=0 \\ even}}^{k+1} + \sum_{\substack{l'=0 \\ odd}}^{k} \sum_{\substack{m'=0 \\ odd}}^{k+1} \right) S_l^{l'}|^2 |S_m^{m'}|^2 |S_s^{s'}|^2 \left(\log\left|\frac{S_l^{l'}}{S_0^{l'}}\right|^2 + \log\left|\frac{S_m^{m'}}{S_0^{m'}}\right|^2 + \log\left|\frac{S_s^{s'}}{S_0^{s'}}\right|^2 \right) =$$

$$-2 \left(\sum_{l' \ even} \frac{1}{2}\left(1 + \delta_{m,\frac{k+1}{2}}\right) + \sum_{l' \ odd} \frac{1}{2}\left(1 - \delta_{m,\frac{k+1}{2}}\right) \right) |S_l^{l'}|^2 \log\left|\frac{S_l^{l'}}{S_0^{l'}}\right|^2 -$$

$$-2 \left(\sum_{m' \ even} \frac{1}{2}\left(1 + \delta_{l,\frac{k}{2}}\right) + \sum_{m' \ odd} \frac{1}{2}\left(1 - \delta_{l,\frac{k}{2}}\right) \right) |S_m^{m'}|^2 \log\left|\frac{S_m^{m'}}{S_0^{m'}}\right|^2 =$$

$$s_{su(2)_k}(l) + \delta_{m,\frac{k+1}{2}}\bar{s}_{su(2)_k}(l) + s_{su(2)_{k+1}}(m) + \delta_{l,\frac{k}{2}}\bar{s}_{su(2)_{k+1}}(m), \qquad (7.89)$$

where we defined the *projected* subleading term as

$$\bar{s}_{su(2)_k}(l) := - \sum_{l'=0}^{k} (-1)^{l'} |S_l^{l'}|^2 \log\left|\frac{S_l^{l'}}{S_0^{l'}}\right|^2. \qquad (7.90)$$

For small values of k we summarize some values of $\bar{s}_{su(2)_k}(l)$ in table 7.2.

k	$\bar{s}_{su(2)_k}(l)$
k odd	$0 \ \forall \ 0 \leq l \leq k$
2	0 for $l = 0, 2$
	$-\log 2$ for $l = 1$
4	0 for $l = 0, 4$
	$-\frac{1}{2}\log 3$ for $l = 1, 3$
	$-\frac{4}{3}\log 2$ for $l = 2$

Table 7.2: List of values of $\bar{s}_{su(2)_k}(l)$ for small values of k

Since the projected terms always come with a delta function the combination is always identically zero for all values of k, thus the entanglement entropy takes the final form

$$S(l, m, s) = \left(\frac{1}{2} - \frac{3}{(k+2)(k+3)} \right) \log L + s_{su(2)_k}(l) + s_{su(2)_{k+1}}(m). \qquad (7.91)$$

As in the parafermionic case the subleading contribution again decouples into its individual parts. Here we didn't write the contribution coming from $su(2)_1$ explicitly since it is identically zero for all values of s. We now consider two examples to illustrate the result.

Example 1: $k = 1$ as Ising model

For $k = 1$ the coset describes the critical point of second order phase transition of the Ising model. The fields and conformal weights are given by

(l, m, s)	$h_{l,m,s}$
$(0, 0, 0)$	0
$(0, 2, 0)$	$\frac{1}{2}$
$(1, 1, 0)$	$\frac{1}{16}$

The entanglement entropies for the given fields are then exactly the ones obtained in section 7.3.2.

Example 2: $k = 2$ as tri-critical Ising model

For $k = 2$ the coset theory is realized by the tri-critical Ising model with $c = 7/10$. The fields and conformal weights of this model are given by

(l, m, s)	$h_{l,m,s}$
$(0, 0, 0)$	0
$(0, 2, 0)$	$\frac{3}{5}$
$(1, 1, 0)$	$\frac{3}{80}$
$(1, 3, 0)$	$\frac{7}{16}$
$(2, 0, 0)$	$\frac{3}{2}$
$(2, 2, 0)$	$\frac{1}{10}$

For the corresponding entanglement entropies we find using the table 7.1

$$S(l, m, s) = \frac{7}{30} \log L + \begin{cases} 0 & \text{for } (0,0,0) \ \& \ (2,0,0) \\ -8(b^2 - a^2) \log \frac{b}{a} & \text{for } (0,2,0) \ \& \ (2,2,0) \\ -\log 2 & \text{for } (1,3,0) \\ -\log 2 - 8(b^2 - a^2) \log \frac{b}{a} & \text{for } (1,1,0) \end{cases} \tag{7.92}$$

7.4.3 $\mathcal{N} = 2$ Superconformal Minimal Models

The superconformal models with $\mathcal{N} = 2$ SUSY can be realized via the coset

$$\frac{su(2)_k \oplus u(1)_2}{u(1)_{k+2}}. \tag{7.93}$$

The central charge and highest weights are given via

$$c = \frac{3k}{k+2}, \tag{7.94}$$

$$h_{l,m,s} = \frac{l(l+2) - m^2}{4(k+2)} + \frac{s^2}{8} \mathrm{mod} 1. \tag{7.95}$$

Here the fields are labeled by three integer numbers (l, m, s) with

$$l = 0, \ldots, k \quad m = 0, \ldots, 2k+3 \ (\mathrm{mod}(2k+4)) \quad s = -1, 0, 1, 2 \ . \tag{7.96}$$

The $\mathbb{Z}_2$ field identifications again are given by

$$(l, m, s) \sim (k - l, k + 2 + m, 2 + s), \tag{7.97}$$

with the restriction

$$l + m + s = 0 \ \mathrm{mod} \ 2. \tag{7.98}$$

We will denote the set of all allowed labels that satisfy (7.96)-(7.98) as J_k. Thereby we can choose a standard range for the labels as

$$J_k = \{(l, m, s) | 0 \le l \le k, \ 0 \le m \le 2k+3, \ s = 0, 1 \ , \ l + m + s = 0 \ \mathrm{mod} \ 2\}. \tag{7.99}$$

Generally $s = -1, 1$ correspond to the R-sector, whereas $s = 0, 2$ correspond to the NS-sector respectively. Again in principle we have to distinguish the two cases where k is even or odd. Remarkably it again turns out that both cases lead to the same results. The modular S-matrix can be written in terms of the individual S-matrices including a normalization constant N as

$$S_{l,m,s}^{l',m',s'} = N S_l^{l'} S_m^{m'} S_s^{s'}. \tag{7.100}$$

As usual we demand for diagonal modular invariant theories

$$\sum_{(l',m',s') \in J_k} |S_{l,m,s}^{l',m',s'}|^2 = 1. \tag{7.101}$$

For the decomposition of the sum one finds

$$\sum_{(l',m',s') \in J_k} = \underbrace{\left(\sum_{l'=0 \ even}^{k} \sum_{m'=0 \ even}^{2k+3} + \sum_{l'=1 \ odd}^{k} \sum_{m'=1 \ odd}^{2k+3} \right) \sum_{s'=0}^{0}}_{\text{NS-sec contribution}} +$$

$$\underbrace{\left(\sum_{l'=0 \ even}^{k} \sum_{m'=1 \ odd}^{2k+3} + \sum_{l'=0 \ even}^{k} \sum_{m'=1 \ odd}^{2k+3} \right) \sum_{s'=1}^{1}}_{\text{R-sec contribution}} . \tag{7.102}$$

This can now be used to determine the normalization constant following a straightforward calculation with the result $N = 2$.

Using the same arguments as in the parafermionic case we find for the subleading term to the entanglement entropy

$$s(l,m,s) = - \sum_{(l',m',s') \in J_k} |S_{l,m,s}^{l',m',s'}|^2 \log \left| \frac{S_{l,m,s}^{l',m',s'}}{S_{0,0,0}^{l',m',s'}} \right|^2 =$$

$$- \frac{N^2}{4} \sum_{l'=0}^{k} |S_l^{l'}|^2 \log \left| \frac{S_l^{l'}}{S_0^{l'}} \right|^2 = s_{su(2)_k}(l). \tag{7.103}$$

For the entanglement entropy this then implies that it is just depending on the data coming from the $su(2)_k$ part of the model and is given via

$$S(l,m,s;k) = \frac{k}{k+2} \log L + s_{su(2)_k}(l). \tag{7.104}$$

As in the parafermionic case it just depends on the data coming from the $su(2)_k$ contribution since the $u(1)_k$ does not contribute to the entanglement entropy.

Example: $k = 1$ as super-parafermion theory

The super-parafermionic theory is realized by twelve fields with one half corresponding to NS-fields and the other half to R-fields. In terms of $\mathcal{N} = 2$ minimal model labels these fields are given as follows

NS	R
$(0, 0, 0)$	$(0, 1, 1)$
$(0, 2, 0)$	$(0, 3, 1)$
$(0, 4, 0)$	$(0, 5, 1)$
$(1, 1, 0)$	$(1, 0, 1)$
$(1, 3, 0)$	$(1, 2, 1)$
$(1, 5, 0)$	$(1, 4, 1)$

The EE is identical for all twelve and given by

$$S(l, m, s; 1) = \frac{1}{3} \log L. \tag{7.105}$$

Note that in the case $k = 1$ we have the equality for the coset:

$$\frac{su(2)_1 \oplus u(1)_2}{u(1)_3} = u(1)_6, \tag{7.106}$$

also leading to twelve distinguished fields with only a leading term contribution to the entanglement entropy.

Chapter 8

Left/Right Entanglement Entropy

8.1 Left/Right Entanglement Entropy

In this section we consider a system with a boundary [60]. As we have seen in section 4.6 the real-space entanglement entropy of a system with boundary receives a correction by the boundary entropy $s = \log g$, where g is the universal non-integer ground-state degeneracy of [38]. The entanglement entropy we are interested in is the left/right entanglement entropy (LREE) considered before in [87] for the free boson and in [88, 89] for generic CFTs. The two subsystems consist of the left- and right-moving part of the Hilbert space. As mentioned in chapter 3, a conformal boundary condition is the maximally reflective solution to the interface conformality condition

$$\lim_{y \searrow 0}(T^{(1)}(x + iy) - \tilde{T}^{(1)}(x - iy)) = \lim_{y \nearrow 0}(T^{(2)}(x + iy) - \tilde{T}^{(2)}(x - iy)). \tag{8.1}$$

For a CFT in the upper half-plane, the components of the bulk energy-momentum tensor satisfy

$$T = \bar{T}|_{\mathbb{R}} . \tag{8.2}$$

As usual we can associate to each boundary condition a boundary state. Again as in section 2.13.3 we map the upper half plane to the unit disc, see figure 2.10, the boundary condition becomes such a boundary state in standard radial quantisation. The defining property for a conformal boundary state $|B\rangle$ is the gluing condition

$$(L_n - \bar{L}_{-n})|B\rangle = 0 . \tag{8.3}$$

This means that the boundary state breaks one half of the conformal charges. As before, we decompose the Hilbert space as

$$\mathcal{H}^{(n)} = \bigoplus_{(i,\bar{i})} M_{i\bar{i}}^{(n)} \mathcal{H}_i \otimes \mathcal{H}_{\bar{i}}. \tag{8.4}$$

As usual we can build a consistent boundary state out of Ishibashi states via

$$|B\rangle = \sum_{\mathbf{i}} b_{B\mathbf{i}}|\mathbf{i}\rangle\rangle. \tag{8.5}$$

In this section, bold-faced indices

$$\mathbf{i} = (i, \alpha, \beta) \tag{8.6}$$

only contain one representation label since by the boundary left- and right-moving degrees of freedom are identified. The sum in (8.5) and in the rest of this section only runs over representations of the bulk space of states with $i = \bar{\imath}$. The multiplicity labels α and β distinguish the different instances where the representation i appears in the holomorphic and anti-holomorphic part of the space of states, respectively.

In our original setup, correlators and fields in the boundary CFT will depend on holomorphic and anti-holomorphic coordinates restricted to the upper half plane. Using the Cardy doubling trick as discussed in section 2.13.2, we regard the dependence on anti-holomorphic coordinates $\bar{z}$ on the upper half plane as a dependence on a holomorphic coordinate $z^* = \bar{z}$ for mirror fields on the lower half plane. This means that we can consider a chiral construction on the full plane, where the stress tensor is continuous everywhere. The boundary condition is then a topological interface in this chiral part of a CFT, located on the real line.

Unfolding the Ishibashi states one obtains interface-like operators $\|\mathbf{i}\|$ that project onto a specific pair of representations $\mathbf{i}$. We, therefore, associate to the boundary state (8.5) an interface operator

$$I(B) = \sum_{\mathbf{i}} b_{B\mathbf{i}} \|\mathbf{i}\| . \tag{8.7}$$

The computation of the (left/right) entanglement entropy now proceeds in analogy with the previous sections. The characters in the expression

$$Z(n) = \sum_{i} \mathrm{Tr} \left(b_{B^*\mathbf{i}} b_{B\mathbf{i}} \right)^n tr_{\mathcal{H}_i} \left(e^{-2\delta H} \right) = \sum_{i} \mathrm{Tr} \left(b_{B^*\mathbf{i}} b_{B\mathbf{i}} \right)^n \chi_i \left(e^{-2\delta n} \right) \tag{8.8}$$

can be written by means of the modular S-matrix as

$$Z(n) = \sum_{i} \mathrm{Tr} \left(b_{B^*\mathbf{i}} b_{B\mathbf{i}} \right)^n S_{ij} \chi_j \left(e^{-\frac{2\pi^2}{\delta n}} \right) \approx \sum_{i} \mathrm{Tr} \left(b_{B^*\mathbf{i}} b_{B\mathbf{i}} \right)^n S_{i0} e^{\frac{2\pi^2 c}{24\delta n}} . \tag{8.9}$$

Again for the general boundary state with open string vacuum multiplicity $\mathcal{N}_{0B}^{B}$ we write the entanglement entropy again in terms of a probability distribution, which is defined by the traces of the matrices [60]

$$p_{\mathbf{i}}^{B} = \frac{b_{B^*\mathbf{i}} b_{B\mathbf{i}} S_{i0}}{\mathcal{N}_{0B}^{B}} . \tag{8.10}$$

In (8.10) we abuse the index notation in the same way as in the previous chapters — while the indices $\mathbf{i}$ on the right-hand side contain one multiplicity label for holomorphic and one for antiholomorphic representations (and we again suppress the summation over interior labels), the index $\mathbf{i}$ on the left-hand side includes two multiplicity labels of the same kind. In this way we can write the LREE for a system with a boundary condition B as

$$\tilde{S} = \frac{c}{6} \log L - \sum_{i} \mathrm{Tr} \, p_{\mathbf{i}}^{B} \log \frac{p_{\mathbf{i}}^{B}}{S_{i0}} . \tag{8.11}$$

In contrast to the 'ordinary' entanglement entropy the coefficient in front of the term $\log L$ is one half the prefactor in the case of the full theory without boundary. This exactly coincides with the area law mentioned in [78]. In order to distinguish the EE and LREE later on we denote the LREE by $\tilde{S}$ and the entanglement entropy by S.

A natural question is whether it is again possible to interpret the result in terms of a Kullback-Leibler divergence. However, for interfaces there is a generic "neutral" interface (the identity defect) with respect to which one can compute the relative entropy. This is no longer the case for boundaries, as there is no "neutral" boundary on the full plane that could serve as a reference point. There will generically always be "information loss" when left movers are scattered by the boundary into right movers. Exceptional cases occur when the boundary condition is a permutation boundary condition obtained by folding an identity or symmetry defect to a boundary condition for a tensor product of identical CFTs.

Technically, one can try to interpret the denominator in the logarithm of (8.11) as a distribution corresponding to the entries S_{i0} times appropriate identity matrices. However, the sum over the traces of these matrices is in general not equal to 1, and, therefore, it is not a probability distribution. In the cases where it is, we indeed obtain the relative entropy with respect to a permutation boundary state, where each $b_{\mathbf{i}}$ is a permutation matrix. However, in general we conclude that the interpretation as a relative entropy fails in the case of the LREE boundary states.

An immediate consequence of losing the interpretation of the LREE as a relative entropy is that the contribution

$$\tilde{s} = - \sum_i \operatorname{Tr} p_{\mathbf{i}}^B \log \frac{p_{\mathbf{i}}^B}{S_{i0}} \tag{8.12}$$

is not necessarily negative anymore. Using the same technique that we applied in chapter 7 yields the upper bound

$$\tilde{s} \leq \log \left(\sum_i S_{i0} \right). \tag{8.13}$$

It is clear that this bound does not need to be negative. To see this we can consider boundary states in diagonal rational models. In these cases the boundary states are labelled by a irreducible representation a of the symmetry algebra. The coefficients b_{ai} of the elementary boundary states in this case are

$$b_{ai} = \frac{S_{ai}}{\sqrt{S_{i0}}}. \tag{8.14}$$

Plugging this into (8.10) and (8.12) we obtain the LREE of diagonal rational models

$$\tilde{S} = \frac{c}{6} \log L - \sum_i |S_{ai}|^2 \log \frac{|S_{ai}|^2}{S_{i0}}. \tag{8.15}$$

This reproduces the result obtained in [88]. For later use we define the subleading contri-

bution to the left/right entanglement entropy as

$$\tilde{s} := -\sum_i |S_{ai}|^2 \log \frac{|S_{ai}|^2}{S_{i0}}. \tag{8.16}$$

It seems plausible that all symmetry-preserving boundary states in a diagonal model have the LREE of the Cardy brane associated to the identity as an upper bound,

$$\tilde{s} \leq -\sum_i S_{0i}^2 \log S_{0i} \,. \tag{8.17}$$

In particular the right-hand side is stricter than the bound (8.13) since $0 \leq S_{0i}^2 \leq 1$, and it is always positive.

8.2   Examples for Left/Right Entanglement Entropies

In this section we consider some simple examples for the left/right entanglement entropy in diagonal rational models. The first four examples 8.2.1, 8.2.3 and 8.2.4 can also be found in [60].

8.2.1   Example: Ising model

The LREE for boundary states of the Ising model has already been discussed in [88]. Here we quote the results for illustration. The Cardy states in the Ising model are explicitly given in terms of Ishibashi states by

$$\begin{aligned}
|id\rangle &= \tfrac{1}{\sqrt{2}}\big(|id\rangle\rangle + |\epsilon\rangle\rangle + 2^{\frac{1}{4}}|\sigma\rangle\rangle\big)\,, \\
|\epsilon\rangle &= \tfrac{1}{\sqrt{2}}\big(|id\rangle\rangle + |\epsilon\rangle\rangle - 2^{\frac{1}{4}}|\sigma\rangle\rangle\big)\,, \\
|\sigma\rangle &= |id\rangle\rangle - |\epsilon\rangle\rangle\,.
\end{aligned} \tag{8.18}$$

The contributions to the LREE we obtain from (8.12) are

$$\tilde{s} = \frac{3\log 2}{4} \ \text{ for } \ |id\rangle\,,\ |\epsilon\rangle\,, \qquad \text{and} \qquad \tilde{s} = 0 \ \text{ for } \ |\sigma\rangle\,. \tag{8.19}$$

With our formula (8.15) using the modular S-matrix for the Ising model (7.31) we exactly reproduce the results.

8.2.2   Example: $u(1)_k$ boundary states

In this short example we calculate the LREE associated to a $u(1)_k$ boundary states. As a reminder the modular S-matrix is given by

$$S_m^{m'} = \frac{1}{\sqrt{2k}} \exp\left(-i\pi\frac{m \cdot m'}{2k}\right). \tag{8.20}$$

Thus we find using (8.15)

$$\tilde{S}(k) = \frac{1}{6} \log L + \tilde{s}_{u(1)_k} = \frac{1}{6} \log L + \frac{1}{2} \log(2k). \tag{8.21}$$

In particular this means that the subleading term $\tilde{s}_{u(1)_k} = \frac{1}{2} \log(2k)$ is independent of the boundary label m and just depends on k. It is commonly known that the $u(1)_k$ theory corresponds to a free boson compactified on a circle of radius $R = \sqrt{2k}$. Thus again we can write the LREE in terms of the radius via

$$\tilde{S} = \frac{1}{6} \log L + \log R. \tag{8.22}$$

8.2.3 Example: $su(2)_k$ boundary states and the $k \to \infty$ limit

Analogously to the example of $su(2)_k$ defects in section 7.3.4 we consider the LREE of boundary states in the WZW models $su(2)_k$ in the limit $k \to \infty$. For finite k, the theory is diagonal and rational, and the formulae of [88] apply. The Cardy states (8.14) are again labelled by spins $s = b/2$ for $b = 0, 1, \ldots, k$. From (8.15), the universal contribution to the LREE by the state B_b is

$$\tilde{s}(b) = - \sum_{i=0}^{k} \frac{2}{k+2} \sin^2(\pi(b+1)\frac{(i+1)}{k+2}) \log \frac{\sin^2(\pi(b+1)\frac{i+1}{k+2})}{\sin(\pi\frac{i+1}{k+2})} + \log \sqrt{\frac{2}{k+2}}. \tag{8.23}$$

Here we have split off a factor depending only on k from the argument of the logarithm, and used that $\sum_i |S_b^i|^2 = 1$. Note that the shift term $-\log(k+2)$ in (8.23) has the right form to be identified with (the logarithm of) the radius of the target space. The target space of the $su(2)_k$ WZW model is the (fuzzy) sphere S^3 at radius $R = \sqrt{k}$.

In the large k limit the sum in (8.23) becomes an integral. By the same methods as in section 7.3.4 we obtain

$$\tilde{s}(b) = -\frac{2b+1}{2b+2} + \frac{1}{2} \log 2 + \log R \qquad , k \to \infty . \tag{8.24}$$

The positive (and infinite) contribution from the radius is similar to the radius contribution to the LREE of Dirichlet branes of the compactified boson [87], see (9.27).

For completeness we also state the subleading contribution to the LREE for small values of k (see table 8.1). We will need them later when discussing coset model boundary states involving $su(2)_k$.

8.2.4 Example: Fusion of defect and boundary in the $su(2)_k$ WZW model

As we have seen in section 3.4 a topological interface can be fused onto a boundary state. Here we are now interested in how the LREE behaves under this fusion. Therefore, we

k	$\tilde{s}_{su(2)_k}(l)$
1	$\frac{1}{2}\log 2$ for $l = 0, 1$
2	$\frac{3}{4}\log 2$ for $l = 0, 2$
	0 for $l = 1$
3	$-\frac{1}{2}\log 2 - 4[a^2\log a + b^2\log b]$ for $l = 0, 3$
	$-\frac{1}{2}\log 2 - 4[(2a^2 - b^2)\log a + (2b^2 - a^2)\log b]$ for $l = 1, 2$
4	$\frac{2}{3}\log 2 + \frac{1}{4}\log 3$ for $l = 0, 4$
	$\log 2 - \frac{1}{4}\log 3$ for $l = 1, 3$
	$\frac{1}{2}\log 3 - 2\log 2$ for $l = 2$

Table 8.1: Values of $\tilde{s}_{su(2)_k}(\mathcal{D}_l)$ for small values of k with $a = \frac{1}{\sqrt{5}}\sin(\pi/5)$ and $b = \frac{1}{\sqrt{5}}\sin(2\pi/5)$.

consider the topological defect

$$\mathcal{D}_a = \sum_i \frac{S_{ia}}{S_{i0}}||i|| \tag{8.25}$$

and the boundary state in a WZW $su(2)_k$ model given by

$$|\mathcal{B}_b\rangle = \sum_i \frac{S_{bi}}{S_{0i}}|i\rangle\rangle. \tag{8.26}$$

Fusion yields a new boundary state $|\mathcal{B}'\rangle$

$$|\mathcal{B}'\rangle = \mathcal{D}_a |\mathcal{B}_b\rangle = \sum_i \frac{S_{ai}S_{bi}}{S_{0i}^{3/2}}|i\rangle\rangle. \tag{8.27}$$

By unfolding we thus obtain the new defect operator with coefficients

$$b_{\mathcal{B}'i} = \frac{S_{ai}S_{bi}}{S_{0i}^{3/2}}. \tag{8.28}$$

The number of open-string vacua in the self-spectrum of $|\mathcal{B}'\rangle$ is

$$\mathcal{N}_{0\mathcal{B}'}^{\mathcal{B}'} = \sum |b_{\mathcal{B}'i}|^2 S_{0i} = \sum_i N_{aa}^i N_{bb}^i = \min(a, b) + 1\,, \tag{8.29}$$

where again N_{ab}^c are the $su(2)_k$ fusion numbers. The number of open-string vacua is exactly the same as in the case of the fusion products of two elementary defects (see section 7.3.4). The subleading contribution to the LREE can thus be written as

$$\tilde{s}(a \times b) = \log(\min(a, b) + 1) - \frac{\sum_i |b_{Bi}|^2 S_{0i}\log|b_{Bi}|^2}{\min(a, b) + 1}\,. \tag{8.30}$$

Observe that $\min(a, b) + 1$ is also again the number of elementary branes in the decomposition

$$|\mathcal{B}'\rangle = \sum_c N_{ab}^{\ c} |c\rangle \tag{8.31}$$

of the fusion product.

In the large k limit of the $su(2)_k$ WZW model, the LREE of the fusion product differs from the entropy of the original boundary state $|\mathcal{B}_b\rangle$ again by a rational term and the logarithm of the number of elementary branes in the decomposition. Indeed, in the limit of large k the numerator in the second term of the right-hand side of (8.30) becomes

$$\sum_i |b_{B'i}|^2 S_{0i} \log |b_{B'i}|^2 \xrightarrow{k \to \infty} \tag{8.32}$$

$$- \log \sqrt{\tfrac{2}{k+2}} + \frac{2}{\pi} \int_0^\pi \frac{\sin^2((a+1)x)\sin^2((b+1)x)}{\sin^2(x)} \log \left(\frac{\sin^2((a+1)x)\sin^2((b+1)x)}{\sin^3(x)} \right) \, dx \, .$$

A similar calculation as in section 7.3.4 leads to

$$\tilde{s}(a \times b) = \log \min(a+1, b+1) + \frac{1}{2}\log 2 + \log R - \frac{p}{q} \quad , k \to \infty, \tag{8.33}$$

for some $p, q \in \mathbb{N}$. The difference between the entanglement entropy of the boundary state after fusion (8.33) and the original boundary state (8.24) for $k = \infty$ is, therefore,

$$\tilde{s}(a \times b) - \tilde{s}(b) = \log(\min(a, b) + 1) - \frac{p}{q} \, . \tag{8.34}$$

8.3   LREE in Coset Models

8.3.1   Parafermionic Coset

We can apply the result (8.15) to parafermionic boundary states with modular S-matrix

$$S_{lm}^{l'm'} = 2 S_l^{l'} S_m^{*m'} . \tag{8.35}$$

Inserting the expression into the subleading term in (8.15) we find

$$\tilde{s}(l, m) = - \sum_{(l',m') \in PF(k)} 4|S_l^{l'}|^2 |S_m^{m'}|^2 \log \frac{2|S_l^{l'}|^2 |S_m^{m'}|^2}{S_0^{l'} S_0^{*m'}} =$$

$$- \sum_{(l',m') \in PF(k)} 4|S_l^{l'}|^2 |S_m^{m'}|^2 \left(\log 2 + \log \frac{|S_l^{l'}|^2}{S_0^{l'}} + \log \frac{|S_m^{m'}|^2}{S_0^{*m'}} \right) =$$

$$-\frac{1}{4} \sum_{l'=0}^{k} \sum_{m'=-k+1}^{k} 4|S_l^{l'}|^2 |S_m^{m'}|^2 \left(\log 2 + \log \frac{|S_l^{l'}|^2}{S_0^{l'}} + \log \frac{|S_m^{m'}|^2}{S_0^{*m'}} \right) =$$

$$-\log 2 + \tilde{s}_{su(2)_k}(l) + \tilde{s}_{u(1)_k}(m). \tag{8.36}$$

Thus the total LREE for the parafermionic case reads

$$\tilde{S}(l,m) = \frac{k-1}{3(k+2)} + \tilde{s}_{su(2)_k}(l) + \tilde{s}_{u(1)_k}(m) - \log 2. \tag{8.37}$$

From the formula we see that the subleading term to the LREE for this specific coset model decomposes into a part coming from $su(2)_k$, a part coming from $u(1)_k$ and an additional term $-\log 2$ that can be associated with the normalization constant. Let us again discuss the two simplest models which can be obtained from this theory

Example 1: $k = 2$ as the Ising model
In section 8.2.1 we already calculated the LREE for the Ising model boundary states. For $k = 2$ the parafermionic theory realizes the Ising model with the three fields of conformal dimension

(l, m)	$h_{l,m}$
$(0, 0)$	0
$(0, 2)$	$1/2$
$(1, 1)$	$1/16$

For (8.37) we thus find

$$\tilde{S}_{LREE} = \frac{1}{12} \log L + \begin{cases} \frac{3}{4} \log 2 & \text{for } (0,0) \ \& \ (0,2) \\ 0 & \text{for } (1,1) \end{cases} \tag{8.38}$$

which exactly reproduces the results from the boundary state case.

Example 2: $k = 3$ as the three state Potts model
Again for $k = 2$ one reproduces the fractional spectrum of the three state Potts model with fields of conformal weight

(l, m)	$h_{l,m}$
$(0, 0)$	0
$(0, 2)$	$2/3$
$(0, -2)$	$2/3$
$(1, -1)$	$1/15$
$(1, 1)$	$1/15$
$(1, 3)$	$2/5$

For the LREE we thus obtain

$$\tilde{S}(l,m) = \frac{2}{15}\log L +$$

$$+\frac{1}{2}\log\frac{3}{4} + \begin{cases} -4[a^2\log a + b^2\log b] & \text{for } (0,0) \ \& \ (0,2) \ \& \ (0,-2) \\ -4[(2a^2-b^2)\log a + (2b^2-a^2)\log b] & \text{for } (1,-1 \ \& \ (1,1) \ \& \ (1,3) \end{cases} \quad (8.39)$$

where again $a := \frac{1}{\sqrt{5}}\sin\frac{\pi}{5}$, $b := \frac{1}{\sqrt{5}}\sin\frac{2\pi}{5}$.

8.3.2 Unitary Minimal Series

As a second example for the left/right entanglement entropy in coset theories we again consider the case of the unitary minimal series realized by the coset

$$\frac{su(2)_k \otimes su(2)_1}{su(2)_{k+1}}. \quad (8.40)$$

The calculation for the subleading term to the left/right entanglement entropy now proceeds in a similar fashion to the calculation of the entanglement entropy of section 7.4.2

$$\tilde{s}(l,m,s) = -4\sum_{\substack{l'+m' \ even \\ s'=0}} |S_l^{l'}|^2 |S_m^{m'}|^2 |S_s^{s'}|^2 \log\left(2\frac{|S_l^{l'}|^2}{S_0^{l'}}\frac{|S_m^{m'}|^2}{S_0^{m'}}\frac{|S_s^{s'}|^2}{S_0^{s'}}\right) =$$

$$-\log 2 - 2\left(\sum_{l' \ even}\sum_{m' \ even} + \sum_{l' \ odd}\sum_{m' \ odd}\right)\left(\log\frac{|S_l^{l'}|^2}{S_0^{l'}} + \log\frac{|S_m^{m'}|^2}{S_0^{m'}} + \log\frac{|S_s^0|^2}{S_0^0}\right) =$$

$$-\log 2 + \tilde{s}_{su(2)_1}(s) - \left(\sum_{l' \ even}(1 + \delta_{m,\frac{k+1}{2}}) + \sum_{l' \ odd}(1 - \delta_{m,\frac{k+1}{2}})\right)\log\frac{|S_l^{l'}|^2}{S_0^{l'}} -$$

$$-\left(\sum_{m' \ even}(1 + \delta_{l,\frac{k}{2}}) + \sum_{m' \ odd}(1 - \delta_{l,\frac{k}{2}})\right)\log\frac{|S_m^{m'}|^2}{S_0^{m'}} =$$

$$-\log 2 + \tilde{s}_{su(2)_k}(l) + \tilde{s}_{su(2)_{k+1}} + \tilde{s}_{su(2)_1}(s) + \delta_{m,\frac{k+1}{2}}\bar{\bar{s}}_{su(2)_k}(l) + \delta_{l,\frac{k}{2}}\bar{\bar{s}}_{su(2)_{k+2}}(m), \quad (8.41)$$

where we defined

$$\bar{\bar{s}}_{su(2)_k}(l) := -\sum_{l'=0}^{k}(-1)^{l'}|S_l^{l'}|^2 \log\frac{|S_l^{l'}|^2}{S_0^{l'}}. \quad (8.42)$$

Again the terms including the delta functions drop identically since either $\bar{\bar{s}}$ is zero or the delta function. Thus we find for the left/right entanglement entropy of the unitary minimal series

$$\tilde{S}(l,m,s) = \left(\frac{1}{4} - \frac{3}{2(k+2)(k+3)}\right)\log L + \tilde{s}_{su(2)_k}(l) + \tilde{s}_{su(2)_{k+1}} + \tilde{s}_{su(2)_1}(s) - \log 2. \quad (8.43)$$

As in the parafermionic case we see that the subleading term decouples into its individual parts. The additional term $-\log 2$ can again be associated with the normalization constant of the coset. As in section 7.4.2 let us consider the two simplest examples corresponding to the Ising and tri-critical Ising model.

Example 1: $k = 1$ as Ising model

The three fields in this model are given by $(0, 0, 0)$, $(0, 2, 0)$ and $(1, 1, 0)$. Their corresponding left/right entanglement entropies read

$$\tilde{S}(l, m, s) = \frac{1}{12} \log L + \begin{cases} \frac{3}{4} \log 2 & \text{for } (0, 0, 0) \ \& \ (0, 2, 0) \\ 0 & \text{for } (1, 1, 0) \end{cases} \tag{8.44}$$

Example 2: $k = 2$ as tri-critical Ising model

The tri-critical Ising model consists of the six fields $(0, 0, 0)$, $(0, 2, 0)$, $(1, 1, 0)$, $(1, 3, 0)$, $(2, 0, 0)$ and $(2, 2, 0)$. For the left/right entanglement entropies we thus find using table 8.1

$$\tilde{S}(l, m, s) = \frac{7}{60} \log L + \begin{cases} -\frac{1}{4} \log 2 - 4(a^2 \log a + b^2 \log b) & \text{for } (0, 0, 0) \ \& \ (2, 0, 0) \\ -\frac{1}{4} \log 2 - 4[(2a^2 - b^2) \log a + (2b^2 - a^2) \log b] & \text{for } (0, 2, 0) \ \& \ (2, 2, 0) \\ -\log 2 - 4[(2a^2 - b^2) \log a + (2b^2 - a^2) \log b] & \text{for } (1, 1, 0) \\ -\log 2 - 4(a^2 \log a + b^2 \log b) & \text{for } (1, 3, 0) \end{cases}$$
$$\tag{8.45}$$

8.3.3 $\mathcal{N} = 2$ Superconformal Minimal Models

For superconformal minimal models with $\mathcal{N} = 2$ supersymmetry the LREE can also be calculated in a similar manner as for the parafermionic case. Using the decomposition of the sum as in (7.102) the subleading term to the LREE in this case is given by

$$\tilde{s}(l, m, s) = - \sum_{(l', m', s') \in J_k} |S_{l,m,s}^{l',m',s'}|^2 \log \frac{|S_{l,m,s}^{l',m',s'}|^2}{S_{0,0,0}^{l',m',s'}} =$$

$$-\frac{N^2}{8(k+2)} \sum_{(l', m', s') \in J_k} |S_l^{l'}|^2 \log \left[\frac{N}{\sqrt{8(k+2)}} \frac{|S_l^{l'}|^2}{S_0^{l'}} \right] =$$

$$-\frac{N^2}{4} \sum_{l'=0}^{k} |S_l^{l'}|^2 \left[\log \frac{N}{\sqrt{8(k+2)}} + \log \frac{|S_l^{l'}|^2}{S_0^{l'}} \right] =$$

$$-\log \frac{1}{\sqrt{4}} - \log \frac{1}{\sqrt{2(k+2)}} - \log 2 - \sum_{l'=0}^{k} |S_l^{l'}|^2 \log \frac{|S_l^{l'}|^2}{S_0^{l'}} =$$

$$\tilde{s}_{su(2)_k}(l) + \tilde{s}_{u(1)_{k+2}}(m) + \tilde{s}_{u(1)_2}(s) - \log 2. \tag{8.46}$$

We see that as in the parafermionic case the subleading term decomposes into the individual parts and an additional term $-\log 2$ related to the normalization constant. For the LREE we thus find

$$\tilde{S}(l, m, s; k) = \frac{k}{2(k+2)} \log L + \tilde{s}_{su(2)_k}(l) + \tilde{s}_{u(1)_{k+2}}(m) + \tilde{s}_{u(1)_2}(s) - \log 2. \tag{8.47}$$

Example: $k = 1$ as super-parafermionic theory

As discussed in section 7.4.3 the super-parafermionic theory consists of twelve individual fields. Nevertheless, the LREE for all these fields is equal and given by

$$\tilde{S}(l, m, s; 1) = \frac{1}{6} \log L + \tilde{s}_{su(2)_1}(l) + \tilde{s}_{u(1)_3}(m) + \tilde{s}_{u(1)_2}(s) - \log 2 =$$

$$\frac{1}{6} \log L + \frac{1}{2} \log 2 + \frac{1}{2} \log 6 + \frac{1}{2} \log 4 - \log 2 =$$

$$\frac{1}{6} \log L + \frac{1}{2} \log(2 \cdot 6) =$$

$$\frac{1}{6} \log L + \tilde{s}_{u(1)_6}. \tag{8.48}$$

Even more obvious as in the case of the entanglement entropy we observe in a nice way the level rank duality

$$\frac{su(2)_1 \otimes u(1)_2}{u(1)_3} = u(1)_6. \tag{8.49}$$

Chapter 9

Results for Bosonic Tori

In this chapter we briefly want to discuss the entanglement entropy (left/right entanglement entropy) through topological interfaces for the case of d free bosons compactified on a torus which can also be found in [60]. For a brief discussion and conventions of the free boson CFT description see appendix B.

9.1 EE through topological defects

For the case of d free bosons compactified on a torus the interface operators are explicitly known [55]. The ground states of the theory form an even, self dual lattice $\Gamma \subset \mathbb{R}^{d,d}$, where the lattice vectors are of the form $\gamma = (p, \bar{p})$. The d-dimensional vectors p and $\bar{p}$ denote left- and right-moving momenta respectively.

We consider topological interfaces that also preserve the full $u(1)^d$ symmetry, i.e. these interfaces are specified by a gluing matrix $\Lambda \in O(d|\mathbb{R}) \times O(d|\mathbb{R})$, which implies on the modes of the d bosons

$$\begin{pmatrix} a_n^1 \\ -\bar{a}_{-n}^1 \end{pmatrix} I_{1,2} = I_{1,2} \Lambda \begin{pmatrix} a_n^2 \\ -\bar{a}_{-n}^2 \end{pmatrix}, \tag{9.1}$$

where the modes of the left and right $u(1)^d$ currents are considered to be d-dimensional vectors. Especially $n = 0$ corresponds to the modes for the charges mentioned above.

Similarly to the rational case discussed earlier, the interface operators can be written as linear combinations of operators between $u(1)^d$ highest weight representations:

$$I_{12}(\Lambda) = \sum_{\gamma \in \Gamma_{12}^\Lambda} d_{\Lambda\gamma} ||\gamma||. \tag{9.2}$$

The projector $||\gamma||$ is an intertwiner of the representation space specified by the lattice vector γ, and $d_{\Lambda\gamma}$ are prefactors constrained by consistency under modular S-transformation. The range of the summation is restricted to a sublattice, given in terms of a gluing condition Λ for the lattices Γ_1 and Γ_2 on the two sides of the interface,

$$\Gamma_{12}^\Lambda = \{\gamma \in \Gamma_1 \,|\, \Lambda\gamma \in \Gamma_2\} = \Gamma_1 \cap \Lambda^{-1}\Gamma_2 \subset \Gamma_1. \tag{9.3}$$

For admissible gluing conditions Λ, the sublattice Γ_{12}^Λ has full rank. Consistency under modular S transformation then demands that $d_{\Lambda\gamma} = g_{12}^\Lambda \exp(2\pi i\varphi(\gamma))$, where $\varphi \in (\Gamma_{12}^\Lambda)^\star$ and

$$(g_{12}^\Lambda)^2 = |\Gamma_1/\Gamma_{12}^\Lambda| \tag{9.4}$$

is the index of the sublattice Γ_{12}^Λ inside the lattice Γ_1. Since the modes of the lattice and oscillating part decouple one may split the interface operator according to

$$I_{12} = I_{12}^0(\Lambda) \prod_{n>0} I_{12}^n(\Lambda) \,, \tag{9.5}$$

where

$$I_{12}^0 = g_{12}^\Lambda \sum_{\gamma \in \Gamma_{12}^\Lambda} e^{2\pi i\varphi(\gamma)} |\Lambda\gamma\rangle \langle\gamma| \tag{9.6}$$

gives the map for the zero modes and the

$$I_{12}^n = \exp\left(-\frac{1}{n}\left(a_{-n}^2 \Lambda_{11} a_n^1 + \tilde{a}_{-n}^2 \Lambda_{22} \tilde{a}_n^1\right)\right) \tag{9.7}$$

for $n > 0$ give the contribution of the higher oscillating modes. As the interface operator acts as a map it is implicitly understood that modes of CFT_1 act from the right and modes of CFT_2 from the left of I_{12}^0.

We are now in the position to determine the entanglement entropy through this topological defects. In order to do this we proceed as before. The partition function of the n-sheeted Riemann surface[1] for the topological defect (7.1) is

$$\begin{aligned} Z(n) &= \mathrm{Tr}\left(\left(II^\dagger\right)^n e^{-2\delta KH}\right) \\ &= (g_{12}^\Lambda)^{2n} \sum_{(p,\bar{p})=\gamma \in \Gamma_{12}^\Lambda} \chi_p(i\frac{\delta}{\pi}n)\bar{\chi}_{\bar{p}}(i\frac{\delta}{\pi}n) \,, \end{aligned} \tag{9.8}$$

where the χ_p are the $u(1)$ characters. As usual we perform a modular S-transformation and express $Z(n)$ in terms of characters depending on the S-transformed variable $i\pi/n\delta$. This leads to a summation over lattice vectors in the dual lattice $\Gamma_{12}^\vee$. In the limit $\delta \ll 1$ we approximate the lattice sum by the dominant contribution of the vacuum $p = \bar{p} = 0$,

$$\begin{aligned} Z(n) &= (g_{12}^\Lambda)^{2n} \sum_{(q,\bar{q})\in\Gamma_{12}^\vee} a_{(q,\bar{q})}\chi_q(i\frac{\pi}{n\delta})\bar{\chi}_{\bar{q}}(-i\frac{\pi}{n\delta}) \\ &\approx (g_{12}^\Lambda)^{2n} a_{(0,0)} e^{\frac{\pi^2 d}{6\delta n}} \,. \end{aligned} \tag{9.9}$$

Using that the interfaces with the normalization (9.4) are elementary, we obtain for $n = 1$ the ordinary defect partition function, where the multiplicity of the vacuum propagating in the S-dual channel is 1. From this we can conclude that $a_{(0,0)} = 1/(g_{12}^\Lambda)^2$.

---

[1]Do not confuse that here n now stands for the number of sheets and not for the index of the modes for the free boson

Using $\delta = \pi^2/\log(L)$, $c = d$ for the central charge of d bosons, and (9.4), the entanglement entropy is given by

$$S = (1 - \partial_n) \log(Z(n))\big|_{n=1} = \frac{c}{3} \log(L) - \log |\Gamma_1/\Gamma_{12}^\Lambda| \,. \tag{9.10}$$

Considering the special case $d = 1$, *i.e.* for a free boson compactified on a circle, conformal interfaces between CFT$_1$ and CFT$_2$ are classified by two winding numbers k_1 and k_2. For generic compactification radii of the two CFTs these interfaces are not topological, but they become so by choosing radii to satisfy the relation $R_1/R_2 = k_2/k_1$ [41], where R_1 is the compactification radius in CFT$_1$ and R_2 is the compactification radius in CFT$_2$. In this case the index of the sublattice has been calculated [41, 55] to be

$$|\Gamma_1/\Gamma_{12}^\Lambda| = |k_1 k_2| \,, \tag{9.11}$$

such that the entanglement entropy through the topological interface is given by

$$S = \frac{1}{3} \log(L) - \log |k_1 k_2| \,. \tag{9.12}$$

The result is in agreement with the one obtained in [82].

All topological toroidal interfaces are duality interfaces according to the definition presented in section 3.1. A subclass of them are symmetry interfaces and describe automorphisms of the toroidal CFT. It can be shown that they are associated to gluing matrices Λ in the T-duality group $O(d, d, \mathbb{Z})$. In particular, for those matrices we get $\Gamma_{12}^\Lambda = \Gamma_1$, which means that the defect couples to the full momentum lattice and no ground states are projected out. If this is the case, there is no contribution coming from the subleading term to the entanglement entropy from the interface.

The broader class of duality interfaces is specified by matrices in $O(d, d, \mathbb{Q})$. In particular these interfaces can be related to orbifold constructions. In the case of a single circle, where $R_1/R_2 = k_2/k_1$ [41, 55], the theory with radius R_1 can be obtained from the theory with radius R_2 by orbifolding with respect to the shift symmetry

$$X \mapsto X + 2\pi R_1 \,. \tag{9.13}$$

The group that is generated by this shift symmetry is $\mathbb{Z}_{|k_1 k_2|}$ and thus obviously has order $|k_1 k_2|$. The operator $II^\dagger$ now projects the theory with R_2 onto the sector invariant under the orbifold group $\mathbb{Z}_{|k_1 k_2|}$. We see that for circle theories the contribution to the sub-leading term of the entanglement entropy is set by the order of this orbifold group,

$$S = \frac{1}{3} \log(L) - \log |G| \,, \tag{9.14}$$

in agreement with the general result (7.29).

9.2   LREE of bosonic tori

In this section we consider the LREE for d free bosons compactified on a torus. The gluing conditions can be written as [3, 55]

$$(a_n + O\tilde{a}_{-n})\,|B\rangle = 0\,, \tag{9.15}$$

where $O \in O(d|\mathbb{R})$. The ground states solving the zero mode condition are given by

$$\Gamma^O = \left\{ \begin{pmatrix} -Ox \\ x \end{pmatrix} \cap \Gamma \mid x \in \mathbb{R}^d \right\}, \tag{9.16}$$

where Γ is the charge lattice of the torus model. As usual the boundary state is a superposition of Ishibashi states $|p, \bar{p}\rangle\rangle$ built on ground states $(p, \bar{p}) \in \Gamma^O$,

$$|B\rangle = g \sum_{(p,\bar{p})\in\Gamma^O} e^{i\varphi(p,\bar{p})}|p, \bar{p}\rangle\rangle\,, \tag{9.17}$$

where the function $\varphi \in (\Gamma^O)^*$ specifies the D-brane moduli and the g-factor is fixed by the condition that the open-string vacuum appears with multiplicity 1. Again by unfolding the boundary state we can associated a defect to it acting on the chiral part of the Hilbert space. For this, we introduce the projections $\pi(\Gamma^O)$ and $\bar{\pi}(\Gamma^O)$ of the lattice Γ^O to the left- and right-moving parts respectively. On the level of ground states, the interface, therefore, maps $\pi(\Gamma^O) \ni p \to -Op \in \bar{\pi}(\Gamma^O)$. The g-factor can be related to the volume of the unit cell of the projected lattice as

$$g = vol(\pi(\Gamma^O)). \tag{9.18}$$

The computation of the entanglement entropy now proceeds in analogy to the case of topological interfaces. The partition functions on the n-sheeted torus can be approximated by

$$Z(n) = g^{2n} \sum_{(p,\bar{p})\in\Gamma^O} \chi_p(i\frac{\delta}{\pi}n) \xrightarrow{S \text{ trsf}, \delta \ll 1} g^{2n-2}e^{\frac{\pi^2}{12\delta n}}\,, \tag{9.19}$$

where we used again that the vacuum in the open string channel has multiplicity 1 for $n = 1$. Since the central charge of d bosons is simply $c = d$ and $\delta = \pi^2/\log(L)$ we obtain from this the LREE

$$S = \frac{c}{6}\log(L) - \log vol(\pi(\Gamma^O)). \tag{9.20}$$

Note that the the subleading part of the LREE is determined by the g factor of the boundary state. We want to relate this quantity to the torus geometry, let us, therefore, recall that Γ is a Narain lattice given by

$$\Gamma = \left\{ \begin{pmatrix} \frac{1}{2}E^{-1}M + E^T(1 + B)N \\ -\frac{1}{2}E^{-1}M + E^T(1 - B)N \end{pmatrix} \mid M, N \in \mathbb{Z}^d \right\}, \tag{9.21}$$

where $G = EE^T$ is the metric and B the Kalb-Ramond field on the target space, and M and N are the momentum and winding quantum numbers, respectively. Here we use capital letters for the momenta and winding numbers to indicate that these are d-dimensional vectors. Let us consider a $D1$ brane in $d = 2$ dimensions for the geometric case where B is zero. If the D1 brane were located in infinite flat space, we would specify the direction of the brane by specifying the momenta perpendicular to it; a localisation of the brane to its world-volume direction would then be achieved by integration over these momenta. On a torus, the momenta are part of a lattice. We can fix our brane by choosing the elementary generator of transverse momenta that couple to the brane to be given by

$$N^0 = \begin{pmatrix} M_1^0 \\ M_2^0 \end{pmatrix}, \tag{9.22}$$

with two integers M_i^0 that we assume to be relatively prime. This choice determines the winding modes our D1 brane can couple to. The elementary winding generator $N^0 = (N_1^0, N_2^0)$ is again specified by two coprime integers N_1^0, N_2^0, and have to satisfy the orthogonality constraint

$$M_1^0 N_1^0 + M_2^0 N_2^0 = 0. \tag{9.23}$$

The equation is solved by $N_1^0 = -M_2^0$, $N_2^0 = M_1^0$. By this we have fixed a D1 brane for which the lattice Γ^O is precisely spanned by the two generators M^0 and N^0 for M and N in (9.21), respectively. It can be checked explicitly that these lattice vectors solve (9.15) with

$$O = \begin{pmatrix} \cos(2\theta) & \sin(2\theta) \\ \sin(2\theta) & -\cos(2\theta) \end{pmatrix} \in O(2, \mathbb{R}), \tag{9.24}$$

where $\theta = \arctan\left(-(E^{-1}M^0)_1/(E^{-1}M^0)_2\right)$ [41]. To compute the g-factor we now have to compute the volume of (the unit cell of) this lattice, projected to the left-movers. After some algebra one obtains

$$g^2 = \frac{1}{2 \det E} \left((M_2^0)^2 G_{11} + (M_1^0)^2 G_{22} - 2G_{12}M_2^0 M_1^0\right). \tag{9.25}$$

Mapping M_i^0 to the winding numbers of the brane $M_1^0 = k_2$, $M_2^0 = -k_1$, we see that

$$g^2 = \frac{length^2}{2 vol}, \tag{9.26}$$

where *length* refers to the length of the brane and *vol* to the volume of the torus. This is in agreement with geometrical expectations. Note also, that in the special case of a rectangular torus with diagonal metric where the radii are related by a rational number the above result agrees with the one for topological interfaces of the previous section.

As states before the left/right entanglement entropy for a single boson compactified on a circle of radius R has been computed in [87]. To compare the results, note that in one dimension the left-moving momenta are given by $a_0 = m/2R + nR$ and the right-moving

momenta by $\bar{a}_0 = m/2R - nR$ (see appendix B) with n the winding number. The matrix O in the gluing condition reduces to a choice of sign. For Dirichlet branes we have $O = 1$, and only ground states without winding contribute to the boundary state. We, therefore, have $\Gamma^O = \{(m/2R, m/2R)\}$, and the volume of the projected unit cell is $1/2R$. Similar considerations also hold for Neumann branes. Our result (9.20) for the LREE of a single boson compactified on a circle thus gives

$$S = \frac{1}{6} \log L - \begin{cases} \log R & \text{for } O = -1 \text{ (Neumann b.c.)} \\ \log \frac{1}{2R} & \text{for } O = 1 \text{ (Dirichlet b.c.)} \end{cases} . \tag{9.27}$$

which in particular reproduces the results of [87].

Chapter 10

Indices with Defects

10.1 Indices from Boundary States

In this section we want to calculated indices in the presence of topological defects for boundary states in $\mathcal{N} = 2$ minimal models. These minimal models can be realized via a coset theory as discussed in section 2.12.6. We consider the model equipped with a vector-like GSO projection [18, 19, 92], where the Hilbert space takes the form

$$\mathcal{H} = \bigoplus_{(l,m,s)} \mathcal{H}_{l,m,s} \otimes \mathcal{H}_{l,m,s}. \tag{10.1}$$

We now first review some general aspects on the construction of Cardy-boundary states in $\mathcal{N} = 2$ minimal models [19] before calculating indices with topological defects.

In $\mathcal{N} = 2$ minimal models there exist both A-branes and B-branes that preserve half of the $(2,2)$ superconformal symmetry. The notion of A- and B-type is related to type IIA and type IIB string theory where those branes naturally arise from the theory. The corresponding boundary states satisfy

$$(L_n - \bar{L}_{-n}) |\mathcal{B}_A\rangle = 0, \quad (J_n - \bar{J}_{-n}) |\mathcal{B}_A\rangle = 0, \tag{10.2}$$

$$(\bar{G}_n^+ - ie^{i\alpha} G_{-n}^-) |\mathcal{B}_A\rangle = 0, \quad (\bar{G}_n^- - ie^{-i\alpha} G_{-n}^+) |\mathcal{B}_A\rangle = 0 \tag{10.3}$$

for A-type with $e^{i\alpha} = 1$ if $s = \pm 1$ and $e^{i\alpha} = 1$ if $s = 0, 2$ and

$$(L_n - \bar{L}_{-n}) |\mathcal{B}_B\rangle = 0, \quad (J_n + \bar{J}_{-n}) |\mathcal{B}_B\rangle = 0, \tag{10.4}$$

$$(\bar{G}_n^+ - ie^{i\beta} G_{-n}^+) |\mathcal{B}_B\rangle = 0, \quad (\bar{G}_n^- - ie^{-i\beta} G_{-n}^-) |\mathcal{B}_B\rangle = 0 \tag{10.5}$$

for B-type with $e^{i\beta} = -1$ for $s = 0$ and $+1$ for $s = 1$.

In the rational case for each kind of boundary condition there exist an associated Ishibashi state given by

$$|A_{l,m,s}\rangle\rangle = \sum_N |l, m, s; N\rangle \otimes \Omega_M U |l, m, s; N\rangle, \tag{10.6}$$

$$|B_{l,m,s}\rangle\rangle = \sum_N |l, m, s; N\rangle \otimes U |l, m, s; N\rangle. \tag{10.7}$$

As always the states $|l, m, s; N\rangle$ form a orthonormal basis of $\mathcal{H}_{l,m,s}$, U is the usual anti-linear operator $U : \mathcal{H}_{l,m,s} \to \mathcal{H}_{l,-m,-s}$ and Ω_M is the mirror automorphism[1] of the $\mathcal{N} = 2$ superconformal algebra.

The states $|A_{l,m,s}\rangle\rangle$ survive the GSO projection for all (l, m, s) while for B-type only the Ishibashi states $|B_{l,0,0}\rangle$, $|B_{l,0,2}\rangle$ and $|B_{\frac{k}{2}, \frac{k+2}{2}, \pm 1}\rangle$ survive where the last one is possible for k even only.

Out of the Ishibashi states one can construct the corresponding boundaries states. For the A-branes these are given by

$$|A_{l,m,s}\rangle = \sum_{(l',m',s') \in J_k} \frac{S_{l,m,s}^{l',m',s'}}{\sqrt{S_{0,0,0}^{l',m',s'}}} |A_{l',m',s'}\rangle\rangle, \tag{10.8}$$

while the B-branes are given as

$$|B_{l,s}\rangle = \sqrt{2(k+2)} \sum_{l' \in 2\mathbb{Z}, \ s'=0,2} \frac{S_{l,-l-s,s}^{l',0,s'}}{\sqrt{S_{0,0,0}^{l',0,s'}}} |B_{l',0,s'}\rangle\rangle. \tag{10.9}$$

Again J_k labels the set of all distinct fields in the coset. The modular S-matrices in this case are given by

$$S_{L,M,S}^{l,m,s} = \frac{1}{k+2} \sin\left(\pi \frac{(L+1)(l+1)}{k+2}\right) e^{i\pi \frac{mM}{k+2}} e^{-i\pi \frac{sS}{2}}. \tag{10.10}$$

For the case that k is even the B-branes with $l = k/2$ further split into two separate boundary states

$$|B_s\rangle = \frac{1}{2} |B_{\frac{k}{2}, s}\rangle + \frac{\sqrt{k+2}}{2} e^{-i\pi \frac{s^2}{2}} \sum_{s'=-1,1} e^{-i\pi \frac{ss'}{2}} |B_{\frac{k}{2}, \frac{k+2}{2}, s'}\rangle\rangle, \quad s = -1, 0, 1, 2. \tag{10.11}$$

As usual the labels l, m, s are subjected to the field identification $(l, m, s) \sim (k - l, k + 2 + m, 2 + s)$ and the restriction $l + m + 2 = 0 \bmod 2$ (see 2.12.6).

Having defined all the possible boundary states we are now in the position to calculate indices, especially *Witten indices* associated to the boundary states. Therefore, we consider an open string in the (a, b) sector where a and b now can correspond to any of the above boundary states. In the open string language the topological intersection index [95] is defined by

$$I(a, b) = tr_{\mathcal{H}_{ab}} (-1)^F e^{-\beta H}. \tag{10.12}$$

In the closed string picture (obtained by modular S-transformation) the index corresponds to an overlap of the Ramond sector boundary states with an additional spectral flow operator insertion, i.e.

$$I(a, b) = 2_{RR} \langle a| e^{-i\pi J_0} e^{-\frac{2\pi^2}{\beta}(L_0 + \bar{L}_0 - \frac{c}{12})} |b\rangle_{RR}. \tag{10.13}$$

---

[1] $\Omega_M : J_n \to -J_n$ and $\Omega_M : G_r^\pm \to G_r^\mp$

The factor 2 gives rise to the right identification related to the GSO projection. In the overlap only the Ramond sector ground states $(l, m, s) = (l, l+1, 1)$ for which $L_0 + \bar{L}_0 - \frac{c}{12} = 0$ contribute so we may alternatively write

$$I(a, b) = 2\,_{RRG}\langle a|\, e^{-i\pi J_0}\, |b\rangle_{RRG}, \tag{10.14}$$

where $|a\rangle_{RRG}$ is the projection on the RR-ground states.

Since we are only interested in the Ramond sector contribution we can restrict the A-branes and B-branes to this sector by

$$|A_{l,m,s}\rangle_{RR} = \sum_{\substack{(l',m',s') \\ s'=\pm 1}} \frac{S^{l',m',s'}_{l,m,s}}{\sqrt{S^{l',m',s'}_{0,0,0}}} |A_{l',m',s'}\rangle\rangle, \tag{10.15}$$

and for the case that k is even

$$|B_s\rangle_{RR} = \frac{\sqrt{k+2}}{2} e^{-i\pi\frac{s^2}{2}} \sum_{s'=\pm 1} e^{-i\pi\frac{ss'}{2}} |B_{\frac{k}{2},\frac{k+2}{2},s'}\rangle\rangle, \quad s = -1, 0, 1, 2. \tag{10.16}$$

The overlap between B-B-branes and A-B-branes is a straight forward calculation (see [18–20]) resulting in

$$I(B_{\pm 1}, A_{l,m,s}) = \mp e^{i\pi\frac{m-s}{2}} \sin\left(\pi\frac{l+1}{2}\right) \in \{-1, 0, 1\}, \tag{10.17}$$

$$I(B_{\pm 1}, B_1) = \pm\frac{k+2}{2}. \tag{10.18}$$

The calculation for the A-A-overlap is a bit more involved thus we review it here in a detailed calculation

$$I(A_{l_1,m_1,s_1}, A_{l_2,m_2,s_2}) = 2\,_{RR}\langle A_{l_1,m_1,s_1}|\, e^{-i\pi J_0} q^H |A_{l_2,m_2,s_2}\rangle_{RR}$$

$$= 2 \sum_{\substack{(l,m,s) \\ s\ odd}} \frac{S^{*l,m,s}_{l_1,m_1,s_1} S^{l,m,s}_{l_2,m_2,s_2}}{S^{l,m,s}_{0,0,0}} e^{-i\pi(\frac{s}{2}-\frac{m}{k+2})} \chi_{l,m,s}(q)$$

$$= \frac{2}{k+2} \sum_{(l,m)\ odd} \frac{\sin\left(\pi\frac{(l_1+1)(l+1)}{k+2}\right) \sin\left(\pi\frac{(l_2+1)(l+1)}{k+2}\right)}{\sin\left(\pi\frac{l+1}{k+2}\right)} e^{i\pi\frac{m(m_2-m_1+1)}{k+2}} e^{-i\pi\frac{s_2-s_1+1}{2}} (\chi_{l,m,1} - \chi_{l,m,-1})$$

$$= e^{i\pi\frac{s_2-s_1}{2}} \sum_l \frac{S^l_{l_1} S^l_{l_2} S^l_{m_2-m_1}}{S^l_0}$$

$$= (-1)^{\frac{s_1-s_2}{2}} N^{n_2-n_1}_{l_1,l_2}, \tag{10.19}$$

where

$$S_i^j = \sqrt{\frac{2}{k+2}} \sin\left(\pi \frac{(i+1)(j+1)}{k+2}\right), \tag{10.20}$$

are the $su(2)_k$ modular S-matrices and $N_{i,j}^l$ the $su(2)_k$ fusion coefficients with

$$N_{i,j}^l = \begin{cases} 1 & \text{for } |i-j| \leq l \leq min(i+j, 2k-i-j) \\ & i+j+l = 0 \bmod 2 \\ 0 & \text{otherwise} \end{cases} \tag{10.21}$$

Note that in the calculation we used

$$\sum_{(l,m)\ odd} = \frac{1}{2} \sum_{l+m\ odd}. \tag{10.22}$$

Further we demanded that s_1, s_2 are both odd in order to preserve the same supersymmetry (s on the other hand can take all possible values). Further it is understood that $N_{i,j}^l$ is zero for all $l = -1 \bmod (2k+4)$ and for general $l < 0$ holds the identification $N_{i,j}^l = -N_{i,j}^{2-l}$ and equally with a period of $k+2$.

10.2 Indices from Boundary States with Topological Defects

Having defined the index between Ramond sector boundary states of $\mathcal{N} = 2$ minimal models we are now in the position to generalize the index by adding a topological defect which is also defined in the Ramond sector

$$D_{L,M,S} = \sum_{\substack{(l,m,s) \\ s\ odd}} \frac{S_{L,M,S}^{l,m,s}}{S_{0,0,0}^{l,m,s}} P^{(l,m,s)}. \tag{10.23}$$

Here $P^{(l,m,s)}$ are projectors on the representations (l, m, s) as usual. We are interested in calculating the enhanced index

$$I(a, b, D_{L,M,S}) = 2_{RR}\langle a| e^{-i\pi J_0} D_{L,M,S} |b\rangle_{RR}. \tag{10.24}$$

Graphically this setup is shown in figure 10.1.
From section 3.4 we know that a topological defect can be fused onto the Cardy state. In our case this results in

$$D_{L,M,S} |A_{l,m,s}\rangle_{RR} = \sum_{l'} N_{L,l}^{l'} |A_{l',M+m,S+s}\rangle_{RR}, \tag{10.25}$$

$$D_{L,M,S} |B_s\rangle_{RR} = \frac{\sqrt{k+2}}{2} e^{-i\pi\frac{s^2}{2}} \sum_{s'=\pm 1} \frac{S_{L,M,S+s}^{\frac{k}{2},\frac{k+2}{2},s'}}{S_{0,0,0}^{\frac{k}{2},\frac{k+2}{2},s'}} |B_{\frac{k}{2},\frac{k+2}{2},s'}\rangle\rangle. \tag{10.26}$$
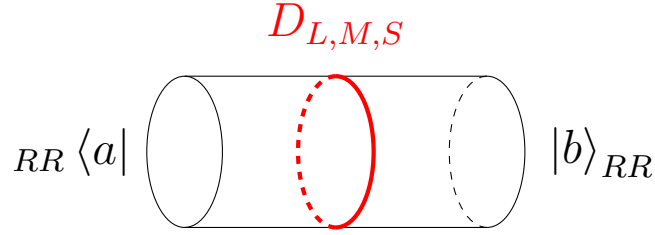
$$D_{L,M,S}$$

Figure 10.1: Topological defect placed along the cylinder with boundaries.

Again $N_{i,j}^l$ are the $su(2)_k$ fusion coefficients, further we see that the action of the defect on the boundary states generates a superposition of boundary states.

It is now straight forward to calculate the indices in presence of the defect by using the results from (10.17)-(10.19). In appendix D we perform the calculation explicitly, i.e. without using the fusion of the defect with the boundary but simply by performing the calculation straight away. The results then are given by

$$I(B_{\pm 1}, A_{l,m,s}, D_{L,M,S}) = \mp \sin\left(\pi \frac{l+1}{2}\right) \sin\left(\pi \frac{L+1}{2}\right) e^{i\pi \frac{M+m-S-s}{2}}, \quad M+S = 0 \text{ mod } 2,$$

(10.27)

$$I(B_{\pm 1}, B_1, D_{L,M,S}) = \pm \frac{k+2}{2} \sin\left(\pi \frac{L+1}{2}\right) e^{i\pi \frac{M-S}{2}}, \quad M+S = 0 \text{ mod } 2,$$ (10.28)

$$I(A_{l_1,m_1,s_1}, A_{l_2,m_2,s_2}, D_{L,M,S}) = (-1)^{\frac{s_1+S-s_2}{2}} \sum_{l'=0}^{k} N_{l_1,l_2}^{l'} N_{L,M+m_2-m_1}^{l'}, \quad S = 0 \text{ mod } 2. \quad (10.29)$$

The restrictions on the labels M and S naturally arise since we want to recover (10.17)-(10.19) for the special case of the identity defect $D_{0,0,0}$. Further the restriction $S = 0 \text{ mod } 2$ for the index between A-type boundaries with defect tells us that the defect preserves the corresponding spin structure of the boundaries.

It is quite simple to generalize to the insertion of several, let's say n defects. By using their fusion with each other and restricting the final result to the Ramond sector

$$D_{L_1,M_1,S_1} D_{L_2,M_2,S_2} = \sum_{\substack{(l,m,s) \\ s \text{ odd}}} N_{L_1,L_2}^l \delta_{s,S_1+S_2}^{(4)} \delta_{m,M_1+M_2}^{(2k+4)} P^{(l,m,s)}.$$ (10.30)

For the index between two A-branes this then results in

$$I(A_{l_1,m_1,s_1}, A_{l_2,m_2,s_2}, D_{L_1,M_1,S_1}, \ldots, D_{L_n,M_n,S_n}) =$$

$$e^{i\pi \frac{s_2-s_1}{2}} \prod_{j=1}^{n} e^{-i\pi \frac{S_j}{2}} \sum_{\tilde{l}_1,\ldots,\tilde{l}_n} N_{l_1,l_2}^{\tilde{l}_1} N_{L_1,\tilde{l}_1}^{\tilde{l}_2} \cdots N_{L_{n-1},\tilde{l}_{n-1}}^{\tilde{l}_n} N_{L_n,\Delta M}^{\tilde{l}_n},$$ (10.31)

where $\Delta M := m_2 - m_1 + \sum_j M_j$ and again with the restriction

$$\sum_{j=1}^{n} S_j = 0 \text{ mod } 2, \quad s_1, s_2 \text{ odd}.$$ (10.32)

For the index between A- and B- branes and B- and B-branes similar generalization hold (see appendix D).

It is commonly known that the $\mathcal{N} = 2$ minimal models arise as the infrared fixed point [97] of the Landau-Ginzburg model consisting of a single chiral superfield X with superpotential W given by

$$W = X^{k+2}, \tag{10.33}$$

where k is the level of the minimal model. It can be shown [18, 19] that there is a nice geometric interpretation of the index between two boundary states in terms of intersection numbers of the associated branes in the Landau-Ginzburg description. We will review the geometric interpretation in the next section and then apply the results to the index obtained with the insertion of a single defect (for several defect insertions the same logic will hold). In this way we can give our formula (10.29) a physical meaning.

10.3   Geometric Interpretation

As stated before $\mathcal{N} = 2$ minimal models can be realized as the IR fixed point of Landau-Ginzburg models [17]. The action for a Landau-Ginzburg model (in superspace formalism [5]) for a single chiral superfield X is given by

$$S_{LG} = \int d^2x \left[d^4\theta K(X, \bar{X}) + \frac{1}{2} \left(\int d^2\theta W(X) + \int d^2\bar{\theta}\bar{W}(\bar{X}) \right) \right]. \tag{10.34}$$

Here $K(X, \bar{X})$ is the Kähler potential which defines the associated Kähler metric

$$g_{i\bar{j}} = \partial_i \partial_{\bar{j}} K(X, \bar{X}). \tag{10.35}$$

Usually $g_{i\bar{j}}$ is taken to be the flat metric. The k-th minimal model can now be described by the superpotential of the form

$$W(X) = X^{k+2}. \tag{10.36}$$

In the Landau-Ginzburg description A-type D-branes are preimages of straight lines on the W-plane starting from critical values which in the cases of the above superpotential are given by the critical points $X = 0$ with a multiplicity $k + 1$ and critical value $w_* = 0$. By performing a deformation of the superpotential with lower powers of X one can obtain $k + 1$ non-degenerate critical points with distinct values w_i. Each of these critical points belongs to a D-brane with the image being a straight half-line starting from w_i and going to $+\infty$ in the positive real direction. The preimage approaches for large X (where the deformation is negligible) the lines

$$\mathcal{L}_n = \left\{ r \exp\left(\frac{2\pi i n}{k+2} \right) \mid n = 0, \ldots, k+1, \quad r \in [0, \infty) \right\}. \tag{10.37}$$

Hence, on the X-plane the D-branes of the deformed theory is a curve that asymptotes to a pair of such lines $\mathcal{L}_{n_1}$ and $\mathcal{L}_{n_2}$ with $n_1 \neq n_2$. The precise combinations of D-branes of this

type depend on the way of deformation of W away from criticality. However, generally the $k+1$ D-branes obtained this way will not intersect on the X-plane because by construction they do not intersect in the W-plane too.

Associating to the pair of numbers a state $|n_1, n_2\rangle$ one may define an intersection index between two branes as

$$\langle n_1, n_2 | r_1, r_2 \rangle = \begin{cases} 1 & n_i = r_i \text{ for some } i \\ 0 & \text{else} \end{cases}. \tag{10.38}$$

At a critical point all the D-branes from the non-critical theories arbitrarily close to it are present. Since all pairs (n_1, n_2) are realized in some deformation of W, all of them exist in the critical theory, which gives us a total of $(k+2)(k+1)$ D-branes. Their preimages in the X-plane are two of the former lines, $\mathcal{L}_{n_1} \cup \mathcal{L}_{n_2}$ with arbitrary (n_2, n_2), $n_1 \neq n_2$.

Following the ideas from [18] we can now make the correspondence to the boundary state description in $\mathcal{N} = 2$ minimal models. The labels of the A-type boundary state $|A_{l,m,s}\rangle$ can be identified with the two integer numbers (n_1, n_2) specifying the D-brane as

$$|n_2 - n_1| = l + 1, \tag{10.39}$$

$$n_1 + n_2 = m, \tag{10.40}$$

$$s = \text{sign}(n_2 - n_1). \tag{10.41}$$

Since we are considering Ramond-boundary states $s = \pm 1$. Geometrically negative values of s correspond to opposite orientations of the D-branes. The intersection index 10.38 can now be identified (up to a phase regarding the orientation of the branes) with the Witten index of two associated A-type boundary states (10.19) with

$$|n_2 - n_1| = l_1 + 1, \quad |r_2 - r_1| = l_2 \tag{10.42}$$

$$n_1 + n_2 = m_1, \quad r_1 + r_2 = m_2 + 1 \tag{10.43}$$

$$s_1 = \text{sign}(n_2 - n_1), \quad s_2 = \text{sign}(r_2 - r_1). \tag{10.44}$$

We now want to discuss the action of a topological defect on the boundary state and its geometric interpretation. The action of a topological defect on a boundary is given by

$$D_{L,M,S} |l, m, s\rangle = \sum_{l'} N_{L,l}^{l'} |l', M + m, S + s\rangle. \tag{10.45}$$

For the new numbers representing the asymptotics of the D-brane this means

$$n_2 = \frac{M + m + l' + 1}{2} \quad , \quad n_1 = \frac{M + m - l' - 1}{2}. \tag{10.46}$$

In comparison to the original orientation of the D-brane associated to the boundary state $|l, m, s\rangle$ we recognize, that M rotates the original brane by an angle $\pi M/(k+2)$ and l' is responsible for the angle that the brane encloses. Especially the enclosed angle is given by
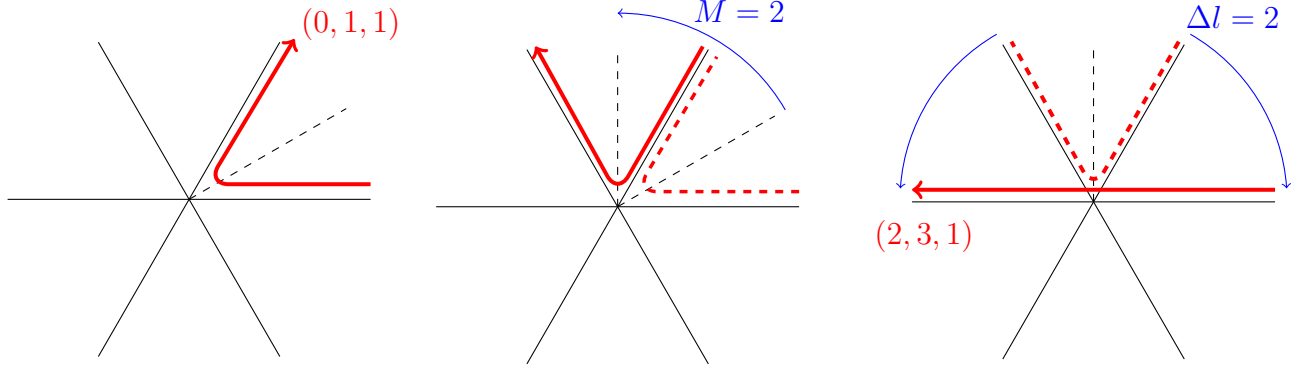
Figure 10.2: Graphical representation for $k = 4$ of one possible transformation of a brane $(0, 1, 1)$ by action of a defect $D_{2,2,0}$, where $\Delta l = l' - l$.
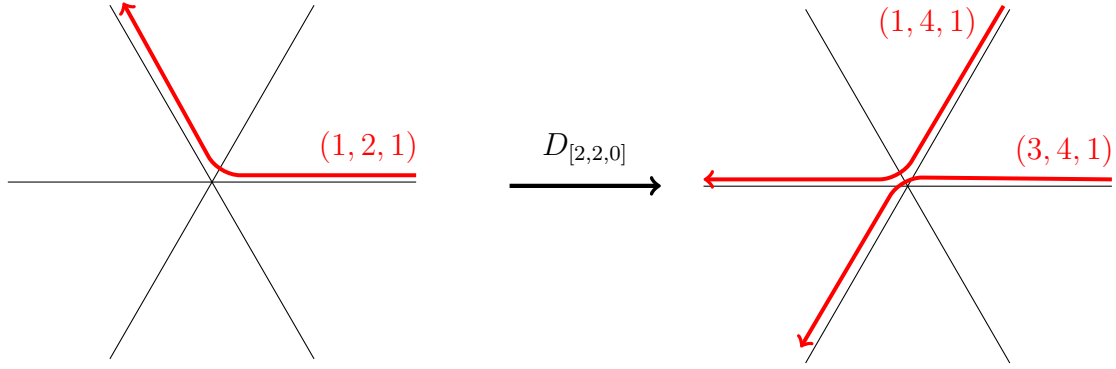

Figure 10.3: left: boundary state with labels $(1, 2, 1)$ in the D-brane picture right: action of $D_{2,2,0}$ on the original boundary state generates two new boundary states in the D-brane picture.

$2\pi(l' + 1)/(k + 2)$. The S label of the defect simply exchanges the orientation of the brane for $S = 2$ and preserves the orientation of the transformed brane compared to the original one for $S = 0$. The dependence of the defect labels is shown as an example in figure 10.2. Note that the D-branes, in fact, lie upon the lines X, nevertheless, here we draw the branes slightly apart thus we get a better graphical representation for the intersections of several branes later on.

The index that we calculated in the presence of one topological defect now exactly counts the number of intersections of the branes generated by the defect and the additional one. Let us consider an illustrative example to get more familiar with the geometric interpretation. We start with an A-type boundary state $|A_{1,2,1}\rangle$ where the level is fixed to be $k = 4$. Geometrically $|A_{1,2,1}\rangle$ then corresponds to a D-brane coming from $X = r$ and approaching $X = r \cdot \exp\left(\frac{2\pi i}{3}\right)$ (see figure 10.3 left). Let us now assume that we act with the topological defect $D_{2,2,0}$ on the boundary. In this case we obtain a superposition of boundary states given by

$$D_{2,2,0}\,|A_{1,2,1}\rangle = |A_{1,4,1}\rangle + |A_{3,4,1}\rangle. \tag{10.47}$$

Graphically the action of the defect on the boundary is illustrated in figure 10.3 right.

The index (10.29) now geometrically corresponds to the number of intersections of D-branes corresponding to the new created boundary states $|A_{1,4,1}\rangle$ and $|A_{3,4,1}\rangle$ with another D-brane associated to the boundary state $|A_{l_1,m_2,s_2}\rangle$. Since our defect produced two new boundaries the maximal number of intersections for the corresponding D-branes with a third brane can be two.

As an example consider the case $|A_{l_2,m_2,s_2}\rangle = |A_{0,5,1}\rangle$. Equation (10.29) then tells us that the intersection number is one. Geometrically the three branes in case can be represented as in figure 10.4.
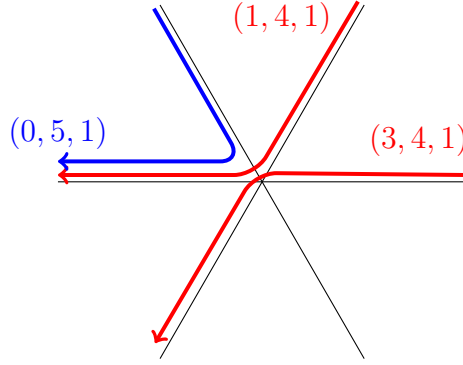

Figure 10.4: Graphical representation for index with one intersection.

We see that the branes with labels $(0,5,1)$ and $(1,4,1)$ indeed intersect at $-\infty$ and that they both have the same orientation for which the index is positive.

As a second example consider the case where $|A_{l_1,m_2,s_2}\rangle = |A_{2,7,1}\rangle$. Equation (10.29) in this case tells us that the brane corresponding to the boundary state intersects with both the other two branes, i.e. that the index is 2. Graphically this can be verified as illustrated in figure 10.5. Indeed the blue brane intersects with both red branes i.e. its intersection number is two.

10.4 Index from Unfolded Boundary States

In section 10.2 we calculated the index corresponding to two boundary states in the presence of a topological defect as the overlap amplitude between the associated boundary states. In this section we will follow a different approach. From section 3.2 we already know that every boundary state can (in principle) be unfolded. We want to apply this procedure to our A- and B-type boundary states. In this way we obtain a corresponding A- or B-type defect acting just on the chiral part of the Hilbert space, i.e.

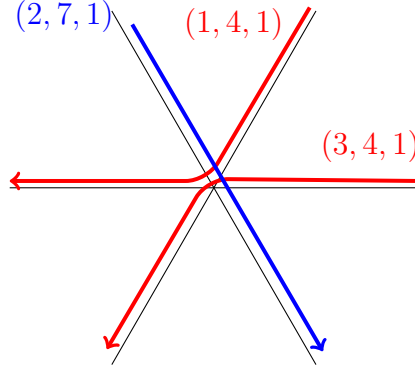$$\mathcal{H}_c = \bigoplus_{(l,m,s)} \mathcal{H}_{l,m,s}. \tag{10.48}$$

Figure 10.5: Graphical representation for index with two intersections.

We start our discussion with A-type boundary states (again only in the Ramond-sector)

$$|A_{l,m,s}\rangle_{RR} = \sum_{\substack{(l',m')\ odd \\ s'\ odd}} \frac{S_{l,m,s}^{l',m',s'}}{\sqrt{S_{0,0,0}^{l',m',s'}}} |A_{l',m',s'}\rangle\rangle. \qquad (10.49)$$

Following the unfolding procedure we find for the defect

$$|A_{l,m,s}\rangle_{RR} \rightarrow D_{l,m,s}^{(A_{RR})} = \sum_{\substack{(l',m')\ odd \\ s'\ odd}} \frac{S_{l,m,s}^{l',m',s'}}{\sqrt{S_{0,0,0}^{l',m',s'}}} P^{(l,m,s)}, \qquad (10.50)$$

where the projector $P^{(l,m,s)}$ is given by

$$P^{(l,m,s)} = \sum_{N} |l,m,s;N\rangle \langle l,m,s;N| . \qquad (10.51)$$

As in the boundary case we now can calculate an index associated to the defect. In the boundary case the index was given by the overlap between two possible different boundary states with the insertion of an operator $\exp(-i\pi J_0)$. This implies that in order to get a similar result we also should consider two possibly different defects together with the insertion of the right charge operator. Since in the boundary case $\exp(-i\pi J_0)$ is just acting on the chiral part of the Hilbert space and our unfolded defect also only acts on the chiral part we can again take the same operator. Our index can then be defined by

$$I(D_{l_1,m_1,s_1}^{\dagger}, D_{l_2,m_2,s_2}) = 2 \cdot \operatorname{tr}_{\mathcal{H}_c} D_{l_1,m_1,s_1}^{(A_{RR})\dagger} e^{-i\pi J_0} D_{l_2,m_2,s_2}^{(A_{RR})} q^{L_0 - \frac{c}{24}}. \qquad (10.52)$$

Note that the position of the charge operator $\exp(-i\pi J_0)$ is for the A-type defect irrelevant but it will be essential for the B-type so we already place it at the right position, further we took for the second defect the adjoint version and further we included a factor of 2, again corresponding to the vector-like GSO projection, in order to get the right correspondence in the open string channel. All steps have to be done in order to get the right boundary state description as in section 10.2.

The calculation of the index is now straight forward

$$I(D^\dagger_{l_1,m_1,s_1}, D_{l_2,m_2,s_2}) =$$

$$2 \cdot \mathrm{tr}_{\mathcal{H}_c} \sum_{\substack{(l',m'),(l'',m'') \ odd \\ s',s'' \ odd}} \frac{S^{*l',m',s'}_{l_1,m_1,s_1}}{\sqrt{S^{l',m',s'}_{0,0,0}}} \frac{S^{l'',m'',s''}_{l_2,m_2,s_2}}{\sqrt{S^{l'',m'',s''}_{0,0,0}}} \cdot$$

$$\cdot |l',m',s'\rangle\rangle \underbrace{\langle\langle l',m',s'|e^{-i\pi J_0}|l'',m'',s''\rangle\rangle}_{\delta_{l',l''}\delta_{m',m''}\delta_{s',s''}\exp(-i\pi(\frac{s'}{2}-\frac{m'}{k+2}))} \langle\langle l'',m'',s''|q^{L_0-\frac{c}{24}} =$$

$$2 \cdot \mathrm{tr}_{\mathcal{H}_c} \sum_{\substack{(l',m') \ odd \\ s' \ odd}} \frac{S^{*l',m',s'}_{l_1,m_1,s_1} S^{l',m',s'}_{l_2,m_2,s_2}}{S^{l',m',s'}_{0,0,0}} |l',m',s'\rangle\rangle\langle\langle l',m',s'|e^{-i\pi(\frac{s'}{2}-\frac{m'}{k+2})}q^{L_0-\frac{c}{24}} =$$

$$2 \sum_{\substack{(l',m') \ odd \\ s' \ odd}} \frac{S^{*l',m',s'}_{l_1,m_1,s_1} S^{l',m',s'}_{l_2,m_2,s_2}}{S^{l',m',s'}_{0,0,0}} e^{-i\pi(\frac{s'}{2}-\frac{m'}{k+2})} \chi_{l',m',s'}(\tau) =$$

$$\frac{2}{k+2} \sum_{\substack{(l',m') \ odd \\ s' \ odd}} \frac{\sin(l',l_1)\sin(l',l_2)}{\sin(l',0)} e^{i\pi\frac{m'(m_2-m_1+1)}{k+2}} e^{i\pi\frac{s'(s_2-s_1+1)}{2}} \chi_{l',m',s'}(\tau). \tag{10.53}$$

Here we again used the abbreviation

$$\sin(i,j) = \sin\left(\pi\frac{(i+1)(j+1)}{k+2}\right). \tag{10.54}$$

As in the boundary case we demand s_1, s_2 to be odd to preserve the same kind of supersymmetry. This then implies for our partition function

$$I(D^\dagger_{l_1,m_1,s_1}, D_{l_2,m_2,s_2}) =$$

$$-i(-1)^{\frac{s_2-s_1}{2}} \frac{2}{k+2} \sum_{(l',m') \ odd} \frac{\sin(l',l_1)\sin(l',l_2)}{\sin(l',0)} e^{i\pi\frac{m'(m_2-m_1+1)}{k+2}} (\chi_{l',m',1} - \chi_{l',m',-1}) =$$

$$(-1)^{\frac{s_2-s_1}{2}} \frac{2}{k+2} \sum_{l'=0}^{k} \frac{\sin(l',l_1)\sin(l',l_2)\sin(l',m_2-m_1)}{\sin(l',0)} =$$

$$(-1)^{\frac{s_1-s_2}{2}} \sum_{l'} \frac{S^{l'}_{l_1} S^{l'}_{l_2} S^{*l'}_{m_2-m_1}}{S^{l'}_0} =$$

$$(-1)^{\frac{s_2-s_1}{2}} N^{m_2-m_1}_{l_1,l_2}. \tag{10.55}$$

$$RR\langle A_{l_1,m_1,s_1}| \bigcirc \quad \times e^{-i\pi J_0} \quad \bigcirc |A_{l_2,m_2,s_2}\rangle RR$$

$$\downarrow \text{unfold}$$

$$D^{(A_{RR})}_{l_2,m_2,s_2}$$

$$\times e^{-i\pi J_0}$$

$$D^{(A_{RR})\dagger}_{l_1,m_1,s_1}$$

Figure 10.6: Performing the unfolding of the boundary states one equivalently can calculate the index in terms of a torus partition function on the chiral Hilbert space.

Here we used from the second to the third line the well know identity for the characters $\chi_{l,m,1}(\tau) - \chi_{l,m,-1}(\tau) = \delta_{m,l+1} - \delta_{m,-l-1}$ (see also appendix D).

We see that we obtain the same result as in the boundary case without a defect insertion (10.19). This is exactly what we expected from the unfolding. For a graphical representation see figure 10.6.

The index for the insertion of topological defects can now equally be calculated. The results then exactly match with (10.31).

Let us now focus on the B-type boundary in the Ramond sector (10.16). Unfolding this boundary yields the associated B-type defect acting on the chiral part of the Hilbert space

$$|B_s\rangle_{RR} \rightarrow D^{(B_{RR})}_s = \frac{\sqrt{k+2}}{2} e^{-i\pi \frac{s^2}{2}} \sum_{s'=\pm 1} e^{-i\pi \frac{ss'}{2}} \hat{P}^{(\frac{k}{2}, \frac{k+2}{2}, s')}, \tag{10.56}$$

with the projector

$$\hat{P}^{(\frac{k}{2}, \frac{k+2}{2}, s')} = \sum_N |\frac{k}{2}, \frac{k+2}{2}, s'; N\rangle \langle \frac{k}{2}, -\frac{k+2}{2}, -s'; N| \tag{10.57}$$

Note that in contrast to the A-type unfolding we have to perform an additional charge conjugation which amounts in replacing $m \to -m$ and $s \to -s$.

The index can now be calculated in a similar manner as for the A-type

$$I(D_{\pm 1}^{(B_{RR})\dagger}, D_1^{(B_{RR})}) = 2 \cdot \text{tr}_{\mathcal{H}_c} \, D_{\pm 1}^{(B_{RR})\dagger} e^{-i\pi J_0} D_1^{(B_{RR})} q^{L_0 - \frac{c}{24}}, \tag{10.58}$$

reproducing the result (10.18). Note that in this case the position of the spectral flow operator is essential, i.e. it has to be placed within the two defects.

10.5 Generalizations to Non-Topological Defects

In sections 10.1 and 10.2 we have calculated the indices between boundary states without and with topological defect insertions. We now want to generalize the calculation to non-topological defects. Thereby we recognize that in the calculation for the indices only the Ramond-ground states with labels $(l, l+1, 1)$ contributed.

We now proceed as follows: first we introduce the concept of a boundary state charge in $\mathcal{N} = 2$ superconformal minimal models. Having defined the charges, which can be seen as forming a charge lattice, we consider the index calculation without defects in terms of the brane-charges before in the end we generalize to (possible) non-topological defects.

This is somewhat clear since we are dealing with a superconformal theory and are considering the insertion of a $(-1)^F$ operator which in our case is given by

$$(-1)^F = \exp(-i\pi J_0). \tag{10.59}$$

For supersymmetric theories the number of bosons and the number of fermions for excited states are equal thus these states cancel out when inserting the $(-1)^F$ operator. Only the number of ground states of bosons and fermions don't coincide (for a graphical representation see figure 10.7). These ground states then are exactly the states that contribute to the index. Let us denote the Ramond ground states by $|l, l+1, 1\rangle$ where $l \in \{0, \ldots, k\}$.

We are interested in the overlap of branes with these ground states. We will just consider the A-type branes since these give rise to non-trivial indices (see section 10.1). We thus define, adopting the notation presented in [19]

$$\tilde{\Pi}_{l,l+1,1}^{l_1, m_1, s_1} := \langle l, l+1, 1 | A_{l_1, m_1, s_1} \rangle_{RR} \tag{10.60}$$

$$\Pi_{l,l+1,1}^{l_1, m_1, s_1} := {}_{RR} \langle A_{l_1, m_1, s_1} | e^{-i\pi J_0} | l, l+1, 1 \rangle. \tag{10.61}$$

These overlaps encode the information about the D-brane charge, namely in the supersymmetric closed string ground states generate space-time gauge potentials. These gauge potentials are called Ramond-Ramond potentials. The overlaps of the boundary states with the Ramond ground states thus measure the charge of the D-brane with respect to the gauge potentials [19]. This results in talking about the D-brane charge and the associated charge lattice Λ_D of the branes. Explicitly for the A-type branes the overlaps are
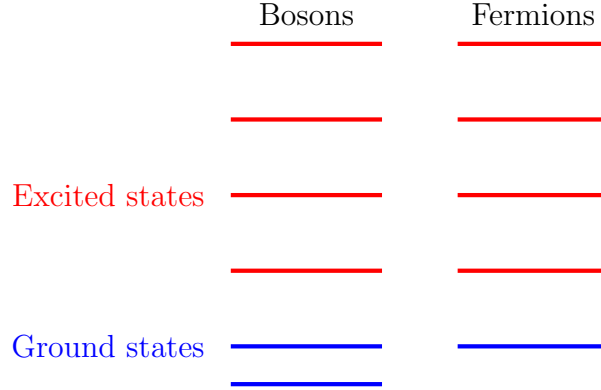
Figure 10.7: Number of fermionic and bosonic states. For a supersymmetry theory the number of bosons and fermions for excited states coincide while for the ground states the equality doesn't have to hold.

given by

$$\tilde{\Pi}_{l,l+1,1}^{l_1,m_1,s_1} = \frac{1}{\sqrt{k+2}} \frac{\sin\left(\pi \frac{(l_1+1)(l+1)}{k+2}\right)}{\sqrt{\sin\left(\pi \frac{l+1}{k+2}\right)}} e^{i\pi \frac{m_1(l+1)}{k+2}} e^{-i\pi \frac{s_1}{2}} \tag{10.62}$$

$$\Pi_{l_1,m_1,s_1}^{l,l+1,1} = \frac{1}{\sqrt{k+2}} \frac{\sin\left(\pi \frac{(l_1+1)(l+1)}{k+2}\right)}{\sqrt{\sin\left(\pi \frac{l+1}{k+2}\right)}} e^{-i\pi \frac{(m_1-1)(l+1)}{k+2}} e^{i\pi \frac{s_1-1}{2}} \tag{10.63}$$

The Witten index (10.29) can thus be expressed in terms of these overlaps as

$$I(A_{l_1,m_1,s_1}, A_{l_2,m_2,s_2}) =$$

$$2\sum_{l,l'} {}_{RR}\langle A_{l_1,m_1,s_1}|e^{-i\pi J_0}|l,l+1,1\rangle\langle l,l+1,1|l',l'+1,1\rangle\langle l',l'+1,1|A_{l_2,m_2,s_2}\rangle_{RR} =$$

$$2\sum_{l,l'} \Pi_{l,l+1,1}^{l_1,m_1,s_1} g_{ll'} \tilde{\Pi}_{l,l+1,1}^{l_2,m_2,s_2}. \tag{10.64}$$

In the formula we introduced the associated metric $g_{ll'} := \langle l, l+1, 1|l', l'+1, 1\rangle$. We see that the index is totally determined by the charges of the branes, i.e. the Witten index defines an integral bilinear form on the charge lattice Λ_D. This concept can now easily be generalized to the inclusion of a (not necessarily topological) defect. Since only Ramond ground states contribute to the index this also has to be true for the case when we include a defect which on the level of the Ramond ground states may be interpreted as a map[2].

---

[2]Note that in general non-topological defects can not be associated with a map from one CFT to another.

Thereby only those ground states survive that again are 'mapped' onto ground states by the defect. In terms of overlaps this can be written as

$$I(A_{l_1,m_1,s_1}, A_{l_2,m_2,s_2}, D_{L,M,S}) = 2 \sum_{l,l'} \Pi_{l,l+1,1}^{l_1,m_1,s_1} g_{ll'}(D_{L,M,S}) \tilde{\Pi}_{l,l+1,1}^{l_2,m_2,s_2}, \qquad (10.65)$$

where we introduced the defect induced metric

$$g_{ll'}(D_{L,M,S}) = \langle l, l+1, 1 | D_{L,M,S} | l', l'+1, 1 \rangle . \qquad (10.66)$$

We see that the induced metric encodes exactly the information which ground states are mapped by the defect onto other ground states. For the case of a topological defect the induced metric is diagonal with elements $g_{ll} = S_{L,M,S}^{l,l+1,1}/S_{0,0,0}^{l,l+1,1}$. For topological twisted theories similar considerations as for the topological case should apply. For non-topological defects in general we also will obtain off diagonal terms. Concluding we see that the index with the insertion of general defects can be computed in terms of the overlaps encoding the charges of the D-branes and the defect induced metric[3].

10.6 Elliptic Genera with Defects

The elliptic genus provides a connection between CFTs with $\mathcal{N} = 2$ supersymmetry and geometric quantities such as the Euler characteristics. E. Witten suggested in his paper [97] that the elliptic genus is a good quantity to understand the relations between Landau-Ginzburg and $\mathcal{N} = 2$ minimal models.
The conformal field theoretic elliptic genus is defined by [7, 96, 97]

$$\mathcal{E}(\tau, z) = \text{tr}_{RR}(-1)^F q^{L_0 - \frac{c}{24}} \bar{q}^{\bar{L}_0 - \frac{c}{24}} y^{J_0}, \qquad (10.67)$$

where $q = \exp(2\pi i \tau)$ and $y = e^{2\pi i z}$ with $z \in \mathbb{C}$. The fermion number operator can be realized as $F = J_0 - \bar{J}_0$. Setting $z = 0$ one reproduces the ordinary Witten index

$$\mathcal{E}(\tau, 0) = \text{tr}_{RR}(-1)^F. \qquad (10.68)$$

If the theory admits a sigma model interpretation it is known [14] that the Witten index gives the Euler characteristic of the target manifold of the sigma model.
It can be shown that the elliptic genus transforms in the following way under generalized modular transformations

$$\mathcal{E}(\tau + 1, z) = \mathcal{E}(\tau, z), \qquad (10.69)$$

$$\mathcal{E}(-\frac{1}{\tau}, \frac{z}{\tau}) = e^{2\pi i \frac{c}{6} \cdot \frac{z^2}{\tau}} \mathcal{E}(\tau, z). \qquad (10.70)$$

---

[3]Alternatively one could fold the defect and calculate the Witten index as an boundary state expectation value.

As in the last section we are interested in calculating an (Witten) index with a topological defect insertion. In order to do this we first perform the slightly more complicated calculation where we consider the elliptic genus with variable z in the presence of such a defect. After we have calculated the associated new genus we set $z = 0$ in order to find the right expression for the index.

Thus the new quantity of interest is given by

$$\mathcal{E}(\tau, z, D_{[L,M,S,\bar{S}]}) = \mathrm{tr}_{RR}(-1)^F D_{[L,M,S,\bar{S}]} q^{L_0 - \frac{c}{24}} \bar{q}^{\bar{L}_0 - \frac{c}{24}} y^{J_0}. \tag{10.71}$$

The topological B-type defect that we insert can be represented via

$$D_{[L,M,S,\bar{S}]} = \sum_{\substack{[l,m,s],\bar{s} \\ s-\bar{s} \text{ even}}} D_{[L,M,S,\bar{S}]}^{[l,m,s,\bar{s}]} P_{[l,m,s,\bar{s}]}, \tag{10.72}$$

where $P_{[l,m,s,\bar{s}]}$ is a projector on the space of states with labels $[l, m, s, \bar{s}]$. Here $[l, m, s, \bar{s}]$ labels the following set

$$[l, m, s, \bar{s}] = \{(l, m, s_i) | 0 \leq l \leq k, \ m \in \mathbb{Z}_{2k+4}, \ s_i \in \mathbb{Z}_4, l + m + s_i = 0 \bmod 2\}/\sim, \tag{10.73}$$

where $(l, m, s_i) \sim (k - l, k + 2 + m, 2 + s_i)$ with $s_i \in \{s, \bar{s}\}$. The standard solution for the defect coefficients, which can be obtained by folding and applying the permutation boundary conditions [21], is

$$D_{[L,M,S,\bar{S}]}^{[l,m,s,\bar{s}]} = e^{-i\pi \frac{\bar{S}(s+\bar{s})}{2}} \frac{S_{[L,M,S-\bar{S}]}^{[l,m,s]}}{S_{[0,0,0]}^{[l,m,s]}}, \tag{10.74}$$

where the different defects are labelled by representation classes $[L, M, S, \bar{S}]$. Further the modular S-matrix is given by

$$S_{[L,M,S]}^{[l,m,s]} = \frac{1}{k+2} e^{-i\pi \frac{Ss}{2}} e^{i\pi \frac{Mm}{k+2}} \sin\left(\pi \frac{(L+1)(l+1)}{k+2}\right). \tag{10.75}$$

The defect acts as a map $D : \mathcal{H} \to \mathcal{H}$ preserving the B-type gluing conditions leading to the associated commutation relations

$$[L_n, D] = 0 = [\bar{L}_n, D] \tag{10.76}$$

$$G_r^{\pm} D - \eta D G_r^{\pm} = 0 = \bar{G}_r^{\pm} D - \bar{\eta} D \bar{G}_r^{\pm}, \tag{10.77}$$

with $\eta, \bar{\eta} \in \{\pm 1\}$. The possible choices of S and $\bar{S}$ are, therefore, related to the spin structures for left and right movers as

$$(-1)^S = \eta \quad (-1)^{\bar{S}} = \bar{\eta}, \tag{10.78}$$

where it is understood

$$D^{[l,m,s+2,\bar{s}]} = \eta D^{[l,m,s,\bar{s}]} \quad \text{and} \quad D^{[l,m,s,\bar{s}+2]} = \bar{\eta} D^{[l,m,s,\bar{s}]}. \tag{10.79}$$

The fusion of two topological defects is now straight forward [21]

$$D_{[L_1,M_1,S_1,\bar{S}_1]} D_{[L_2,M_2,S_2,\bar{S}_2]} = \sum_L N^L_{L_1 L_2} D_{[L,M_1+M_2,S_1+S_2,\bar{S}_1+\bar{S}_2]}, \tag{10.80}$$

where N^l_{ij} are the $su(2)_k$ fusion coefficients. The calculation of the elliptic genus with defect insertion now proceeds as follows

$$\mathcal{E}(\tau, z, D_{[L,M,S,\bar{S}]}) = \sum_{\substack{(l,m,s) \\ s,\bar{s}\ odd}} \frac{S^{[l,m,s,\bar{s}]}_{[L,M,S,\bar{S}]}}{S^{[l,m,s,\bar{s}]}_{[0,0,0,0]}} \text{tr}_{\mathcal{H}_{[l,m,s,\bar{s}]}} (-1)^{J_0-\bar{J}_0} q^{L_0-\frac{c}{24}} \bar{q}^{\bar{L}_0-\frac{c}{24}} y^{J_0}. \tag{10.81}$$

The Hilbert space is given by

$$\mathcal{H}_{[l,m,s,\bar{s}]} = (\mathcal{H}_{l,m,s} \oplus \mathcal{H}_{l,m,s+2}) \otimes (\bar{\mathcal{H}}_{l,m,\bar{s}} \oplus \bar{\mathcal{H}}_{l,m,\bar{s}+2}). \tag{10.82}$$

Adopting the notation presented in [96] for the difference of characters

$$I^l_m(\tau, z) = \chi_{l,m,1}(\tau, z) - \chi_{l,m,-1}(\tau, z), \tag{10.83}$$

we find

$$\mathcal{E}(\tau, z, D_{[L,M,S,\bar{S}]}) =$$

$$\sum_{(l,m)\ odd} \left(D^{[l,m,1,1]}_{[L,M,S,\bar{S}]} \chi_{l,m,1}(\tau, z) - D^{[l,m,-1,1]}_{[L,M,S,\bar{S}]} \chi_{l,m,-1}(\tau, z) \right) \bar{\chi}_{l,m,1}(\bar{\tau}, 0) -$$

$$- \left(D^{[l,m,1,-1]}_{[L,M,S,\bar{S}]} \chi_{l,m,1}(\tau, z) - D^{[l,m,-1,-1]}_{[L,M,S,\bar{S}]} \chi_{l,m,-1}(\tau, z) \right) \bar{\chi}_{l,m,-1}(\bar{\tau}, 0). \tag{10.84}$$

We now demand $S, \bar{S}$ to be even in order to preserve the corresponding spin structure. We thus find for the genus with defect insertion

$$\frac{1}{2}(-1)^{\frac{S+\bar{S}}{2}} \sum_{l=0}^{k} \sum_{m=-k-1}^{k+2} \frac{\sin(l,L)}{\sin(l,0)} e^{i\pi\frac{mM}{k+2}} I^l_m(\tau, z) \bar{I}^l_m(\bar{\tau}, 0). \tag{10.85}$$

Here we used in the last step that

$$\sum_{(l,m)\ odd} = \frac{1}{2} \sum_{l=0}^{k} \sum_{m=-k-1}^{k+2}, \tag{10.86}$$

which is true since $\bar{I}_m^l(\bar{\tau}, 0)$ automatically makes $l + m$ odd (see (E.9)). Some aspects of the functions $I_m^l(\tau, z)$ and characters $\chi_{l,m,s}(\tau, z)$ are summarized in appendix E and can also be found in [96].

We are now interested in performing a generalized modular S-transformation via

$$I_m^l(-1/\tau, z/\tau) = (-i)e^{\frac{c\pi i}{3}\frac{z^2}{\tau}} \sum_{l'=0}^{k} \sum_{m'=k-1}^{k+2} S_l^{l'} S_m^{*m'} I_{m'}^{l'}(\tau, z), \tag{10.87}$$

$$\bar{I}_m^l(-1/\bar{\tau}, 0) = i \cdot \sum_{l'=0}^{k} \sum_{m'=k-1}^{k+2} S_l^{l'} S_m^{m'} \bar{I}_{m'}^{l'}(\tau, 0), \tag{10.88}$$

with

$$S_l^{l'} = \sqrt{\frac{2}{k+2}} \sin\left(\pi \frac{(l+1)(l'+1)}{k+2}\right) \tag{10.89}$$

$$S_m^{m'} = \frac{1}{\sqrt{2(k+2)}} e^{-i\pi\frac{mm'}{k+2}}. \tag{10.90}$$

Plugging this into (10.85) one obtains

$$\mathcal{E}(\tau, z, D_{[L,M,S,\bar{S}]}) = \frac{1}{2}(-1)^{\frac{S+\bar{S}}{2}} e^{-\frac{c\pi i}{3}\frac{z^2}{\tau}} \sum_{l_1,l_2} \sum_{m_1} N_{l_1,l_2}^L \left(\delta_{m_1,l_2+M+1}^{(2k+4)} - \delta_{m_1+M-l_2-1}^{(2k+4)}\right) I_{m_1}^{l_1}(-1/\tau, z/\tau). \tag{10.91}$$

We are now in the position to specialize to the specific value $z = 0$ in which case

$$\mathcal{E}(\tau, 0, D_{[L,M,S,\bar{S}]}) = \frac{1}{2}(-1)^{\frac{S+\bar{S}}{2}} \sum_{l_1,l_2}^{k} N_{l_1,l_2}^L \left(\delta_{l_1,l_2+M}^{(2k+4)} + \delta_{l_1,l_2-M}^{(2k+4)} - \delta_{l_1,M-l_2-2}^{(2k+4)} - \delta_{l_1,-M-l_2-2}^{(2k+4)}\right). \tag{10.92}$$

This gives us the Witten index (10.68) in the presence of a single defect. The equation is of the form

$$(number \ of \ bosons) \ - \ (number \ of \ fermions)$$

where topological bosons appear if

$$l_1 = l_2 \pm M \mod (2k+4), \tag{10.93}$$

and the topological fermions arrise for

$$l_1 = -l_2 - 2 \pm M \mod (2k+4). \tag{10.94}$$

If we consider the case of the insertion of two defects $D_{[L_1,M_1,S_1,\bar{S}_1]}$ and $D_{[L_2,M_2,S_2,\bar{S}_2]}^\dagger$ one obtains for the Witten index using the fusion for the topological defects (10.80)

$$\mathcal{E}(\tau, 0, D_{[L_1,M_1,S_1,\bar{S}_1]}, D_{[L_2,M_2,S_2,\bar{S}_2]}^\dagger) =$$

$$\frac{1}{2}(-1)^{\frac{S_1+\bar{S}_1-S_2-\bar{S}_2}{2}} \sum_{l,l_1,l_2} N^l_{L_1,L_2} N^l_{l_1,l_2} \left(\delta^{(2k+4)}_{l_1,l_2+\Delta M} + \delta^{(2k+4)}_{l_1,l_2-\Delta M} - \delta^{(2k+4)}_{l_1,\Delta M-l_2-2} - \delta^{(2k+4)}_{l_1,-\Delta M-l_2-2} \right),$$

$$(10.95)$$

where $\Delta M := M_1 - M_2$. In this case we see that the topological 'bosons' are determined by $l_1 = l_2 \pm \Delta M \mod (2k+4)$, whereas the topological 'fermions' are given by $l_1 = -l_2 - 2 \pm \Delta M \mod (2k+4)$.

This is in exact agreement with the result obtained in [21] (up to a factor $1/2$ coming from a different normalization) where they considered the spectrum between permutation branes[4] and identified the topological 'bosons' and 'fermions' which can be related (in matrix factorisation language) to the Landau-Ginzburg model.

The result can now easily be generalized to the insertion of n defects by repeatedly performing the fusion (10.80), i.e.

$$\prod_{i=1}^{n} D_{[L_i,M_i,S_i.\bar{S}_i]} = \sum_{\tilde{L}_1,...,\tilde{L}_{n-1}} N^{\tilde{L}_1}_{L_{n-1}L_n} N^{\tilde{L}_2}_{L_{n-2}\tilde{L}_1} \cdots N^{\tilde{L}_{n-1}}_{L_1\tilde{L}_{n-2}} D_{[\tilde{L}_{n-1},\sum_i M_i,\sum_i S_i,\sum_i \bar{S}_i]}. \quad (10.96)$$

As a remark we want to note that if we consider the case, where the defect labels $S, \bar{S}$ are both odd we don't need the operator $(-1)^F$ in the partition function to get the same result for the elliptic genus. This is clear since $(-1)^F$ acts as a spectral flow operator acting on the defect as $D_{[L,M,S,\bar{S}]} \to D_{[L,M,S+1,\bar{S}+1]}$.

Note that the Witten index can also be calculated for non-topological defects whereas it is not clear if this can be done easily also for the elliptic genus.

10.7 EE in the Ramond Sector with $(-1)^F$ Insertion

Here we want to briefly comment on the entanglement entropy through Ramond-sector topological interfaces in the presence of $(-1)^F$. Again we consider B-type defects given by (10.72). Following the usual arguments for obtaining the partition function on the n-sheeted Riemann surfaces we want to calculate

$$Z(n) = \mathrm{tr}_{RR} \left(D_{[L,M,S,\bar{S}]} D^\dagger_{[L,M,S,\bar{S}]} \right)^n (-1)^F e^{-2n\delta H}. \quad (10.97)$$

Using the fusion (10.80) we find

$$\left(D_{[L,M,S,\bar{S}]} D^\dagger_{[L,M,S,\bar{S}]} \right)^n = \sum_{l_1,...,l_{2n-1}} N^{l_1}_{L,L} N^{l_2}_{L,l_1} \cdots N^{l_{2n-1}}_{L,l_{2n-2}} D_{[l_{2n-1},0,0,0]}. \quad (10.98)$$

We now can make use of the result for the elliptic genus with $z = 0$ (10.92) to find

$$Z(n) = \sum_{l_1,...,l_{2n}} N^{l_1}_{L,L} N^{l_2}_{L,l_1} \cdots N^{l_{2n-1}}_{L,l_{2n-2}} N^{l_{2n-1}}_{l_{2n},l_{2n}} = \sum_{l=0}^{k} \left(\frac{\sin(L,l)}{\sin(0,l)} \right)^{2n} \in \mathbb{N}. \quad (10.99)$$

---

[4]As we have seen before permutation branes are the folded versions of the B-type defects considered in the calculation

It is interesting to see directly from (10.92) that only the 'bosons' contribute to the partition function. For the Ramond sector contribution to the entanglement entropy then follows

$$S_R(L,k) = (1-\partial_n)\log Z(n)|_{n=1} = \log[(L+1)(k+1-L)] - \frac{\sum_l \frac{\sin^2(L,l)}{\sin^2(0,l)}\log\frac{\sin^2(L,l)}{\sin^2(0,l)}}{(L+1)(k+1-L)}, \quad (10.100)$$

where we used

$$\sum_{l=0}^{k} \frac{\sin^2(L,l)}{\sin^2(0,l)} = \sum_{l_1,l_2} N_{L,L}^{l_1} N_{l_2,l_2}^{l_1} = (L+1)(k+1-L). \quad (10.101)$$

It is interesting that the Ramond-sector contribution to the EE is independent of M, S and $\bar{S}$ and is just a function of L. Further the result shows in a nice way the field identification since $S_R(L,k)$ is invariant under $L \to k - L$.

Chapter 11

Conclusion and Future Directions

Here we summarize the results of the thesis. First we have generalized the supersymmetric twist fields introduced in [86] to general chiralities and calculated with their help the supersymmetric versions of the Renyi and entanglement entropies. In particular we have seen that for a single interval the leading term of the SRE is simply the entanglement entropy independent of the choices for the chiralities. We highlighted the construction for SUSY twist fields and generalized the construction procedure in obtaining the twist fields. Thereby we recognized that it is important in which way one applies the spectral flow, in particular we learned that depending on the number of applications of the spectral flow we end up in the NS- or R-sector respectively.

Next we have considered entanglement through topological interfaces. After a short introduction how to derive the partition function on the n-sheeted Riemann surface we calculated the entanglement entropy an showed that it takes the form

$$S = \frac{c}{3} \log L + S_{sub}, \tag{11.1}$$

where all the information coming from the topological defect are encoded in the subleading term S_{sub}. Discussing several examples we highlighted the obtained formula. Especially we considered RCFT, e.g. models based on $su(2)_k$ and also specific coset models that are free of field identification fixed points. For the later ones we showed in several examples that the subleading contribution decomposes into the individual coset parts.

Afterwards we considered the left/right entanglement entropy which we derived by unfolding a Cardy boundary state and performed the same calculational steps as in the chapter before for just the chiral part of the algebra corresponding to the unfolded boundary. We motivated our results with a class of examples.

As a last big topic we discussed indices in the presence of defects. Thereby we calculated the indices between boundary states and gave a detailed geometric interpretation in terms of an intersection number of D-branes living in a Landau-Ginzburg model with superpotential $W = X^{k+2}$. By calculating the elliptic genus in the presence of a single defect we managed to obtain an expression for the Witten index with a defect insertion and showed that we reproduce the results obtained in [21].

For future directions it would be interesting to see how coset models with fixed point field identification behave in the subleading term of the entanglement entropy. It is possible that there is the same decomposition as for the fixed-point free models but with an additional contribution reflecting the fixed point. Quite generally it would be interesting to see the decomposition for general coset models.

Also it would be interesting to see if the action of a defect could be phrased in terms of extended twist fields carrying additional structure.

Further let us comment on $\mathcal{N} = 2$ supersymmetric theories. It is known that these theories can be topologically twisted with the gluing conditions of boundaries and defects compatible under the topological twist. On this level a topological twisted defect can be calculated in the same manner as we did for the 'purely' topological defects. In the case of topological twisted defects the entanglement entropy should have a topological interpretation.

Finally we proposed a method for calculating indices in terms of a defect induced metric. It would be interesting to work this out for specific non-topological defects an also give a geometric interpretation. Apart from that we also calculated the elliptic genus in presence of a topological defect. It would be interesting to find some applications of the obtained quantity and also to find some geometric interpretation. In addition it would be interesting to know if a generalization to non-topological interfaces is possible.

Appendix A

Properties of Vertex Operators

From theories with a free scalar field $H(z, \bar{z}) = H_L(z) + H_R(\bar{z})$ one can construct another primary field called the *vertex operators*. The scalar field is no good conformal field because on the one hand it is no primary field and on the other hand because of its logarithmic behaviour of the two point function

$$\langle H(z, \bar{z})H(w, \bar{w}) \rangle = -\log|z - w|^2. \tag{A.1}$$

There are two possible ways of getting rid of the logarithm either by considering derivatives of the scalar field, e.g. the current $J \sim \partial H$, or by taking the exponential of this field combined with a normal ordering description. It turns out that exponentiating results in a primary field. This so called *vertex operator* is then defined by

$$V_\alpha(z, \bar{z}) = \quad : \exp(i\alpha H(z, \bar{z})) : . \tag{A.2}$$

The OPE with the energy-momentum tensor of the theory is given by

$$T(z)V_\alpha(w, \bar{w}) = \frac{\alpha^2}{2} \cdot \frac{1}{(z - w)^2}V_\alpha(w, \bar{w}) + \frac{1}{(z - w)}\partial_w V_\alpha(w, \bar{w}) + reg. \tag{A.3}$$

Comparing this to the general OPE for primary fields (2.24) (and similar for the anti-holomorphic part) one see that the conformal weight of the vertex operator is $(h, \bar{h}) = (\alpha^2/2, \alpha^2/2)$. For theories compactified on a circle of radius R the highest weight of left- and right-mover can be related to the the zero modes of the free boson $(\alpha^2/2, \alpha^2/2) = (p_L, p_R)$, in particular this means that the weights depend on the momentum and winding number (see section B).

Consider next the slightly different vertex operator defined by

$$V_\alpha(z, \bar{z}; \epsilon, \bar{\epsilon}) = \exp(i\alpha(\epsilon H_L + \bar{\epsilon}H_R)), \tag{A.4}$$

where $\epsilon, \bar{\epsilon} \in \{\pm 1\}$. The conformal weights of the vertex operator is unchanged under the redefinition. Of special interest are n-point functions of these vertex operators which can all be compute using Wick's theorem [1, 2]. As a result one finds

$$\langle \prod_{i=1}^{n} V_\alpha(z_i, \bar{z}_i; \epsilon_i, \bar{\epsilon}_i) \rangle = \prod_{j>i}^{n} (z_j - z_i)^{\epsilon_i \epsilon_j \alpha^2} (\bar{z}_j - \bar{z}_i)^{\bar{\epsilon}_i \bar{\epsilon}_j \alpha^2} \delta_{0, \sum_i \epsilon_i} \delta_{0, \sum_i \bar{\epsilon}_i}, \tag{A.5}$$

where we assumed that the insertion points are ordered according to $|z_i| < |z_j|$ for $i < j$. The Kronecker-delta appearing in the equation ensure that the n-point function is zero unless the balance of the 'charges' $\sum_i \epsilon_i = 0$ (and same for the right-movers) is kept.

Appendix B

CFT Description of the Free Boson

In this chapter we summarize some conventions for the free massless chiral boson in the CFT description. In complex coordinates the equation of motion for a free complex scalar field $\Phi(z, \bar{z})$ with central charge is given by

$$\partial_z \partial_{\bar{z}} \Phi(z, \bar{z}) = 0. \tag{B.1}$$

The solution to the equation of motion results in the mode expansion for the free boson

$$\Phi(z, \bar{z}) = q_L + q_R - i(p_L \log z + p_R \log \bar{z}) + i \sum_{n \neq 0} \frac{1}{n} \left(a_n z^{-n} + \bar{a}_n \bar{z}^{-n} \right). \tag{B.2}$$

Here q_L and q_R are the left- and right-moving space operators whereas p_L and p_R are the momentum operators respectively. In string language $q = q_L + q_R$ determines the center of mass coordinate of the string. The non-trivial commutation relations between these operators are given by

$$[q_L, p_L] = i, \tag{B.3}$$
$$[q_R, p_R] = i, \tag{B.4}$$
$$[a_n, a_m] = n\delta_{n+m,0}, \tag{B.5}$$
$$[\bar{a}_n, \bar{a}_m] = n\delta_{n+m,0} \tag{B.6}$$

One can split the field into left and right chiral components $\Phi(z, \bar{z}) = \Phi_L(z) + \Phi_R(\bar{z})$, with

$$\Phi_L(z) = q_L - ip_L \log z + i \sum_{n \neq 0} \frac{1}{n} a_n z^{-n}, \tag{B.7}$$

$$\Phi_R(\bar{z}) = q_R - ip_R \log \bar{z} + i \sum_{n \neq 0} \frac{1}{n} \bar{a}_n \bar{z}^{-n}. \tag{B.8}$$

The holomorphic part of energy-momentum tensor associated with the free boson can be written as

$$T(z) = -\frac{1}{2} : \partial_z \Phi_z \partial_L \Phi_L : \tag{B.9}$$

For the Virasoro generators this implies

$$L_n = \frac{p_L^2}{2} + \sum_{m>0} a_m a_{n-m}, \tag{B.10}$$

and similar for the anti-holomorphic part. One also calls p_L and p_R the zero modes for the holomorphic and anti-holomorphic Virasoro generator, i.e. $a_0 = p_L/\sqrt{2}$.

We now want to consider the case when the boson is compactified on a circle of radius R. In this case we identify

$$X \equiv X + 2\pi R. \tag{B.11}$$

The identification has two consequences: first the momenta are quantized. This can be seen from the fact that the operator $\exp(2\pi i Rp)$ that translates states around the circle has to be trivial. Here $p = p_L + p_R$ is the total momentum operator of left- and right-movers. The momentum eigenvalue thus has to take the form m/R, where on calls $m \in \mathbb{Z}$ the momentum number. The second consequence is that there are new 'winding' states that can wrap around the circle since the boundary conditions

$$\Phi(e^{2\pi i}z, e^{-2\pi i}\bar{z}) = \Phi(z, \bar{z}) + 2\pi Rn, \quad n \in \mathbb{Z} \tag{B.12}$$

are allowed by the identification (B.11). One calls n the winding number. The eigenvalues of the zero modes (p_L, p_R) are thus quantized and given by

$$(p_L, p_R) = \left(\frac{m}{R} + \frac{nR}{2}, \frac{m}{R} - \frac{nR}{2} \right). \tag{B.13}$$

The non-zero modes a_n, $\bar{a}_n$ are unaffected by the identification (B.11) and thus remain unchanged. Obviously the zero-modes, or also called charges, form a charge lattice $\Lambda(R)$. A highest weight state is now label by the winding and momentum numbers $|m, n\rangle$ and for the partition function holds

$$Z_{circ}(\tau, \bar{\tau}) = \frac{1}{|\eta(\tau)|^2} \sum_{m,n} q^{\frac{1}{2}\left(\frac{m}{R} + \frac{nR}{2}\right)^2} \bar{q}^{\frac{1}{2}\left(\frac{m}{R} - \frac{nR}{2}\right)^2}, \tag{B.14}$$

with

$$\eta(\tau) = q^{\frac{1}{24}} \prod_{n=1}^{\infty} (1 - q^n). \tag{B.15}$$

Appendix C

Prove of Specific Formulas

In this chapter we prove some specific formulas that appear in the context of coset models. We consider a $su(2)_k$ theory with modular S-matrix

$$S_l^{l'} = \sqrt{\frac{2}{k+2}} \sin\left(\pi \frac{(l+1)(l'+1)}{k+2}\right). \tag{C.1}$$

Here $l, l' \in \{0, 1, \ldots, k\}$. We are now interested in calculating the sum over even (odd) labels of the modular S-matrix absolute value squared. We consider the case k even first. The calculation proceeds as follows:

$$\sum_{\substack{l'=0 \\ l' \, even}}^{k} |S_l^{l'}|^2 = -\frac{1}{2(k+2)} \sum_{\substack{l'=0 \\ l' \, even}}^{k} \left(e^{2\pi i \frac{(l+1)(l'+1)}{k+2}} - 2 + e^{-2\pi i \frac{(l+1)(l'+1)}{k+2}}\right) \tag{C.2}$$

Substituting $l = 2(n-1)$ one obtains

$$\sum_{\substack{l'=0 \\ l' \, even}}^{k} |S_l^{l'}|^2 = -\frac{1}{2(k+2)} \sum_{n=1}^{\frac{k}{2}+1} \left(e^{-2\pi i \frac{l+1}{k+2}} e^{2\pi i \frac{n}{\frac{k}{2}+1}} - 2 + e^{2\pi i \frac{l+1}{k+2}} e^{-2\pi i \frac{n}{\frac{k}{2}+1}}\right) =$$

$$\frac{1}{2} - \frac{1}{2(k+2)} \sum_{n=1}^{\frac{k}{2}+1} \left(e^{-2\pi i \frac{l+1}{k+2}} e^{2\pi i \frac{m}{\frac{k}{2}+1}} + e^{2\pi i \frac{l+1}{k+2}} e^{-2\pi i \frac{m}{\frac{k}{2}+1}}\right). \tag{C.3}$$

Using the identity

$$\sum_{n=1}^{N} e^{2\pi i n m / N} = N \delta_{m,0}^{(N)}, \tag{C.4}$$

we finally obtain for the even summation assuming also k to be even:

$$\sum_{\substack{l'=0 \\ l' \, even}}^{k} |S_l^{l'}|^2 = \frac{1}{2}\left(1 + \delta_{l', \frac{k}{2}}\right). \tag{C.5}$$

In a similar fashion the case for the summation over the odd labels can be worked out. Using

$$1 = \sum_{l'=0}^{k} |S_l^{l'}|^2 = \sum_{\substack{l'=0 \\ l'\ even}}^{k} |S_l^{l'}|^2 + \sum_{\substack{l'=0 \\ l'\ odd}}^{k} |S_l^{l'}|^2, \tag{C.6}$$

the result or the odd summation is using (C.5):

$$\sum_{\substack{l'=0 \\ l'\ odd}}^{k} |S_l^{l'}|^2 = \frac{1}{2}\left(1 - \delta_{l',\frac{k}{2}}\right). \tag{C.7}$$

For the cases where k is odd one can use the symmetry $|S_l^{l'}|^2 = |S_l^{k-l'}|^2$ to show

$$\sum_{\substack{l'=0 \\ l'\ even}}^{k} |S_l^{l'}|^2 = \sum_{\substack{l'=0 \\ l'\ odd}}^{k} |S_l^{l'}|^2 = \frac{1}{2}. \tag{C.8}$$

Since l is an integer the formulas (C.5) and (C.7) apply for all possible k.

Appendix D

Explicit Calculation of the Boundary Index

In this chapter we explicitly calculate the overlap between two branes in the Ramond sector [18–20] with the insertion of $\exp(-i\pi J_0)$ (spectral flow[1]) and a topological defect $D_{L,M,S}$.

For the index between A-branes we find with $q^H = \exp(-\frac{2\pi^2}{\beta}(L_0 + \bar{L}_0 - \frac{c}{12}))$

$$I(A_{l_1,m_1,s_1}, A_{l_2,m_2,s_2}, D_{L,M,S}) = 2\,_{RR}\langle A_{l_1,m_1,s_1}|\, e^{-i\pi J_0} q^H D_{L,M,S} |A_{l_2,m_2,s_2}\rangle_{RR} =$$

$$2 \sum_{\substack{(l,m,s) \\ s\ odd}} \sum_{\substack{(l',m',s') \\ s'\ odd}} \frac{S^{l,m,s}_{l_1,m_1,s_1} S^{*\ l',m',s'}_{l_2,m_2,s_2}}{\sqrt{S^{l,m,s}_{0,0,0} S^{l',m',s'}_{0,0,0}}} \cdot \frac{S^{l,m,s}_{L,M,S}}{S^{l,m,s}_{0,0,0}} e^{-i\pi\left(\frac{s}{2} - \frac{m}{k+2}\right)} \langle\langle A_{l,m,s}|q_H|A_{l',m',s'}\rangle\rangle \tag{D.1}$$

Using

$$\langle\langle A_{l,m,s}|q_c^{H_c}|A_{l',m',s'}\rangle\rangle = \delta_{ll'}\delta_{mm'}\delta_{ss'}\chi_{l,m,s}(2\tau), \tag{D.2}$$

with $\tau = i\pi/\beta$ we can write our expression in a more compact form as

$$I(A_{l_1,m_1,s_1}, A_{l_2,m_2,s_2}, D_{L,M,S}) = 2 \sum_{\substack{(l,m,s) \\ s=\pm 1}} \frac{S^{l,m,s}_{l_1,m_1,s_1} S^{*\ l,m,s}_{l_2,m_2,s_2}}{S^{l,m,s}_{0,0,0}} \cdot \frac{S^{l,m,s}_{L,M,S}}{S^{l,m,s}_{0,0,0}} e^{-i\pi\left(\frac{s}{2} - \frac{m}{k+2}\right)} \chi_{l,m,s} =$$

$$= \frac{2}{k+2} \sum_{(l,m)\ odd} \frac{\sin(l,l_1)\sin(l,l_2)\sin(l,L)}{\sin^2(l,0)} e^{i\pi \frac{m(M+m_2-m_1+1)}{k+2}} \times$$

$$\left(e^{-i\pi \frac{s_1+S+1-s_2}{2}} \chi_{l,m,1} + e^{i\pi \frac{s_1+S+1-s_2}{2}} \chi_{l,m,-1}\right). \tag{D.3}$$

---

[1]On the level of boundary states $\exp(-i\pi J_0)$ acts on the s-label as $s \to s - 1$. In this sense we change from the NS-sector to the R-sector and vice versa. In this sense $\exp(-i\pi J_0)$ resembles a spectral flow

Here again we used the short hand notation

$$\sin(i,j) := \sin\left(\pi \frac{(i+1)(j+1)}{k+2}\right). \tag{D.4}$$

If we now demand

$$S + s_1 - s_2 = 0 \bmod 2 \tag{D.5}$$

we find for the overlap

$$I(A_{l_1,m_1,s_1}, A_{l_2,m_2,s_2}, D_{L,M,S}) =$$

$$-\frac{2i}{k+2} e^{-i\pi \frac{S+s_1-s_2}{2}} \sum_{(l,m)\ odd} \frac{\sin(l,l_1)\sin(l,l_2)\sin(l,L)}{\sin^2(l,0)} e^{i\pi \frac{m(M+m_2-m_1+1)}{k+2}} \left(\chi_{l,m,1} - \chi_{l,m,-1}\right). \tag{D.6}$$

Note that we assume s_1, s_2 to bee odd in order to obtain old result (10.19) for the identity defect. Equation (D.5) then tells us that $S = 0 \bmod 2$ which means that only boundary condition preserving defects are allowed, i.e. we cannot switch an A-type boundary condition into a B-type condition.

It is now commonly known that $\chi_{l,m,1} - \chi_{l,m,-1} = \delta_{m,l+1} - \delta_{m,-l-1}$. Plugging this into the equation above and noting

$$\sum_{(l,m)\ odd} = \frac{1}{2} \sum_{l=0}^{k} \sum_{\substack{m=-k-1 \\ l+m=1\ \bmod\ 2}}^{k+2} , \tag{D.7}$$

we find

$$I(A_{l_1,m_1,s_1}, A_{l_2,m_2,s_2}, D_{L,M,S}) =$$

$$\frac{2}{k+2} e^{-i\pi \frac{S+s_1-s_2}{2}} \sum_{l=0}^{k} \frac{\sin(l,l_1)\sin(l,l_2)\sin(l,L)\sin(M+m_2-m_1,l)}{\sin^2(l,0)}. \tag{D.8}$$

This can be rewritten in terms of $su(2)_k$ modular S-matrices as

$$I(A_{l_1,m_1,s_1}, A_{l_2,m_2,s_2}, D_{L,M,S}) = e^{-i\pi \frac{S+s_1-s_2}{2}} \sum_{l=0}^{k} \frac{S_{l_1}^l S_{l_2}^l S_L^l S_{M+m_2-m_1}^l}{S_0^l S_0^l}. \tag{D.9}$$

Using the identity

$$\delta_{a,b} = \sum_{c=0}^{k} S_a^c S_b^c, \tag{D.10}$$

as well as the definition of the fusion coefficients for $su(2)_k$ in terms of modular S-matrices

$$N_{a,b}^c = \sum_{l=0}^{k} \frac{S_a^l S_b^l S_c^l}{S_0^l}, \qquad (D.11)$$

we finally obtain

$$I(A_{l_1,m_1,s_1}, A_{l_2,m_2,s_2}, D_{L,M,S}) = e^{i\pi \frac{s_2-S-s_1}{2}} \sum_{l=0}^{k} N_{l_1,l_2}^l N_{L,M+m_2-m_1}^l. \qquad (D.12)$$

Here it is understood that

$$N_{L\ \Delta m}^l = \begin{cases} N_{L,-\Delta m-2k-6}^l & \text{for } \Delta m \in \{-2k-3,\ldots,-k-4\} \\ -N_{L,-\Delta m-2}^l & \text{for } \Delta m \in \{-k-2,\ldots,-2\} \\ N_{L\ \Delta m}^l & \text{for } \Delta m \in \{0,\ldots,k\} \\ -N_{L,2k+2-\Delta m}^l & \text{for } \Delta m \in \{k+2,\ldots,2k+2\} \\ N_{L,4k+6-\Delta m}^l & \text{for } \Delta m \in \{2k+4,\ldots,3k+4\} \\ -N_{L,6k+10-\Delta m}^l & \text{for } \Delta m \in \{3k+6,\ldots,4k+6\} \\ 0 & \text{for } \Delta m = -1 \bmod (k+2) \end{cases} \qquad (D.13)$$

where $\Delta m = M + m_2 - m_1$. Since we want to reproduce (10.19) for the identity defect $(L, M, S) = (0, 0, 0)$ we have s_1, s_2 odd for which follows from (D.5)

$$S = 0 \bmod 2. \qquad (D.14)$$

Let us now consider the overlap between B-type boundaries. The calculation now follows similar steps as before

$$I_B(B_s, B_{\tilde{s}}, D_{L,M,S}) = 2\,_{RR}\langle B_s| \, D_{L,M,S} \, q^H \, |B_{\tilde{s}}\rangle_{RR} =$$

$$\frac{k+2}{2} \sum_{l',m',s'\ odd} \frac{S_{LMS}^{l'm's'}}{S_{000}^{l'm's'}} e^{i\pi \frac{s^2-\tilde{s}^2}{2}} e^{i\pi \frac{s'(s-\tilde{s})}{2}} \langle\langle B_{\frac{k}{2},\frac{k+2}{2},s'}|e^{-i\pi J_0} q^H |B_{\frac{k}{2},\frac{k+2}{2},s'}\rangle\rangle. \qquad (D.15)$$

The labels for the B-type boundaries are restricted to $s, \tilde{s} \in \{\pm 1\}$. For the expectation value holds

$$\langle\langle B_{\frac{k}{2},\frac{k+2}{2},s'}|e^{-i\pi J_0} q_c^{H_c}|B_{\frac{k}{2},\frac{k+2}{2},s'}\rangle\rangle = e^{-i\pi(\frac{1}{2}-\frac{k+2)}{2(k+2)})} \delta_{s',1} \delta_{m',\frac{k+2}{2}} \delta_{l',\frac{k}{2}}, \qquad (D.16)$$

Thus is follows

$$I_B(B_s, B_{\tilde{s}}, D_{L,M,S}) = \frac{k+2}{2} \sin\left(\frac{\pi}{2}(L+1)\right) e^{i\pi \frac{s^2+s-\tilde{s}^2-\tilde{s}}{2}} e^{i\pi \frac{M-S}{2}} \in \{0, \pm\frac{k+2}{2}\}. \qquad (D.17)$$

In order to reproduce (10.18) for the identity defect we have to restrict to values satisfying

$$M - S = 0 \mod 2. \tag{D.18}$$

The last possible case is to consider a defect between an A-type and a B-type boundary, i.e.

$$I_{AB}(B_{\tilde{s}}, A_{l,m,s}, D_{L,M,S}) = 2_{RR} \langle B_{\tilde{s}}| D_{L,M,S} \, q_c^{H_c} |A_{l,m,s}\rangle_{RR} =$$

$$\sqrt{k+2} \sum_{l',m',s' \; odd} \frac{S_{lms}^{l'm's'}}{\sqrt{S_{000}^{l'm's'}}} \frac{S_{LMS}^{l'm's'}}{S_{000}^{l'm's'}} e^{-i\pi \frac{\tilde{s}^2 + \tilde{s}s'}{2}} \langle\langle B_{\frac{k}{2}, \frac{k+2}{2}, s'}|e^{-i\pi J_0} q_c^{H_c}|A_{l',m',s'}\rangle\rangle. \tag{D.19}$$

Using the same ideas as in the previous case we find for the final case under the assumption $\tilde{s} \in \{\pm 1\}$

$$I_{AB}(B_{\tilde{s}}, A_{l,m,s}, D_{L,M,S}) = e^{-i\pi \frac{\tilde{s}^2 + \tilde{s}}{2}} \sin\left(\pi \frac{l+1}{2}\right) \sin\left(\pi \frac{L+1}{2}\right) e^{i\pi \frac{M-S}{2}}, \tag{D.20}$$

with the restriction $M - S = 0 \mod 2$. Again the result can be simply generalized to several defects

$$I_{AB}(B_{\tilde{s}}, A_{l,m,s}, D_{L_1,M_1,S_1}, \ldots, D_{L_K,M_K,S_K}) =$$

$$e^{-i\pi \frac{\tilde{s}^2 + \tilde{s}}{2}} \sin\left(\pi \frac{l+1}{2}\right) \prod_{n=1}^{K} \sin\left(\pi \frac{L_n+1}{2}\right) e^{i\pi \frac{M_n - S_n}{2}} \in \{\pm 1, 0\}, \tag{D.21}$$

with the restriction

$$\sum_{n=1}^{K} M_n - S_n = 0 \mod 2. \tag{D.22}$$

Appendix E

Properties of $I_m^l(\tau, z)$

Here we summarize some properties of the functions $I_m^l(\tau, z)$ which can also be found in [96]. By definition $I_m^l(\tau, z)$ is given by

$$I_m^l(\tau, z) = (\chi_{l,m,1} - \chi_{l,m,-1})(\tau, z) , \tag{E.1}$$

where

$$\chi_{l,m,s}(\tau, z) = \sum_{j \in \mathbb{Z}} c_{m-s+4j}^l(\tau) q^{\frac{k+2}{2k}\left[\frac{m}{k+2} - \frac{s}{2} + 2j\right]^2} e^{2\pi i z \left(\frac{m}{k+2} - \frac{s}{2} + 2j\right)}. \tag{E.2}$$

Alternatively the characters can be written in terms of generalized theta functions

$$\chi_{l,m,s}(\tau, z) = \sum_{j=1}^{k} c_{m-s-4j}^l(\tau) \Theta_{-2m+(4j+s)(k+2),2k(k+2)}(\tau, z), \tag{E.3}$$

where

$$\Theta_{a,b}(\tau, z) = \sum_{n \in \mathbb{Z}} q^{b(n + \frac{a}{2b})^2} y^{b(n + \frac{a}{2b})}. \tag{E.4}$$

The functions $c_a^b(\tau)$ are so called sting functions [1,3]. We see that for the case $z = 0$ the characters are exactly given by the the characters of the $\mathcal{N} = 2$ unitary minimal models (2.142).

Here we used the short notation $q = \exp(2\pi i \tau)$ and $y = \exp(2\pi i z)$. The following identifications hold

$$I_m^l(\tau + 1, z) = \exp[\pi i (h_{l,m,1} - \frac{c}{24})] I_m^l(\tau, z), \tag{E.5}$$

$$I_m^l(-1/\tau, z/\tau) = (-i) \exp[2\pi i \frac{c}{6} \cdot \frac{z^2}{\tau}] I_m^l(\tau, z), \tag{E.6}$$

$$I_m^l(\tau, z) = -I_{-m}^l(\tau, z) = I_{k+2-m}^{k-l}(\tau, z), \tag{E.7}$$

$$I_m^l(\tau, z) = I_{m+2(k+2)\mathbb{Z}}^l(\tau, z) \tag{E.8}$$

$$I_m^l(\tau, 0) = \delta_{m,l+1} - \delta_{m,-l-1}. \tag{E.9}$$

Bibliography

[1] R. Blumenhagen and E. Plauschinn, *Introduction to Conformal Field Theory*, Lecture Notes in Physics. Springer-Verlag Berlin Heidelberg, 2009.

[2] P. di Francesco, P. Mathieu, D. Sénéchal, *Conformal Field Theory*, Graduate Texts in Contemporary Physics, Springer-Verlag New York, 1997.

[3] R. Blumenhagen, D. Lüst and S. Theisen, *Basic Concepts of String Theory*, Theoretical and Mathematical Physics, Springer Berlin Heidelberg, Berlin, Heidelberg, 2013.

[4] A. Recknagel and V. Schomerus, *Boundary Conformal Field Theory and the World-sheet Approach to D-Branes*, Cambridge University Press on Mathematical Physics, Cambridge, 2013.

[5] J. Wess and J. Bagger, *Supersymmetry and Supergravity*, Princeton Series in Physics, Princeton, 1992.

[6] P. Ginsparg, *Applied Conformal Field Theory*, in Les Houches Summer School in Theoretical Physics: Fields, Strings, Critical Phenomena Les Houches, France, June 28-August 5, 1988, pp. 1-168, 1988, [hep-th/9108028v1].

[7] K. Wendland, *Snapshots of conformal field theory*, in: Mathematical Aspects of Quantum Field Theories, D. Calaque and Th. Strobl, eds., Springer-Verlag, 2015, pp. 89-129, [hep-th/1404.3108].

[8] H. Weyl, *Gravitation and Electricity*, Sitz. Berichte d. Preuss. Akad. d. Wissenschaften, 465 (1918).

[9] A.M. Polyakov, *Nonhamiltonian approach to conformal quantum field theory*, Zh. Eksp. Teor. Fiz. 66: 23-42, (1974).

[10] J.M. Maldacena, *The Large N limit of superconformal field theories and supergravity*, Int.J.Theor.Phys. **38**, 1113-1133 (1999), [hep-th/9711200].

[11] M. Virasoro, *Subsidy conditions and ghosts in dual-resonance models*, Phys. Rev. D **1**, 2933 (1970).

[12] J.L. Gervais and B. Sakita, *Field theory interpretation of supergauges in dual models*, Nucl.Phys. B *34*, 632-639 (1971).

[13] J. Wess and B. Zumino, *Supergauge transformations in four dimensions*, Nucl.Phys. B **70**, 39-50 (1974).

[14] E. Witten, *Constraints on Supersymmetry Breaking*, Nucl. Phys. B **202**, 253-316 (1982).

[15] W. Lerche, C. Vafa and N. P.Warner, *Chiral Rings in $\mathcal{N} = 2$ Superconformal Theories*, Nucl. Phys. B **324**, 427-474 (1989).

[16] W. Lerche and J. Walcher, *Boundary rings and $\mathcal{N} = 2$ coset models*, Nucl. Phys. B **625**, 97-127 (2002).

[17] C. Vafa, N. Warner, *Catastrophes and the Classification of Conformal Theories*, Phys. Lett. B **218**, 51 (1988).

[18] K. Hori, A. Iqbal and C. Vafa, *D-branes And Mirror Symmetry*, [hep-th/0005247v2].

[19] K. Hori, S. Katz, A. Klemm, R. Pandharipand, R. Thomas, C. Vafa, R. Vakil and E. Zaslow, *Mirror Symmetry*, Clay Mathematics Monographs Volume 1, Cambridge (2000).

[20] I. Brunner, M.R. Douglas, A. Lawrence and C. Römelsberger, *D-branes on the qunitic*, JHEP **0008** (2000) 015, [hep-th/9906200].

[21] I. Brunner and M. Gaberdiel, *Matrix factorisations and permutation branes*, JHEP **0507** (2005) 012, [hep-th/0503207].

[22] A. Cappelli, C. Itzykson and J.B. Zuber, *Modular Invariant Partition Functions in Two-Dimensions*, Nucl. Phys. B **280** [FS18] 445 (1987).

[23] A. Cappelli, C. Itzykson and J.B. Zuber, *The A-D-E Classification of Minimal and $A_1^{(1)}$ Conformal Invariant Theories*, Commun. Math. Phys. **113**, 1-26 (1987).

[24] T. Gannon, *The Classification of SU(3) Modular Invariants Revisited*, Comm. Math. Phys. **161**, 233-263 (1994), [hep-th/9404185].

[25] J. Fuchs, B. Gato-Rivera, A.N. Schellekens and C. Schweigert, *Modular invariants and fusion rule automorphism from Galois theory*, Phys. Lett. B **334**, 113 (1994).

[26] J. Fuchs, A.N. Schellekens and C. Schweigert, *Galois modular invariants of WZW models*, Nucl. Phys. B **437**, 667 (1995).

[27] P. Goddard, A. Kent and D. Olive,*Virasoro algebras and coset space models* , Phys. Lett. **152**, 88 (1995).

[28] P. Goddard, A. Kent and D. Olive,*Unitary representations of the Virasoro and Super-virasoro algebras* , Commun. Math. Phys. **103**, 105 (1986).

[29] M. Yu. Lashkevich, *Coset Construction of Minimal Models*, Int. J. Mod. Phys. A **8**, 5673 (1993), [hep-th/9304116].

[30] A.N. Schellekens and S. Yankielowicz, *Field Identification Fixed Points in the Coset Construction*, Nucl. Phys. B **334**, 67 (1990), (App. B).

[31] G. Mussardo, G. Sotkov and M. Stanishkov, $\mathcal{N} = 2$ *Superconformal Minimal Models*, Int. J. Mod. Phys. A **4**, 1135 (1989).

[32] P. DiVecchia, J.L. Peterson and H. B. Zheng, *N = 2 Superconformal Theory In Two Dimensions*, Phys. Lett. B **162**, 327 (1985).

[33] P. DiVecchia, J.L. Petersen and M. Yu, *On The Unitary Representations of N = 2 Superconformal Theory*, Phys. Lett. B **172**,211 (1986).

[34] J. Cardy, *Boundary Conformal Field Theory*, in Encyclopedia of Mathematical Physics, ed J.-P. Francoise, G. Naber, and S. Tsun Tsou, (Elsevier, Amsterdam, 2006), [hep-th/0411189v2].

[35] J.L. Cardy, *Boundary Conditions, Fusion Rules and the Verlinde Formula*, Nuclear Physics B **324**, 581-596 (1989).

[36] D. Abanin and E. Demler, *Measuring entanglement entropy of a generic many-body system with a quantum switch*, Phys. Rev. Lett. 109, 020504 (2012), [arxiv:1204.2819v1].

[37] J.L. Cardy, O.A. Castro-Alvaredo and B. Dyon, *Form factors of branch-point twist fields in quantum integrable models and entanglement entropy*, J. Stat. Phys. **130**, 139 (2007), [hep-th/0706.3384].

[38] I. Affleck and A. Ludwig, *Universal noninteger ground-state degeneracy in critical quantum systems*, Phys. Rev. Lett. **67**, 161 (1991).

[39] C. Bachas, J. de Boer, R. Dijkgraaf and H. Ooguri, *Permeable conformal walls and holography*, JHEP **6**, 1-32 (2002), [hep-th/0111210v2].

[40] C. Bachas and M. Gaberdiel, *Loop operators and the Kondo problem*, JHEP **11** (2004) 065, [hep-th/0411067].

[41] C. Bachas and I. Brunner, *Fusion of conformal interfaces*, JHEP **0802** (2008) 085, [hep-th/0712.0076v3].

[42] V. Petkova and J. Zuber, *Generalized twisted partition functions*, Phys.Lett. B **504**, 157-164 (2001), [hep-th/0011021v3].

[43] V. Petkova and J. Zuber, *Conformal Boundary Conditions and what they teach us* (2001), [hep-th/0103007v1].

[44] K. Graham and G.M.T. Watts, *Defect Lines and Boundary Flows*, JHEP **04**, 019 (2004), [hep-th/0306167].

[45] J. Fröhlich, J. Fuchs, I. Runkel and C. Schweigert, *Kramers-Wannier duality from conformal defects*, Phys. Rev. Lett. **93** (Aug., 2004) 070601, [hep-th/0404051].

[46] J. Fröhlich, J. Fuchs, I. Runkel and C. Schweigert, *Duality and defects in rational conformal field theory*, Nucl. Phys. B **763**, 354-430 (2007), [hep-th/061196].

[47] C.L. Kane and M.P.A. Fischer, *Transmission through barriers and resonant tunneling in an interaction one-dimensional elctron gas*, Phys. Rev. **B** Volume 46, Number 23, 1992.

[48] M. Oshikawa and I. Affleck, *Defect lines in the Ising model and boundary states on orbifolds*, Phys. Rev. Lett. **77**, 2604-2607 (1996), [hep-th/9606177].

[49] T. Quella, I. Runkel, G. Watts, *Reflection and Transmission for Conformal Defects*, JHEP **0704** (2007) 095, [hep-th/0611296v2].

[50] T. Quella and V. Schomerus, *Symmetry Breaking Boundary States and Defect Lines*, JHEP **06** (2002) 028, [hep-th/0203161].

[51] G. Sarkissian, *Defects and Permutation branes in the Liouville field theory*, Nucl. Phys. B **821**, 607-625 (2009), [hep-th/0903.4422].

[52] N. Drukker, D. Gaiotto and J. Gomis, *The Virtue of Defects in 4D Gauge Theories and 2D CFTs*, [hep-th/1003.1112].

[53] I. Runkel, *Perturbed Defects and T-Systems in Conformal Field Theory*, J. Phys. A **41**,105401 (2008), [hep-th/0711.0102].

[54] J. Fuchs, M. Gaberdiel, I. Runkel, C. Schweigert, *Topological Defects for the Free Boson CFT*, J. Phys. A **40**, 11403-11440 (2007), [hep-th/0705.3129].

[55] C. Bachas, I. Brunner, D. Roggenkamp, *A worldsheet extension of $O(d,d;\mathbb{Z})$*, JHEP **1210** (2012) 039, [hep-th/1205.4647].

[56] S. Kullback and R. Leibler, *On information and sufficiency*, Annals of Mathematical Statistics **22** (1951) 79-86.

[57] A. YU. Alekseev and V. Schomerus, *D-branes in the WZW model*, Phys. Rev. D **60**, 061901 (1999), [hep-th/9812193].

[58] C. Bachas, M.R. Douglas and C. Schweigert, *Flux stabilisation of D-branes*, JHEP **05** (2000) 048, [hep-th/0003037].

[59] J. M. Figueroa-O'Farrill and S. Stanciu, *D-branes in $AdS_3 \times S^3 \times S^3 \times S^1$* , JHEP **04** (2000) 005, [hep-th/0001199].

[60] E. Brehm, I. Brunner, D. Jaud, C. Schmidt-Colinet, *Entanglement and topological interfaces*, Fortsch. Phys. **64** (2016) 516-535, [hep-th/1512.05945v2].

[61] A. Einstein, B. Podolski and N. Rosen, *Can quantum-mechanical description of physical reality be considered complete?*, Phys. Rev. vol. **47**, no. 10, p. 777 (1935).

[62] J.S. Bell, *On the Einstein-Podolsky-Rosen Paradox*, Pyhsics, vol. 1, no. 3,pp. 195-200 (1964).

[63] P.W. Shor, *Polynomial-time algorithms for prime factorization and discrete logarithms on a quantum computer*, SIAM journal of computing, vol. 26, no. 5, pp. 1484-1509 (1997).

[64] M.A. Nielsen and I.L. Chuang, *Quantum computation and quantum information*, Cambridge University Press, Cambridge, 2010.

[65] C.H. Bennett, G. Brassard, C. Crepeau, R. Jozsa, A. Peres and Â´ W. K. Wootters, *Teleporting an unknown quantum state via dual classical and einstein-podolsky-rosen channels*, Phys. Rev. Lett. vol. **70**, no. 13, p. 1895 (1993).

[66] R.P. Feynman, *Simulating physics with computers*, International journal of theoretical physics, vol. **21**, no. 6/7, pp. 467-488 (1982).

[67] A. Recknagel, *Permutation Branes*, JHEP **0304** (2003) 041, [hep-th/0208119v1].

[68] G. Sarkissian and M. Zamaklar, *Symmetry breaking, permutation D-branes on group manifolds: Boundary states and geometric description*, Nucl. Phys. B **696** (2004) 66, hep-th/0312215

[69] J. Fuchs, I. Runkel and C. Schweigert, *Boundaries, defects and Frobenius algebras*, Fortsch. Phys. **51** (2003) 850.

[70] L. Amico, R. Fazio, A. Osterloh and V. Vedral, *Entanglement in many-body systems*, Reviews of Modern Physics, vol. 80, no. 2, p. 517 (2008).

[71] R. Islam, R. Ma, P. M. Preiss, M. E. Tai, A. Lukin, M. Rispoli and M. Greiner, *Measuring entanglement entropy through the interference of quantum many-body twins*, Nature **528**, 77 (2015), [arxiv:1509.01160v1].

[72] T. Nishioka, S. Ryu and T. Takayanagi, *Holographic entanglement entropy: an overview*, Journal of Physics A: Mathematical and Theoretical, vol. 42, no. 50, p. 504008 (2009), [hep-th/0905.0932].

[73] S. Ryu and T. Takayanagi, *Holographic derivation of entanglement entropy from AdS/CFT*, Phys. Rev. Lett. **96**, 181602 (2006), [hep-th/0603001].

[74] S. Ryu and T. Takayanagi, *Aspects of Holographic Entanglement Entropy*, JHEP **0608** (2006) 045, [hep-th/0605073].

[75] A. Renyi, *On Measures of entropy and Information*, Proc. Fourth Berkeley Symp. on Math. Statist. and Prob, Vol. 1 (Univ. of Calif. Press, 1961), 547-561.

[76] M.B. Plenio and S. Virmani, *An introduction to entanglement measures*, Quant. Inf. Comp. **7**, 1, [quant-ph/0504163v3].

[77] P. Calabrese and J. Cardy, *Entanglement Entropy and Quantum Field Theory*, J.Stat.Mech. **0406** (2004) P06002, [hep-th/0405152].

[78] P. Calabrese and J. Cardy, *Entanglement entropy and conformal field theory*, J. Phys. A **42**, 504005 (2009), [hep-th/0905.4013v2].

[79] C.G. Callan Jr and F. Wilczek, *On geometric entropy*, Phys. Lett. B **333**, 55-61 (1994), [arXiv:hep-th/9401072].

[80] S. Furukawa, V. Pasquier and J. Shiraishi, *Mutual Information and Compactification Radius in a $c = 1$ Critical Phase in One Dimension*, Phys. Rev. Lett. **102**, 170602 (2009), [arxiv:0809.5113v3].

[81] H. Casini and M. Huerta, *Entanglement entropy in free quantum field theory*, J. Phys. A **42**, 504007 (2009), [arXiv:0905.2562].

[82] K. Sakai and Y. Satho, *Entanglement through conformal interfaces*, JHEP **0812** (2008) 001, [hep-th/0809.4548].

[83] E. Brehm and I. Brunner, *Entanglement entropy through conformal interfaces in the 2D Ising model*, JHEP **09**, 080 (2015), [hep-th/1505.02647].

[84] R. Argurio, A. Giveon and A. Shomer, *Superstrings on AdS_3 and Symmetric Products*, JHEP **0012**, 003 (2000), [hep-th/0009242].

[85] L. Borisov, M.B. Halpern and C. Schweigert, *Systematic approach to cyclic orbifolds*, Int. J. Mod. Phys. A **13** (1998) 125, [hep-th/9791961].

[86] A. Giveon and D. Kutasov, *Supersymmetric Renyi entropy in CFT_2 and AdS_3* , JHEP **03**, 058 (2016), [hep-th/1510.08872].

[87] L.A. Pando Zayas and N. Quiroz, *Left-right entanglement entropy of boundary states*, JHEP **01**, 100 (2015), [hep-th/1407.7057].

[88] D. Das and S. Datta, *Universal features of left-right entanglement entropy*, Phys. Rev. Lett. **115**, 131602 (2015), [hep-th/1504.0247].

[89] I. Affleck, N. Laflorencie and E.S. Sørensen, *Entanglement entropy in quantum impurity systems and systems with boundaries*, J. Phys. A **42** (2009) 504009.

[90] N. Ishibashi, *The boundary and crosscap states in conformal field theories* (1889), Modern Physics Letters A **4** (1989) 251-264.

[91] J. Maldacena, G. Moore and N. Seiber, *Geometrical interpretation of D-branes in gauged WZW models*, JHEP **0107** (2001) 046, [hep-th/0105038v1].

[92] M. Gaberdiel, *Boundary conformal field theory and D-branes* (2003), [http://www.phys.ethz.ch/∼mrg/lectures2.pdf].

[93] D.C. Lewellen, *Sewing constraints for conformal field theories on surfaces with boundaries*, Nucl. Phys. B **372**, 654 (1992).

[94] C.L. Cardy and D.C. Lewellen, *Bulk and boundary operators in conformal field theory*, Phys. Lett. B **259**, 274 (1992).

[95] M.R. Douglas and B. Fiol, *D-branes and discrete torsion. II*, JHEP **0509** (2005) 053, [hep-th/9903031]

[96] T. Kawai, Y. Yamanda and S. Yang, *Elliptic Genera and $\mathcal{N} = 2$ Superconformal Field Theory*, Nucl. Phys. B **414**, 191-212 (1994), [hep-th/9306096].

[97] E. Witten, *On the Landau-Ginzburg description of $\mathcal{N} = 2$ minimal models*, Int. J. Mod. Phys. A **9** (1994) 4783, [hep-th/9304026].

[98] S. Goh, *Chebyshev polynomials and spread polynomials*, Honours Thesis, School of Mathematics and Statistics, UNSW (2005).

Acknowledgements